Studies on the enzymatic synthesis of chiral hydroxyl nitriles

March, 2022

Daijun Zheng

CONTENTS

INTRODUCTION

Chiral hydroxyl nitrile (α-hydroxyl nitriles and β-hydroxyl nitriles) is a common motif that can be transformed into chiral amino nitrile(*1-3*), chiral amino acid(*4*, *5*), chiral hydroxyl amine(*6*, *7*), etc. These molecules derived from chiral hydroxyl nitriles are involved in lots of pharmaceuticals and biologically active molecules (**Scheme 1**).

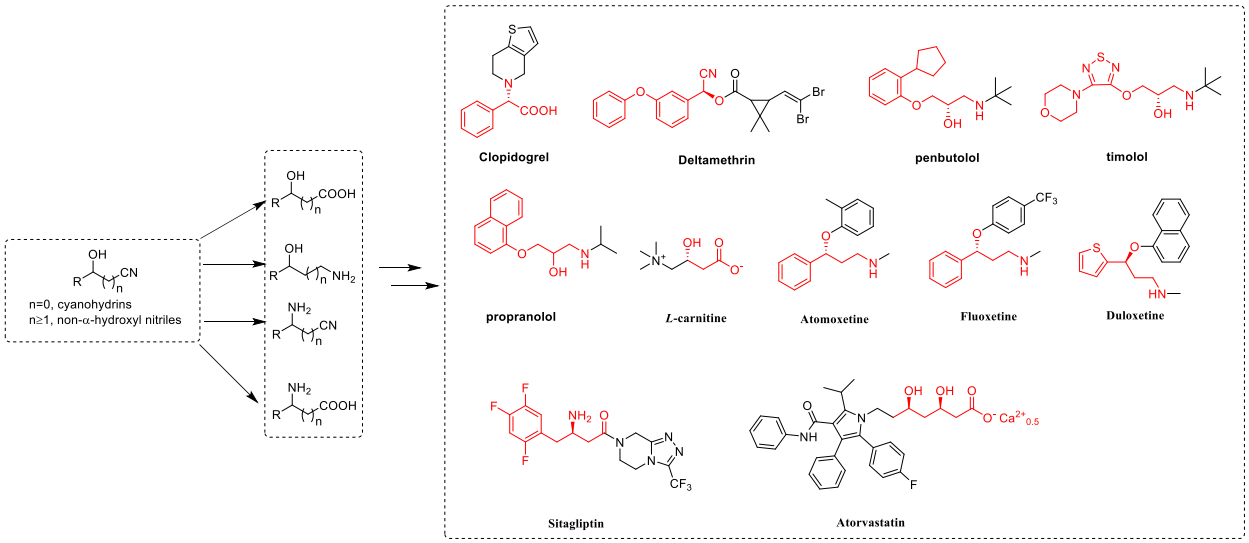

Scheme 1. Active molecules containing the motif derived from hydroxyl nitriles.

The common method used for chiral α-hydroxyl nitriles is asymmetric cyanation of carbonyl compounds using hydroxynitrile lyases (*8-10*) or chiral small molecules(*11*) as catalysts (**Scheme 2**). Alternatively, it can be also synthesized by kinetic resolution of racemic α-hydroxyl nitriles using lipases (*12*).

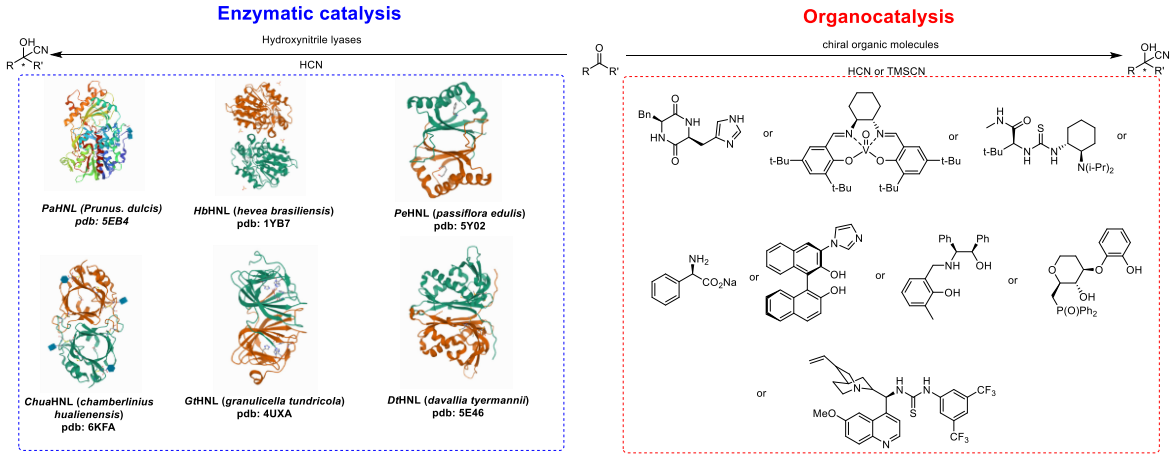

Scheme 2. Examples of asymmetric cyanation of carbonyl compounds catalyzed by enzymes or organocatalysts.

Hydroxynitrile lyase (HNL) is a class of enzyme participating in the process of cyanogenesis, in which it was identified to catalyze the decomposition of cyanohydrins to corresponding carbonyl compounds and toxic hydrogen cyanide (HCN). To date, known HNLs' structures can be classified into 7 superfamilies that include FAD-binding oxidoreductase (*Pa*HNL, derived from *Prunus amygdalus* (*13-16*), *Pm*HNL, derived from *Prunus mume* (*17*), *Ps*HNL, derived from *prunus serotina ehrh* (*18*), *Ej*HNL, derived from *Eriobotrya japonica* (*19, 20*)), α/β-hydrolase fold (*At*HNL, derived from *Arabidopsis thaliana* (*21, 22*), *Me*HNL, derived from *Manihot esculenta* (*23-30*), *Hb*HNL, derived from *Hevea brasiliensis* (*31-34*), *Sb*HNL, derived from *Sorghum bicolor* (*35-37*), *Bm*HNL derived from *Baliospermum montanum* (*38, 39*)), dimeric α+β barrel (*Pe*HNL, derived from *Passiflora edulis* (*40, 41*)), lipocalin like fold (*Chua*HNL, derived from *Chamberlinius hualienensis* (*42-44*), *Plam*HNL, derived from *Parafontaria laminate* (*45*), *Ogra*HNL, derived from *Oxidus gracilis*), cupin (*Ac*HNL, derived from *Acidobacterium capsulatum* (*46*), *Psm*HNL, derived from *Pseudomonas mephitica* (*47*), *Bp*HNL, derived from *Burkholderia phytofirmans* (*47*), *Gt*HNL, derived from *Granulicella tundricola* (*48*)), bet-v1 like fold (*Dt*HNL, derived from *Davallia tyermanii* (*49*)), and Zn^{2+}-dependent alcohol dehydrogenase (*Lu*HNL, derived from *Linum usitatissimum* (*50-53*)). Among them, the *Lu*HNL is one of the few enzymes that can catalyze the cyanation of ketones (*54, 55*) as shown in **Scheme 3**. Noteworthy, the *Lu*HNL showed different enantioselectivity on the asymmetric cyanation of different ketones. However, due to the lack of structure information of *Lu*HNL, the catalytic mechanism of *Lu*HNL is still a mystery. To reveal the catalytic mechanism will help us to understand this enzyme better and provide us a model on the enzyme engineering for its application on chiral ketone cyanohydrin synthesis.

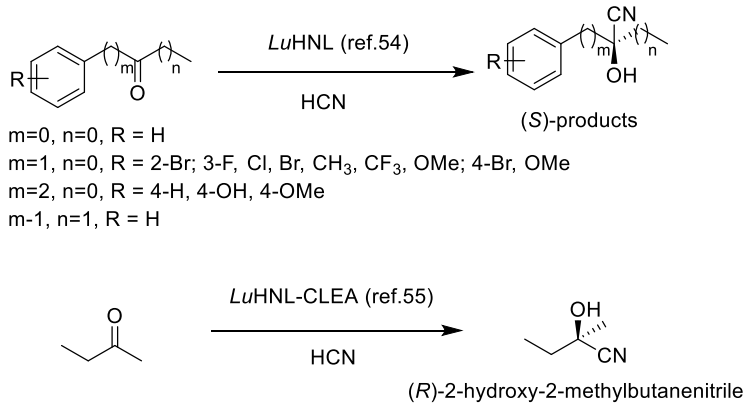

Scheme 3. The application of *Lu*HNL on ketone cyanohydrins synthesis.

To address these issues, in the Chapter I of this dissertation, the crystal structures of *Lu*HNL were determined using X-ray crystallography. In total, three structures of *Lu*HNL were determined: ligand-free *Lu*HNL (*Lu*HNL_lig_free, PDB ID: 7VB3), acetone cyanohydrin-complexed *Lu*HNL (*Lu*HNL_CNH, PDB ID: 7VB5), and (*R*)-2-butanone cyanohydrin-complexed *Lu*HNL (*Lu*HNL_BCN, PDB ID: 7VB6). Based on these crystal structures and site-directed mutagenesis analysis results, we proposed a catalytic mechanism for *Lu*HNL on cyanohydrin decomposition and elucidated the function of NAD^+ and Zn^{2+} in *Lu*HNL.

As for the asymmetric synthesis of β-hydroxyl nitriles, the asymmetric transfer hydrogenation of *pre*-ketones (ATH) using Ru (*56-58*) or Ir (*59-61*) transition metal complexes as catalyst is commonly adopted as shown in **Scheme 4**.

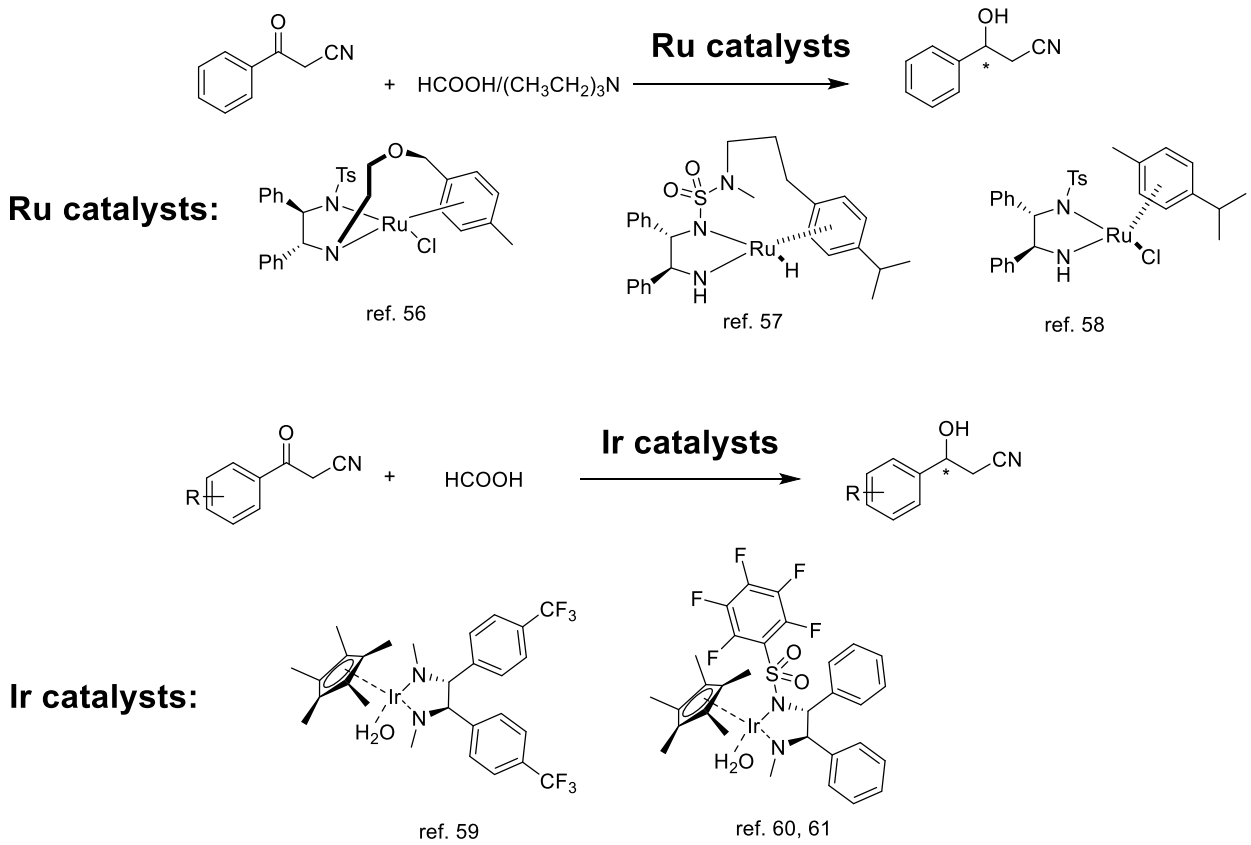

Scheme 4. Asymmetric transfer hydrogenation of β-ketone nitriles to corresponding chiral β-hydroxyl nitriles.

In addition, alternative methods using the β-borylation of organoborane compounds with acceptor of α, β-unsaturated nitriles catalyzed by copper-complex following with oxidation to synthesize corresponding alcohols have been reported (**Scheme 5**) (*62-64*).

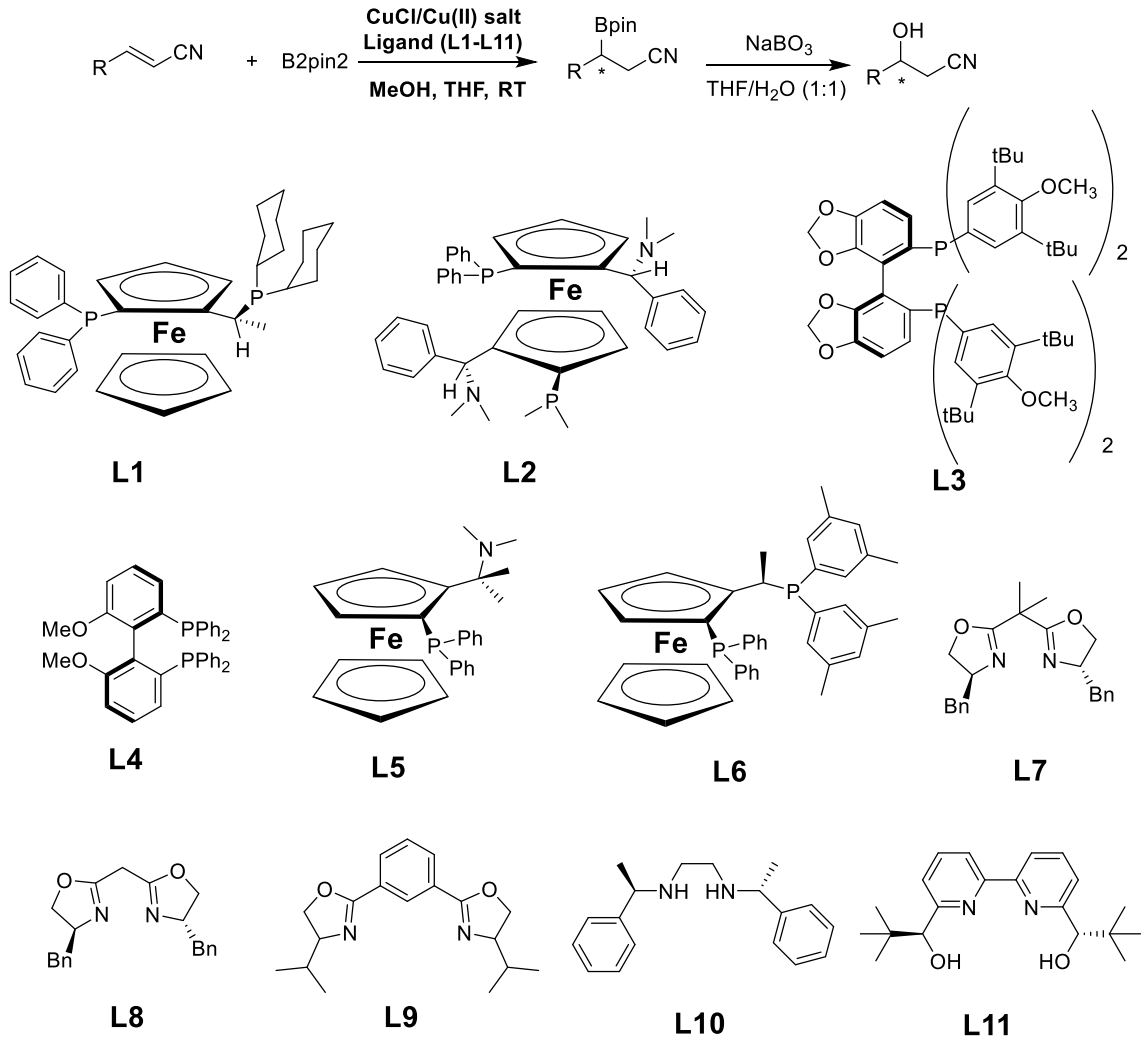

Scheme 5. The β-borylation of organoborane compounds with acceptor of α, β-unsaturated nitriles.

What's more, the asymmetric cross aldol reaction of aldehydes with different nucleophilic addition donors and catalysts, such as acetonitrile/Cu alkoxide-chiral phosphine complex (*65*, *66*), organolithium reagents (*67*), cyanomethylzinc bromide/DPMPM (*68*) have been well developed (**Scheme 6**).

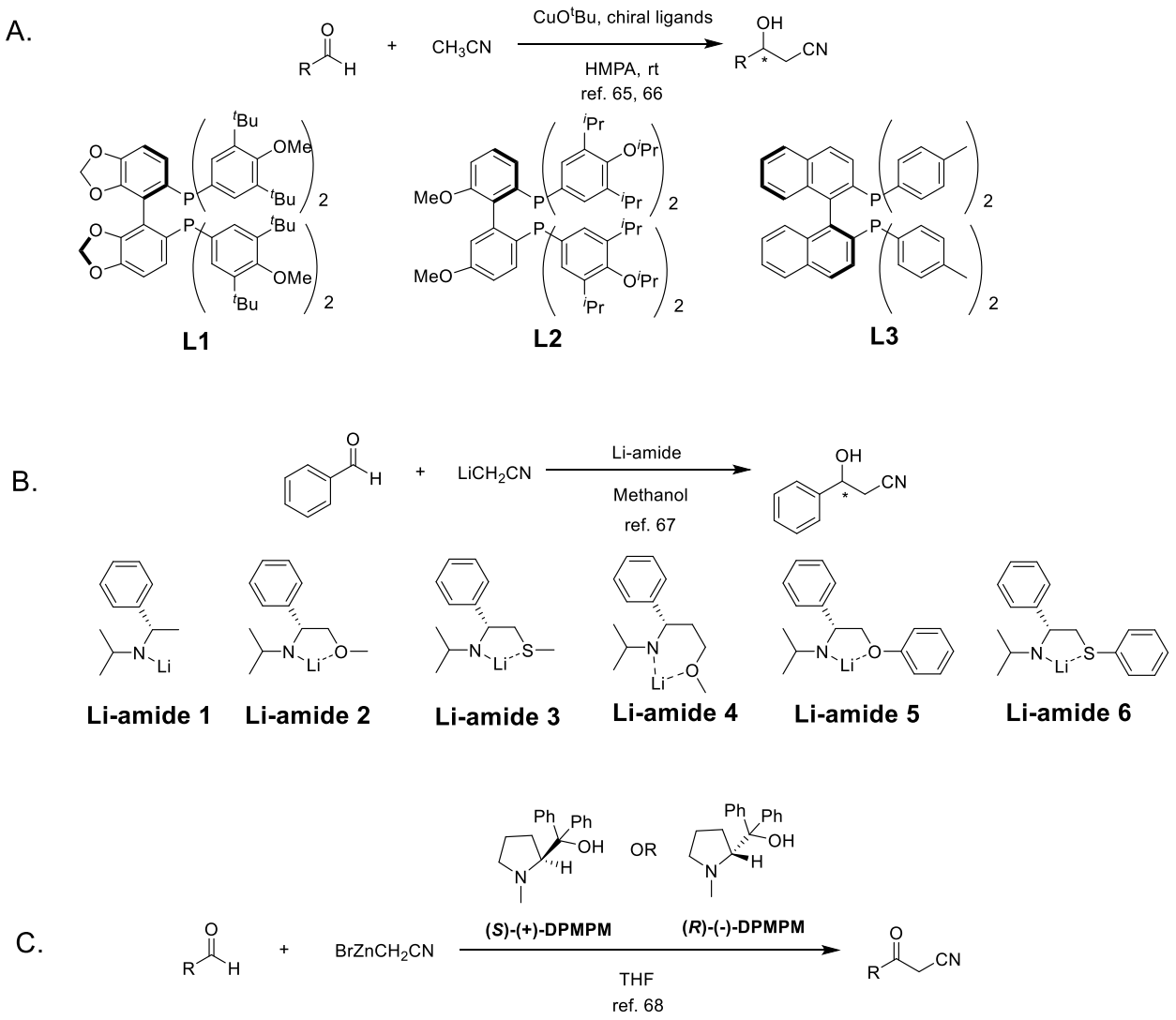

Scheme 6. Asymmetric cross aldol reaction of aldehydes with different nucleophilic addition donors and catalysts.

Benefitting from the great development of biotechnology and green chemistry, a variety of synthetic strategies to β-hydroxy nitriles have been developed using purified enzymes or whole cell catalysts. Among them, lipases (*69*, *70*), reductases (*71-74*), dehydrogenases (*75*), and nitrilases (*76*, *77*), have been mostly employed toward the synthesis of chiral β-hydroxyl nitriles via the kinetic resolution of racemic hydroxyl nitriles or the asymmetric reduction of β-oxo-nitriles. In addition, few publications have reported the use of monooxygenase for the asymmetric hydroxylation of 3-phenylpropanenitrile (*78*) or multi-enzymatic biosynthesis

system of alcohol dehydrogenase/halohydrin dehalogenase treating on α-halo ketones and cyanide (*79*) to form this class of chiral compounds (**Scheme 7**).

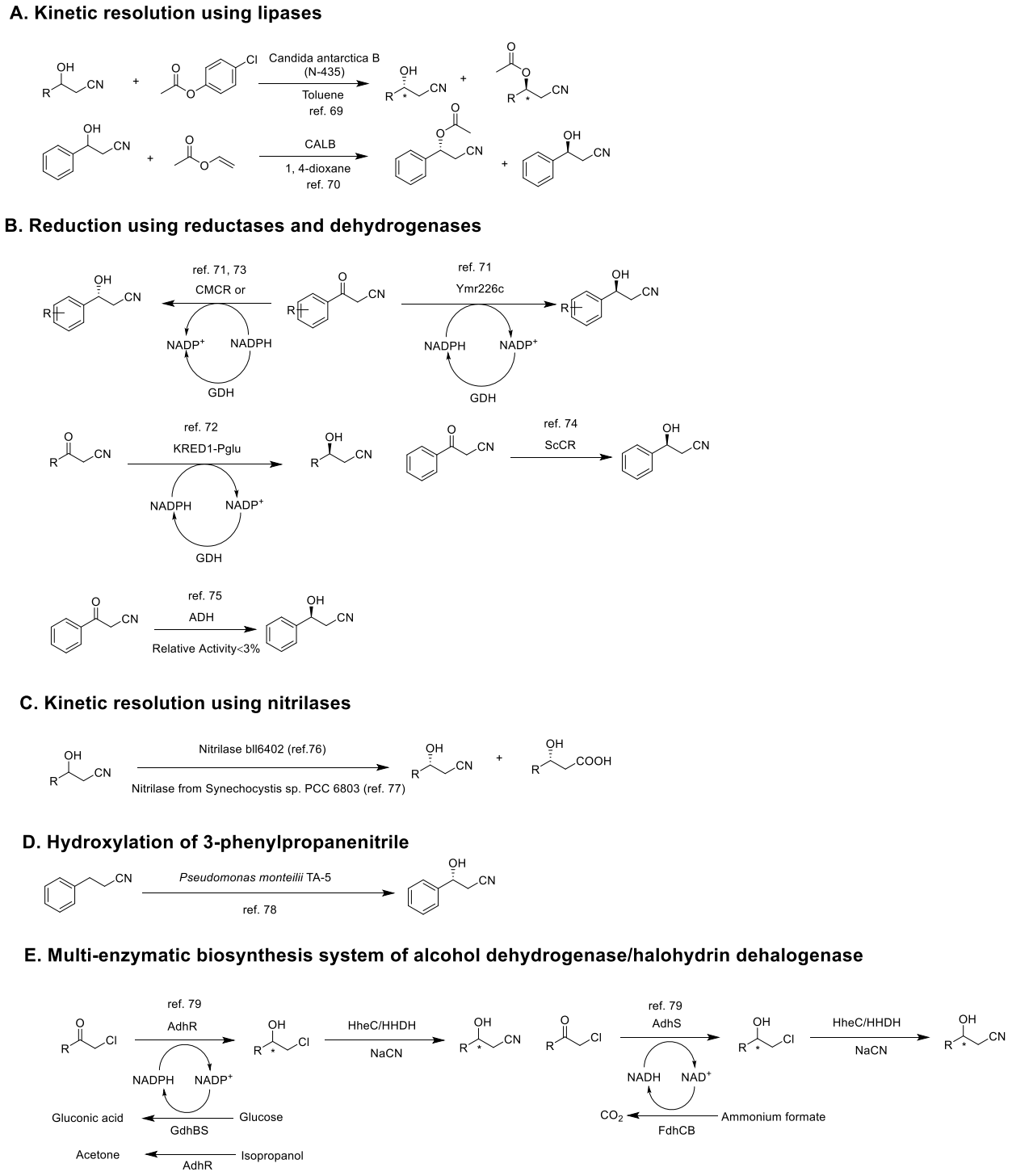

Scheme 7. Enzymatic reactions for chiral β-hydroxyl nitriles synthesis.

In general, most of the organic synthetic routes inevitably use costly chiral transition-metal complexes as catalysts to construct the chiral center. The biocatalytic methods overcome the use of costly transition-metal catalysts, but are confined to a limited scope of precursors, including keto-nitriles and racemic hydroxyl nitriles.

In the Chapter II and Chapter III of this dissertation, a novel enzymatic method is described to synthesize complementary enantiomers of β-hydroxyl nitriles using aldoxime dehydratases as catalyst. This method starts from readily available alkenes, but avoids using toxic cyanide for nitrile group construction.

Chapter I: Structural characterization of *Linum usitatissimum* hydroxynitrile lyase: a new cyanohydrin decomposition mechanism involving a cyano-zinc complex

In early 1987, *Lu*HNL, the only member of the Zn^{2+}-dependent alcohol dehydrogenase superfamily, was purified for the first time from young seedings of flax (*Linum usitatissimum* L.). It was characterized as a dimer with a subunit molecular mass of 42,000 Da (*50*). In 1997, the full-length cDNA encoding *Lu*HNL was isolated and cloned into *Escherichia coli*. The amino acid sequence of *Lu*HNL showed significant similarities to the alcohol dehydrogenase (ADH) family, rather than to other known HNLs. The phylogenetic evolution analysis on *Lu*HNL by amino acid alignment in NCBI shows that *Lu*HNL possesses the closest clade with alcohol dehydrogenase (**Fig.1**).

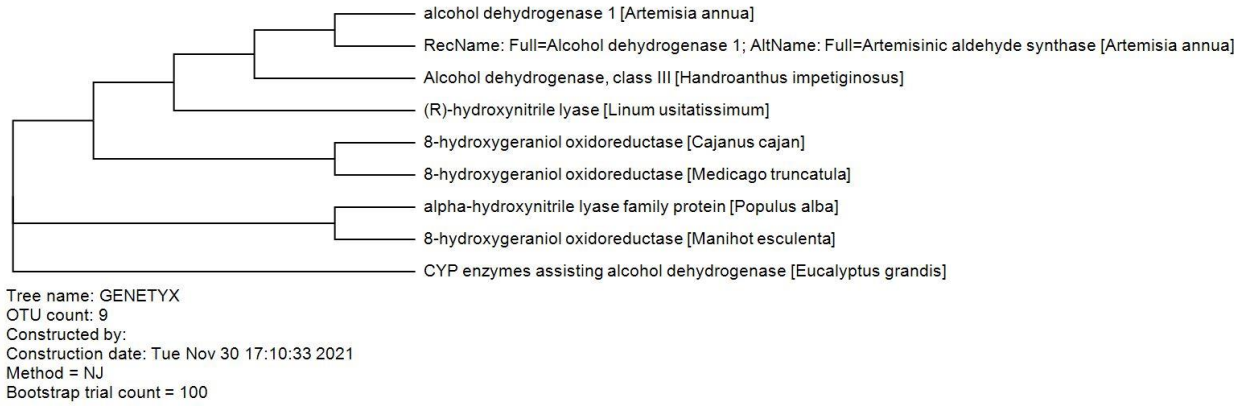

Fig.1. Phylogenetic evolution analysis of *Lu*HNL.

In addition, from the sequence alignment of *Lu*HNL and ADHs, it was found the residues coordinating with Zn^{2+} ions and the ADP-binding βαβ unit motif in ADHs were highly conserved in *Lu*HNL. However, neither ADH activity in *Lu*HNL nor HNL activity in ADH was detected. From the loss of inhibition of *Lu*HNL activity with the addition of Zn^{2+} chelators, it was concluded that the Zn^{2+} ions were not directly involved in the catalysis of cyanohydrin cleavage (*51*). Furthermore, the subsequent site-directed mutagenesis analysis of *Lu*HNL by its overexpression in *Pichia pastoris* indicated that the residues involved in catalysis of Zn^{2+}-ADHs were also functionally important in *Lu*HNL. From these results, it was presumed that all the Zn^{2+}

ions in *Lu*HNL possess only the function of stabilizing the structure and not participating in the catalysis (*52*). All these conclusions seem reasonable based on the experimental results, but not from direct evidence. Until now, no convincing evidence has been described to clarify these questions, and the catalytic mechanism of *Lu*HNL is also unknown. Hence, the structures of *Lu*HNL were solved by X-ray crystallography here to help to clarify the reaction mechanism of the enzyme on the decomposition of cyanohydrins.

Experimental procedures

Overexpression of *Lu*HNL and purification

The gene for *Lu*HNL from *Linum usitatissimum* (GenBank accession number AF024588.1) was cloned into pET-15b vector (Novagen, Darmstadt, Germany) with ***NdeI*** (CATATG) and ***BamHI*** (GGATCC) restriction sites, and a His-tag peptide and a thrombin recognition sequence (MGSSHHHHHHSSGLVPRGSHM) were attached to the N-terminal. The resulting plasmid was transformed into competent JM109 *E.coli* cells, and the copied plasmid was extracted using the Gene elute^{TM} Plasmid Miniprep Kit (Sigma-Aldrich, St. Louis, MO, USA). The extracted recombinant plasmid sequence was confirmed by Genetic Analyzer 3500 (ThermoFisher Scientific, MA, USA) using T7 promoter primer (5'-TAATACGACTCACTATAGGG-3') and T7 terminator primer (5'-ATGCTAGTTATTGCTCAGCGG-3'). Then the recombinant plasmid was transformed into SHuffle T7 Express Competent *E.coli* (New England Biolabs, Ipswich, MA, USA) for expression.

A single colony of SHuffle T7 *E.coli* harboring the plasmid of pET-15b-*Lu*HNL was inoculated into a 5 mL lysogeny broth (LB) medium containing 100 μg/mL ampicillin (Amp), and cultivated at 30°C, 300 RPM overnight. Then, 3 mL pre-culture was transferred into 500 mL LB medium containing 100 μg/mL Amp and cultivated at 30 °C, 150 RPM for 5 h (OD_{600} = 0.64), then 1 mM isopropyl β-D-1-thiogalactopyranoside (IPTG) was added to induce the protein expression, and the cells were continued to cultivate at 16 °C, 120 RPM for 24 h. The cells from 4 L of medium (500 mL×8) were harvested by centrifugation (6000 × *g*, 10 min, 4 °C) and the pellet was re-suspended in 100 mL lysis buffer (20 mM potassium phosphate buffer (KPB), 20 mM imidazole, 500 mM NaCl, pH 7.4). The cells were disrupted by sonication in an ice-bath for 30 min. Then, the debris and insoluble protein were removed by centrifugation (15000 × *g*, 30

min, 4 °C). The supernatant was loaded onto a 15 mL of Ni Sepharose™ 6 Fast flow column (GE Healthcare, IL, USA) equilibrated with lysis buffer (10 column volume (CV)), followed by washing with lysis buffer (10 CV). A gradient elution program was performed using 15 CV of lysis buffer (buffer A) and 15 CV of buffer B (20 mM KPB, 500 mM imidazole, 500 mM NaCl, pH 7.4) to elute the bound protein. The fractions were collected in volumes of 10 mL per tube. The active fractions were pooled and dialyzed against 20 mM KPB (pH 7.4, 5 L×2, 4 °C). Subsequently, the active fraction was concentrated and applied to Mono Q 5/50 GL column (bed volume: 1 mL; GE Healthcare, IL, USA) for further purification. The bound protein was eluted with a linear gradient of 0-0.15 M NaCl (40 CV), 0.15 M-0.25 M NaCl (20 CV), 0.25 M-0.5 M NaCl (10 CV) in 20 mM KPB (pH 7.4). The purity of active fractions was analyzed by SDS-PAGE and pure fractions were pooled and concentrated to 10.5 mg/mL (measured by BCA method, Takara, Otsu, Japan) for further crystallization.

Crystallization

The crystals of N-His-*Lu*HNL were prepared using the vapor diffusion sitting drop method at 20 °C in 96-well Intelli-Plates (Art Robbins Instruments, Sunnyvale, CA, USA). The sitting drop was prepared by mixing 1 µL of N-His-*Lu*HNL (10.5 mg/mL) with 1 µL crystallization buffer (0.1 M BIS-TRIS, pH 6.5, 20% w/v polyethylene glycol monomethyl ether 5,000, HAMPTON RESEARCH, Index™, Reagent 46) (HAMPTON RESEARCH, CA, USA). A total of 50 µL of crystallization buffer was used as reservoir solution.

Data collection, processing, model building, and refinement

Before subjecting the crystals to flash-freezing for X-ray diffraction, the sample for ligand-free structure of *Lu*HNL determination was prepared by soaking the crystal in solution I (crystallization buffer containing 15 % (v/v) glycerol) and cryoprotectant solution II (crystallization buffer containing 25% (v/v) glycerol) successively. Similarly, the sample for *Lu*HNL-acetone cyanohydrin complex structure determination was performed by soaking the crystal in cryoprotectant solution I and cryoprotectant solution III (cryoprotectant solution II/acetone cyanohydrin: 90/10 (v/v)) for 20 min. The sample for *Lu*HNL-2-butanone cyanohydrin complex structure determination was similarly prepared by soaking the crystal in

cryoprotectant solution I and cryoprotectant solution IV (cryoprotectant solution II/(*rac*)-2-butanone cyanohydrin cyanohydrin: 98/2 (v/v)) for 5 min.

The X-ray diffraction data of ligand-free *Lu*HNL and *Lu*HNL_CNH were collected at 100 K at the beamline BL-5A of KEK-PF (Tsukuba, Japan) with a reflection record of 0.2° per image. Another data set of *Lu*HNL soaked by (*rac*)-2-butanone cyanohydrin was collected using an in-house X-ray generator and an imaging plate (MicroMax-007HF and R-AXIS VII, Rigaku, Tokyo, Japan) with a reflection record of 0.5° per image. All data sets were integrated using iMosflm (*80*) and scaled using SCALA (*81*). The initial model for molecular replacement was built using the automatic molecular replacement pipeline program of BALBES (*82*). All models were corrected using COOT (*83*) and refined using REFMAC5 (*84*) and *Phenix* (*85*). R_{free} values were computed from 5% of the randomly chosen reflections that were not used for refinement. Water molecules were inserted automatically and manually into the potential electron density map. The validation of the water molecules was automatically performed according to the geometric criteria and their refined B-factors (B<60 Å2). The statistics for data collection and refinement are showed in **Table 1**.

The figures of the protein structure were displayed by Pymol *(86)* and the secondary structure was displayed by ESPript 3.0 server (http://espript.ibcp.fr/) (*87*).

Site-directed mutagenesis of *Lu*HNL

The *Lu*HNL mutants were prepared via site-directed mutagenesis using the PrimeSTAR® Mutagenesis Basal kit (Takara, Otsu, Japan) with forward and reverse primers of a 27-mer oligonucleotide designed as indicated by the kit manual. The PCR was performed for 30 cycles: (denaturation 98°C/10s, annealing 55°C/15s, elongation 72 °C/40s). The amplified PCR product was purified using a Wizard® SV gel and PCR clean-up system (Promega, WI, USA). The resulting PCR product was transformed into JM109 *E.coli* competent cell. The recombinant plasmids were extracted from the JM109 *E.coli* and sequenced by Genetic Analyzer 3500 (ThermoFisher Scientific, MA, USA) using T7 promoter primer (5'-TAATACGACTCACTATAGGG-3') and T7 terminator primer (5'-ATGCTAGTTATTGCTCAGCGG-3'). The confirmed plasmids were transformed into SHuffle

T7 Express Competent *E.coli* (New England Biolabs, Ipswich, MA, USA) for expression. All the mutants were purified as the wild type did for activity assay.

Table 1: Statistics for data collection and refinement of *Lu*HNL structures.

crystals	*Lu* HNL_lig_free	Complex structures of *Lu* HNL	
		Lu HNL_CNH	*Lu* HNL_BCN
PDB ID	7VB3	7VB5	7VB6
X-ray source	KEK-PF BL-5A	KEK-PF BL-5A	Rigaku MicroMax-007HF
Space group	$P2_1$	$P2_1$	$P2_1$
Unit cell dimensions			
***a, b, c* (Å)**	94.12, 52.18, 168.51	94.12, 51.57, 170.00	94.18, 52.10, 169.85
α, β, γ (°)	90.00, 95.01, 90.00	90.00, 94.67, 90.00	90.00, 94.80, 90.00
Wavelength (Å)	1.000	1.000	1.542
Resolution range (outer shell)	85.08-1.48 (1.56-1.48)	93.81-1.58 (1.67-1.58)	56.46-1.72 (1.82-1.72)
Total No. of reflections	1648102 (242127)	1381304 (203937)	1048056 (129043)
No. of unique reflections	269690 (38964)	223351 (32471)	168508 (20676)
Completeness	99.6 (99.2)	100.0 (100.0)	97.0 (84.7)
Mean (I/σ(I))	10.5 (2.7)	8.9 (1.3)	9.9 (2.4)
R_{merge} [a]	0.092 (0.661)	0.121 (1.323)	0.113 (0.663)
Multiplicity	6.1 (6.2)	6.2 (6.3)	6.2 (6.2)
Mn(I) half-set correlation $CC_{1/2}$	0.998 (0.835)	0.997 (0.612)	0.996 (0.845)
Average mosaicity	0.64	0.36	0.67
Protomers in asymmetric unit	4	4	4
R_{work} [b]	0.156	0.171	0.163
R_{free} [b]	0.183	0.205	0.206
RMSD of the geometry			
Bond length (Å)	0.0129	0.0099	0.0100
Bond angle (°)	1.808	1.593	1.635
Ramachandran outlier (%)	0	0	0
Ramachandran favored (%)	97.59	97.05	96.97

[a] $R_{merge} = \Sigma|(I_{hkl} - \langle I_{hkl}\rangle)| / (\Sigma I_{hkl})$, where $\langle I_{hkl}\rangle$ is the mean intensity of all reflections equivalent to reflection *hkl*.

[b] R_{work} (R_{free}) = $\Sigma||F_{obs}|-|F_{calc}|| / \Sigma|F_{obs}|$, where 5 % of randomly selected data were used for R_{free}.

*Lu*HNL activity measurement

The acetone cyanohydrin degradation activity of *Lu*HNL was determined by monitoring the formation of CN^- ion (*88*). The reaction mixture was composed of appropriate enzyme amount, 10 mM acetone cyanohydrin (added by 100 µL of 100 mM acetone cyanohydrin that prepared in 0.1 M citric acid solution), and 400 mM citrate buffer (pH 4.5) in a total volume of 1 mL, which was monitored at room temperature for 7 min by cyanide detection. For cyanide detection, 1 µL enzymatic reaction mixture was added to 199 µL oxidants solution (27 mM succinimide and 2 mM N-chlorosuccinimide in DIW), followed by the addition of 50 µL coupling reagent (0.2 M barbituric acid and 24% pyridine (V/V) in DIW). The resulting mixture was incubated at room

temperature for 10 min, then measured at 580 nm. 1 U enzyme activity was defined as the enzyme amount to catalyze the formation of 1 μmol CN^- in 1 min.

Quantitative measurement on the metal ions in *Lu*HNL

The concentration of *Lu*HNL was measured by BCA method (Takara, Otsu, Japan) and the *Lu*HNL molecular mass of 48 kDa was used for calculation. Analysis method: to 10 mL of *Lu*HNL enzyme solution with different concentrations (8.6 nM-610 nM) was added by 50 μL nitric acid solution (V_{acid}/V_{H2O}=1/2). The resulted solution was applied to Inductively Coupled Plasma Mass Spectrometry (ICP-MS, Agilent 7700, CA, USA) analysis.

Quantitative measurement of the NAD^+ in *Lu*HNL

5 mg/mL *Lu*HNL (measured by BCA method, Takara, Otsu, Japan) was incubated with 4 M guanidine in ice-bath for 1 h. The denatured *Lu*HNL and NAD^+ cofactor were separated by filtration (12, 000×g, 20 min, 4 °C, Amicon Ultra 10K, Merck Millipore, MA, USA). The NAD^+ in the filtrate was measured at wavelength of 260 nm and quantitatively calculated using a calibration curve prepared from standard NAD^+ compound (Fujifilm Wako, Osaka Japan).

LC-MS/MS for protein determination

The protein cut from the SDS-PAGE was transfer into 1.5 mL tube. 300 μL destaining solution I (25 mM NH_4HCO_3, 50% MeOH) was added, which was incubated at 40 °C for 30 min. The resulting sample was centrifuged (2000 ×g) and the destaining solution was removed. Then 300 μL destaining solution II (25 mM NH_4HCO_3, 50% acetonitrile) was added, which was incubated at 40 °C for 30 min. The resulting sample was centrifuged (2000 ×g) and the destaining solution was removed. Then the gel was washed by 25 mM NH_4HCO_3 for two times. The dehydration of the washed gel was performed by addition of 200 μL acetonitrile. The acetonitrile was removed by pipette and the residual acetonitrile was removed by treating the sample in vacuum for 5 min. To the treated sample, 50 μL of reducing solution (10 mM DTT, 25 mM NH_4HCO_3) was added and the sample was incubated at 56°C for 45 min. Then the sample was centrifuged (2000 ×g) and the reducing solution was removed by pipette. The resulting sample was washed by addition of 50 μL NH_4HCO_3 (25 mM), which was shaken for 5 min to remove DTT. Then 50 μL alkylation reagent (55 mM iodoacetamide, 25 mM NH_4HCO_3) was added, which was shaken at

r.t for 30 min (protect from light) to alkylate the Cysteines. The alkylation solution was removed by pipette after centrifugation (2000 ×g). Then the sample was washed by 500 μL NH_4HCO_3 (25 mM) for 2 times, followed by addition of 200 μL acetonitrile to dehydrate the gel completely. The acetonitrile was removed by pipette and the residual acetonitrile was removed by keeping the sample in vacuum for 5 min. Then the protein was digested in the gel by addition of 30 μL trypsin solution (10 ng/μL in 25 mM NH_4HCO_3), the resulting sample was shaken by Voltex until the gel become transparent (about 10 min). The sample was centrifuged (2000×g) and excess trypsin solution was removed by pipette. To the gel, 50 μL of NH_4HCO_3 (25 mM) was added, and the resulting sample was incubated at 37 °C overnight. Then the solution was removed by pipette and the digested protein was extracted by addition of 50 μL extraction solution I (50% acetonitrile, 0.1% trifluoroacetic acid). After centrifugation (2000×g), the supernatant solution was transferred to a new tube and the remaining gel was extracted for two times by using 50 μL extraction solution II (100% acetonitrile, 0.1% trifluoroacetic acid). The supernatant solutions were combined with previous supernatant in the new tube, which was analyzed by LC-MS/MS.

CD-spectrum measurement for *Lu*HNL

The CD spectrum were measured using 0.05 mg/mL protein concentration (BCA method, Takara, Otsu, Japan), rt, 2 mm pathlength of cuvette. The data was processed using CAPITO program (*89*).

Results

The overall structure of *Lu*HNL

Because of the low sequence identity of *Lu*HNL with structures of known proteins, the initial structure model of ligand-free *Lu*HNL (*Lu*HNL_lig_free) was built using the BALBES program (*82*). BALBES suggested a possible initial model of the human σσ alcohol dehydrogenase (PDB ID: 1D1T, 32.47% sequence identity with *Lu*HNL) (*90*) and a subsequent molecular replacement was successfully processed. Further refinement was performed using REFMAC5 (*84*) and *Phenix* (*85*). The crystal belongs to the monoclinic space group $P2_1$ with unit-cell parameters a = 94.12 Å, b = 52.18, c = 168.51; α = 90.00, β = 95.01, γ = 90.00. The R_{work} and R_{free} values of the

refined coordinate are 0.156 and 0.183 at 1.48 Å as shown in the **Table 1**. Two dimers (dimer 1: chain A + B and dimer 2: chain C + D) in parallel as shown in the **Fig. 2A** were found in the asymmetric unit.

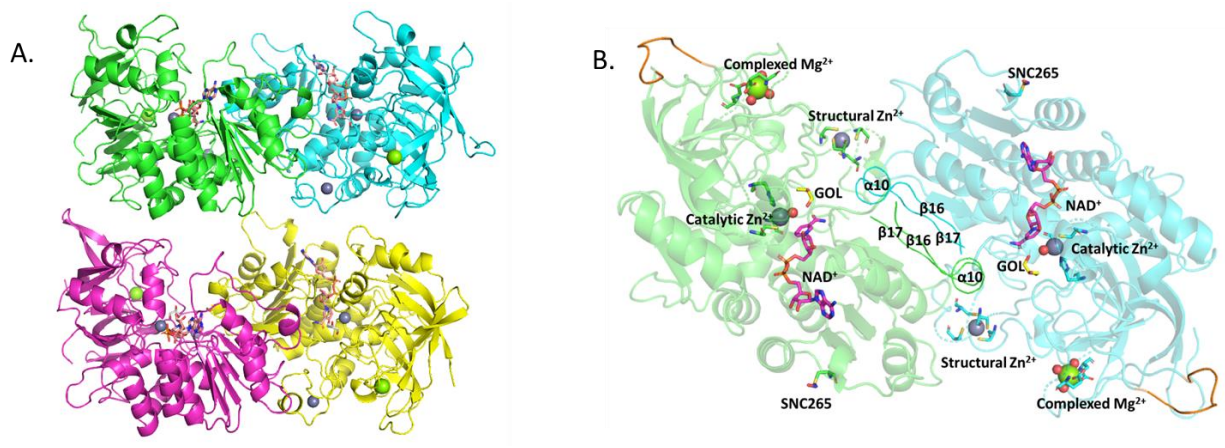

Fig.2. Structure view of *Lu*HNL. (A) Overall structure of *Lu*HNL with two parallel dimers observed in per asymmetric unit. The four chains are colored in green (chain A), cyan (chain B), magenta (chain C), yellow (chain D), respectively. (B) Structure features observed in *Lu*HNL. As indicated in the picture, two Zn^{2+} ions (grey spheres), one NAD^{+} molecule, one Mg^{2+} ion (green spheres), S-nitrosylation of Cys265 were identified in each chain. The water molecules complexed with metal ions were shown as red spheres. The GOL refers to glycerol molecule. The interface of two subunits (β16α10β17 moiety) was highlighted by ribbon. The parts with poor electron density map were marked as gold color. The protein structures were displayed using the program of PyMOL (*86*).

The secondary structure of *Lu*HNL consists of thirteen α-helices, six 3_{10}-helices, nineteen β-sheets, ten strict β-turns, and one strict α-turn, as shown in the **Fig. 3.** The root-mean-square deviation (RMSD) between the Cα atoms of two dimers was 0.514 Å. Each of the two chains in dimer 1 (chain A + B) and dimer 2 (chain C + D) superimposed with an RMSD of 0.308 Å and 0.278 Å at the Cα atoms, respectively. Large conformational variations were observed in the β-turn between β7 and β8, β-turn between η2 and α8, and around η4 and β16, which may be disordered as the electron density is not well-defined. The conformational changes among four chains (Chain A, B, C, D) in terms of RMSD are 0.093-0.248 Å for β-turn between β7 and β8 (aa 146-158), 0.317-0.792 Å for β-turn between η2 and α8 (aa 268-283), and 0.092-0.327 Å for the residues around η4 and β16 (aa 326-334), respectively.

The interface region between two subunits in one dimer was in the β16α10β17 area **(Fig. 2B)**, which contains twelve hydrophobic residues (Ile331, Phe332, Phe333, Phe335, Phe338, Leu339,

Phe340, Gly341, Gly342, Val344, Val345, Gly346), four electrically charged residues (Arg330, Asp334, Lys336, Asp337), and one polar uncharged residue (Asn343). The central area of this βαβ unit is occupied by hydrophobic residues. The electrically charged residues and polar uncharged residue were located on the periphery and extended outward. A salt bridge between the ε-amino group in Lys336 and the carboxyl group in Glu136 of another chain was observed at 2.7-3.0 Å. (**Fig. 4A**)

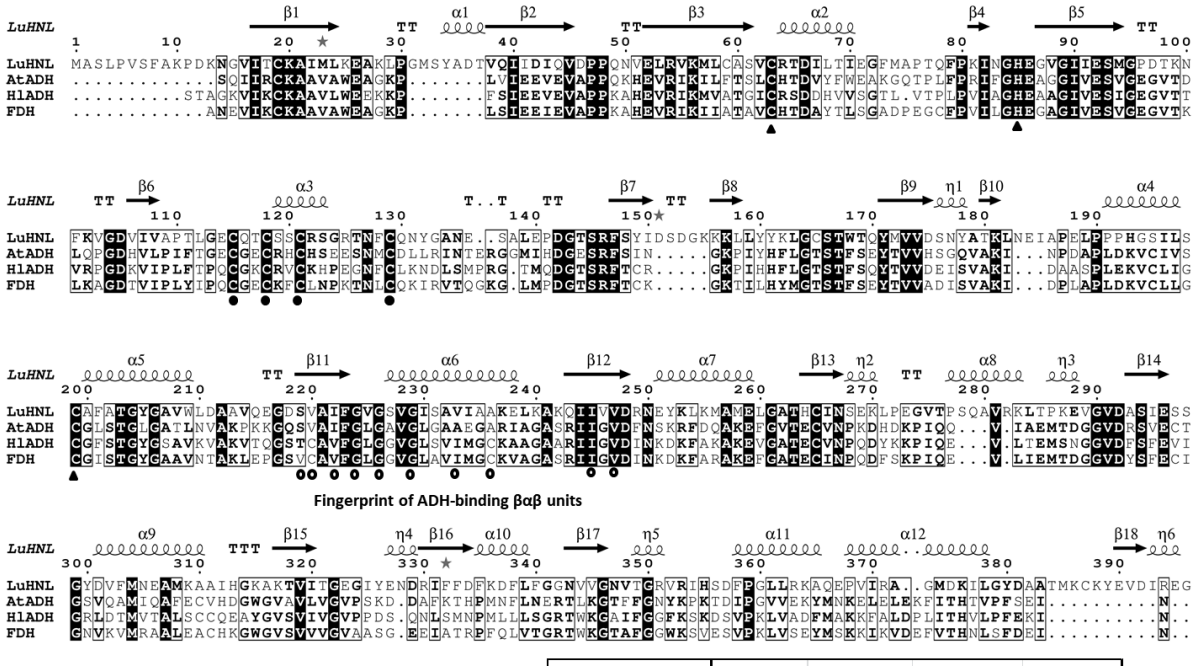

Identity/%	LuHNL	AtADH	HlADH	FDH
LuHNL	100	34	33	36
AtADH	34	100	52	54
HlADH	33	52	100	62
FDH	36	54	62	100

Fig. 3. Secondary structure-based multiple sequence alignment of *Lu*HNL with alcohol dehydrogenase (*At*ADH, derived from *Arabidopsis thaliana* (PDB ID: 4RQU); *Hl*ADH, derived from *Equus caballus* (PDB ID: 6ADH) (*91*, *92*), and formaldehyde dehydrogenase, derived from *Homo sapiens* (FDH, PDB ID: 1M6H) (*93*). The secondary structure elements are shown as α-helices (medium squiggles with α symbols), 3_{10}-helices (small squiggles with η symbols), β-strands (arrows with β symbols), strict β-turns (TT letters), and strict α-turns (TTT letters). The residues for catalytic Zn^{2+} coordination that conserved in all four proteins are highlighted as triangle symbols. The four cysteines for structural Zn^{2+} coordination that conserved in all four proteins are marked by bold dots. The fingerprint of ADH-binding βαβ units (*94*) are indicated as circles. The alignment was done using ESPript 3.0 server (http://espript.ibcp.fr/) (*87*).

The electron density of NAD^+ was observed in the crystal without the addition of exogenous NAD^+ during enzyme crystallization, nor soaking of the crystal to a NAD^+ solution before X-ray diffraction (**Fig. 4B**). The NAD^+ molecule was bound to the β11α6β12 fold, a classic binding domain for ADP, which is consistent with the fingerprint for ADP-binding that identified from the amino acid sequence of *Lu*HNL (**Fig. 3**) (*94*). Furthermore, two classical tetra-coordinated complexes of Zn^{2+} ions were observed. One was bonded to Cys115, Cys118, Cys 121, Cys 129 at a distance of 2.3-2.4 Å (**Fig. 4C**), and the second Zn^{2+} complex formed bonds with Cys63, His85, Cys199, and one molecule of water at a distance of 2.0-2.4 Å (**Fig. 4D)**. Beyond the water

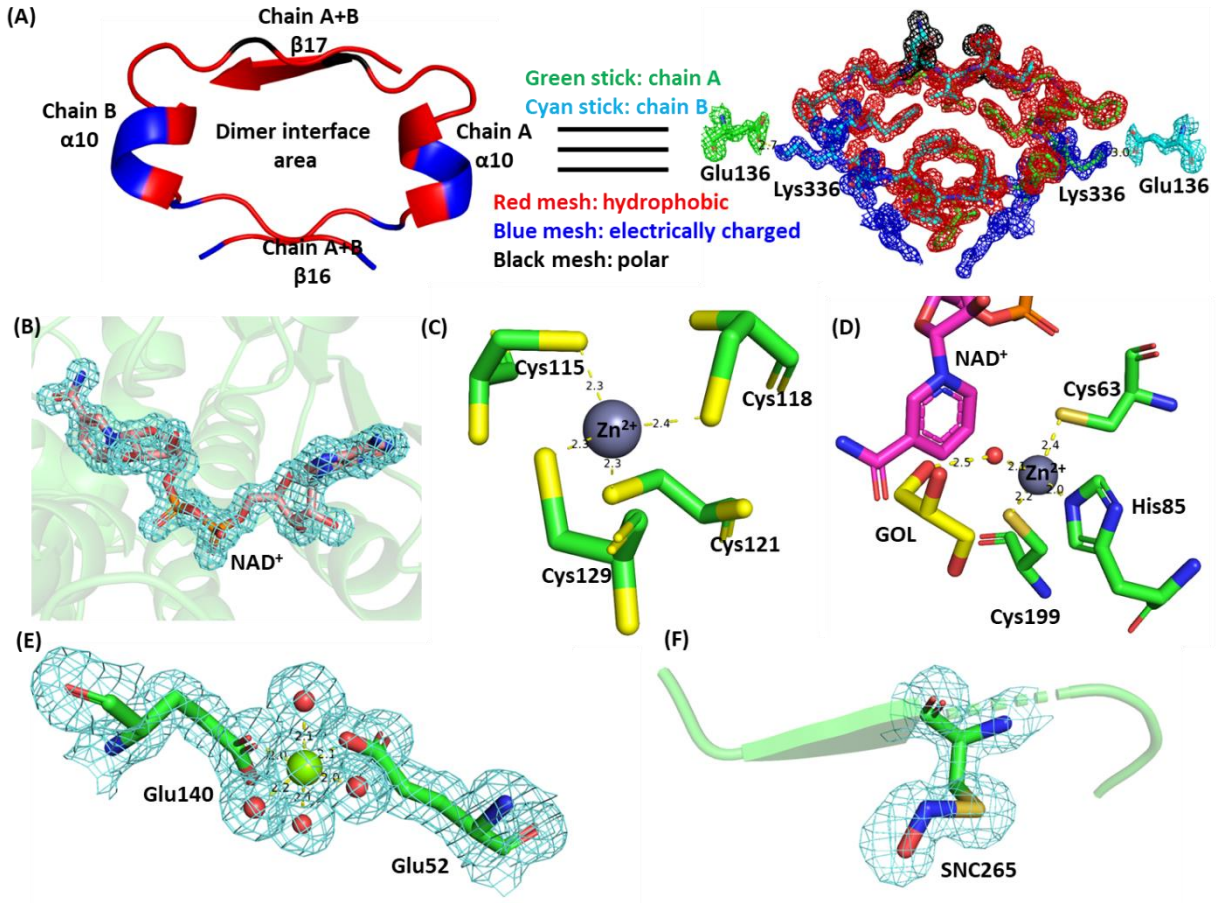

Fig. 4. Structure features of *Lu*HNL in detail. (A) The interface area in a dimer; (B) The NAD^+ molecule electron density map observed in structure refinement; (C) The structural Zn^{2+} ion complexed with four cysteines; (D) The catalytic Zn^{2+} complexed with two cysteines and one histidine; (E) The complexed structure of Mg^{2+} coordinated with four water molecules (red spheres) and two glutamic acid residues. (F) The S-nitrosylation of Cys265. The GOL in the Fig. 4D refers to glycerol. The $2F_0$-F_c map is contoured at 1 e-/Å3. The protein structures are displayed using the program of PyMOL (*86*).

molecule that bonded to the second Zn^{2+} ion, a glycerol molecule was trapped via hydrogen bond interaction with the water molecule and residues of Thr111, Lys162, Glu323, and Thr349 (**Fig. 5A**), which implies that the second Zn^{2+} area is the catalytic site of *Lu*HNL. In addition, a hexa-coordinated complex of Mg^{2+} ion was observed on the enzyme surface that bonded with residues of Glu52, Glu140 and four molecules of water at 2.0-2.2 Å (**Fig. 4E**). The quantitative measurement of metal ions in *Lu*HNL using Inductively Coupled Plasma Mass Spectrometry (ICP-MS) indicated that the contents of metal ions were 2.22 Zn^{2+} and 0.35 Mg^{2+} in each subunit, respectively (**Table 2**). Moreover, it was noted that a positive F_{obs}-F_{calc} map was attached to the thiol group of Cys265 in β13 during structure refinement, which suggests that the Cys265 was

Table 2: Quantitative measurement of metal ions in *Lu*HNL using ICP-MS[a].

Samples	LuHNL loading (nM)[a]	Mg^{2+} (nM)	Zn^{2+} (nM)
sample1	86.5	14.9	204.3
sample2	8.6	4.8	20.8
sample3	610	156.2	1088.6
sample4	122	51.4	284.7
Average	1	0.35	2.22

[a] The concentration of *Lu*HNL was measured by BCA method (Takara, Otsu, Japan) and the *Lu*HNL molecular mass of 48 kDa was used for calculation.

modified in *Lu*HNL. According to the possible modification forms of cysteine in protein (*95*), an S-nitrosylation form of Cys265 was proposed in *Lu*HNL, which fits the observed electron density (**Fig. 4F**). However, we failed to detect the S-nitrosyl group in *Lu*HNL solution by Saville's method (*96*). Interestingly, the S-nitrosyl group can be detected in lyophilized *Lu*HNL. The results suggest that the S-nitrosylation of Cys265 may be formed during crystallization or X-ray diffraction, rather than the post-translational modification of *Lu*HNL.

The complex structures of *Lu*HNL

The structures for acetone cyanohydrin (CNH) complexed *Lu*HNL (*Lu*HNL_CNH) and (*R*)-2-butanone cyanohydrin (BCN) complexed *Lu*HNL (*Lu*HNL_BCN) were determined at a resolution of 1.58 Å and 1.72 Å, respectively. These two complex structures have similar unit cell dimensions with *Lu*HNL_lig_free, as summarized in **Table 1**. The RMSD between *Lu*HNL_lig_free and *Lu*HNL_CNH, *Lu*HNL_lig_free and *Lu*HNL_BCN was 0.524 Å and 0.309 Å, respectively, at Cα atoms of all four subunits. This indicates that the complex structures of *Lu*HNL did not change significantly as compared to the ligand-free *Lu*HNL structure. Large conformational variations were observed in the N-terminal, β-turns between β7 and β8, β-turns between η2 and α8. The electron density of all the structural features that observed in the *Lu*HNL_lig_free structure were also well-defined in the complex structures, such as tightly bound NAD^+ molecule, two tetra-coordinated Zn^{2+} ions, one hexa-coordinated Mg^{2+} ion, and S-nitrosylation of Cys265 in each subunit. Additionally, the RMSD between *Lu*HNL_CNH and *Lu*HNL_BCN was 0.297 Å for the Cα atoms of all four chains. In the *Lu*HNL_CNH structure, the electron density of the acetone cyanohydrin (CNH) in the catalytic pocket was only observed in subunits of A, B, and C. However, the electron density of (*R*)-2-butanone cyanohydrin in the catalytic pocket of the *Lu*HNL_BCN structure was well defined in all four subunits. These two complexes indicate the same substrate binding pattern in the catalytic site (**Fig. 5D** and **Fig. 5F**), which is different from the glycerol binding pattern in *Lu*HNL_lig_free as described above (**Fig. 5B**). In the substrate complexed structures, the nitrile group of the substrate replaced the water molecule observed in the *Lu*HNL_lig_free structure (**Fig. 5B**) to bond with the catalytic zinc ion coordinated with Cys63, His85, Cys199 at a distance of 2.2-2.3 Å. The hydroxyl group of cyanohydrins oriented to form direct hydrogen bond interaction with Glu323 at a distance of 2.7 Å and indirect interaction with Lys162 via one molecule of water at a distance of 2.6 Å-2.8 Å for each hydrogen bond. Furthermore, the hydrogen bond relay was extended to the O2D of NAD^+ from Glu323 via Thr65 residue at 2.7 Å for each hydrogen bond.

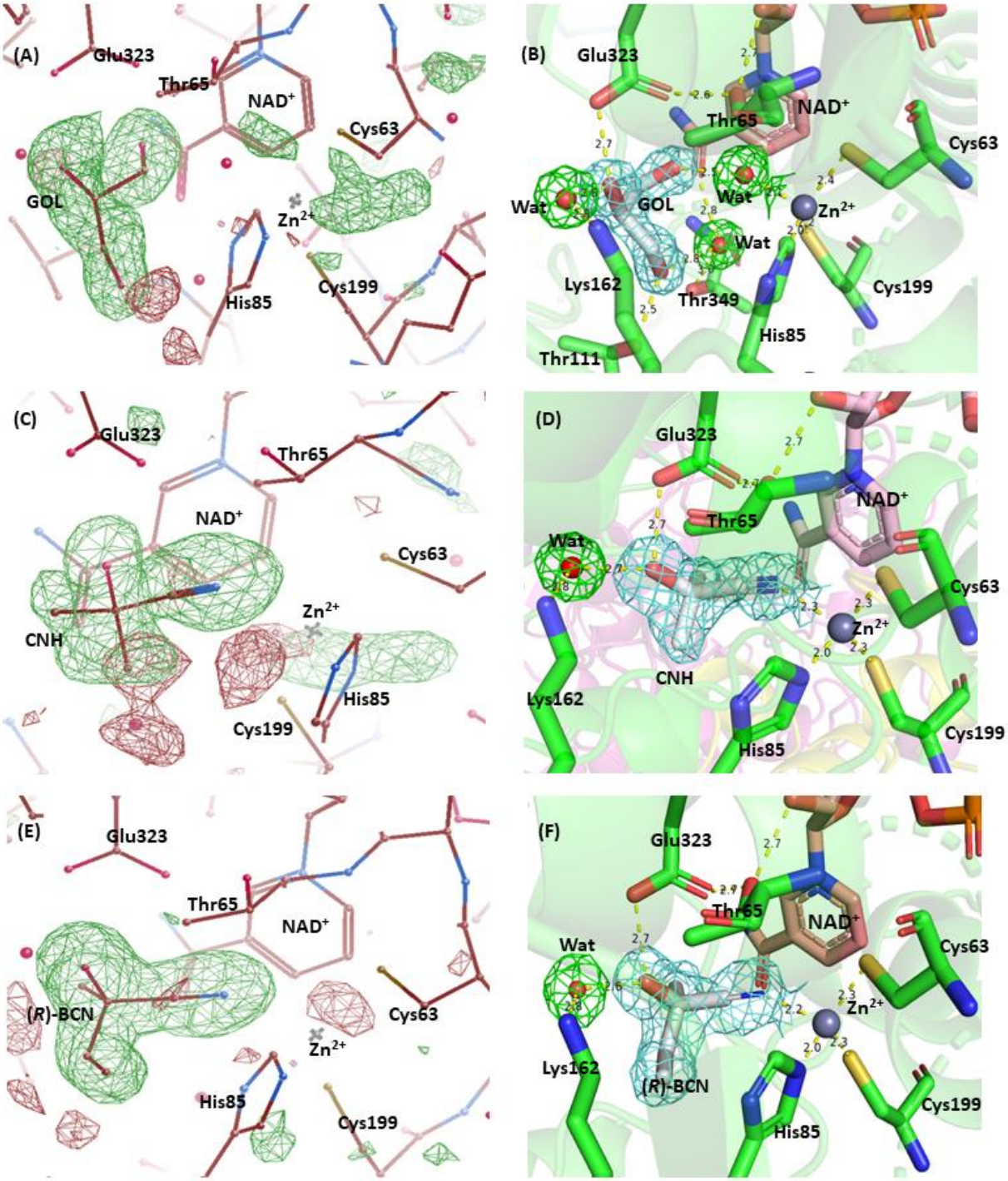

Fig. 5. Catalytic sites in *Lu*HNL. (A) The F_o-F_c omit map (green) of GOL in ligand-free structure of *Lu*HNL before inserting GOL; (B) The ligand-free structure of *Lu*HNL; (C) The F_o-F_c omit map (green) of CNH in *Lu*HNL-CNH complex before inserting CNH molecule; (D) The complex structure of *Lu*HNL with acetone cyanohydrin; (E) The F_o-F_c omit map (green) of (*R*)-BCN in *Lu*HNL-BCN complex before inserting (*R*)-BCN molecule; (F) The complex structure of *Lu*HNL with (*R*)-2-butanone cyanohydrin. The GOL refers to glycerol; the CNH refers to

acetone cyanohydrin; the (*R*)-BCN refers to (*R*)-2-butanone cyanohydrin; the Wat refers to water molecule. The F_o-F_c map was displayed in COOT (*83*) and contoured at 3.0 σ. The positive omit map was displayed as green and the negative omit map was displayed as red. The $2F_o$-F_c map were displayed using PyMOL (*86*) and contoured at 1 e^-/$Å^3$. The protein structures were displayed using PyMOL (*86*).

In addition, two substrate entry tunnels were observed in the subunit of *Lu*HNL, as shown in **Fig. 6A**. The substrate entry tunnel 1 is a long and tortuous channel that connects the surface of the protein with the bottom of the catalytic pocket. Oppositely, the substrate entry tunnel 2 is

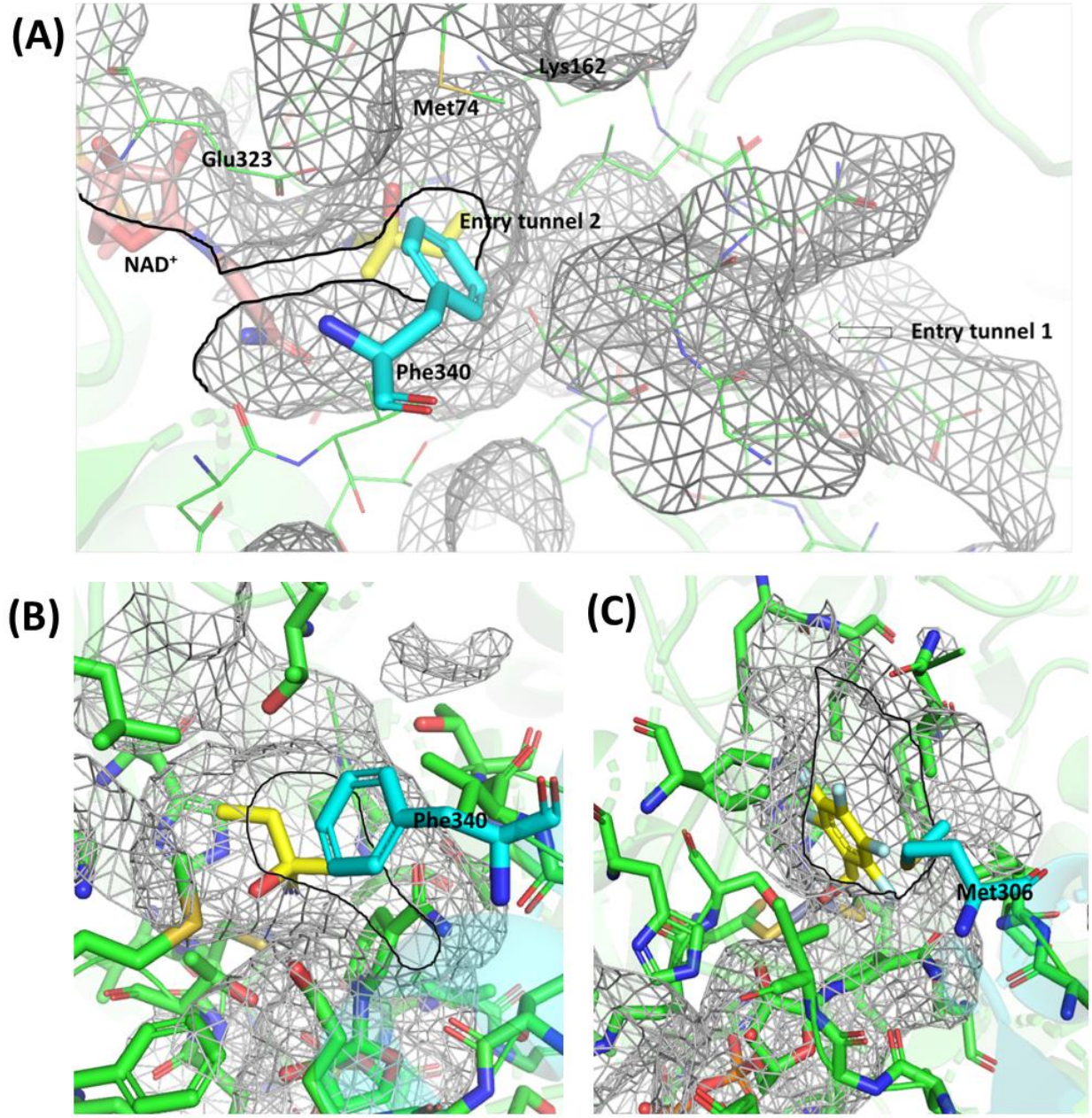

Fig. 6. Substrate entry tunnels in *Lu*HNL and Hl_ADH. (A) Substrate entry tunnels in *Lu*HNL_BCN; (B) Substrate entry tunnel 2 in *Lu*HNL_BCN; (C) Substrate entry tunnel in Hl_ADH (PDB ID: 4NFH) (*97*). The subunit A was displayed as green color and the subunit B was displayed as cyan color. The entry tunnel 1 in *Lu*HNL was indicated by arrows. The entry tunnel 2 of *Lu*HNL and the entry tunnel of Hl_ADH were marked by bold black line. The ligands in Fig. A and Fig. B were displayed as yellow color, which refer to 2-butanone cyanohydrin. The ligand in Fig. C was displayed as yellow color, which refers to 2,3,4,5,6-pentafluorobenzyl alcohol. The protein structures were displayed using PyMOL (*86*).

located at the upper part of catalytic pocket and close to the interface of the dimer (β16α10β17 fold). However, in the dimer structure of *Lu*HNL, the substrate entry tunnel 2 was completely shielded by the Phe340 on the helix α10 fragment of another subunit (**Fig. 6A**), resulting in a closed upper part of catalytic pocket.

The framework of NAD^+ binding cavity

The well-defined electron density of NAD^+ in *Lu*HNL suggests that the cofactor NAD^+ is tightly bound to the enzyme. The subsequent quantitative measurement of NAD^+ by denaturing the

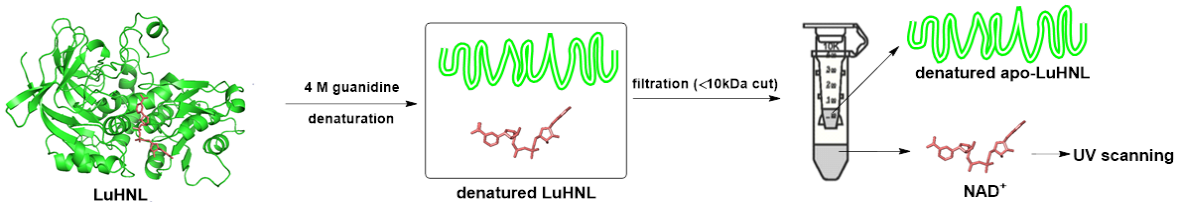

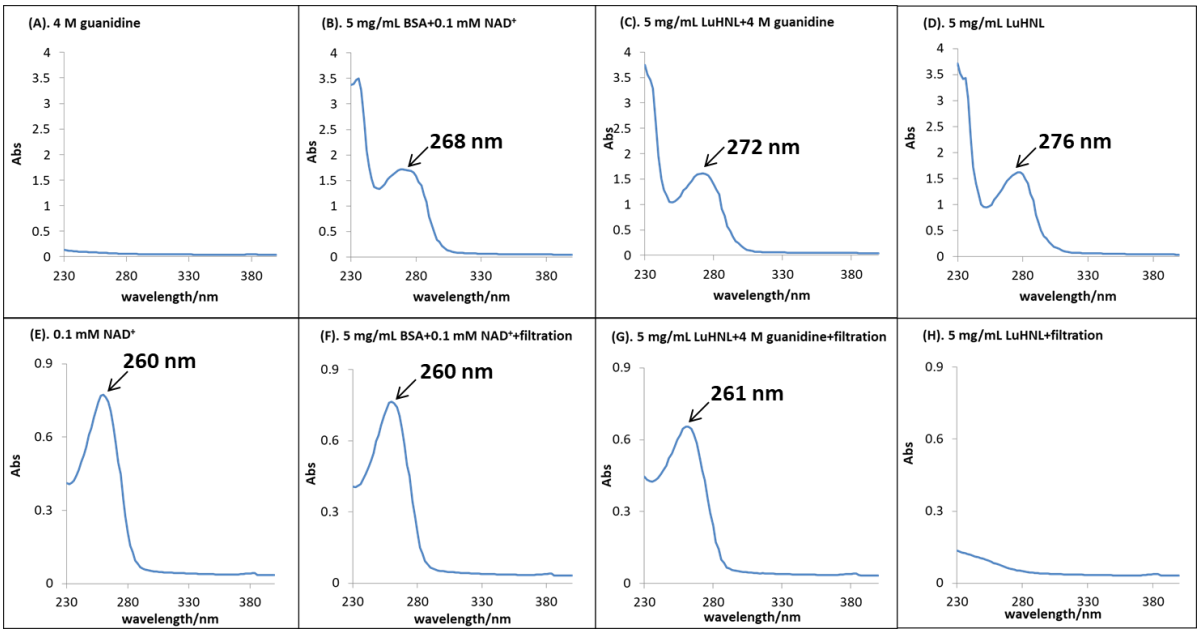

Fig. 7. Quantitative measurement of NAD^+ in *Lu*HNL. (A) The UV scanning spectrum of 4 M guanidine; (B) The UV scanning spectrum of mixture of 5 mg/mL BSA and 0.1 mM NAD^+; (C) The UV scanning spectrum of mixture of 5 mg/mL *Lu*HNL and 4 M guanidine; (D) The UV scanning spectrum of mixture of 5 mg/mL *Lu*HNL; (E) The UV scanning spectrum of 0.1 mM NAD^+; (F) The UV scanning spectrum of the filtrate of 5 mg/mL BSA and 0.1 mM NAD^+; (G) The UV scanning spectrum of the filtrate of 5 mg/mL *Lu*HNL and 4 M guanidine; (H) The UV scanning spectrum of the filtrate of 5 mg/mL *Lu*HNL.

*Lu*HNL in 4 M guanidine showed that one subunit of *Lu*HNL contains approximately 0.68 molecule of NAD^+ (**Fig. 7**), which suggests that NAD^+ is trapped in the cavity via hydrogen bonding interactions rather than covalent bonding. From the anti-conformation of NAD^+, it was

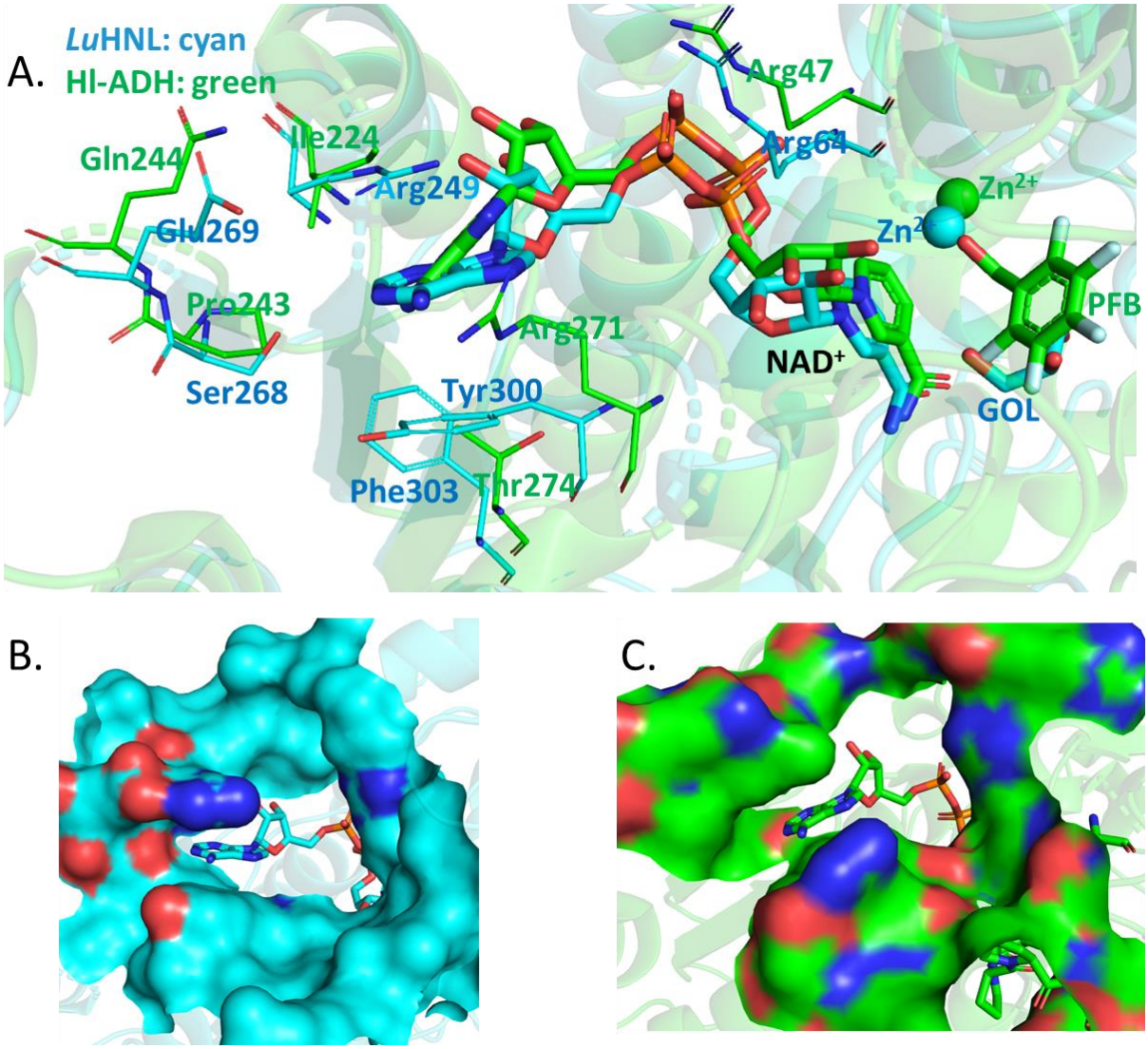

Fig. 8. Comparison of NAD^+ binding cavities of *Lu*HNL and Hl_ADH. (A) The superposition of NAD^+ binding cavities of *Lu*HNL-lig-free and Hl_ADH (PDB ID: 4NFH) (*92*). (B) The protein surface at the entrance of NAD^+ binding cavity in *Lu*HNL-lig-free structure. (C) The protein surface at the entrance of NAD^+ binding cavity in Hl_ADH structure. The GOL refers to glycerol and PFB refers to 2,3,4,5,6-pentafluorobenzyl alcohol. The *Lu*HNL-lig-free structure was colored as cyan and Hl_ADH structure was colored as green. The protein structures were displayed using the program of PyMOL (*86*).

noted that it is the *re*-face of nicotinamide in NAD^+ that approaches the catalytic sites, suggesting that the NAD^+ in *Lu*HNL belongs to the A-form (*98*). Considering the diversity of ADHs and simplifying the description, we focus on the comparison of *Lu*HNL and well-studied horse liver ADH (Hl_ADH) in the following narrative. The superposition of the *Lu*HNL_lig_free structure with horse liver ADH (Hl_ADH, PDB ID: 4NFH) (*99*) showed a significant difference in the residues located at the entrance of the NAD^+ bound cavity. In *Lu*HNL, the adenine part is buried in a "sandwich-structure" of Arg249/adenine of NAD+/Tyr300, resulted in a twisted NAD^+ molecule in the cavity (**Fig. 8A**). In such a situation, the twisted NAD^+ molecule becomes less flexible, which may restrain its free movement. Moreover, the comparison of the protein surface in the entrance of NAD^+ binding cavities of *Lu*HNL (**Fig. 8B**) and Hl_ADH (**Fig. 8C**) give us a more intuitive vision on the buried NAD^+ of *Lu*HNL, in which the adenine part of NAD^+ is embedded in a narrow space, rather than an open space as shown in Hl_ADH.

Site-directed mutagenesis analysis of *Lu*HNL

Site-directed mutagenesis of the catalytic residues was carried out according to the substrate binding geometry in *Lu*HNL. Activity measurements on the acetone cyanohydrin decomposition revealed that the mutants of T65A, K162G, K162A, E323A, E323H, C63S, C199S, H85A, H85C, and C63S/C199S completely lost activity as compared to the wild type (**Fig. 9A**). Additionally, the mutation of Cys121 to alanine also inactivated the enzyme completely, which is consistent with the findings of a previous report (*52*). Moreover, alanine mutation analysis of the residues that coordinated with Mg^{2+} was also performed. The E52A was expressed in an insoluble form using the *E.coli* as the host, but E140A was successfully expressed and purified. The activity analysis suggests that the mutant of E140A possesses approximately 61% activity compared to the wild type (**Fig. 9A**). Moreover, the mutation of Cys265 to alanine also showed a

negligible effect on enzyme activity, and approximately 80% residual activity was detected for C265A (**Fig. 9A**).

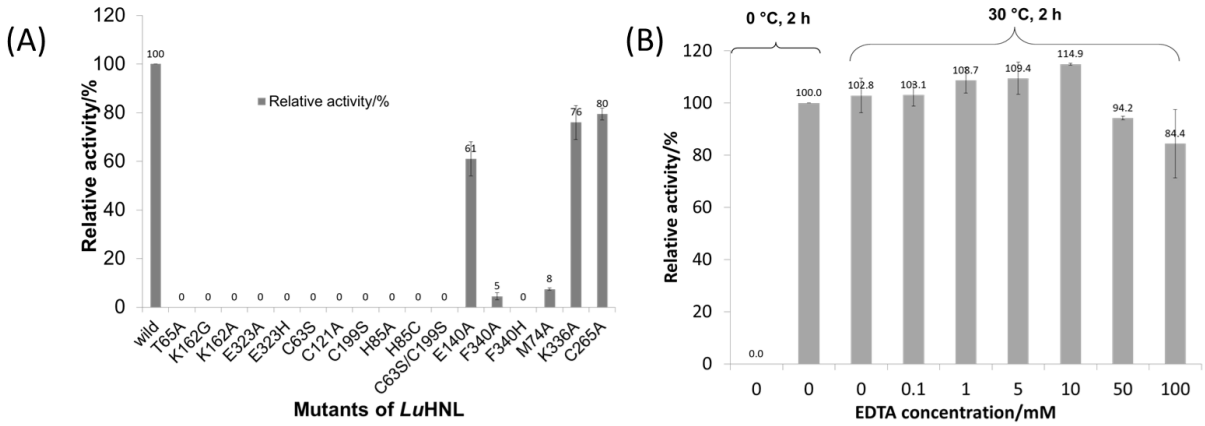

(C)

Entry	Enzymes	V_{max} (mM/min)	K_M (mM)	k_{cat} (S^{-1})
1	*Lu* HNL-wild	0.87±0.08	2.7±0.3	70.0±6.0
2	*Lu* HNL-K336A	0.40±0.02	1.6±0.07	31.8±1.8
3	*Lu* HNL-C265A	0.56±0.02	2.4±0.11	44.5±2.0
4	*Lu* HNL-E140A	0.28±0.04	2.1±0.03	22.5±3.1
5	*Lu* HNL-F340A	0.12±0.05	5.4±2.3	1.0±0.33
6	*Lu* HNL-M74A	0.13±0.01	1.9±0.2	1.0±0.1

Fig. 9. **Mutagenesis analysis and EDTA effect investigation on *Lu*HNL.** (A) Site-directed mutagenesis analysis on *Lu*HNL. The activity of *Lu*HNL-wild type was set at 100%. (B) The EDTA effect on *Lu*HNL activity. The *Lu*HNL enzymes were incubated with a range of concentration of EDTA (0-100 mM) at 30 °C for 2 h. The activity of *Lu*HNL incubated at 0 °C for 2 h was set at 100%. (C) The kinetic parameters for active mutants of *Lu*HNL.

Additionally, a mutant of R249G/S268A/E269L on the entrance of NAD^+ bound cavity was constructed and successfully expressed. However, in enzyme purification using an ion-exchange column of Mono Q 5/50 GL, three proteins of the same size in SDS-PAGE were eluted out at different ionic strengths. The LC-MS/MS analysis revealed that all the proteins were *Lu*HNLs. The CD-spectrum analysis showed that the secondary structure of the first to be eluted enzyme was different from the latter two. The latter two enzymes had similar secondary structures to the *Lu*HNL wild type. However, except for the protein which was eluted last, the enzymes showed no activity. The specific activity of the last enzyme on acetone cyanohydrin decomposition is 11.5 U/mg, about 23% of the wild type enzyme activity (49.8 U/mg). Furthermore, 0.35

molecule of NAD^+/monomer was detected in the last protein, about 56% of the NAD^+ content that was detected in the wild type (0.62 molecule NAD^+/monomer), whereas the other proteins lost NAD^+ completely.

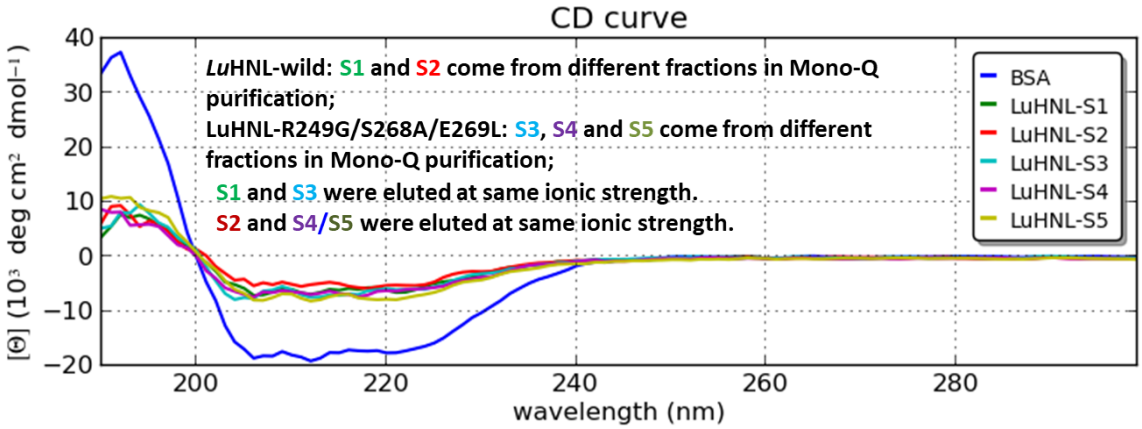

sample	specific activity U/mg		NAD^+ cofactor contens	Circular dichroism		
	NAD^+ (-)	NAD^+ (+)		helix	β-strand	irregular
S1	0	0	0	0.14	0.33	0.53
S2	49.8	48.8	0.62	0.03	0.38	0.54
S3	0	0	0	0.1	0.32	0.49
S4	0	0	0	0.04	0.33	0.52
S5	11.5	12	0.35	0.04	0.32	0.49

Fig. 10. Quantitative analysis of *Lu*HNL-R249G/S268A/E269L. The activity measurement with NAD^+ was performed by addition 10 mM NAD^+ to reaction mixture. The CD spectrum were measured with 0.05 mg/mL protein concentration (BCA method, Takara, Otsu, Japan), rt, 2 mm pathlength of cuvette. The data was processed using CAPITO program (*100*).

We also found that the enzyme activity could not be recovered by the addition of external NAD^+, and no improvement in activity was observed for the active fractions of the *Lu*HNL-R249G/S268A/E269L (12 U/mg) or *Lu*HNL-wild (48.8 U/mg) in the presence of NAD^+ (**Fig. 10**). Subsequently, the mutation analysis on the residues of F340, K336 that located at the interaction area (on the helix α10) of two subunits was also carried out. Compared to the wild type, the F340A showed 5% residual activity, whereas the F340H lost activity completely (**Fig. 9A**). The mutant of *Lu*HNL-K336A did not show significant change in enzyme activity, and

approximately 76% residual activity was detected (**Fig. 9A**). Notably, when the Met74, a residue located at the top of catalytic pocket (**Fig. 6A**), was mutated to alanine, it resulted in a significant decrease in enzyme activity, and only 8% residual activity was detected (**Fig. 9A**). Then the kinetic parameters of *Lu*HNL-wild and its active mutants were determined. As shown in **Fig.9C**, the K_M value of the mutants are similar to the wild type enzyme (K_M=2.7±0.3 mM) except for the mutant of *Lu*HNL-F340A (K_M=5.4±2.3 mM). It means the mutation of Phe340 to Ala340 decreases the affinity of enzyme to the substrate.

Effects of EDTA on *Lu*HNL activity

In a previous study (*51*), it was observed that the *Lu*HNL activity cannot be inhibited by addition of o-phenanthroline (dissociation constant of monophenanthroline-zinc: K_d=3.7×10^{-7} (*101*)), a competitive inhibitor of horse liver alcohol dehydrogenase (Hl_ADH) chelating with Zn^{2+} ion in the enzyme (*102*). The findings suggested that Zn^{2+} ions in *Lu*HNL are not directly involved in cyanohydrin decomposition (*51*). Here, we tested the effect of another Zn^{2+} chelator (dissociation constant of EDTA-zinc: K_d=2.3×10^{-14}(*103*)) on the activity of *Lu*HNL by incubation of the enzyme with 0-100 mM EDTA at 30 °C for 2 h, as a previous study did on yeast alcohol dehydrogenase (YADH), in which 64% of Zn^{2+} ions were removed by incubating the YADH with 100 mM EDTA at 30 °C for 2 h, resulting in a strong inhibitory effect of EDTA on YADH activity (*104*). However, the results showed that approximately 84% residual activity was detected on acetone cyanohydrin decomposition after incubation of *Lu*HNL with 100 mM EDTA at 30 °C for 2 h (**Fig. 9B**). And the metal content analysis showed that there is still 68 % residual Zn^{2+} in the *Lu*HNL after incubation with 100 mM EDTA for 2 h. It suggests that the low extracting efficiency of EDTA on the Zn^{2+} from *Lu*HNL is the reason of slight inhibition effect of EDTA on *Lu*HNL activity. Compared with the EDTA effect on YADH, it implies that Zn^{2+} ion is bound tightly in *Lu*HNL and important for *Lu*HNL activity. The essential of Zn^{2+} ion for *Lu*HNL activity is also supported by the results that the enzyme activity were improved 1.03 fold~1.20 fold by addition of 0.1 mM~50 mM of Zn^{2+} in the activity assay mixture.

Discussion

*Lu*HNL, as a hydroxynitrile lyase that independently evolved from an ancestor protein possessing an ADP-binding βαβ domain, has unique structural features that differ from those of

all known hydroxynitrile lyases. The sequence alignment of *Lu*HNL suggests that its structure is closer to that of Zn^{2+}-containing alcohol dehydrogenase (ADH), sharing the substrate and NAD^+ binding domains. The *Lu*HNL_lig_free and Hl_ADH superimposed with a RMSD of 8.40 Å at 669 Cα atoms, reflecting the similarity of structures to some extent. However, the difference in activity indicates the existence of very significant structural changes.

Absence of ADH activity in *Lu*HNL and vice versa

In Hl_ADH, the hydroxyl group of the substrate was bonded to the catalytic Zn^{2+} that coordinated with Cys46, His67, and Cys174 (**Fig. 11A**). The deprotonation of the hydroxyl group is carried out by a general base of His51 via a hydrogen bonding relay consisting of Ser48 and O2D of NAD^+. The following hydride transfer from the α-carbon atom of the substrate to C4N of NAD^+ occurs at a distance of 3.3 Å-3.5 Å via substrate mobility (PDB IDs: 4NFH and 1MG0) ((*105, 106*)). However, in *Lu*HNL, it is the nitrogen atom of the substrate nitrile group that coordinates with catalytic Zn^{2+}, rather than the oxygen atom of the substrate hydroxyl group. His51, which acts as a general base for deprotonation in Hl_ADH, is replaced by Leu68 in *Lu*HNL. Additionally, the residues of Phe140 and Val294 in Hl_ADH were replaced by Lys162 and Glu323 in *Lu*HNL, which act as catalytic sites in the decomposition of cyanohydrin in *Lu*HNL (**Fig. 11B**). The distance of cyanohydrin alfa-C atom to C4N of NAD^+ is about 5.1 Å-5.4 Å, much further than that in Hl_ADH, suggesting the C4N of NAD^+ in *Lu*HNL is not directly involved in the reaction mechanism. In addtion, the binding geometry of glycerol, a pseudo-substrate that bound in the catalytic pocket of ligand free *Lu*HNL structure (*Lu*HNL-lig-free) suggests that a hydroxyl group cannot replace the water molecule to bond with catalytic Zn^{2+}, even in the absence of a nitrile group (**Fig. 5B**). This may explain the slight inhibitory effect of EDTA on the activity of *Lu*HNL. The two different substrate-binding patterns provide the insights into differences in the activities of *Lu*HNL and Hl_ADH.

The catalytic pocket in *Lu*HNL

In enzymatic dehydrogenation reactions, a free NAD(P)H or $NAD(P)^+$ is essential to catalyze the redox reaction by providing or accepting a hydride ion. An exception is formaldehyde dehydrogenase derived from *Pseudomonas putida* (PFDH), which catalyzes the disproportionation of aldehydes without the external addition of cofactor. The structural origin is

a long insertion loop in PFDH, shielding the adenine part of the bound NAD^+ molecule from the solvent (*107*). However, the reaction catalyzed by *Lu*HNL is not a disproportionation reaction, so the tightly rather than covalently bound cofactor suggests that NAD^+ is unlikely to play a redox role in *Lu*HNL. However, the loss of activity in the correctly folded apo-*Lu*HNL-R249G/S268A/E269L indicates the importance of NAD^+ in *Lu*HNL activity. Once the *Lu*HNL loses NAD^+, the activity will also be lost and can no longer be recovered. Presumably, instead of acting as a redox role to participate in the reaction, the NAD^+ in *Lu*HNL is part of the catalytic pocket to define a specific microenvironment. The similar function of cofactor for an enzyme was reported in the FAD-containing *Pa*HNL, in which the oxidized cofactor of FAD is solely required for electrostatic reason, rather than a redox role (*16*).

In addition, it is noteworthy that in Hl_ADH, the substrate entry tunnel is located beside the interface of two subunits, same position as the substrate entry tunnel 2 observed in *Lu*HNL, but the tunnel in Hl_ADH is still open when the substrate is bound to catalytic sites in a dimer structure, as observed from ligand-complexed structure (PDB: 4NFH) (*99*) (**Fig. 6C**). However, in *Lu*HNL, the substrate entry tunnel 2 was completely shielded by the helix-α10 of another chain when two subunits assemble into a dimer. The residue of Phe340 on the helix-α10, acting as a hydrophobic lid, completely covered the entire entry tunnel 2, resulting in the formation of a specific microenvironment (**Fig. 6B**). The significant decrease on the activity of *Lu*HNL by site-directed mutagenesis of Phe340 and Met74 to alanine supports this viewpoint that a semi-closed catalytic pocket is indispensable for enzyme activity.

Obviously, compared with the long and winding substrate entry tunnel 1, the substrate entry tunnel 2 is a more suitable channel for substrate to enter enzyme if it's not shielded by the residue Phe340 (**Fig. 6A**). Thus, in the process of substrate binding and product release, whether there is conformational change of two subunits in one dimer is an interesting issue. Unfortunately, in the ligand-free structure of *Lu*HNL, a pseudo-substrate of glycerol was trapped in the catalytic pocket. Thus, whether the conformation of enzyme varies with the absence or presence of a compound in the catalytic pocket remains to be studied.

The function of Zn^{2+} in *Lu*HNL

The presence of two Zn^{2+} ions in each subunit of *Lu*HNL was confirmed by quantitative measurement. One of them that located in the catalytic pocket is presumably involved in the catalysis of cyanohydrins decomposition via the nitrile-Zn^{2+} complex. The positively charged Zn^{2+} is responsible for the stabilization of the cyanide anion. Another Zn^{2+} complex with four cysteine residues is structurally important for the correct folding of protein. The inactivation of the enzyme by mutating the Cys121 to alanine strengthens this viewpoint.

The Mg^{2+} ion and the S-nitrosylation of Cys265 on the surface of *Lu*HNL

Magnesium is the most abundant divalent cation in cells with diverse biochemical functions (*108*). Statistical studies of the inner-sphere binding mode of Mg^{2+} revealed that approximately 77% of all Mg−X bonds are Mg−O bonding situations in which either water or negatively charged oxygen functionalities such as carboxylates (Asp, Glu) are the preferred ligands (*109*). Moreover, the distances between the cation and the oxygen atom of proteins and small molecules, as determined by crystal structure studies, vary from 2.05 to 2.25 Å , much more constrained than hexa-coordinated Ca^{2+} (*108*). The magnesium complex in *Lu*HNL that coordinated with Glu52, Glu140, and four molecules of waters in distance of 2.0-2.2 Å is consistent with these descriptions. However, the low content of Mg^{2+} (approximately 0.35 per subunit) and active mutant of E140A suggest that it is not essential for *Lu*HNL activity. To some extent it cannot be ruled out that the Mg^{2+} was bound on the surface coincidently, because of the availability of a suitable location. However, the failed detection of S-nitrosylation in *Lu*HNL solution ruled out that the Cys265 was modified during enzyme expression in *E.coli*. The formation of S-nitrosylation may occur in crystallization step or diffraction experiment when exposed in high-energy X-ray. The negligible effect of C265A on enzyme activity strengthens this viewpoint.

Catalytic mechanism of *Lu*HNL

In a common catalytic mechanism of hydroxynitrile lyases, one residue acts as a base to extract the proton from the hydroxyl group, and the left cyanide anion is stabilized in a microenvironment with a positive electrostatic potential (*110*). Based on the complex structure of *Lu*HNL and site-directed mutagenesis results, the reaction presumably occurred in the catalytic Zn^{2+} pocket. The deprotonated Lys162 acts as a base to extract the proton from the hydroxyl group via one molecule of water, and the electrostatic interaction between positively charged

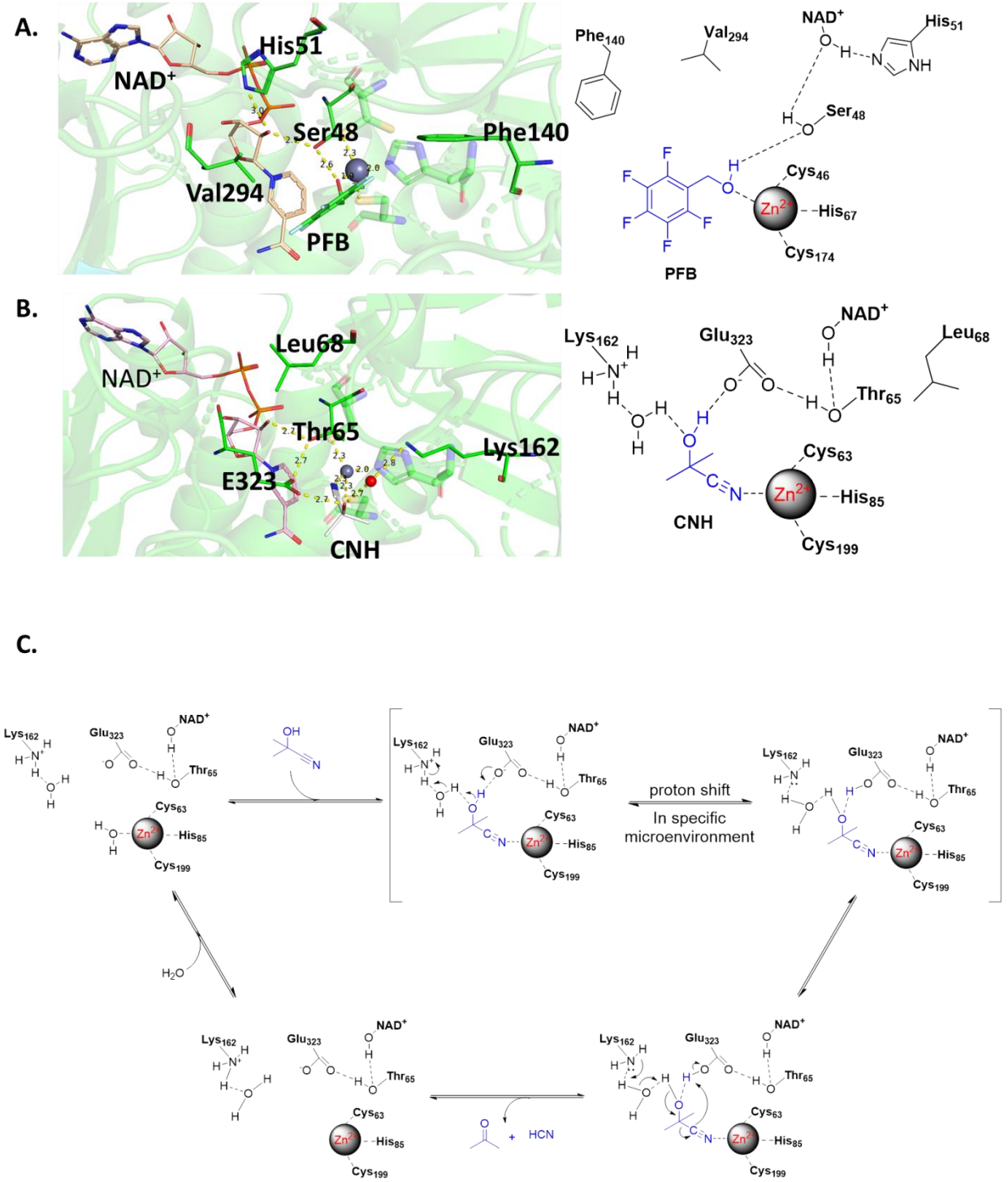

Fig. 11. Substrate binding patterns and proposed reaction mechanism. (A) Substrate binding pattern in Hl_ADH; (B) Substrate binding pattern in *Lu*HNL; (C)Proposed reaction mechanism for *Lu*HNL. The CNH refers to acetone cyanohydrin and PFB refers to 2,3,4,5,6-pentafluorobenzyl alcohol. The protein structures were displayed using the program of PyMOL (*86*).

Zn^{2+} and cyanide ion renders the cyanide a better leaving group. Then, the proton in the protonated Glu323 is transferred to the cyanide anion to release HCN (**Fig. 11C**). Unlike the utilization of histidine as a general base to extract the proton in the first step, as observed in *Pa*HNL (*16*), *Hb*HNL (*34*), *At*HNL ((*22*)), *Pe*HNL ((*41*)), Lys162 acts as the base for proton extraction in *Lu*HNL. However lysinium has much higher *pK*a value than histidinium, let alone to glutamic acid. How the enzyme stabilizes the transition state consisting of deprotonated Lys162 and protonated Glu323 especially in a weak acidic solution is a fascinating issue. Such proton transfer from lysinium to aspartate followed with proton extraction from substrate by the deprotonated lysine has been reported in *Chua*HNL. The deprotonated lysine in *Chua*HNL was proposed to be stabilized by the desolvation effect in the hydrophobic active site (*43*). The desolvation effect by placing the side chain into a specific microenvironment can significantly perturb the pKa of a nucelophile, as detected for the buried lysine (*111*) and glutamic acid (*112*) in the interior of proteins. In *Lu*HNL, the catalytic sites (Lys162, Glu323) are located in the upper part of the catalytic pocket as shown in the **Fig. 6A**. When the substrate is bound to the enzyme, the substrate entry tunnel 1 is blocked by the substrate molecule. The catalytic sites are partially removed from the bulky water by shielding the substrate entry tunnel 2 in a dimer form bearing only one molecule of water for proton delivery, which may result in the *pKa* shift of Lys162 and Glu323.

In summary, this study elucidates the reaction mechanism of *Lu*HNL on cyanohydrin degradation and provides insights into differences in activities of *Lu*HNL and ADH, which has long been a challenge. This understanding of the novel reaction mechanism will contribute to the study of hydroxynitrile lyases and provide a new model for designing enzymes.

Chapter II. Biocatalytic asymmetric ring-opening of dihydroisoxazoles: a cyanide-free route to complementary enantiomers of β-hydroxy nitriles from olefins

Aldoxime dehydratase is a class of Heme-containing enzyme involved in the cyanogenesis pathway observed in nature, which catalyses the dehydration of aldoximes to their corresponding nitrile derivatives (*10*). Using the dehydration function of the enzyme, we established a cyanide-free platform for the synthesis of nitriles utilizing aldoxime precursors (*113-117*). Recently, we discovered the enzyme catalyses the Kemp elimination reaction via a -Fe-N- complex catalytic pathway (*118*), which is different from the classic acid-base mechanism (*119, 120*). In this enzymatic elimination reaction, the N-O bond is initially opened with the action of the –Fe-N- complex (Heme Fe-proximal histidine) followed by deprotonation by a distal histidine residue to form the nitrile triple-bond. Upon investigation of the catalytic mechanism, it has been reported that the Kemp elimination reaction can also occur based on the redox catalysis of Heme-containing P450-BM_3 via heterolysis to liberate an intermediate containing a nitrogen radical moiety (Fe(III)-N·) and phenoxyl anion. The product is formed by bond rotation and proton-transfer to the resulting phenoxyl anion (*121*). It was also mentioned that the metabolism of leflunomide, an immunomodulatory therapeutic drug, could be transferred into teriflunomide via isoxazole ring-opening catalysed by human cytochrome P450. This provides the idea of synthesizing a chiral β-hydroxy nitrile product using a prochiral substrate containing the dihydroisoxazole motif. In this work, by combination of cyanide-free synthesis of chiral nitriles (**Scheme 8a**) (*117*) and the Kemp elimination reaction (**Scheme 8b**) (*118*) catalysed by aldoxime dehydratases (EC 4.99.1.5, EC 4.99.1.6, EC 4.99.1.7), we report a novel cyanide-free enzymatic approach to construct the chiral hydroxyl group and nitrile group in one-step toward the efficient synthesis of the complementary enantiomers of β-hydroxy nitriles via the asymmetric ring-opening of 5-sub-4,5-dihydroisozazoles (**Scheme 8c**). Totally, three aldoxime dehydratases were investigated in this work. One is OxdA that derived from *Pseudomonas chlororaphis* B23. This strain was first isolated as an excellent whole cell catalyst to produce acrylamide in industry by Asano as early as 1982 (*122*) and subsequently identified to be one of the strains possessing aldoxime dehydration activity in 2000 (*123*). Then further studies to clone and characterize the aldoxime dehydratase were carried out, in which the enzyme was named as OxdA (*124, 125*). Another enzyme is OxdB that derived from *Bacillus* sp.OxB-1, which is the first report of

aldoxime dehydratase co-existing with nitrile degrading enzymes in bacteria (*126-128*). The last one, OxdRE, is derived from *Rhodococcus sp*. N-771, which is the first aldoxime dehydratase that revealed the reaction mechanism by X-ray crystal structure determination (*129, 130*).

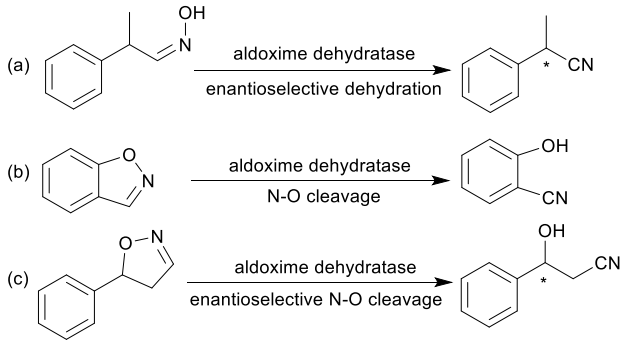

Scheme 8. (a) Enantioselective dehydration catalysed by aldoxime dehydratase. (b) The Kemp elimination reaction catalysed by aldoxime dehydratase. (c) Asymmetric ring-opening of dihydroisoxazole catalysed by aldoxime dehydratase.

General remarks

Reagents were purchased from commercial sources and were directly used unless otherwise noted. The reaction process was monitored by TLC. ^{1}H NMR and ^{13}C NMR (400 and 100 MHz, respectively) spectra were recorded in $CDCl_3$ and DMSO-d_6. ^{1}H NMR chemical shifts are reported in ppm relative to tetramethylsilane (TMS) with the solvent resonance employed as the internal standard ($CDCl_3$ at 7.26 ppm, DMSO-d_6 at 2.50 ppm). Data are reported as follows: chemical shift, multiplicity (s = singlet, br s = broad singlet, d = doublet, t = triplet and m = multiplet), coupling constants (Hz) and integration. ^{13}C NMR chemical shifts are reported in ppm relative to tetramethylsilane (TMS) with the solvent resonance as the internal standard ($CDCl_3$ at 77.16 ppm, DMSO-d_6 at 39.51 ppm). Silica gel column chromatography was performed with Merck silica gel 60 (200-300 mesh) as column material. TLC analysis was performed with precoated Silica Gel 60 F254 TLC-plate and the compounds were visualized with UV light.

Experimental procedures

Construction of Oxd A recombinant and its expression, purification

The Oxd A gene was amplified from previous recombinant plasmid (*118*) using forward primer 5′-GTGCCGCGCGGCAGCCATATGGAAAGCGCAATTGATAC-3′ with restriction site of *Nde* I (bold font) and reverse primer 5′-TCGACGGAGCTCGAATTCTCAGGTCGGTGCAACAAC-3′ with restriction site of *EcoR* I (bold font). The resulting PCR product was purified and ligated with *Nde* I/*EcoR* I-digested pET-28b vector. The ligating mixture was transformed into $JM_{109}(DE_3)$ *E.coli* competent cell via thermal shock. Positive transformants were selected on LB agar plates containing 50 μg/mL kanamycin by incubating at 37 °C overnight. New plasmid DNA (pET-28-N-His-OxdA) was isolated and sequenced to verify that no mutation had been introduced during gene amplification. For enzyme production, the positive colony was picked up and inoculated into 5 mL LB medium containing 50 μg/mL kanamycin, which was incubated at 37 °C overnight. Then 5 mL pre-culture was transferred into 1.4 L TB medium containing 50 μg/mL kanamycin, the resulting mixture was incubated at 30 °C for 12 h, then final concentration of 1 mM IPTG was added to induce the expression of target protein at 26 °C for 24 h. The recombinant cells were harvested by centrifugation (6000 ×*g*, 15 min, 4 °C) and the pellet was re-suspended into lysis buffer (20 mM Tris-HCl, 300 mM NaCl, 20 mM imidazole, pH 8.0), which was applied to sonication (ice-bath, 15 min) for cell disruption. The debris was removed by centrifugation (20,000 × *g*, 30 min, 4 °C) and the supernatant was loaded onto Ni Sepharose™ 6 Fast flow column equilibrated by lysis buffer (20 bed volumes). The unbound protein was washed with lysis buffer (30 bed volumes) and the bound protein was eluted by elution buffer (20 mM Tris-HCl, 300 mM NaCl, 300 mM imidazole, pH 8.0), the fractions were analyzed by SDS-PAGE containing 12% acrylamide and those fractions containing Oxd A were pooled. The combined fractions were dialyzed against KPB (10 mM, pH 7.0, 4 °C, 5 L×2). The partially purified enzyme was used for reaction.

Oxd B and Oxd RE cultivation and purification

The recombinant of $BL_{21}(DE_3)$-pET-22b-His-Oxd-B and $BL_{21}(DE_3)$-pET-22b-His-Oxd RE constructed previously (*118*) were used directly for enzyme production. The positive colony was picked up and inoculated into 5 mL LB medium containing 100 μg/mL ampicillin, which was incubated at 37 °C overnight. Then 5 mL pre-culture was transferred into 1.4 L TB medium containing 100 μg/mL ampicillin, the resulting mixture was incubated at 30 °C for 12 h, then final concentration of 1 mM IPTG was added to induce the expression of target protein at 26 °C

for 24 h. The recombinant cells were harvested by centrifugation (6000 ×*g*, 15 min, 4 °C) and the pellet was re-suspended into lysis buffer (20 mM Tris-HCl, 300 mM NaCl, 20 mM imidazole, pH 8.0), which was applied to sonication (ice-bath, 15 min) for cell disruption. The debris was removed by centrifugation (20,000 × *g*, 30 min, 4 °C) and the supernatant was loaded onto Ni Sepharose™ 6 Fast flow column equilibrated by lysis buffer (20 bed volumes). The unbound protein was washed with lysis buffer (30 bed volumes) and the bound protein was eluted by elution buffer (20 mM Tris-HCl, 300 mM NaCl, 300 mM imidazole, pH 8.0), the fractions were analyzed by SDS-PAGE containing 12% acrylamide and those fractions containing Oxds were pooled. The combined fractions were dialyzed against KPB (10 mM, pH 7.0, 4 °C, 5 L×2). The partially purified enzyme was used for reaction. For kinetic parameter assay, a further purification of the partially purified enzyme from Ni Sepharose™ 6 Fast flow column was performed by loading it onto the ÄKTA Protein Purification System equipped with Mono-Q 5/50 GL column, which was equilibrated by low-salt buffer (20 mM KPB, pH 7.0, 20 bed volumes). After loading the sample, the unbound protein was washed by low-salt buffer (20 bed volumes), followed to elute the target protein by increasing the ratio of high-salt buffer (20 mM KPB, pH 7.0, 500 mM NaCl) to 20% in 20 bed volumes and kept at 20% high-salt buffer to elute for additional 20 bed volumes. The purity of the fractions was checked by SDS-PAGE containing 12% acrylamide, and pure fractions were pooled to dialyze against KPB (20 mM, pH 7.0, 5L ×2).

Enzyme activity assay

Oxd A activity assay (*124*): the aldoxime dehydration activity was measured with appropriate amount of enzyme in 500 μL mixture of 5 mM butyraldoxime, 5 mM $Na_2S_2O_4$ in 100 mM KPB (pH 7.0), which was incubated at 30 °C for 5 min. Then 1 mL methanol containing 3 mM isobutyrnitrile (internal standard substance) was added to stop the reaction, the resulting mixture was centrifuged at 20000×*g* for 10 min, 1 mL supernatant was used for Gas Chromatograph analysis (Shimadazu Gas Chromatograph equipped with Agilent J&W DB-WAX column, carrier gas: He, pressure: 3 kg/cm^2, temperature program: 80 °C-5 min, 10 °C/min to 150 °C, 150 °C-2 min). 1 U enzyme was defined as the amount of enzyme to catalyze the formation of 1 μmol product in 1 min.

Oxd B activity assay (*126*): the aldoxime dehydration activity was measured with appropriate amount of enzyme in 500 μL mixture of 10 mM Z-phenylacetoxime, 1 mM $Na_2S_2O_5$, 0.25 mM

FMN, in 100 mM KPB (pH 7.0), which was incubated at 30 °C for 5 min. Then 1 mL ethyl acetate containing 2 mM benzonitrile (internal standard substance) was added to stop the reaction, the resulting mixture was centrifuged at 13,000×*g* for 1 min, 500 μL upper organic solvent was mixed with 500 μL *iso*-propanol and applied for High Performance Liquid Chromatography analysis (Shimadazu-HPLC equipped with Daicel AD-H chiral column, n-hexane/*iso*-propanol=90/10, flow rate 1mL/min, column temperature 30 ºC, injection volume 5 μL, detection wavelength 220 nm). 1 U enzyme was defined as the amount of enzyme to catalyze the formation of 1 μmol product in 1 min.

Oxd RE activity assay (*129*): the aldoxime dehydration activity was measured with appropriate amount of enzyme in 500 μL mixture of 5 mM Z-phenylacetoxime, 1 mM Na_2S, 10% DMSO, in 100 mM KPB (pH 7.0), which was incubated at 30 °C for 10 min. Then 1 mL ethyl acetate containing 2 mM benzonitrile (internal standard substance) was added to stop the reaction, the resulting mixture was centrifuged at 13,000×*g* for 1 min, 500 μL upper organic solvent was mixed with 500 μL *iso*-propanol and applied for High Performance Liquid Chromatography analysis (Shimadazu-HPLC equipped with Daicel AD-H chiral column, n-hexane/*iso*-propanol=90/10, flow rate 1mL/min, column temperature 30 ºC, injection volume 5 μL, detection wavelength 220 nm). 1 U enzyme was defined as the amount of enzyme to catalyze the formation of 1 μmol product in 1 min.

Synthesis of aromatic dihydroisoxazoles (*131*, *132*)

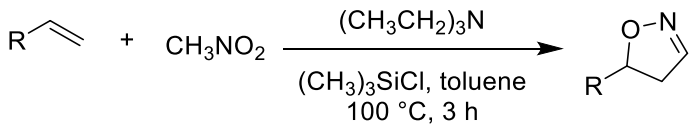

To the 50 mL toluene solution containing styrene derivatives (20 mmol), nitromethane (30 mmol), triethylamine (30 mmol) was added with 30 mmol chlorotrimethylsilane in room temperature. Then the resulting mixture was stirred at 100 °C for 24 h. When it finished, the reaction mixture was filtered and the solvent was removed in reduced pressure, the residual was applied to silica-column for purification (EA/hexane=1/5) (The corresponding NMR spectra are shown in **Appendix I**).

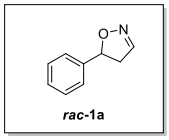

5-phenyl-4,5-dihydroisoxazole: pale yellow Oil, yield 54%. ^{1}H NMR ^{1}H NMR (400 MHz, $CDCl_3$) δ 7.40-7.28 (m, 5H), 7.20 (td, *J* = 1.8, 0.6 Hz, 1H), 5.52 (dd, *J* = 11.2, 8.1 Hz, 1H), 3.44 (ddd, *J* = 17.6, 11.2, 1.8 Hz, 1H), 2.98 (ddd, *J* = 17.6, 8.1, 1.8 Hz, 1H); ^{13}C NMR (100 MHz, $CDCl_3$) δ 145.62, 140.98, 128.75, 128.16, 125.79, 79.89, 43.75. HRMS (ESI): calcd for $C_9H_{10}NO$ $[M + H]^+$, 148.0757; found: 148.0755; calcd for C_9H_9NNaO $[M + Na]^+$, 170.0576; found: 170.0577.

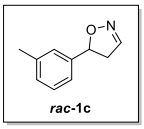

5-(m-tolyl)-4,5-dihydroisoxazole: colourless oil, yield 23%. ^{1}H NMR (400 MHz, $CDCl_3$) δ 7.18 (dd, *J* = 8.5, 6.6 Hz, 1H), 7.13 (td, *J* = 1.8, 0.6 Hz, 1H), 7.10-7.01 (m, 3H), 5.42 (dd, *J* = 11.2, 8.1 Hz, 1H), 3.35 (ddd, *J* = 17.6, 11.2, 1.8 Hz, 1H), 2.90 (ddd, *J* = 17.6, 8.1, 1.9 Hz, 1H), 2.29 (s, 3H); ^{13}C NMR (100 MHz, $CDCl_3$) δ 145.53, 140.80, 138.41, 128.81, 128.56, 126.32, 122.77, 79.86, 43.64, 21.35. HRMS (ESI): calcd for $C_{10}H_{12}NO$ $[M + H]^+$, 162.0913; found: 162.0911; calcd for $C_{10}H_{11}NNaO$ $[M + Na]^+$, 184.0733; found: 184.0734.

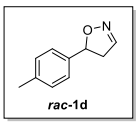

5-(p-tolyl)-4,5-dihydroisoxazole: yellow oil, yield 32%. ^{1}H NMR (400 MHz, $CDCl_3$) δ 7.29-7.04 (m, 5H), 5.47 (dd, *J* = 11.1, 8.2 Hz, 1H), 3.39 (ddd, *J* = 17.6, 11.1, 1.8 Hz, 1H), 2.95 (ddd, 17.6, 8.2, 1.8 Hz, 1H), 2.33 (s, 3H); ^{13}C NMR (100 MHz, $CDCl_3$) δ 145.64, 137.95, 137.90, 129.40, 125.81, 79.91, 43.66, 21.16. HRMS (ESI): calcd for $C_{10}H_{12}NO$ $[M + H]^+$, 162.0913; found: 162.0910; calcd for $C_{10}H_{11}NNaO$ $[M + Na]^+$, 184.0733; found: 184.0744.

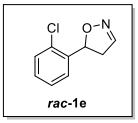

5-(2-chlorophenyl)-4,5-dihydroisoxazole: colorless oil, yield 17%. ^{1}H NMR (400 MHz, $CDCl_3$) δ 7.42-7.40 (m, 1H), 7.33-7.27 (m, 1H), 7.25-7.13 (m, 2H), 7.13-7.08 (m, 1H), 5.75 (dd, *J* = 11.3, 6.9 Hz, 1H), 3.52(ddd, *J* = 17.8, 11.3, 1.8 Hz, 1H), 2.79 (ddd, *J* = 17.8, 6.9, 1.9 Hz, 1H); ^{13}C NMR (100 MHz, $CDCl_3$) δ 145.78, 139.01, 131.26, 129.65, 129.15, 127.28, 126.61, 76.97, 43.46. HRMS (ESI): calcd for $C_9H_8ClNNaO$ $[M + Na]^+$, 204.0187; found: 204.0186.

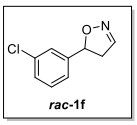

5-(3-chlorophenyl)-4,5-dihydroisoxazole: yellow oil, yield 5%. ^{1}H NMR (400 MHz, $CDCl_3$) δ 7.32-7.26 (m, 3H), 7.20-7.18 (m, 2H), 5.49 (dd, *J* = 11.2, 7.7 Hz, 1H), 3.45 (ddd, *J* = 17.6, 11.3, 1.7 Hz, 1H), 2.95 (ddd, *J* = 17.6, 7.7, 1.6 Hz, 1H); ^{13}C NMR (100 MHz, $CDCl_3$) δ 145.49, 143.10, 134.64, 130.10, 128.27, 125.86, 123.87, 79.00, 43.82. HRMS (ESI): calcd for $C_9H_8ClNNaO$ $[M + Na]^+$, 204.0187; found: 204.0182.

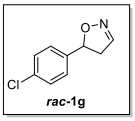

5-(4-chlorophenyl)-4,5-dihydroisoxazole: yellow oil, yield 18%. ^{1}H NMR (400 MHz, $CDCl_3$) δ 7.33-7.20 (m, 5H), 5.51-5.46 (m, 1H), 3.58-3.21 (m, 1H), 2.96-2.89 (m, 1H); ^{13}C NMR (100 MHz, $CDCl_3$) δ 145.51, 139.51, 133.91, 128.90, 127.16, 79.13, 43.78. HRMS (ESI): calcd for $C_9H_8ClNNaO$ $[M + Na]^+$, 204.0187; found: 204.0185.

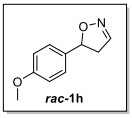

5-(4-methoxyphenyl)-4,5-dihydroisoxazole: colorless oil, yield 25%. ^{1}H NMR (400 MHz, $CDCl_3$) δ 7.26-7.19 (m, 3H), 6.90-6.86 (m, 2H), 5.46 (dd, *J* = 10.9, 8.6 Hz, 1H), 3.79 (s, 3H), 3.37 (ddd, *J* = 17.6, 11.1, 1.7 Hz, 1H), 2.95 (ddd, *J* = 17.6, 8.4, 1.7 Hz, 1H); ^{13}C NMR (100 MHz, $CDCl_3$) δ 159.55,

145.71, 132.80, 127.26, 114.11, 79.81, 55.33, 43.48. HRMS (ESI): calcd for $C_{10}H_{11}NNaO_2$ $[M + Na]^+$, 200.0682; found: 200.0696.

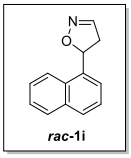

5-(naphthalen-1-yl)-4,5-dihydroisoxazole: yellow oil, yield 18%. ^{1}H NMR (400 MHz, $CDCl_3$) δ 7.90-7.88 (m, 1H), 7.85-7.81 (m, 2H), 7.63-7.62 (d, *J* = 7.1 Hz, 1H), 7.58-7.43 (m, 3H), 7.25 (s, 1H), 6.21 (dd, *J* = 11.3, 7.7 Hz, 1H), 3.65 (dd, *J* = 17.4, 11.4 Hz, 1H), 3.02 (dd, *J* = 17.4, 7.6 Hz, 1H); ^{13}C NMR (100 MHz, $CDCl_3$) δ 145.85, 136.06, 133.97, 129.67, 129.14, 128.50, 126.36, 125.76 , 125.51, 122.85, 122.74, 77.62, 43.51. HRMS (ESI): calcd for $C_{13}H_{11}NNaO$ $[M + Na]^+$, 220.0733; found: 220.0748.

Synthesis of 5-(o-tolyl)-4,5-dihydroisoxazole

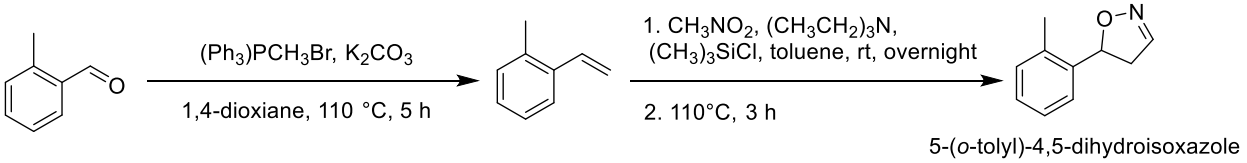

5-(*o*-tolyl)-4,5-dihydroisoxazole

To 30 mL 1, 4-dioxane solution containing 2-methylbenzaldehyde (2.65 g, 22 mmol) and K_2CO_3 (3.03 g), 7.86 g methyltriphenylphosphonium was added. The resulting solution was refluxed at 110 °C for 5 h. Then the solution was cooled down to room temperature and filtered, the solvent in filtrate was removed in reduced pressure. The residual was dissolved in 50 mL toluene, then 1.32 g CH_3NO_2, 2.22 g $(CH_3CH_2)_3N$ and 2.2 g $(CH_3)_3SiCl$ were added. The resulting solution was stirred at room temperature for 48 h, followed with refluxing at 110 °C for 3 h. After cooling down, the solvent was removed in vacuum and the residual was purified by silica-column, (Eluent: EA/hexane=1/5). **(**The corresponding NMR spectra are shown in **Appendix I)**

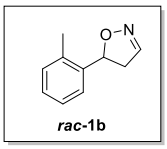

5-(o-tolyl)-4,5-dihydroisoxazole: colorless oil, yield 21%. ^{1}H NMR (400 MHz, $CDCl_3$) δ 7.38 – 7.27 (m, 1H), 7.23 – 7.04 (m, 4H), 5.62 (dd, *J* = 11.2, 8.1 Hz, 1H), 3.39 (ddd, *J* = 17.4, 11.3, 1.4 Hz, 1H), 2.77 (ddd, *J* = 17.4, 8.0, 0.9 Hz, 1H), 2.26 (s, 3H); ^{13}C NMR (100 MHz, $CDCl_3$) δ 145.48, 139.08, 134.21, 130.59, 127.84, 126.38, 124.97, 77.45, 42.84, 19.30. HRMS (ESI): calcd for $C_{10}H_{12}NO$ $[M + H]^+$, 162.0913; found: 162.0914; calcd for $C_{10}H_{11}NNaO$ $[M + Na]^+$, 184.0733; found: 184.0733.

Synthesis of 5-(thiophen-2-yl)-4,5-dihydroisoxazole

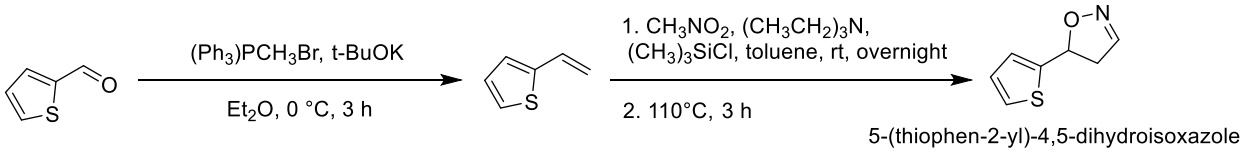

5-(thiophen-2-yl)-4,5-dihydroisoxazole

To 50 mL Et_2O solution containing thiophene-2-carbaldehyde (3.36 g, 30 mmol) and t-BuOK (6.6 g, 48 mmol), 12.86 g methyltriphenylphosphonium was added. The resulting solution was stirred at 0 °C for 3 h. Then the solution was cooled down to room temperature and filtered, the solvent in filtrate was removed in reduced pressure. The residual was dissolved in 50 mL toluene, then 1.80 g CH_3NO_2, 3.03 g $(CH_3CH_2)_3N$ and 3.30 g $(CH_3)_3SiCl$ were added. The resulting solution was stirred at room temperature overnight, followed with refluxing at 110 °C for 3 h. After cooling down, the solvent was removed in vacuum and the residual was purified by silica-column (Eluent: EA/hexane=1/5). (The corresponding NMR spectra are shown in **Appendix I**)

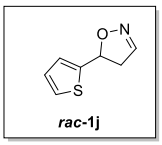

5-(thiophen-2-yl)-4,5-dihydroisoxazole: brown oil, yield 7%. ^{1}H NMR (400 MHz, $CDCl_3$) δ 7.29 – 7.23 (m, 1H), 7.22 (t, *J* = 1.5 Hz, 1H), 7.06 – 7.00 (m, 1H), 7.00 – 6.93 (m, 1H), 5.72 (dd, *J* = 10.8, 7.8 Hz, 1H), 3.39 (ddd, *J* = 17.6, 10.8, 1.8 Hz, 1H), 3.10 (ddd, *J* = 17.6, 7.8, 1.8 Hz, 1H); ^{13}C NMR (100 MHz, $CDCl_3$) δ 145.84, 143.46, 126.96, 125.71, 125.38, 75.89, 43.49. HRMS (ESI): calcd for C_7H_7NNaOS $[M + Na]^+$, 176.0141; found: 176.0139.

Synthesis of aliphatic dihydroisoxazoles (*132*)

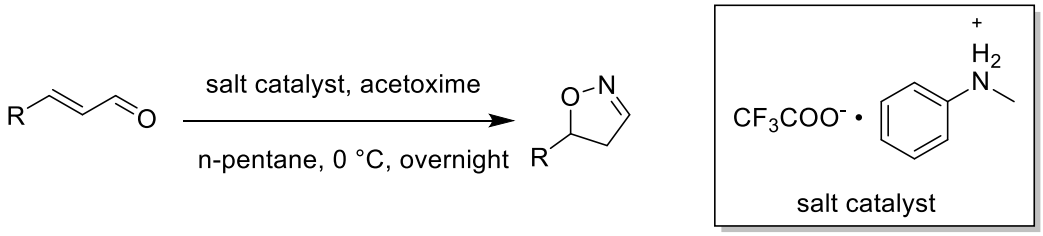

To 50 mL n-pentane solution containing 3.65 g (50 mmol) acetoxime and 2.65 g (20 mol%) salt catalyst was slowly added with 60 mmol aliphatic aldehyde at 0 °C. The resulting solution was stirred at 0°C overnight, then the upper *n*-pentane layer was separated out and the lower layer was washed with *n*-pentane (50 mL ×2). The combined *n*-pentane was concentrated in vacuum and the residual was applied to silica-column for purification (eluent: *n*-pentane/Et_2O=5/1). (The corresponding NMR spectra are shown in **Appendix I**)

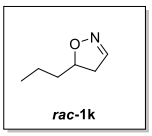

5-propyl-4, 5-dihydroisoxazole: light yellow oil, yield 10%. ^{1}H NMR (400 MHz, $CDCl_3$) δ 7.09 (t, *J* = 1.7 Hz, 1H), 4.58 – 4.33 (m, 1H), 3.02 (ddd, *J* = 17.3, 10.5, 1.8 Hz, 1H), 2.59 (ddd, *J* = 17.3, 8.1, 1.9 Hz, 1H), 1.78 – 1.55 (m, 1H), 1.56 – 1.23 (m, 3H), 1.03 – 0.79 (m, 3H); ^{13}C NMR (100 MHz, $CDCl_3$) δ 145.90, 78.52, 40.42, 37.18, 18.79, 13.86. HRMS (ESI): calcd for $C_6H_{11}NNaO$ $[M + Na]^+$, 136.0733; found: 136.0708.

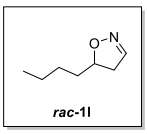

5-butyl-4, 5-dihydroisoxazole: light yellow oil, yield 32%. ^{1}H NMR (400 MHz, $CDCl_3$) δ 7.03 (s, 1H), 4.43 (ddt, *J* = 14.3, 10.4, 7.0 Hz, 1H), 2.97 (ddd, *J* = 17.3, 10.5, 1.8 Hz, 1H), 2.54 (ddd, *J* = 17.4, 8.1, 1.8 Hz, 1H), 1.64-1.58 (m, 1H), 1.49-1.41 (m, 1H), 1.38 – 1.22 (m, 4H), 0.84 (t, *J* = 8.0 Hz, 3H); ^{13}C NMR (100 MHz, $CDCl_3$) δ 145.90, 78.77, 40.41, 34.77, 27.64, 22.49, 13.94. HRMS (ESI): calcd for $C_7H_{13}NNaO$ $[M + Na]^+$, 150.0889; found: 150.0900.

Synthesis of racemic β-alcohol nitriles

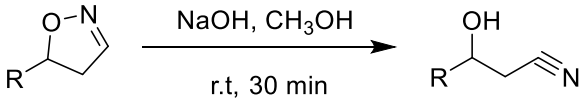

To 10 mL methanol solution containing 200 mg NaOH was added with dihydroisoxazole derivatives (1.5 mmol), then stirred at room temperature for additional 30 min. The solvent was removed in reduced pressure and the residual was applied to silica-column for purification (EA/hexane=1/5). (The corresponding NMR spectra are shown in **Appendix I**)

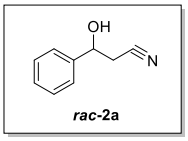

3-hydroxy-3-phenylpropanenitrile: pale yellow oil, 63% yield. ^{1}H NMR (400 MHz, $CDCl_3$) δ 7.47-7.30 (m, 5H), 5.05 (m, 1H), 2.81-2.74 (m, 2H), 2.40 (s, 1H); ^{13}C NMR (100 MHz, $CDCl_3$) δ 141.02, 128.97, 128.88, 125.54, 117.31, 70.15, 27.95. HRMS (ESI): calcd for C_9H_9NNaO $[M + Na]^+$, 170.0576; found: 170.0575.

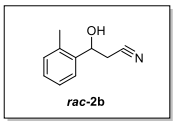

3-hydroxy-3-(o-tolyl)propanenitrile: colorless oil, yield 77%. ^{1}H NMR (400 MHz, $CDCl_3$) δ 7.48-7.46 (m, 1H), 7.26-7.17 (m, 2H), 7.16-7.10 (m, 1H), 5.25-5.13 (m, 1H), 3.16 (s, 1H), 2.64 (dd, *J* = 6.1, 1.3 Hz, 2H), 2.30 (s, 3H); ^{13}C NMR (100 MHz, $CDCl_3$) δ 139.24, 134.36, 130.75, 128.43, 126.72, 125.04, 117.71, 66.31, 26.66, 18.96. HRMS (ESI): calcd for $C_{10}H_{11}NNaO$ $[M + Na]^+$, 184.0733; found: 184.0733.

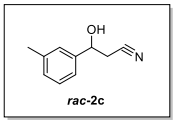

3-hydroxy-3-(m-tolyl)propanenitrile: colorless oil, yield 41%. ^{1}H NMR (400 MHz, $CDCl_3$) δ 7.30-7.26 (m, 1H), 7.21-7.15 (m, 3H), 5.00 (td, *J* = 6.2, 3.7 Hz, 1H), 2.76 (dd, *J* = 6.2, 1.8 Hz, 2H), 2.43 (d, *J* = 3.6 Hz, 1H), 2.37 (s, 3H); ^{13}C NMR (100 MHz, $CDCl_3$) δ 140.98, 138.79, 129.63, 128.87, 126.16, 122.57, 117.33, 70.23, 27.90, 21.46. HRMS (ESI): calcd for $C_{10}H_{11}NNaO$ $[M + Na]^+$, 184.0733; found: 184.0735.

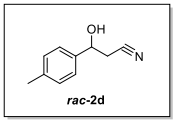

3-hydroxy-3-(p-tolyl)propanenitrile: colorless oil, yield 54%. ^{1}H NMR (400 MHz, $CDCl_3$) δ 7.30-7.22 (m, 2H), 7.19 (d, *J* = 7.9 Hz, 2H), 4.96 (t, *J* = 5.9 Hz, 1H), 2.79 (s, 1H), 2.71 (dd, *J* = 12.5, 6.6 Hz, 2H), 2.35 (s, 3H); ^{13}C NMR (100 MHz, $CDCl_3$) δ 138.66, 138.15, 129.57, 125.50, 117.50, 69.90, 27.89, 21.18. HRMS (ESI): calcd for $C_{10}H_{11}NNaO$ $[M + Na]^+$, 184.0733; found: 184.0733.

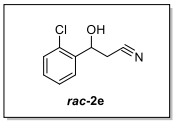

3-(2-chlorophenyl)-3-hydroxypropanenitrile: colorless oil, yield 60%. ^{1}H NMR (400 MHz, $CDCl_3$) δ 7.74-7.60 (m, 1H), 7.38-7.30 (m, 2H), 7.27 (m, 1H), 5.40 (dt, *J* = 7.3, 3.8 Hz, 1H), 3.28 (d, *J* = 3.8 Hz, 1H), 2.88 (dd, *J* = 16.8, 4.0 Hz, 1H), 2.70 (dd, *J* = 16.7, 7.1 Hz, 1H); ^{13}C NMR (100 MHz, $CDCl_3$) δ 138.41, 131.29, 129.67, 129.57, 127.56, 127.05, 117.31, 66.31, 26.32. HRMS (ESI): calcd for $C_9H_8ClNNaO$ [M + Na]$^+$, 204.0187; found: 204.0182.

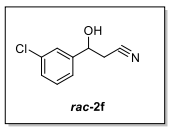

3-(3-chlorophenyl)-3-hydroxypropanenitrile: colorless oil, yield 50%. ^{1}H NMR (400 MHz, $CDCl_3$) δ 7.42-7.41 (m, 1H), 7.37-7.31 (m, 2H), 7.31-7.26 (m, 1H), 5.03 (td, *J* = 6.2, 3.7 Hz, 1H), 2.76 (d, *J* = 6.2 Hz, 2H), 2.65 (d, *J* = 3.8 Hz, 1H); ^{13}C NMR (100 MHz, $CDCl_3$) δ 142.97, 134.92, 130.27, 129.00, 125.79, 123.74, 116.93, 69.49, 27.98. HRMS (ESI): calcd for $C_9H_8ClNNaO$ [M + Na]$^+$, 204.0187; found: 204.0184.

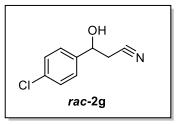

3-(4-chlorophenyl)-3-hydroxypropanenitrile: light yellow oil, yield 65%. ^{1}H NMR (400 MHz, $CDCl_3$) δ 7.39-7.25 (m, 4H), 4.98 (t, *J* = 6.1 Hz, 1H), 3.23 (s, 1H), 2.71 (dd, *J* = 6.2, 1.0 Hz, 2H); ^{13}C NMR (100 MHz, $CDCl_3$) δ 139.54, 134.49, 129.05, 127.01, 117.27, 69.19, 27.98. HRMS (ESI): calcd for $C_9H_8ClNNaO$ [M + Na]$^+$, 204.0187; found: 204.0182.

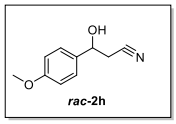

3-hydroxy-3-(4-methoxyphenyl)propanenitrile: colorless oil, yield 59%. ^{1}H NMR (400 MHz, $CDCl_3$) δ 7.30-7.26 (m, 2H), 6.93-6.86 (m, 2H), 4.94 (t, *J* = 5.3 Hz, 1H), 3.79 (s, 3H), 2.96 (s, 1H), 2.71 (dd, *J* = 6.2, 2.2 Hz, 2H); ^{13}C NMR (100 MHz, $CDCl_3$) δ 159.82, 133.27, 126.91, 117.56, 114.24, 69.62, 55.36, 27.90. HRMS (ESI): calcd for $C_{10}H_{11}NNaO_2$ [M + Na]$^+$, 200.0682; found: 200.0688.

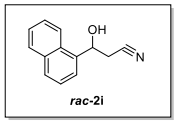

3-hydroxy-3-(naphthalen-1-yl)propanenitrile: colorless oil, yield 56%. ^{1}H NMR (400 MHz, $CDCl_3$) δ 7.97-7.81 (m, 2H), 7.77 (d, *J* = 8.2 Hz, 1H), 7.64 (d, *J* = 7.2 Hz, 1H), 7.58-7.35 (m, 3H), 5.67 (s, 1H), 3.24 (s, 1H), 2.81 (ddd, *J* = 24.4, 16.8, 6.0 Hz, 2H); ^{13}C NMR (100 MHz, $CDCl_3$) δ 136.46, 133.78, 129.64, 129.28, 129.16, 126.76, 125.97, 125.53, 123.25, 122.16, 117.76, 66.75, 27.10. HRMS (ESI): calcd for $C_{13}H_{11}NNaO$ [M + Na]$^+$, 220.0733; found: 220.0733.

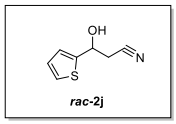

3-hydroxy-3-(thiophen-2-yl)propanenitrile: yellow oil, yield 50%. ^{1}H NMR (400 MHz, $CDCl_3$) δ 7.31 (dd, *J* = 5.0, 1.2 Hz, 1H), 7.11-7.03 (m, 1H), 7.00 (dd, *J* = 5.0, 3.6 Hz, 1H), 5.26 (t, *J* = 6.2 Hz, 1H), 3.23 (s, 1H), 2.85 (dd, *J* = 6.2, 0.9 Hz, 2H); ^{13}C NMR (100 MHz, $CDCl_3$) δ 144.51, 127.12, 125.75, 124.72, 117.07, 66.19, 28.21. HRMS (ESI): calcd for C_7H_7NNaOS [M + Na]$^+$, 176.0141; found: 176.0139.

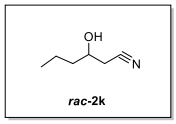

3-hydroxyhexanenitrile: yellow oil, yield 85%. ^{1}H NMR (400 MHz, $CDCl_3$) δ 3.98-3.85 (m, 1H), 2.68 – 2.38 (m, 3H), 1.65 – 1.25 (m, 4H), 0.98 – 0.87 (m, 3H); ^{13}C NMR (100 MHz, $CDCl_3$) δ 117.87, 67.44, 38.57, 26.10, 18.62, 13.75. HRMS (ESI): calcd for $C_6H_{11}NNaO$ [M + Na]$^+$, 136.0733; found: 136.0729.

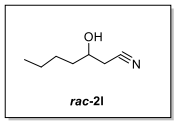

3-hydroxyheptanenitrile: yellow oil, yield 89%. ^{1}H NMR (400 MHz, $CDCl_3$) δ 3.93 – 3.79 (m, 1H), 2.98 (s, 1H), 2.47 (qd, *J* = 16.6 Hz, *J* = 6.4 Hz, 2H), 1.60 – 1.44 (m, 2H), 1.43 – 1.13 (m, 4H), 0.91 – 0.76 (m, 3H); ^{13}C NMR (100 MHz, $CDCl_3$) δ 118.01, 67.57, 36.15, 27.49, 26.03, 22.39, 13.90. HRMS (ESI): calcd for $C_7H_{13}NNaO$ $[M + Na]^+$, 150.0889; found: 150.0886.

Assay procedure for determination of kinetic parameters of Oxd B and Oxd RE

Kinetic assays for Oxd B were performed with 10 µg pure Oxd B and varying substrate concentrations (0.2 mM-50 mM) of 5-phenyl-4,5-dihydroisoxazole (**1a)** in 100 mM KPB (100 mM, pH 6.0) containing 0.05 mM FMN, 1 mM fresh $Na_2S_2O_5$ at 30 °C and kinetic assays for Oxd RE were performed with 20 µg pure Oxd RE and varying substrate concentrations (0.2 mM-20 mM) of **1a** in 100 mM KPB (100 mM, pH 7.0) containing 1 mM fresh Na_2S at 30 °C, respectively. The reactions were initiated by addition of substrate and each sample was measured at different time points of 2 min, 4 min, 6 min for Oxd B, 5 min, 10 min, 20 min for Oxd RE, respectively, by taking 200 µL reaction mixture, which was extracted by addition of 400 µL ethyl acetate containing 2 mM benzonitrile. Initial rates (mM/min) determined by subtracting the slope of the control were plotted versus the concentration of **1a**. The data was fitted to the Michaelis-Menten equation and determine the kinetic parameters.

HPLC/GC analysis methods (*59, 61*)

The substrates (**1a-1l**) and corresponding products (**2a-2l**) were analyzed by Shimadazu-HPLC equipped with Daicel chiral columns and Shimadazu Gas Chromatograph equipped with chiral GC columns as showed in **Table 3**.

Table 3: Analysis methods for compounds **1a-1l** and **2a-2l**

analysis method	Substrate			product		
	structure	retention time		structure	retention time	
Daicel Chiral OJ-H, 1 mL/min, Hexane/iso-propanol=9/1, 30 °C	5-phenyl-4,5-dihydroisoxazole	t1=19.027 min	t2=19.696 min	3-hydroxy-3-phenylpropanenitrile	t1=21.838 min	t2=27.085 min
Daicel Chiral OD-H, 1 mL/min, Hexane/iso-propanol=9/1, 30 °C	5-(o-tolyl)-4,5-dihydroisoxazole	t1=10.527 min	t2=11.268 min	3-hydroxy-3-(o-tolyl)propanenitrile	t1=13.419 min	t2=17.597 min
Daicel Chiral OJ-H, 1 mL/min, Hexane/iso-propanol=9/1, 30 °C	5-(m-tolyl)-4,5-dihydroisoxazole	t1=14.420 min	t2=15.420 min	3-hydroxy-3-(m-tolyl)propanenitrile	t1=17.248 min	t2=20.816 min
Daicel Chiral OD-H, 1 mL/min, Hexane/iso-propanol=9/1, 30 °C	5-(p-tolyl)-4,5-dihydroisoxazole	t1=9.067 min	t2=10.731 min	3-hydroxy-3-(p-tolyl)propanenitrile	t1=16.307 min	t2=17.437 min
Daicel Chiral OD-H, 1 mL/min, Hexane/iso-propanol=95/5, 30 °C	5-(2-chlorophenyl)-4,5-dihydroisoxazole	t1=9.025 min	t2=9.908 min	3-(2-chlorophenyl)-3-hydroxypropanenitrile	t1=18.919 min	t2=19.710 min
Daicel Chiral OJ-H, 1 mL/min, Hexane/iso-propanol=9/1, 30 °C	5-(3-chlorophenyl)-4,5-dihydroisoxazole	t1=15.971 min	t2=16.419 min	3-(3-chlorophenyl)-3-hydroxypropanenitrile	t1=21.532 min	t2=25.850 min
Daicel Chiral OD-H, 1 mL/min, Hexane/iso-propanol=95/5, 30 °C	5-(4-chlorophenyl)-4,5-dihydroisoxazole	t1=14.083 min	t2=14.403 min	3-(4-chlorophenyl)-3-hydroxypropanenitrile	t1=34.262 min	t2=39.309 min
Daicel Chiral OJ-H, 1 mL/min, Hexane/iso-propanol=9/1, 30 °C	5-(4-methoxyphenyl)-4,5-dihydroisoxazole	t1=39.105 min	t2=40.344 min	3-hydroxy-3-(4-methoxyphenyl)propanenitrile	t1=42.091 min	t2=43.587 min
Daicel Chiral OJ-H, 1 mL/min, Hexane/iso-propanol=9/1, 30 °C	5-(naphthalen-1-yl)-4,5-dihydroisoxazole	t1=22.175 min	t2=35.406 min	3-hydroxy-3-(naphthalen-1-yl)propanenitrile	t1=39.632 min	t2=47.051 min
Daicel Chiral OD-H, 1 mL/min, Hexane/iso-propanol=95/5, 30 °C	5-(thiophen-2-yl)-4,5-dihydroisoxazole	t1=19.657 min	t2=20.803 min	3-hydroxy-3-(thiophen-2-yl)propanenitrile	t1=39.119 min	t2=41.094 min
BGB-174， 40 °C-2 min, 1 °C/min to 100 °C, 100 °C-10 min, 2 °C/min to 150 °C, 150 °C-30 min	5-propyl-4,5-dihydroisoxazole	t1=68.616 min	t2=72.214 min	3-hydroxyhexanenitrile	t1=103.731 min	t2=104.495 min
BGB-174， 40 °C-2 min, 1 °C/min to 100 °C, 100 °C-10 min, 2 °C/min to 150 °C, 150 °C-30 min	5-butyl-4,5-dihydroisoxazole	t1=78.849 min	t2=80.736 min	3-hydroxyheptanenitrile	t1=110.752 min	t2=111.740 min

Oxd B homology model and mutants activity assay to aldoxime dehydration

The Oxd B homology model was constructed based on the structure of Oxd RE using SWISS-MODEL online. And the docking experiments between homology model and substrates were performed by the software of Molecular Operating Environment (MOE). The Alanine mutants of Oxd B were constructed by QuikChange Lightning Site-Directed Mutagenesis Kit (Agilent) with standard PCR. The Oxd B mutant enzymes were produced and purified as described above. Then the activity of the mutants to substrate Z-phenylacetoxime were assayed with the reaction mixture of 10 mM substrate, 0.25 mM FMN, 1 mM $Na_2S_2O_5$, 2 μg pure enzymes in 100 mM KPB (pH 7.0) at 30 °C for 5 min.

Results and discussion

In the initial screening process, the reaction of ring-opening of 5-phenyl-4, 5-dihydroisoxazole catalyzed by Oxd B was carried out in the absence of a reductant, which showed excellent enantioselectivity on the cleavage of the N-O bond as expected, but the activity was barely satisfactory. In view of the important role of a reductant in the aldoxime dehydration (*129*) and

Kemp elimination reactions (*118*), which can significantly enhance the enzyme activity, different reductants were tested for the asymmetric ring-opening of 5-phenyl-4,5-dihydroisoxazole (**Fig. 12**). The enhanced effect on the enzymatic activity upon the addition of a reductant was observed, which showed the activity can be improved 1.9–6.0 fold using a variety of reductants. In addition, the enantioselectivity of the enzyme was not affected by the additives with the *ee* of the product being maintained at ⩾99% in each case. The reductant effect implies a ferrous-Heme active state was involved in the reaction, which is consistent with the sensitivity of Oxd B to oxygen (*133*).

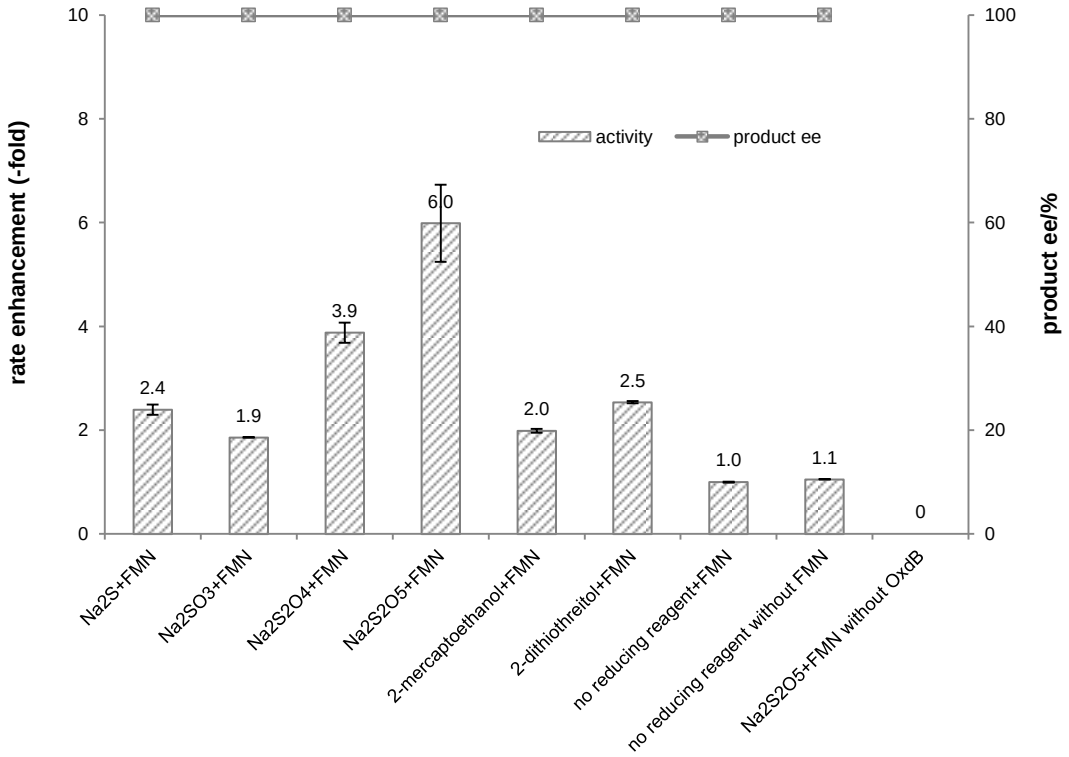

Fig. 12. Reductants effect to the activity of Oxd B in the catalysis of asymmetric ring-opening of 5-phenyl-4, 5-dihydroisoxazole. The partially purified Oxd B from Ni Sepharose^{TM} 6 Fast flow column was used. Initially, different reductants were used for screening on the activity of asymmetric ring-opening of 5-phenyl-4,5-dihydroisoxazole catalyzed by Oxd B, The reactions were performed in 500 μL scale with 100 mM KPB (pH 7.0), 1 U Oxd-B, 20 mM 5-phenyl-4, 5-dihydroisoxazole, 0.25 mM FMN and 1 mM reducing reagent at 30 ºC for 10 min. The yield and ee were detected by chiral HPLC as shown above.

The classic Kemp elimination reaction can take place under alkaline conditions via an acid-base mechanism (*120*). Accordingly, this reaction was investigated in a range of different pH buffers (**Fig. 13a**). Although the yield varied significantly at different pH in a various buffer types, the enzyme could work at pH 5.0 – 10.0 with the desired product formed in 2 – 36% yield, and the optical purity of the product was maintained at ⩾99% at pH 5.0 – 8.0. From the control results, spontaneous reactions were detected in pH 9.0–10.0 (**Fig. 13b**), which caused a sharp decrease in the product *ee*. Enlightened by these results, an useful method to prepare racemic β-hydroxy nitriles is described from alkenes via a 5-sub-4, 5-dihydroisoxazole intermediate upon treatment with a methanolic NaOH solution at room temperature as shown above. The result is consistent with the previous reports that β-hydroxy nitriles were formed by treating dihydroisoxazoles with bases (Such as trimethylamine (*134*), 1, 8-diazabicyclo[5.4.0]undec-7-ene (*135*), NaOMe (*136*), ring-opening of 3-bromo-2-isoxazolines upon treatment with an alkanethiolate (*137*).

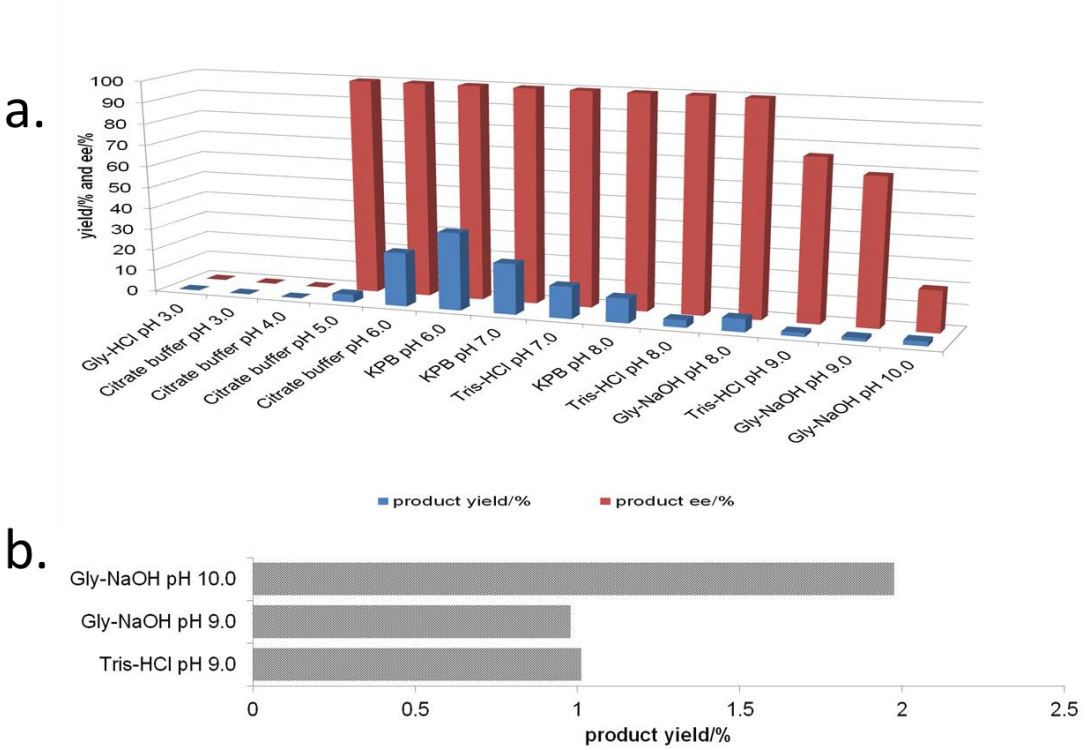

Fig 13. (a) The pH effect on the activity of Oxd B in the catalytic asymmetric ring-opening of 5-phenyl-4,5-dihydroisoxazole. The reactions were performed on a 500 μL scale using 100 mM buffer (pH 3.0–10.0), 1 U Oxd-B, 20 mM 5-phenyl-4,5-dihydroisoxazole, 0.05 mM FMN, and 1 mM $Na_2S_2O_5$ at 30 °C for 30 min. The buffer solutions used were Gly-HCl (pH 3.0), Citrate-buffer (pH 3.0, 4.0, 5.0, and 6.0), KPB (pH 6.0, 7.0, and 8.0), Tris-

HCl (pH 7.0, 8.0, and 9.0), and Gly-NaOH (pH 8.0, 9.0, and 10.0). (b) The control experiments were carried out without Oxd B at pH 9.0 and pH 10.0. The yield and ee were determined using chiral HPLC (n = 2).

To further improve the product yield, the reaction was monitored for a prolonged time of 3 h (**Fig. 14**). During the enantioselective transformation of the substrate, the *ee* of the substrate 5-phenyl-4, 5-dihydroisoxazole (**1a**) increased to 99% over 2 h and the product (**2a**) *ee* was maintained at 99%, indicating the excellent catalytic enantioselectivity of Oxd B on this substrate.

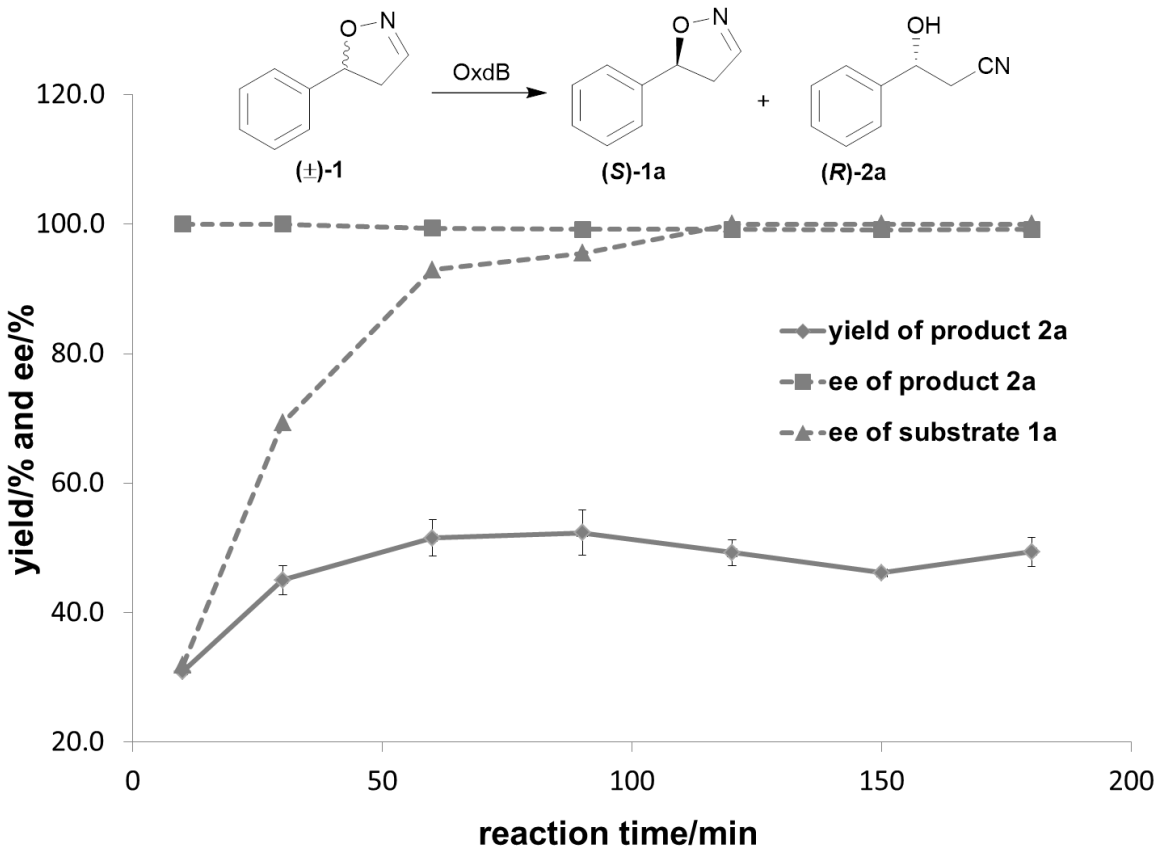

Fig 14. Time course of the asymmetric ring-opening of 5-phenyl-4,5-dihydroisoxazole using Oxd B. The reactions were performed on a 500 µL scale using 100 mM KPB buffer (pH 6.0), 1 U Oxd B, 20 mM 5-phenyl-4,5-dihydroisoxazole, 0.05 mM FMN, and 1 mM $Na_2S_2O_5$ at 30 °C. The yield and *ee* were determined using chiral HPLC (n = 2).

Additionally, it is often beneficial to agitate a reaction to improve the mass transfer process and as a result, enhance the reaction rate. However, a ~5-fold decrease in the yield of the β-hydroxy nitrile product was observed upon shaking the reaction when compared to the static-state

reaction over 1 h. As reported in the dehydration of aldoximes, the activity of Oxd B can be increased by 5-fold under anaerobic conditions (*126*). Therefore, the oxygen sensitivity of Oxd B seems to be the reason of the decrease in the enzymatic activity in a shaking mode. By shaking, the enzyme is much more susceptible to exposure to oxygen in the air, which leads to the oxidation of ferrous-Heme to ferric-Heme, the resting-state of Heme in the ring-opening reaction of dihydroisoxazole (*138*, *139*).

With the optimized reaction conditions, a series of substrates were investigated using Oxd B (**Table 4**). Oxd B exhibited good selectivity toward most aromatic substrates with desired product S/R-2 formed in 48–99% *ee*. Among them, substrates bearing an electron-donating group on the aryl ring showed relatively higher *ee* values than those bearing an electron-withdrawing group. In addition, the enzyme preferred substrates bearing a substituent at the para-position (**Table 4**, **1d**, **1g**, and **1h**), rather than the ortho- (**Table 4**, **1b** and **1e**) or meta-position (**Table 4**, **1c** and **1f**). The selectivity toward heterocyclic aromatic substrates (**Table 4**, **1j**) was also very excellent, but a slight decrease in activity was observed. However, increasing the size of the aromatic ring to a naphthalene group leads to the reaction conversion becoming negligible (**Table 4**, **1i**), which may be caused by the lower solubility of the substrate in water. For aliphatic substrates (**Table 4**, **1k** and **1l**), Oxd B exhibited a deterioration in the reaction selectivity.

To establish an efficient catalytic system for aliphatic substrates, another two aldoxime dehydratases obtained from *Pseudomonas chlororaphis* B23 (Oxd A) (*124*, *125*), and *Rhodococcus* sp. N-771 (Oxd RE) (*140*, *141*), were selected and investigated using a range of different substrates. They were found to display higher activity toward aliphatic substrates when compared to aromatic substrates in the aldoxime dehydration reaction.

Table 4. Investigation of the substrate scope of Oxd A, B, and RE.[a]

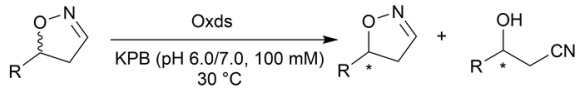

(±)-1 **S/R-1** **S/R-2**

1a: R = Ph; **1b:** R = 2-Me-Ph; **1c:** R = 3-Me-Ph; **1d:** R = 4-Me-Ph;
1e: R = 2-Cl-Ph; **1f:** R = 3-Cl-Ph; **1g:** R = 4-Cl-Ph; **1h:** R = 4-MeO-Ph;
1i: R =1-naphthalene; **1j:** R = 2-thiophene; **1k:** R = *n*-propyl; **1l:** R = *n*-butyl

Substrate (±)-1	Enzyme	Conv. [%] [b]	*ee* of *S/R*-1 [%]	*ee* of *S/R*-2 [%] [c]	Relative activity [%] [d]
1a	Oxd A	93	24 (*S*)	2 (*R*)	100
	Oxd B	51	99 (*S*)	96 (*R*)	100
	Oxd RE	64	68 (*S*)	38 (*R*)	100
1b	Oxd A	70	25 (*R*)	11 (*S*)	75
	Oxd B	31	43 (*S*)	95 (*R*)	8
	Oxd RE	21	10 (*R*)	36 (*S*)	33
1c	Oxd A	70	77 (*S*)	33 (*R*)	75
	Oxd B	47	76 (*S*)	86 (*R*)	42
	Oxd RE	20	17 (*S*)	66 (*R*)	32
1d	Oxd A	95	21 (*S*)	1 (*R*)	102
	Oxd B	32	45 (*S*)	97 (*R*)	8
	Oxd RE	23	12 (*S*)	41 (*R*)	36
1e	Oxd A	67	25 (*R*)	12 (*S*)	74
	Oxd B	47	47 (*S*)	53 (*R*)	55
	Oxd RE	59	18 (*R*)	13 (*S*)	93
1f	Oxd A	52	19 (*S*)	18 (*R*)	55
	Oxd B	53	64 (*S*)	56 (*R*)	38
	Oxd RE	38	38 (*S*)	62 (*R*)	59
1g	Oxd A	94	99 (*S*)	6 (*R*)	101
	Oxd B	40	63 (*S*)	95 (*R*)	28
	Oxd RE	39	18 (*S*)	28 (*R*)	61
1h	Oxd A	74	77 (*S*)	27 (*R*)	79
	Oxd B	47	87 (*S*)	99 (*R*)	25
	Oxd RE	23	23 (*S*)	77 (*R*)	36
1i	Oxd A	0.5	0 (---)	13 (---)	0
	Oxd B	8	6 (---)	71 (---)	7
	Oxd RE	9	1 (---)	6 (---)	15
1j	Oxd A	77	9 (*S*)	3 (*R*)	83
	Oxd B	49	96 (*S*)	99 (*R*)	79
	Oxd RE	79	75 (*S*)	20 (*R*)	123
1k	Oxd A	83	84 (*R*)	17 (*S*)	89
	Oxd B	67	99 (*R*)	48 (*S*)	12
	Oxd RE	31	39 (*R*)	87 (*S*)	48
1l	Oxd A	88	87 (*R*)	11 (*S*)	95
	Oxd B	59	94 (*R*)	66 (*S*)	80
	Oxd RE	38	49 (*R*)	82 (*S*)	58

(a) For Oxd A, the reactions were performed on a 500 µL scale using 100 mM KPB buffer (pH 7.0), 10 U Oxd A, 20 mM substrate, and 4 mM $Na_2S_2O_4$ at 30 °C for 3 h (n = 2); for Oxd B, the reactions were performed on a 500 µL scale using 100 mM KPB buffer (pH 6.0), 20 U Oxd-B, 20 mM substrate, 0.05 mM FMN, and 1 mM $Na_2S_2O_5$ at 30 °C for 2 h (n = 2); and for Oxd RE, the reactions were performed on a 500 µL scale using 100 mM KPB buffer (pH 7.0), 1 U Oxd RE, 6 mM substrate, 1 mM Na_2S at 30 °C for 2 h (n = 2). (b) The conversion was calculated using conv = $ee_s/(ee_s+ee_p)$ (*142*). (c) The *ee* was determined using chiral HPLC and chiral GC. (d) The activity for substrate **1a** was taken to be 100%. The relative activity for Oxd B was determined on a 500 µL scale using 100 mM KPB buffer (pH 6.0), 1 U Oxd B, 20 mM substrate, 0.05 mM FMN, and 1 mM $Na_2S_2O_5$ at 30 °C for 2 h (n = 2)

Prior to investigating the substrate scope, optimization of the reductant was also carried out. Oxd A showed the best activity with sodium dithionite ($Na_2S_2O_4$), which was ~79-fold higher than that observed in the control experiment performed in the absence of a reductant (**Fig. 15a**). Oxd RE preferred sodium sulfide (Na_2S), which exhibited a ~8.2-fold higher activity than the

control (**Fig. 15c**). The optimal reductant concentration for Oxd A and Oxd RE were 4 mM (**Fig. 15b**) and 1 mM (**Fig. 15d**), respectively.

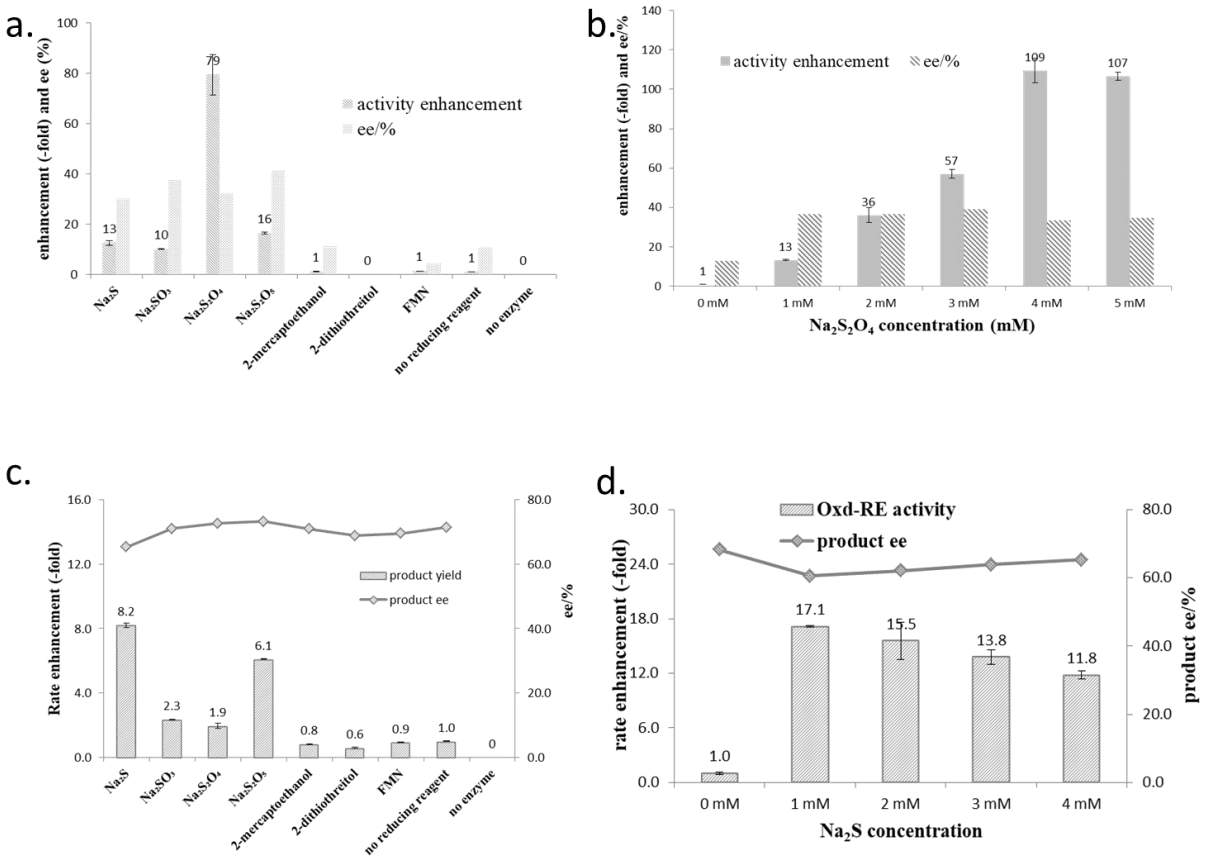

Fig 15. (a) Reductants effect on the activity of Oxd A in the catalysis of asymmetric ring-opening of 5-phenyl-4,5-dihydroisoxazole. The activity without reductant was taken as 1.0. (b). $Na_2S_2O_4$ effect to the activity of Oxd A in the catalysis of asymmetric ring-opening of 5-phenyl-4, 5-dihydroisoxazole. The activity without reductant was taken as 1.0. The partially purified Oxd A from Ni Sepharose^{TM} 6 Fast flow column was used. Initially, different reductants were used for screening on the activity of asymmetric ring-opening of 5-phenyl-4, 5-dihydroisoxazole catalyzed by Oxd A, the reactions were performed in 500 µL scale with 100 mM KPB (pH 7.0), 10 U Oxd-A, 20 mM 5-phenyl-4,5-dihydroisoxazole and 1 mM reducing reagent at 30 ºC for 10 min. The yield and *ee* were detected by chiral HPLC as showed above. Subsequently, the best concentration of $Na_2S_2O_4$ was investigated by performing the reaction in 500 µL scale with 100 mM KPB (pH 7.0), 10 U Oxd A, 20 mM 5-phenyl-4, 5-dihydroisoxazole and 0 mM-5 mM $Na_2S_2O_4$ at 30 ºC for 10 min. The yield and ee were detected by chiral HPLC as shown above. (c) Reductants effect on the activity of Oxd RE in the catalysis of asymmetric ring-opening of 5-phenyl-4,5-dihydroisoxazole. The activity without reductant was taken as 1.0. (d) Na_2S effect to the activity of Oxd RE in the catalysis of asymmetric ring-opening of 5-phenyl-4, 5-dihydroisoxazole. The activity without reductant was taken as 1.0. The partially purified Oxd RE from Ni Sepharose^{TM} 6 Fast flow column was used. Initially, different reductants

were used for screening on the activity of asymmetric ring-opening of 5-phenyl-4,5-dihydroisoxazole catalyzed by Oxd RE, the reactions were performed in 500 μL scale with 100 mM KPB (pH 7.0), 1 U Oxd RE, 20 mM 5-phenyl-4,5-dihydroisoxazole and 1 mM reducing reagent at 30 ºC for 10 min. The yield and *ee* were detected by chiral HPLC as shown above. Subsequently, the best concentration of Na_2S was investigated by performing the reaction in 500 μL scale with 100 mM KPB (pH 7.0), 1 U Oxd RE, 20 mM 5-phenyl-4, 5-dihydroisoxazole and 0 mM-4 mM Na_2S at 30 ºC for 30 min. The yield and *ee* were detected by chiral HPLC as shown above.

Upon monitoring the asymmetric ring-opening reaction of 5-phenyl-4, 5-dihydroisoxazole with time, Oxd A could catalyse the reaction in 83% yield over 3 h, but gave a nearly racemic product (**Fig. 16a**). The same result was also obtained using Oxd RE, the product was formed in 28% yield and 53% *ee* at pH 6.0, and 48% yield and 55% *ee* at pH 7.0 over 2 h, respectively (**Fig. 16b**).

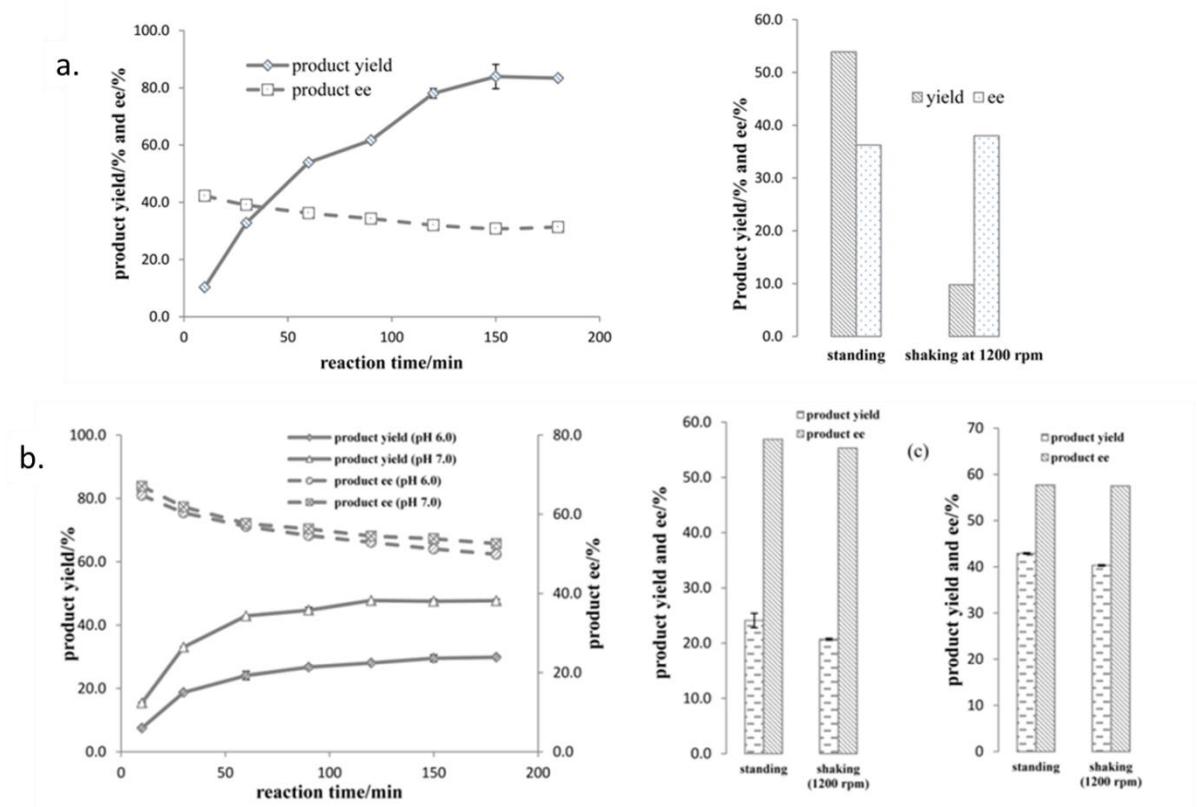

Fig. 16. (a) Reaction time curve for the asymmetric ring-opening of 5-phenyl-4, 5-dihydroisoxazole with catalysis of Oxd A; The partially purified Oxd A from Ni Sepharose^{TM} 6 Fast flow column was used. The reaction was monitored in time of 10 min to 180 min with the reaction condition of 500 μL reaction scale containing 100 mM KPB (pH 7.0), 10 U Oxd A, 20 mM 5-phenyl-4,5-dihydroisoxazole and 4 mM $Na_2S_2O_4$ at 30 ºC. The yield and *ee* were detected by chiral HPLC as shown above. And the different reaction modes of resting and shaking were

compared in 60 min. (b). Reaction time curve for the asymmetric ring-opening of 5-phenyl-4, 5-dihydroisoxazole with catalysis of Oxd RE. The partially purified Oxd RE from Ni Sepharose™ 6 Fast flow column was used. The reaction was monitored in time of 10 min to 180 min with the reaction condition of 500 µL reaction scale containing 100 mM KPB (pH 6.0 or pH 7.0), 1 U Oxd RE, 20 mM 5-phenyl-4,5-dihydroisoxazole and 1 mM Na_2S at 30 ºC. The yield and *ee* were detected by chiral HPLC as shown above. And the different reaction modes of resting and shaking were compared in 60 min.

Our substrate specificity investigations show that Oxd A exhibited very poor enantioselectivity toward the substrates studied, though the conversion is high (**Table 4**). Oxd RE showed relatively better results toward aliphatic substrates when compared to aromatic substrates. In addition, it also exhibited slightly better enantioselectivity than Oxd B in the asymmetric ring-opening of aliphatic substrates (**Table 4**; **1k** and **1l**). Interestingly, Oxd A and Oxd RE exhibited different selectivity toward ortho-substituted aromatic substrates when compared with Oxd B (**Table 4**; **1b** and **1e**). What causes this difference in selectivity compared with other substrates and Oxd B is still not clear. The absolute configuration of products were determined using HPLC using the same analysis methods as published data as shown in **Table 3** (*59, 61*). As for the compounds without reference data, their absolute configurations were measured by Mosher method as shown in **Appendix II** (*143*).

The kinetic parameters for both Oxd B and Oxd RE were determined under the optimized reaction conditions. The turnover number of Oxd B reached 11 s^{-1} with a specific activity of 18 U/mg, which is about one third of the activity observed for (Z)-phenylacetaldoxime dehydration (53 U/mg) using the assay method containing $Na_2S_2O_5$. However, the Oxd RE activity was lower than Oxd B at 4 U/mg with a turnover number of 3 s^{-1}, ~15% of the activity observed for the (Z)-phenylacetaldoxime dehydration reaction (30 U/mg). In addition, the catalytic efficiency of Oxd B ($K_{cat}/K_M = 3.7 \times 10^4\ M^{-1}s^{-1}$) is ~9-fold higher than Oxd RE ($K_{cat}/K_M = 4.3 \times 10^3\ M^{-1}s^{-1}$). An obvious substrate inhibition effect was observed using 1 U of the enzyme upon increasing the substrate concentration to 30 mM for Oxd B and 6 mM for Oxd RE, but no any effect on the optical purity of the product. Therefore, a scale-up reaction was performed based on a substrate concentration of 20 mM and 1 U Oxd B. Under the optimal conditions, the reaction concentration reach 150 mM with the product formed with 50% conversion and 99% *ee* (**Table 5**).

Table 5. Scale up for asymmetric ring-opening of 5-phenyl-4, 5-dihydroisoxazole with catalysis of Oxd B.[a]

entry	substrate concentration (mM)	Oxd B (U)	$Na_2S_2O_5$ concentration (mM)	FMN concentration (mM)	substrate ee (%)	product ee (%)	conversion (%)
1	20	1	1	0.05	99	98.7	50.1
2	40	2	2	0.1	99	98.6	50.1
3	60	3	3	0.15	99	98.8	50.1
4	80	4	4	0.2	99	98.6	50.1
5	100	5	5	0.25	99	98.7	50.1
6	120	6	6	0.3	99	98.7	50.1
7	150	7.5	7.5	0.375	99	99.0	50.0
8	200	10	10	0.5	49.4	98.9	33.3

(a) The reactions were performed in 500 μL scale with equally proportional amplification of optimal reaction conditions (100 mM KPB buffer (pH 6.0), 1 U Oxd-B, 20 mM 5-phenyl-4,5-dihydroisoxazole, 0.05 mM FMN and 1 mM $Na_2S_2O_5$) at 30 ºC for 2 h. The conversion was calculated by the enantiomer excess of substrate and product, as conversion = $ee_s/(ee_s+ee_p)$ (*142*). The yield and ee were detected by chiral HPLC as shown above.

To elucidate the reaction mechanism, a homology model of Oxd B was established based on the crystal structure of Oxd-RE (*130*). In addition, the corresponding residues located in the catalytic pocket of the Heme were selected for an alanine-scanning study (**Fig. 17a**). In this scanning study, L128A, T202A, Q204A, H282A, F289A, and H306A mutants were constructed via site-mutagenesis, which were purified as the wild type of Oxd B to obtain the pure enzyme and used for activity comparison. To begin with, the activity of the mutants toward (Z)-phenylacetaldoxime was assayed. As reported in previous publication, no activity was detected for the T202A, H282A, and H306A mutants, which are corresponding to the S219, H299, and H320 residues in Oxd RE, the crucial residues in the dehydration of butyraldehyde oxime (*118*). These results reveal that the homology model of Oxd B is workable to some extent, although the protein sequence homology between Oxd B and Oxd RE is only 31%. After verifying the reliability of the homology model, the mutants were used in the 5-phenyl-4,5-dihydroisoxazole ring-opening reaction. As expected, the H282A mutant showed no activity toward the substrate because the proximal axial residue ligating to iron is thought to affect the redox potential of the Heme, thus leading to a great difference in the catalytic activity for bond cleavage (*144*, *145*). Surprisingly, the activity of the mutants was determined to be 20% for T202A and 5% for

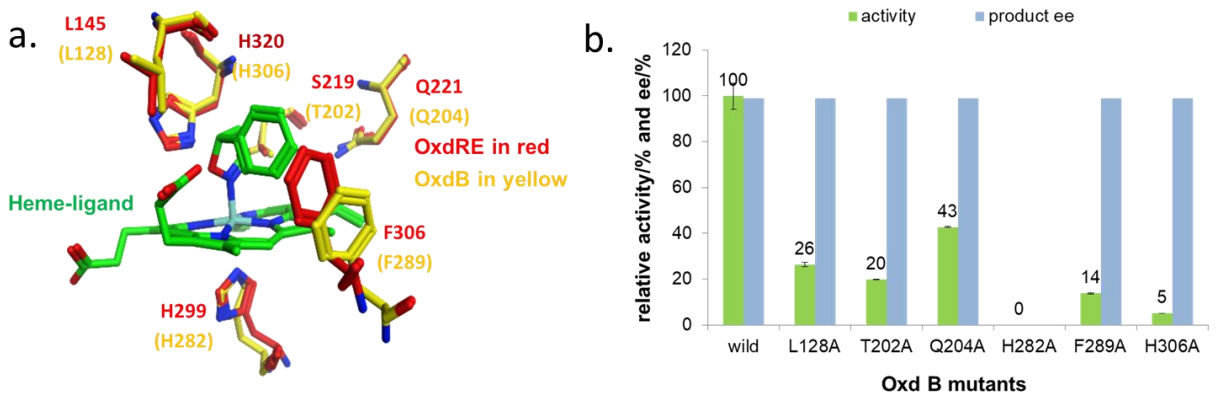

Fig 17. (a) Oxd B homology model and superposition to Oxd RE structure docking with substrate **1a**; (b) Comparison of the Oxd B mutants' activity for substrate **1a**. The reactions were performed on a 500 µL scale using 100 mM KPB buffer (pH 6.0), 2 µg of Oxd-B mutants, 20 mM 5-phenyl-4, 5-dihydroisoxazole, 0.05 mM FMN, and 1 mM $Na_2S_2O_5$ at 30 °C for 10 min. The yield and *ee* were determined using chiral HPLC (n = 2).

H306A when compared with wild-Oxd B (**Fig. 17b**), which is similar to that reported in the Kemp elimination reaction (*118*). To confirm the transformation in mutant of H306A, the amount of Oxd B-H306A was increased 10-fold , and the product could be obtained in 3.8% yield and 99% *ee* over 10 min, 21% yield and 95% *ee* in 1 h, respectively. This implied a discriminating catalytic mechanism between the ring-opening of dihydroisoxazole and aldoxime dehydration reactions(*125*). It seems that the ring-strain in dihydroisoxazole could facilitate the cleavage of the N-O bond via redox of ferrous-Heme without the assistance of the other residues (T202 and H306 in the (Z)-phenylacetaldoxime dehydration reaction), even though its catalytic efficiency was slower than that observed under the assistance of the other residues. In particular, weak activity was detected for H306A, which is thought to play an important role in the next deprotonation step to form the nitrile triple-bond (**Scheme 9a**). This suggests that in addition to the efficient deprotonation step by histidine (H306), it may have another route for deprotonation, which we refer to as the oxygen anion deprotonation pathway. After ring-opening upon attack of the ferrous-Heme, the resulting oxygen anion will approach the hydrogen atom of H-C=N- (via single bond rotation) followed by deprotonation and electron transfer back to ferric-Heme to produce the active state of ferrous-Heme, which undergoes the next catalytic cycle (**Scheme 9b**). We also noticed that the product *ee* did not change significantly in the presence of any mutants.

This reveals the cooperative control of the enantioselectivity with the surrounding residues of the Heme, not only from certain residues in the catalytic pocket.

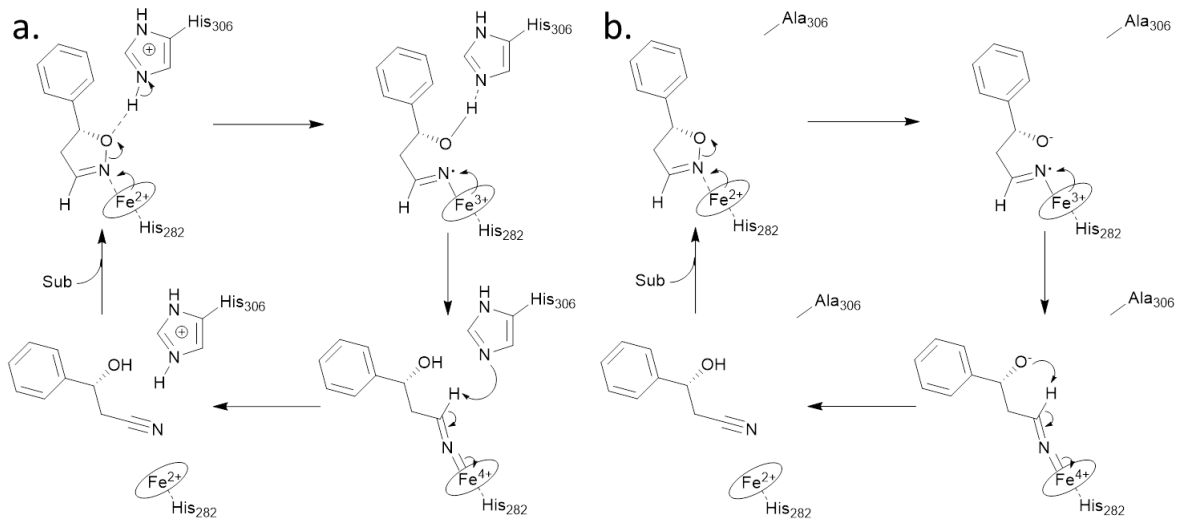

Scheme 9. Proposed reaction mechanism for Oxd B-wild (a) and oxd B-H306A (b).

To verify the practicability of this novel method in organic synthesis, a preparative scale reaction of 5-phenyl-4, 5-dihydroisoxazole (**1a**) was performed at 30 °C using 5 mmol of substrate, 0.25 mM FMN, 500 U Oxd B, and 5 mM $Na_2S_2O_5$ in 50 mL KPB (pH 6.0, 100 mM) stirred slowly for 2 h. After purification by silica gel column chromatography, (*R*)-3-hydroxy-3-phenylpropanenitrile (***R*-2a**) was isolated in 42% yield and 99% *ee*, and (*S*)-5-phenyl-4,5-dihydroisoxazole (***S*-1a**) was isolated in 48% yield and 99% *ee*. The obtained (*S*)-5-phenyl-4,5-dihydroisoxazole (***S*-1a**) was transformed into (*S*)-3-hydroxy-3-phenylpropanenitrile (***S*-2a**) in 95% yield and 94% *ee* upon treatment with 2% NaOH methanol solution (10 mL) for 30 min (**Scheme 10**).

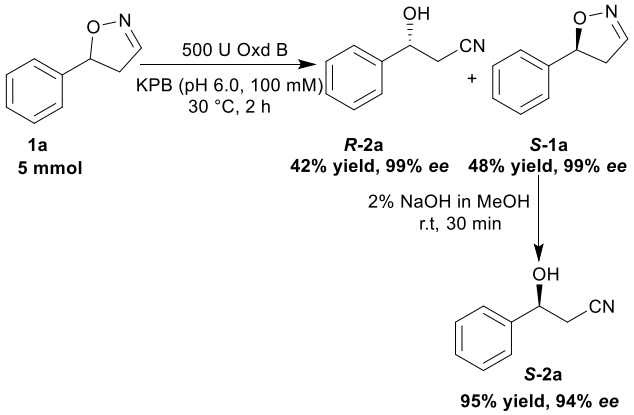

Scheme 10. Preparative scale reaction using substrate **1a** with Oxd B. The reaction was performed on a 50 mL scale using 100 mM KPB buffer (pH 6.0), 500 U Oxd B, 100 mM 5-phenyl-4,5-dihydroisoxazole, 0.25 mM FMN, and 5 mM $Na_2S_2O_5$ at 30°C for 2 h. The isolated yield was calculated after purification by silica gel column chromatography and the *ee* was determined by chiral HPLC.

In addition, for the assay of absolute configuration of **2e**, **2g**, **2k** and **2l**, 50 mL large scale reactions were performed with 5 mmol corresponding substrates, 0.25 mM FMN, 5 mM fresh $Na_2S_2O_5$ and 500 U Oxd B in 100 mM KPB (pH 6.0) at 30 °C for 2 h (slowly stirred by magnetic bar). The products were extracted by ethyl acetate, following with solvent removing in vacuum and the residue was applied for silica gel column chromatography purification (**Table 6**).

Table 6: Large scale reaction catalyzed by Oxd B.

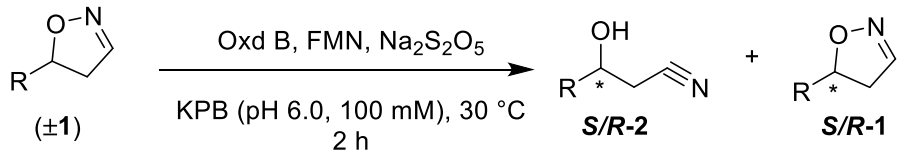

substrate	*S/R*-2	*S/R*-1
R = 2-Cl-phenyl (**1e**),	yield 13%, ee 96% (R)	yield 61%, ee 32%(S)
4-Cl-phenyl (**1g**),	yield 13%, ee 99% (R)	yield 64%, ee 31%(S)
n-propyl (**1k**),	yield 21%, ee 98% (S)	yield 32%, ee 58%(R)
n-butyl (**1l**)	yield 35%, ee 98% (S)	yield 39%, ee 77%(R)

The isolated β-alcohol nitriles were derived with (*R*)-MTPA-Cl and (*S*)-MTPA-Cl using pyridine as base in dichloromethane to produce corresponding (*S*)-MTPA-ester and (*R*)-MTPA-ester. The products were purified by silica-chromatography and applied for ^{1}H NMR analysis. The compound configuration was deduced by the proton relative chemical shift in ^{1}H NMR data as the model established in published literature (*143*). When the substrate group locates at the same side with phenyl group of MTPA, a smaller chemical shift was observed because of the shielding effect. And same shielding effect of phenyl on the substrate to the -OMe group in MTPA was also observed. The NMR spectra results were shown in appendices (**Appendix II**).

Chapter III. A cyanide-free biocatalytic process for synthesis of complementary enantiomers of 4-chloro-3-hydroxybutanenitrile from allyl chloride

Chiral 4-chloro-3-hydroxybutanenitrile is a versatile building block for the synthesis of *L*-carnitine (*146*) and Atorvastatin (*147-149*). Significant efforts have been made to synthesize this compound mainly focused on the regioselective addition of cyanide to epichlorohydrin (*150-152*). The enzymatic methods for preparation of chiral epichlorohydrin (*153*) include the enantioselective oxidation of allyl chloride catalysed by chloroperoxidase (*154*), enantioselective ring-closure of dichloropropanol catalysed by halohydrin dehalogenase (*147, 155, 156*), kinetic resolution catalyzed by epoxide hydrolase (*157-159*) (**Scheme 11A**). In addition, a microbial resolution method for producing chiral 4- chloro-3-hydroxybutanenitrile has also been reported via enantioselective dehalogenation on the racemic substrate (*160*). Most of these enzymatic methods inevitably use highly toxic cyanide as nucleophilic reagent to construct the nitrile group. However, in 1973, a cyanide-free strategy for accessing β-hydroxy nitriles, by treating the methyl 4, 5-dihydroisoxazole-5-carboxylate with trimethylamine, was reported (*134*). Subsequently, isomerization of 4, 5-dihydroisoxazoles to the corresponding β-hydroxy nitriles was reported using a variety of alkali conditions, such as alkanethiolate(*137*), sodium methoxide(*136*), DBU(*135*), alumina (*161*). Moreover, the synthesis of the 4, 5-dihydroisoxazoles mainly involved two methods: one is [3+2] cycloaddition of nitrile oxides with alkenes (*131, 162*), which is a popular method to construct 2-isoxazoline ring except for that it's lack of chirality control strategies on chiral 2-isoxazoline compounds synthesis; another one is conjugate addition of oximes with α, β-unsaturated aldehydes (*132, 135, 163, 164*), which is an ideal synthetic route to synthesize chiral 2-isoxazoline compounds if the availability and cost of starting materials are not taken into consideration. The first method enables the efficient synthesis of racemic β-hydroxy nitriles via a 2-isoxazoline motif from readily available alkenes in a cyanide-free reaction; however, the lack of chirality controlling means limits its application in asymmetric synthesis of chiral β-hydroxy nitriles. To solve this problem, in the chapter II, we reported an aldoxime dehydratase catalyzed kinetic resolution method for the synthesis of chiral β-hydroxy nitriles from racemic 2-isoxazolines substrates (*165*). In the substrate scope investigation, we found that all three enzymes exhibited poor enantioselectivity on aliphatic substrates, restricting its application on aliphatic β-hydroxy nitriles synthesis. Considering the

usefulness of chiral 4-chloro-3-hydroxybutanenitrile as a versatile building block in pharmaceuticals synthesis, we developed an efficient biocatalyst for the asymmetric synthesis of this compound by enzyme engineering (**Scheme 11B**).

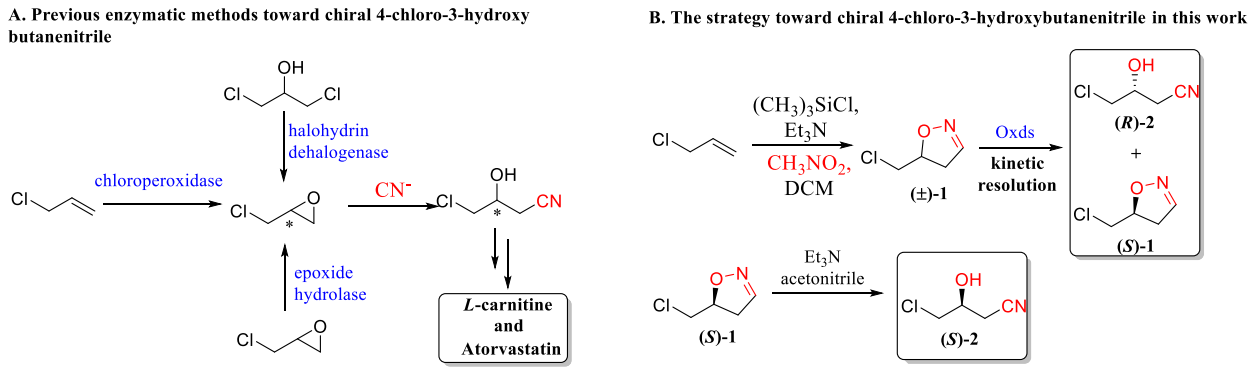

Scheme 11. (A). The enzymatic routes to chiral 4-chloro-3-hydroxybutanenitrile; (B). The proposed cyanide-free strategy to complementary enantiomers of 4-chloro-3-hydroxybutanenitrile in this work.

General remarks

Reagents were purchased from commercial sources and were directly used unless otherwise noted. The reaction process was monitored by TLC. ^{1}H NMR and ^{13}C NMR (400 and 100 MHz, respectively) spectra were recorded in $CDCl_3$ and DMSO-d_6. ^{1}H NMR chemical shifts are reported in ppm relative to tetramethylsilane (TMS) with the solvent resonance employed as the internal standard ($CDCl_3$ at 7.26 ppm, DMSO-d_6 at 2.50 ppm). Data are reported as follows: chemical shift, multiplicity (s = singlet, br s = broad singlet, d = doublet, t = triplet and m = multiplet), coupling constants (Hz) and integration. ^{13}C NMR chemical shifts are reported in ppm relative to tetramethylsilane (TMS) with the solvent resonance as the internal standard ($CDCl_3$ at 77.16 ppm). Silica gel column chromatography was performed with Merck silica gel 60 (200-300 mesh) as column material. TLC analysis was performed with precoated Silica Gel 60 F254 TLC-plate and the compounds were staining in alkali $KMnO_4$ solution.

Experimental procedures

Site-saturated mutagenesis and screening

The site-saturated mutagenesis of OxdA was performed using the PrimeSTAR® Mutagenesis Basal kit (Takara) with forward and reverse primers of 27-mer oligonucleotide designed as the kit manual indicated. The PCR reaction was performed for 30 cycles: (denaturation 98°C/10 s,

annealing 55°C/15 s, elongation 72 °C/40 s). The amplified PCR product was purified by Wizard® SV gel and PCR clean-up system (Promega). The resulting PCR product was transformed into JM109 *E.coli* competent cell. Then the plasmids were extracted from the JM109 E.coli and transformed into $BL_{21}DE_3$ E.coli for expression. The colonies picked up from plate were inoculated into 96-well plate with 1 mL auto-induction medium, at 37 °C, 1000 rpm for 24 h. The cell were harvested by centrifugation (3, 000 rpm, 30 min, 4 °C) and re-suspended into 200 µL reaction mixture containing 100 mM KPB (pH = 7.0), 50 mM **(±)-1**, 4 mM $Na_2S_2O_4$ and 10% DMSO. The resulting reaction mixture was incubated at 30 °C, 1000 rpm for 5 h, followed by extraction using 250 µL ethyl acetate. The contents of substrate and product in the reaction mixture were evaluated by thin layer chromatography (TLC). The candidates were analyzed by gas chromatography after derivatization using triethylamine and acetyl chloride. The positive mutants were sequenced by Genetic Analyzer 3500 (ThermoFisher) using T7 promoter primer (5'-TAATACGACTCACTATAGGG-3') and T7 terminator primer (5'-ATGCTAGTTATTGCTCAGCGG-3').

Enzyme purification

The recombinants of $BL_{21}DE_3$-pET-28a-N-His-OxdA, $BL_{21}(DE_3)$-pET-22b-C-His-Oxd-B and $BL_{21}(DE_3)$-pET-28a-N-His-Oxd RE were cultivated in the same way as previous work (*165*). The enzymes were purified with minor modification. The recombinant cells were harvested by centrifugation (6, 000 ×*g*, 15 min, 4 °C) and the pellet was re-suspended into lysis buffer (20 mM Tris-HCl, 300 mM NaCl, 20 mM imidazole, pH 8.0), which was applied to sonication (ice-bath, 15 min) for cell disruption. The debris was removed by centrifugation (20,000 × *g*, 30 min, 4 °C) and the supernatant was loaded onto Ni Sepharose™ 6 Fast flow column (GE Healthcare) equilibrated by lysis buffer (20 bed volumes). The unbound protein was washed with lysis buffer (30 bed volumes) and the bound protein was eluted by elution buffer (20 mM Tris-HCl, 300 mM NaCl, 300 mM imidazole, pH 8.0), the active fractions were pooled and dialyzed against 20 mM KPB (pH 7.0, 5 L, 4 °C). Then the resulting enzyme solution was loaded onto the manual Toyopearl DEAE-650M column (TOSOH BIOSCIENCE), which was equilibrated by equilibration buffer (20 mM KPB, pH 7.0, 10 bed volumes). After loading the sample, the unbounded protein was washed by equilibration buffer (5 bed volumes), following with further washing by 6 bed volume of 10% elution buffer (20 mM KPB, pH 7.0, 500 mM NaCl)/90%

equilibration buffer. Then the bound protein was eluted by 6 bed volume of 20% elution buffer/80% equilibration buffer, 6 bed volume of 30% elution buffer/70% equilibration buffer, 6 bed volume of 40% elution buffer/60% equilibration buffer. The purity of the fractions was checked by SDS-PAGE containing 12% acrylamide, and pure fractions were pooled and dialyzed against KPB (20 mM, pH 7.0, 5 L ×2).

Activity assay and reaction analysis by GC

The purified OxdA and its mutant were measured with appropriate amount of enzyme containing 10 mM **(±)-1**, 10% DMSO, 5 mM $Na_2S_2O_4$, 100 mM KPB (pH 7.0) in 500 μL, which was incubated at 30 °C for 5 min and followed by addition of 100 μL 6 N HCl to quench the reaction. The resulting solution was extracted using 900 μL ethyl acetate containing 20 mM octanenitrile as internal standard substance. The mixture was centrifuged at 12,000×*g* for 1 min, 500 μL supernatant was used for gas chromatograph analysis (Shimadazu gas chromatograph equipped with BGB-174 column (BGB Analytic), carrier gas: He, flow rate: 50 mL/min, detector temperature: 230°C, temperature program: 100 °C-2 min, 10 °C/min to 160 °C, 20 °C/min to 200 °C, 200 °C-10 min. Retention time for **(*R*)-1** is 10.393 min and 10.676 min for **(*S*)-1**. 1 U enzyme was defined as the amount of enzyme to consume 1 μmol substrate in 1 min. The kinetic parameters for (R) and (S) configuration of the substrate were measured in the same way using racemic substrate with substrate concentration varying from 0.5 mM to 50 mM. The initial reaction velocity at each concentration was measured by monitoring the reaction at different time.

For whole cell activity assay, the reaction was performed in 2 mL containing 100 mM **(±)-1**, 25% DMSO, 20 mM $Na_2S_2O_4$, 100 mM KPB (pH 7.0) and 10 mg lyophilized whole cell. The reaction mixture was stirred in 400 rpm at room temperature and monitored by GC analysis within 6 min.

The product 4-chloro-3-hydroxybutanenitrile **(±)-2** can't be separated in the GC analysis condition described above, the retention time for both **(*R*)-2** and **(*S*)-2** are 14.820 min. To measure the *ee* of the product, it was needed to transform 4-chloro-3-hydroxybutanenitrile **(±)-2** into corresponding 1-chloro-3-cyanopropan-2-yl acetate **(±)-3** by derivatization using triethylamine and acetyl chloride as the reagents. The retention time for (*R*)-1-chloro-3-cyanopropan-2-yl acetate (**(*R*)-3**) is 11.551 min and for (*S*)-1-chloro-3-cyanopropan-2-yl acetate

(**(*S*)-3**) is 11.355 min. The absolute configuration of product was confirmed using commercial chiral 4-chloro-3-hydroxybutanenitrile compounds (TCI).

Substrate concentration effect on enzyme activity

The reactions were performed in 400 µL mixture containing 10 mM-250 mM of **(±)-1**, 2 U of OxdA-L318I, 10% DMSO, 5 mM $Na_2S_2O_4$, 100 mM KPB (pH 7.0), and incubated at 30 °C for 30 min. The conversion and enantiomeric excess of substrate were detected using GC.

Synthesis of 5-(chloromethyl)-4,5-dihydroisoxazole (±)-1 compound (*131*)

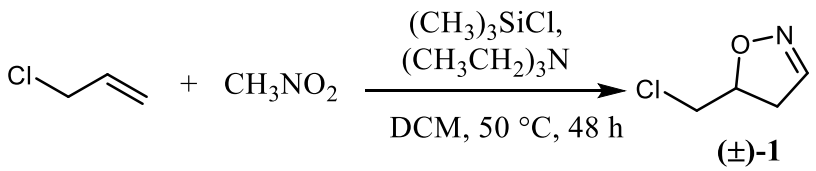

To 600 mL dichloromethane, 18.3 g CH_3NO_2 (300 mmol), 30.3 g $(CH_3CH_2)_3N$ (300 mmol) were added. The resulting mixture was incubated in ice-bath, followed with addition of 32.6 g $(CH_3)_3SiCl$ (300 mmol) and 15.32 g allyl chloride (200 mmol). Then the mixture was stirred at room temperature overnight, followed with refluxing at 50 °C for 48 h. Before work-up, the mixture was cooled down in ice-bath followed with 300 mL DIW addition. The dichloromethane layer was dried against anhydrous $MgSO_4$ and concentrated in vacuum. The residue was purified using silica column chromatography (ethyl acetate/Hexane=1/5 to 1/3). The target product 5-(chloromethyl)-4, 5-dihydroisoxazole **(±)-1** was purified in light yellow oil with 22% yield (5.3 g). The NMR spectra were shown in **Appendix III.** ^{1}H NMR (400 MHz, $CDCl_3$) δ 7.14 (t, 1H), 4.85 – 4.71 (m, 1H), 3.60 (dd, *J*=11.4, 4.5, 1H), 3.49 (dd, *J*=11.3, 6.8, 1H), 3.14 (ddd, *J*=17.9, 10.7, 1.7, 1H), 2.97 (ddd, *J*=17.9, 6.4, 1.8, 1H). ^{13}C NMR (100 MHz, $CDCl_3$) δ 145.73, 77.15, 44.84, 39.01. HRMS (ESI): calcd for C4H7ClNO $[M + H]^+$, 120.0211, found: 120.0211; calcd for C4H6ClNNaO $[M + Na]^+$, 142.0030, found: 142.0030.

Synthesis of 4-chloro-3-hydroxybutanenitrile (±)-2 compound (*134*)

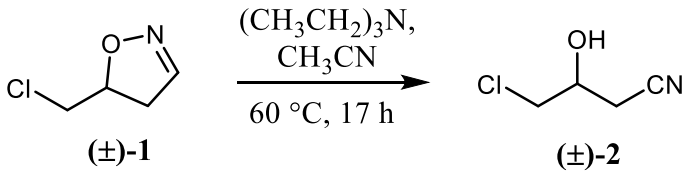

To 10 mL CH_3CN solution, 1.195 g 5-(chloromethyl)-4, 5-dihydroisoxazole (10 mmol) and 202 mg $(CH_3CH_2)_3N$ (2 mmol, 0.2 eq) were added. The resulting solution was heated in 60 °C for 17 h. After cooling down, 30 mL 1 M HCl was added, the resulting solution was extracted using ethyl acetate (20 mL×3). Then the ethyl acetate layer was dried against anhydrous $MgSO_4$ and concentrated in vacuum. The residue was purified by silica chromatography (ethyl acetate/Hexane=1/3). The target product **(±)-2** was isolated in light-yellow oil with 88% yield (1.05 g). The NMR spectra were shown in **Appendix III.** ^{1}H NMR (400 MHz, $CDCl_3$) δ 4.24-4.18 (m, 1H), 3.66 (d, J = 5.3 Hz, 2H), 3.25 (s, 1H), 2.76 (dd, J = 16.8, 5.3 Hz, 1H), 2.70 (dd, J = 16.8, 6.4 Hz, 1H). ^{13}C NMR (100 MHz, $CDCl_3$) δ 116.90, 67.35, 47.36, 23.28. HRMS (ESI): calcd for C4H6ClNNaO $[M + Na]^+$, 142.0030; found: 142.0032.

Biotransformation and product isolation

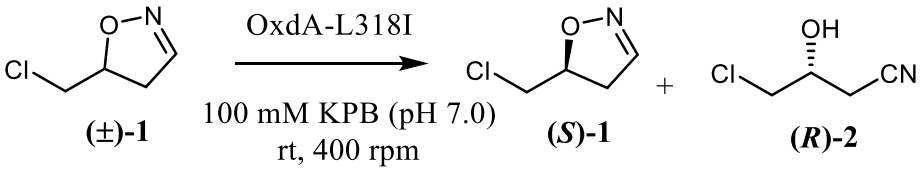

In the gram-scale reactions, the reactions were carried out in 40 mL reaction mixture containing 1.19 g **(±)-1**, 25% DMSO, 100 mM KPB (pH 7.0), 20 mM $Na_2S_2O_4$, 250 U enzyme or 65 mg lyophilized whole cell (5 U/mg). The reaction was performed at room temperature with stirring at 400 rpm. In the scheduled time, the reaction was stopped by addition of 5 mL 6 N HCl and extracted by 50 mL×3 ethyl acetate or diethyl ether. The organic solvent layer was dried against anhydrous $MgSO_4$, followed by concentration in vacuum, the residue was purified by silica column chromatography (ethyl acetate/hexane=1/3). The NMR spectra were shown in **Appendix III**. The *ee* of **(*S*)-1** was measured by GC directly and the *ee* of **(*R*)-2** was measured by mixing 2 μL of **(*R*)-2**, 11.2 μL $(CH_3CH_2)_3N$ and 7.1 μL CH_3COCl in 100 μL dichloromethane followed with addition of 500 μL of DIW and 900 μL ethyl acetate. The resulting solution was centrifuged in 20, 000×*g* for 1 min. 500 μL supernatant was used for GC analysis. (**Appendix IV)**.

(*S*)-1: 99% *ee*, 39% isolated yield, $[\alpha]_D^{25}$=+180.90 (c 1.00, MeOH), ^{1}H NMR (400 MHz, $CDCl_3$) δ 7.16 (t, 1H), 4.83-4.76 (m, 1H), 3.63 (dd, *J* = 11.3, 4.4 Hz, 1H), 3.50 (dd, *J* = 11.3, 7.1 Hz, 1H), 3.16 (ddd, *J* = 17.9, 10.7, 1.7 Hz, 1H), 3.00 (ddd, *J* = 17.9, 6.4, 1.9 Hz, 1H). ^{13}C NMR (100 MHz, $CDCl_3$) δ 145.63, 77.20, 44.73, 39.06. **(*R*)-2:** 90% *ee*, 39% isolated yield, ^{1}H NMR (400 MHz, $CDCl_3$) δ 4.28 – 4.14 (m, 1H), 3.66 (d, *J* = 5.3 Hz, 2H), 3.28 (s, 1H), 2.76 (dd, J = 16.8, 5.4 Hz, 1H), 2.70 (dd, J = 16.8, 6.4 Hz, 1H). ^{13}C NMR (100 MHz, $CDCl_3$) δ 116.90, 67.35, 47.36, 23.28.

Chiral (*S*)-4-chloro-3-hydroxybutanenitrile synthesis

5.1 Chemical reaction

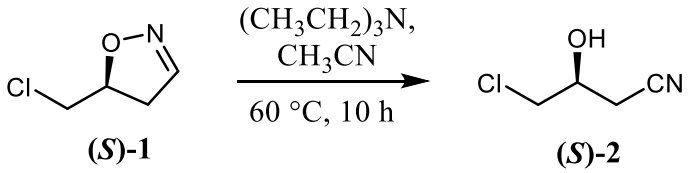

To 1 mL CH_3CN solution, 119.5 mg (*S*)-5-(chloromethyl)-4, 5-dihydroisoxazole (99% *ee*, 1 mmol) and 20.2 mg $(CH_3CH_2)_3N$ (0.2 mmol, 0.2 eq) were added. The resulting solution was heated in 60 °C for 10 h. After cooling down, 3 mL 1 M HCl was added, the resulting solution was extracted using ethyl acetate (10 mL×3). Then the ethyl acetate layer was dried against anhydrous $MgSO_4$ and concentrated in vacuum. The residue was purified by silica chromatography (ethyl acetate/Hexane=1/3). The target product **(*S*)-2** was isolated in light-yellow oil with 72% yield (86 mg) and 99% *ee* (**Appendix IV-6**). The NMR spectra were shown in **Appendix III**. ^{1}H NMR (400 MHz, $CDCl_3$) δ 4.27 – 4.13 (m, 1H), 3.66 (dd, *J* = 5.3, 0.7 Hz, 2H), 3.26 (s, 1H), 2.75 (dd, *J* = 16.8, 5.4 Hz, 1H), 2.70 (dd, J = 16.8, 6.5 Hz, 1H). ^{13}C NMR (100 MHz, $CDCl_3$) δ 116.91, 67.35, 47.36, 23.28.

5.2 Enzymatic reaction

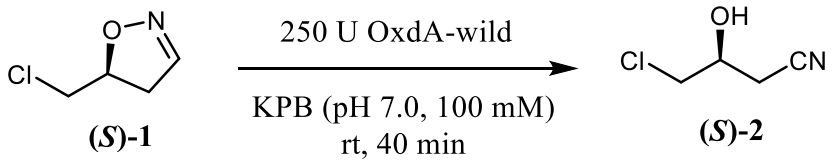

The reactions were carried out in 4 mL reaction mixture containing 119 mg **(*S*)-1**, 25% DMSO, 100 mM KPB (pH 7.0), 20 mM $Na_2S_2O_4$, 250 U of OxdA-wild enzyme. The mixture was stirred at 400 rpm in room temperature. The reaction was stopped in 40 min by addition of 5 mL 6 N HCl and extracted by 50 mL×3 diethyl ether. The organic solvent layer was dried against anhydrous $MgSO_4$, followed by concentration in vacuum, the residue was purified by silica column chromatography (ethyl acetate/hexane=1/3). The target product **(*S*)-2** was isolated in light-yellow oil with 88% yield (105 mg) and 99% *ee* (**Appendix IV-2**). The NMR spectra were shown in **Appendix III**. ^{1}H NMR (400 MHz, $CDCl_3$) δ 4.27 – 4.15 (m, 1H), 3.67 (dd, *J* = 5.2, 2.1 Hz, 2H), 2.85 (s, 1H), 2.74 (dd, *J* = 15.9, 4.7 Hz, 1H), 2.69 (dd, *J* = 15.9, 5.4 Hz, 1H). ^{13}C NMR (100 MHz, $CDCl_3$) δ 116.60, 67.42, 47.50, 23.27.

Results and Discussion

First, the precursor of **(±)-1** was synthesized using [3+2] cycloaddition of silyl nitronate with allyl chloride by minor modification of the published method (*131*). And the **(±)-2** was synthesized in 88% yield from **(±)-1** by treating it with triethylamine in acetonitrile. However, the desired product was not obtained when NaOMe or K_2CO_3 were used as alkali reagents in the ring-opening reaction for **(±)-2** synthesis. Under these conditions, a by-product with higher polarity than the target product was mainly formed, which may be caused by the instability of 4-chloro-3-hydroxybutanenitrile in strong alkali conditions (*150*).

Next, three aldoxime dehydratases (OxdA, OxdB, OxdRE) were selected for testing the enantioselective ring scission of 5-(chloromethyl)-4, 5-dihydroisoxazole. A number of subsequent studies established that all these three enzymes exhibited better enantioselectivity on aromatic substrates as compared to aliphatic substrates in the asymmetric synthesis of nitriles from achiral aldoxime precursors. However, for aliphatic chiral nitriles synthesis, the OxdA showed better selectivity than OxdB and OxdRE (*113-117, 166*).

The tested results on this new reaction showed that all three enzymes are active on the selective N-O bond cleavage of the precursor **(±)-1** and prefer *R* configuration rather than *S* configuration. This means **(*R*)-2** and **(*S*)-1** are produced in the kinetic resolution of racemic substrate **(±)-1**.

Table 7. The kinetic parameters for Oxds on the kinetic resolution of (±)-1.

Enzymes [a]	k^{R}_{cat} (S^{-1})[b]	K^{R}_{M} (mM)	k^{S}_{cat} (S^{-1})[c]	K^{S}_{M} (mM)	E[d]
OxdA	**173.2**	**9.6**	**12.7**	**7.6**	**10.8**
OxdA-L318I	**193**	**13.1**	**1.9**	**8.8**	**68.2**
OxdB	**26.8**	**14.1**	**5.4**	**9.5**	**3.3**
OxdRE	**4.2**	**3.1**	**2.9**	**5.1**	**2.4**

[a] The racemic **(±)-1** was used for determination by monitoring the consumption of R/S substrate and the details were available in experimental section. [b] R means for R configuration of substrate. [c] S means for S configuration of substrate. [d] $E=(k^{R}_{cat}/K^{R}_{M})/(k^{S}_{cat}/K^{S}_{M})$. (*167*)

Among them, the OxdA can catalyse the reaction with the highest velocity (k_{cat}^{R} =173.2 s^{-1}, k_{cat}^{S}=12.7 s^{-1}) as compared to OxdB (k_{cat}^{R}=26.8 s^{-1}, k_{cat}^{S}=5.4 s^{-1}) and OxdRE (k_{cat}^{R}=4.2 s^{-1}, k_{cat}^{S}=2.9 s^{-1}). However, the enantiomeric ratio of all three enzymes are not very high, the best enantiomeric ratio was obtained from the OxdA and was only E=11 (**Table 7**). In kinetic resolution, the low enantiomeric ratio of the enzyme restricts its application on the chiral product synthesis, but the enzyme can be exploited to produce the substrate in high enantiopurity at the expense of yield (*168*). To improve the practicality of this method in asymmetric organic synthesis, site-saturated mutagenesis of OxdA on the residues around the substrate was carried out to screen positive mutants possessing better enantiomeric ratio (E) on this kinetic resolution.

From the docking simulation of OxdA with **(*R*)-1** and **(*S*)-1** using MOE platform (**Fig. 18**), we found that they were bound in the catalytic pocket in different orientations, which resulted in the different distance of oxygen (O1) in the substrate to His320-Nδ. However, in aldoxime dehydration reaction mechanism, the first step is protonation of hydroxyl group in aldoxime by proton migration from Nδ of His320 (*125*). The distance of Nδ to the O1 in **(*R*)-1** (3.2 Å) is much closer than that in **(*S*)-1** (4.2 Å) (Figure 1), which suggests the **(*R*)-1** is the preferred substrate of OxdA rather than **(*S*)-1**. If the substrate can twist more in clockwise direction, the distance of O1 in **(*S*)-1** to His320-Nδ will further increase and may result in a decrease in activity. Based on this tentative idea, the residues of Met29, Leu145, Ala147 and Leu318, which are located around the 5-chloromethyl group of the substrate, were selected as the targets for saturated mutagenesis. Compared to the wild type enzyme, several positive mutants of M29N, L318I and L318T were obtained from the initial screening by GC analysis. Then the best mutant of L318I was purified and its kinetic parameter, enantiomeric ratio were measured (**Table 7**). As shown in table 7, the significant difference between the OxdA-wild (k_{cat}^{S}=12.7 s^{-1}) and OxdA-L318I (k_{cat}^{S}=1.9 s^{-1}) is the k_{cat} value for the S configuration of substrate. An approximately 6-fold decrease in activity was determined, which resulted in about 6-fold improvement of enantiomeric ratio E (E=68) on the kinetic resolution of **(±)-1**. At the same 50% conversion rate, the substrate ee using OxdA-L318I as catalyst was significantly improved from 72% to 88% as compared to the use of OxdA-wild type as catalyst.

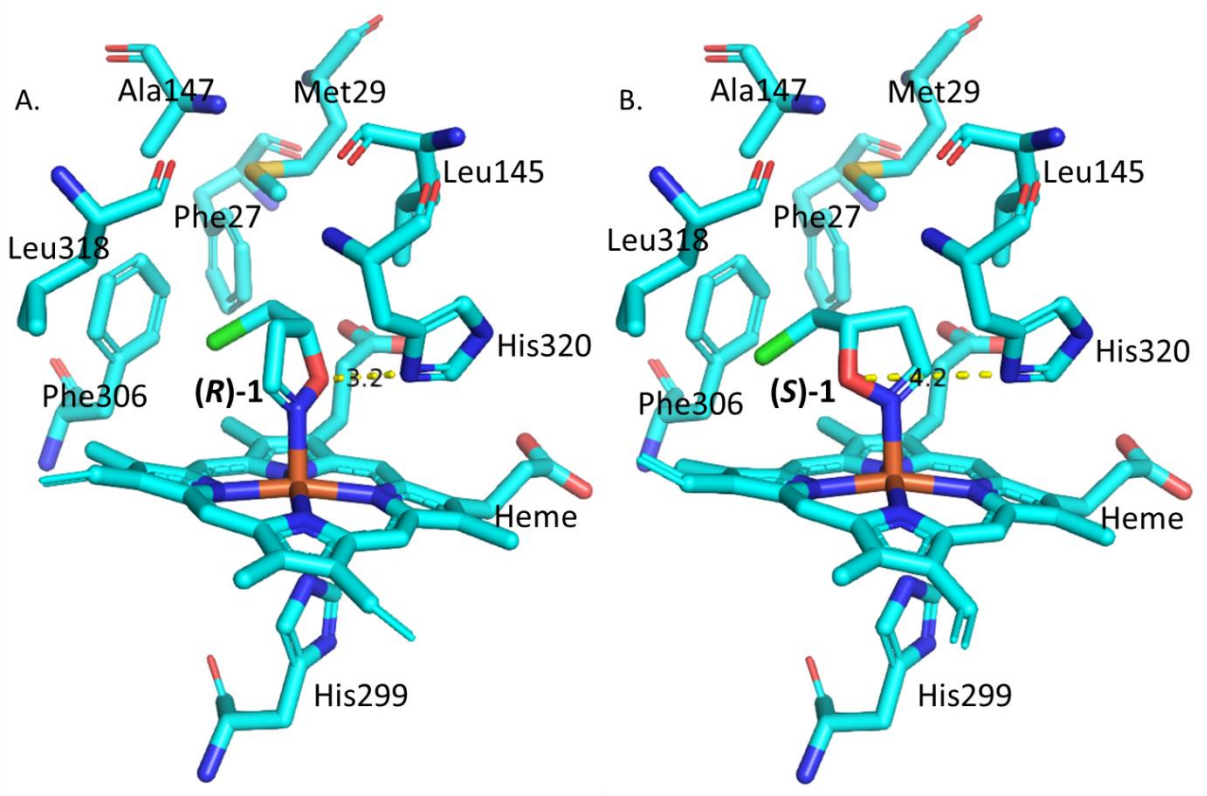

Fig 18. (A). Docking simulation of (R)-1 with OxdA; (B). Docking simulation of (S)-1 with OxdA.

The optimization of the reaction conditions showed that the OxdA-L318I can tolerate a maximum of 30% DMSO in the reaction mixture with approximately 77% residual activity compared with the non-DMSO addition (100% activity). However, the addition of DMSO greatly improved the *ee* of substrate and product as shown in the **Table 8**, which may be due to the better dispersion of substrate in the presence of DMSO. Without the addition of co-solvent DMSO, the substrate tends to aggregate together to form oil droplets in a pure water solvent, and the static reaction mode further deteriorates the mass transfer process. Moreover, the reductive additive is essential to recover enzyme activity from inactive state (*139, 169*). In this work, the reductant $Na_2S_2O_4$, which has been identified as the best reductive additive for OxdA (*165*), was used in the experiments. As shown in the **Table 8**, no any inhibitory effect on the enzyme activity was observed up to 50 mM $Na_2S_2O_4$, and slight activity enhancement was detected with the increase of $Na_2S_2O_4$ concentration. In the absence of $Na_2S_2O_4$, almost no activity can be detected, which implies that the reaction occurred in a ferrous-Heme catalytic pocket, as previously reported (*118, 165, 169*). Furthermore, no substrate inhibition effect was observed up

to 250 mM substrate concentration, which suggests the feasibility of this method in asymmetric organic synthesis.

Table 8. DMSO and $Na_2S_2O_4$ effects on enzyme activity

Entry[a]	DMSO[b] content/%	$Na_2S_2O_4$ conc/mM	*ee* of substrate/%[c]	Conv/%[d]
1	0	5	46	70
2	10	5	97	67
3	20	5	96	62
4	30	5	86	54
5	40	5	1	0
6	50	5	0	0
7	10	0	1	0
8	10	10	99	76
9	10	20	99	76
10	10	30	98	77
11	10	40	99	79
12	10	50	99	80

[a] The reactions were performed in 400 μL mixture containing 100 mM of **(±)-1**, 10 U of OxdA-L318I, 100 mM KPB (pH 7.0), and incubated at 30 °C for 30 min. [b] The content of DMSO is volume ratio (V/V). [c] The *ee* of the substrate was measured by GC. [d] The conversion of the substrate was measured by GC.

Though the enantiomeric ratio of mutant OxdA-L318I (E=68) improved 6-fold as compared to the wild type, it was still not as effective as E=∞. To quench the reaction at a proper time is an effective mean to synthesize chiral substrate or chiral product with acceptable yield when the enantiomeric excess has been improved to the desired value. Therefore, the reaction was monitored for 3 h and the results showed that 98% *ee* of **(*R*)-2** could be obtained, but in low yield of 16%. With an acceptable 47% conversion, **(*R*)-2** and **(*S*)-1** were formed with 90% *ee* and 80% *ee* in 10 min, respectively. To produce **(*S*)-1** with 99% *ee*, the reaction can be stopped at 30 min with 57% conversion and 74% *ee* of **(*R*)-2** remaining (**Fig. 19B**). This result was a significant

improvement over the use of OxdA-wild type as catalyst (**Fig. 19A**), in which the best result for **(*R*)-2** synthesis is 90% *ee* in 9% yield and for **(*S*)-1** is 99% *ee* in 34% yield, respectively.

In addition, it was noticed that the *ee* of product **(*R*)-2** decreased approximately 16% when the *ee* of substrate **(*S*)-1** increased from 80% to 99%, which is greatly different from the initial reaction stage in which the product *ee* decreased by only about 10% when the substrate *ee* increased from 0 to 80%. According to the time course of the reaction, it can be calculated that approximately 10 mM **(*R*)-1** and 119 mM **(*S*)-1** remained when the substrate *ee*

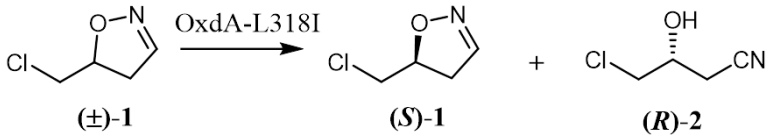

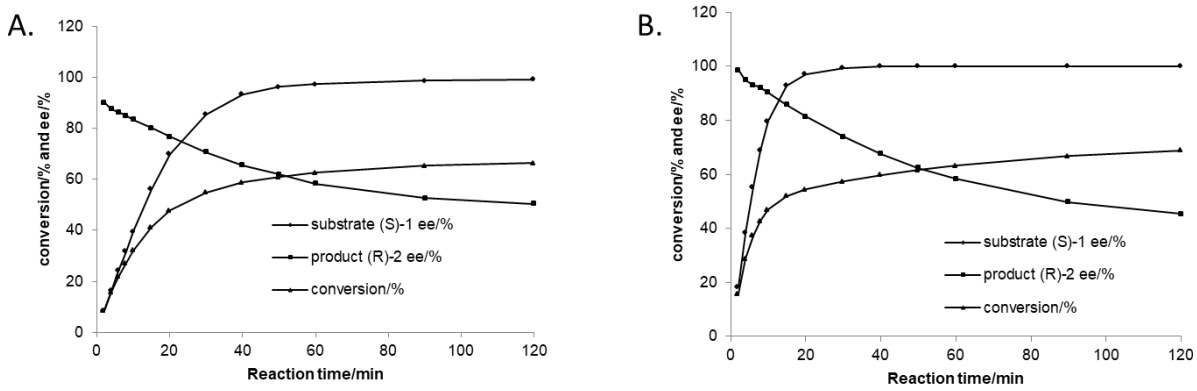

Fig 19. (A). The time course of the kinetic resolution of **(±)-1** catalysed by OxdA-wild. (B). The time course of the kinetic resolution of **(±)-1** catalysed by OxdA-L318I. The reactions were performed in 4 mL reaction mixture containing 250 mM substrate **(±)-1**, 25% DMSO, 25 U of enzymes, 100 mM KPB (pH 7.0), 20 mM $Na_2S_2O_4$, room temperature, stirred at 400 rpm. The substrate *ee* and product *ee* were assayed by GC and the conversion was evaluated by Conv=$ee_s/(ee_s+ee_p)$ (*168*).

increased to 80%. However, the K_M value of OxdA-L318I on R and S configurations of the substrate showed that the reaction velocity of **(*R*)-1** decreased to half of the maximum reaction velocity when **(*R*)-1** concentration decreased to 13.1 mM. This means when the substate *ee* reaches about 80%, the difference in reaction velocity for **(*R*)-1** and **(*S*)-1** will decrease, resulting in a significant decline on the *ee* value of **(*R*)-2** in the final stage of conversion to synthesize enantiopure **(*S*)-1** (*ee*>99%). Furthermore, it was also observed that the reaction velocity on **(*S*)-1** became faster when the competition from **(*R*)-1** became weaker, which further deteriorates the enantioselective conversion of the substrate in the final stage of reaction.

To verify the practicability of this method in asymmetric organic synthesis, gram-scale reactions were performed with 40 mL reaction mixture at different scheduled times. With a reaction time of 10 min, **(*R*)-2** was isolated in 39% yield with 90% *ee* and **(*S*)-1** was isolated in 50% yield with 83% *ee* by silica column chromatography (**Table 9, entry 1**). Alternatively, with a reaction time of 30 min, **(*S*)-1** was isolated in 39% yield with 99% *ee* and **(*R*)-2** was isolated in 47% yield with 80% *ee* by silica column chromatography (**Table 9, entry 2**). Furthermore, we attempted to carry out the reaction using lyophilized whole cell as catalyst in gram-scale reactions, which is a common reaction mode in industry. As summarized in **table 9**, **(*S*)-1** can be isolated with more than 96% *ee* when the reaction time was prolonged more than 2 h. In less than 1 h of reaction time, **(*R*)-2** can be obtained with more than 86% *ee* in the current reaction conditions.

Table 9. Gram-scale reactions using enzyme or whole cell as catalyst in different scheduled times.

Entry[a]	Catalyst[b]	Reaction time/min	(*S*)-1[c]		(*R*)-2[d]	
			Yield /%	*ee* /%	Yield /%	*ee* /%
1	enzyme	10	50	83	39	90
2	enzyme	30	39	99	47	80
3	cell	40	46	74	43	87
4	cell	60	37	80	44	86
5	cell	120	37	96	50	80
6	cell	180	30	99	53	69

[a] The details are available in biotransformation part of experimental section. [b] The catalysts are purified enzyme of OxdA-L318I or lyophilized whole cell of OxdA-L318I. [c] Isolated yield and the ee was detected using chiral GC. [d] Isolated yield and the *ee* was detected by chiral GC after derivatization using Et3N and CH_3COCl in dichloromethane.

In addition, **(*S*)-2** with 99% *ee* was successfully synthesized in 72% yield from enantiopure **(*S*)-1** by treating it at 60 °C with triethylamine in acetonitrile. Alternatively, it can be also achieved using OxdA-wild as catalyst with 100% conversion and without formation of any by-products at room temperature, in which the product can be easily isolated by a simple work-up process.

Conclusion

In this study, the author reveals a novel cyanohydrin decomposition mechanism, which makes a contribution on the enzymatic synthesis of ketone cyanohydrins by ketone cyanation. In addition, a novel enzymatic reaction is discovered for complementary enantiomers synthesis of chiral β-hydroxy nitriles, which makes it feasible to synthesize chiral β-hydroxy nitriles from alkenes without utilization of highly toxic cyanide. Moreover, a new biocatalyst with better enantioselectivity on the synthesis of chiral 4-chloro-3-hydroxybutanenitrile is developed by enzyme engineering.

Chapter I: Structural characterization of *Linum usitatissimum* hydroxynitrile lyase: a new cyanohydrin decomposition mechanism involving a cyano-zinc complex

In this chapter, the ligand-free 3D structure of *Lu*HNL and the structures of its complex formed with acetone cyanohydrin and (*R*)-2-butanone cyanohydrin were determined using X-ray crystallography. The structures reveal an A-form of NAD^+ molecule was tightly rather than covalently bound to each subunit of *Lu*HNL. The structure origin is a "sandwich-structure" on the adenine part of NAD^+, restraining the free movement of the NAD^+ molecule. Moreover, the structures and mutagenesis analysis reveal a novel reaction mechanism for cyanohydrin decomposition involving the cyano-zinc complex and hydrogen-bonded interaction of the hydroxyl group with Glu323/Thr65 and H_2O/Lys162. The deprotonated Lys162 and protonated Glu323 residues are presumably stabilized by a partially desolvated microenvironment. In general, the substrate-binding geometry of *Lu*HNL provides insights into the differences in activities of *Lu*HNL and ADH. Identifying this novel reaction mechanism is an important contribution to the study of hydroxynitrile lyases.

Chapter II. Biocatalytic asymmetric ring-opening of dihydroisoxazoles: a cyanide-free route to complementary enantiomers of β-hydroxy nitriles from olefins

In this chapter, a new application of aldoxime dehydratase in the asymmetric ring-opening of 5-sub-4, 5-dihydroisoxazoles to synthesize chiral β-hydroxy nitriles with broad substrate scope, excellent enantioselectivity (up to 99% *ee*), and good turnover number (up to 11 s^{-1}) was reported by combination of the cyanide-free synthesis of chiral nitriles and the Kemp elimination reaction catalyzed by aldoxime dehydratases. Upon simple isolation and treatment with an

alkaline reagent, the remaining chiral 5-sub-4, 5-dihydroisoxazoles can be easily transformed into their corresponding β-hydroxy nitriles. Using site-directed mutagenesis, a ferrous Heme-containing active site was confirmed and two possible deprotonation pathways were proposed. To the best of our knowledge, this is the first enzymatic reaction used to construct a chiral hydroxyl group and nitrile group in one-step starting from a simple alkene, which provides a novel and useful strategy for the synthesis of complementary enantiomers of β-hydroxy nitriles.

Chapter III. A cyanide-free biocatalytic process for synthesis of complementary enantiomers of 4-Chloro-3-hydroxybutanenitrile from allyl chloride

In this chapter, a biocatalyst used for selective ring scission of (±)-5-(chloromethyl)-4, 5-dihydroisoxazole to synthesize chiral (*R*)-4-chloro-3-hydroxybutanenitrile (90% *ee*, 39% isolated yield) and (*S*)-5-(chloromethyl)-4, 5-dihydroisoxazole (99% *ee*, 39% isolated yield) was developed by site-saturated mutagenesis on aldoxime dehydratase derived from *Pseudomonas chlororaphis* B23 (OxdA). The positive mutant (OxdA-L318I, E=68) improved the enantiomeric ratio E by 6-fold as compared to the wild type enzyme (OxdA-wild, E=11). The racemic precursor of (±)-5-(chloromethyl)-4, 5-dihydroisoxazole, used in the reaction, can be synthesized from readily available allyl chloride without utilizing highly toxic cyanide. The enantiopure (*S*)-5-(chloromethyl)-4, 5-dihydroisoxazole remaining in the kinetic resolution can be transformed into corresponding chiral (*S*)-4-chloro-3-hydroxybutanenitrile without loss of enantiomeric excess by treating it with triethylamine in acetonitrile (99% *ee*, 72% isolated yield) or catalysis of OxdA-wild enzyme (99% *ee*, 88% isolated yield).

ACKNOWLEDGMENT

Time flies. The six-year doctoral research career is coming to an end. Looking back, everything seemed to occur yesterday. I vaguely remember the beautiful scenery on the journey from Zunyi to Toyama, and the excitement and anxiety along the way. Now I turned more than thirty years old, and finally it is the time to harvest. Looking at the photos under the Sakura tree pasted in the laboratory and recalling the little by little of nearly two thousand days, it's so sentimental at this moment.

During the six years of research career, I learned a lot and grew a lot. On the occasion of graduation, I would like to thank Prof. Asano sincerely for his careful guidance on my researches. In addition, I would like to thank Hibi sensei, Matsui sensei, Yamaguchi sensei, Iwasaki sensei and Kawakami sensei for their help on the experiments.

I would like to thank Dr. Metzner and Dr. Shichida for their help and encouragement in the darkest period of my PhD course; In addition, I would like to thank Dr. Zhai， Dr. Miao， Dr. Nakabayashi, Dr. Shinoda, Dr. Siriporn, Dr. Bo and Dr. Aem for their help on life and experiments.

I appreciate Kuchiki san and Morikawa san for their hard work on the daily affairs of laboratory. I would like to thank everyone in the laboratory for their kindly teaching in my Japanese learning and help in life. No matter you are studying or already worked, I sincerely wish you a better and better future!

I am grateful for the support from ERATO project and the Grant-in-Aid for Scientific Research (S) from the Japan Society for Promotion of Sciences.

At last，I would like to thank my family for their encouragement and support during these six years.

The Chapter I of this dissertation was reproduced from "D. Zheng, M. Nakabayashi and Y. Asano, *J. Biol, Chem*., 2022, in press, DOI: 10.1016/j.jbc.2022.101650" with permission from the American Society for Biochemistry and Molecular Biology.

The Chapter II of this dissertation was reproduced from "D. Zheng and Y. Asano, *Green Chem*., 2020, 22, 4930-4936, DOI: 10.1039/D0GC01445A" with permission from the Royal Society of Chemistry.

The Chapter III of this dissertation was reproduced from "D. Zheng and Y. Asano, *ChemCatChem*., 2021, 13, 4237–4242, DOI: 10.1002/cctc.202100835" with permission from the Chemistry Europe.

References

1. T.-L. Liu *et al.*, Cyano-borrowing: titanium-catalyzed direct amination of cyanohydrins with amines and enantioselective examples. *Chemical Communications* **56**, 651-654 (2020).
2. Z. Li, Z. Zhou, L. Wang, Q. Zhou, C. Tang, Enantioselective reaction of secondary alcohols with phthalimide in the presence of a chiral tri-coordinate phosphorus reagent in Mitsunobu reaction. *Tetrahedron: Asymmetry* **13**, 145-148 (2002).
3. E. G. J. C. Warmerdam, J. Brussee, C. G. Kruse, A. van der Gen, Inversion of the configuration of cyanohydrins by a mitsunobu esterification reaction. *Tetrahedron* **49**, 1063-1070 (1993).
4. M.-X. Wang, S.-J. Lin, Practical and Convenient Enzymatic Synthesis of Enantiopure α-Amino Acids and Amides. *The Journal of Organic Chemistry* **67**, 6542-6545 (2002).
5. R. E. Steiger, dl-a-AMINOPHENYLACETIC ACID. *Organic Syntheses* **22**, 23 (1942).
6. O. Pàmies, J.-E. Bäckvall, Efficient Lipase-Catalyzed Kinetic Resolution and Dynamic Kinetic Resolution of β-Hydroxy Nitriles. Correction of Absolute Configuration and Transformation to Chiral β-Hydroxy Acids and γ-Amino Alcohols. *Advanced Synthesis & Catalysis* **344**, 947-952 (2002).
7. T. M. Koenig, D. Mitchell, A convenient method for preparing enantiomerically pure norfluoxetine, fluoxetine and tomoxetine. *Tetrahedron Letters* **35**, 1339-1342 (1994).
8. P. Bracco, H. Busch, J. von Langermann, U. Hanefeld, Enantioselective synthesis of cyanohydrins catalysed by hydroxynitrile lyases – a review. *Organic & Biomolecular Chemistry* **14**, 6375-6389 (2016).
9. L. Elisa *et al.*, Mini-Review: Recent Developments in Hydroxynitrile Lyases for Industrial Biotechnology. *Recent Patents on Biotechnology* **7**, 197-206 (2013).
10. M. Dadashipour, Y. Asano, Hydroxynitrile Lyases: Insights into Biochemistry, Discovery, and Engineering. *ACS Catalysis* **1**, 1121-1149 (2011).
11. X.-P. Zeng, J.-C. Sun, C. Liu, C.-B. Ji, Y.-Y. Peng, Catalytic Asymmetric Cyanation Reactions of Aldehydes and Ketones in Total Synthesis. *Advanced Synthesis & Catalysis* **361**, 3281-3305 (2019).
12. L. Veum, U. Hanefeld, Enantioselective formation of mandelonitrile acetate: investigation of a dynamic kinetic resolution II. *Tetrahedron: Asymmetry* **15**, 3707-3709 (2004).
13. I. Dreveny, C. Kratky, K. Gruber, The active site of hydroxynitrile lyase from Prunus amygdalus: Modeling studies provide new insights into the mechanism of cyanogenesis. *Protein Science* **11**, 292-300 (2002).
14. I. Dreveny, K. Gruber, A. Glieder, A. Thompson, C. Kratky, The Hydroxynitrile Lyase from Almond: A Lyase that Looks Like an Oxidoreductase. *Structure* **9**, 803-815 (2001).
15. T. Pavkov-Keller *et al.*, Structures of almond hydroxynitrile lyase isoenzyme 5 provide a rationale for the lack of oxidoreductase activity in flavin dependent HNLs. *Journal of Biotechnology* **235**, 24-31 (2016).
16. I. Dreveny, A. S. Andryushkova, A. Glieder, K. Gruber, C. Kratky, Substrate Binding in the FAD-Dependent Hydroxynitrile Lyase from Almond Provides Insight into the Mechanism of Cyanohydrin Formation and Explains the Absence of Dehydrogenation Activity. *Biochemistry* **48**, 3370-3377 (2009).
17. Y. Fukuta *et al.*, Characterization of a New (R)-Hydroxynitrile Lyase from the Japanese Apricot Prunus mume and cDNA Cloning and Secretory Expression of One of the Isozymes in Pichia pastoris. *Bioscience, Biotechnology, and Biochemistry* **75**, 214-220 (2011).
18. R. Yemm, J. Poulton, Isolation and characterization of multiple forms of mandelonitrile lyase from mature black cherry (Prunus serotina Ehrh.) seeds. *Archives of biochemistry and biophysics* **247 2**, 440-445 (1986).
19. T. Ueatrongchit, A. Kayo, H. Komeda, Y. Asano, A. H-Kittikun, Purification and Characterization of A Novel (R)-Hydroxynitrile Lyase from Eriobotrya japonica (Loquat). *Bioscience, Biotechnology, and Biochemistry* **72**, 1513-1522 (2008).

20. G.-J. Zhao, Z.-Q. Yang, Y.-H. Guo, Cloning and expression of hydroxynitrile lyase gene from Eriobotrya japonica in Pichia pastoris. *Journal of Bioscience and Bioengineering* **112**, 321-325 (2011).
21. J. Andexer *et al.*, An R-Selective Hydroxynitrile Lyase from Arabidopsis thaliana with an α/β-Hydrolase Fold. *Angewandte Chemie International Edition* **46**, 8679-8681 (2007).
22. J. N. Andexer *et al.*, Hydroxynitrile Lyases with α/β-Hydrolase Fold: Two Enzymes with Almost Identical 3D Structures but Opposite Enantioselectivities and Different Reaction Mechanisms. *ChemBioChem* **13**, 1932-1939 (2012).
23. J. Hughes, J. P. C. Decarvalho, M. A. Hughes, Purification, Characterization, and Cloning of α-Hydroxynitrile Lyase from Cassava (Manihot esculenta Crantz). *Archives of Biochemistry and Biophysics* **311**, 496-502 (1994).
24. H. Wajant, S. Förster, H. Böttinger, F. Effenberger, K. Pfizenmaier, Acetone cyanohydrin lyase from Manihot esculenta (cassava) is serologically distinct from other hydroxynitrile lyases. *Plant Science* **108**, 1-11 (1995).
25. H. Wajant, K. Pfizenmaier, Identification of Potential Active-site Residues in the Hydroxynitrile Lyase from Manihot esculenta by Site-directed Mutagenesis*. *Journal of Biological Chemistry* **271**, 25830-25834 (1996).
26. J. Hughes, J. H. Lakey, M. A. Hughes, Production and characterization of a plant α-hydroxynitrile lyase in Escherichia coli. *Biotechnology and Bioengineering* **53**, 332-338 (1997).
27. Y. Asano, M. Dadashipour, M. Yamazaki, N. Doi, H. Komeda, Functional expression of a plant hydroxynitrile lyase in Escherichia coli by directed evolution: creation and characterization of highly in vivo soluble mutants. *Protein engineering, design & selection : PEDS* **24 8**, 607-616 (2011).
28. M. Dadashipour, Y. Fukuta, Y. Asano, Comparative expression of wild-type and highly soluble mutant His103Leu of hydroxynitrile lyase from Manihot esculenta in prokaryotic and eukaryotic expression systems. *Protein Expression and Purification* **77**, 92-97 (2011).
29. H. Lauble *et al.*, Structure determinants of substrate specificity of hydroxynitrile lyase from Manihot esculenta. *Protein Science* **11**, 65-71 (2002).
30. H. Lauble, S. Forster, B. Miehlich, H. Wajant, F. Effenberger, Structure of hydroxynitrile lyase from Manihot esculenta in complex with substrates acetone and chloroacetone: implications for the mechanism of cyanogenesis. *Acta Crystallographica Section D* **57**, 194-200 (2001).
31. M. Hasslacher *et al.*, Molecular Cloning of the Full-length cDNA of (S)-Hydroxynitrile Lyase from Hevea brasiliensis: FUNCTIONAL EXPRESSION IN ESCHERICHIA COLI AND SACCHAROMYCES CEREVISIAE AND IDENTIFICATION OF AN ACTIVE SITE RESIDUE (∗). *Journal of Biological Chemistry* **271**, 5884-5891 (1996).
32. U. G. Wagner, M. Hasslacher, H. Griengl, H. Schwab, C. Kratky, Mechanism of cyanogenesis: the crystal structure of hydroxynitrile lyase from Hevea brasiliensis. *Structure* **4**, 811-822 (1996).
33. G. Gartler, C. Kratky, K. Gruber, Structural determinants of the enantioselectivity of the hydroxynitrile lyase from Hevea brasiliensis. *Journal of Biotechnology* **129**, 87-97 (2007).
34. K. Gruber, G. Gartler, B. Krammer, H. Schwab, C. Kratky, Reaction Mechanism of Hydroxynitrile Lyases of the α/β-Hydrolase Superfamily: THE THREE-DIMENSIONAL STRUCTURE OF THE TRANSIENT ENZYME-SUBSTRATE COMPLEX CERTIFIES THE CRUCIAL ROLE OF LYS²³⁶*. *Journal of Biological Chemistry* **279**, 20501-20510 (2004).
35. H. Wajant, K.-W. Mundry, Hydroxynitrile lyase from Sorghum bicolor: a glycoprotein heterotetramer. *Plant Science* **89**, 127-133 (1993).
36. H. Wajant, K.-W. Mundry, K. Pfizenmaier, Molecular cloning of hydroxynitrile lyase from Sorghum bicolor (L.). Homologies to serine carboxypeptidases. *Plant Molecular Biology* **26**, 735-746 (1994).
37. H. Lauble, B. Miehlich, S. Förster, H. Wajant, F. Effenberger, Crystal Structure of Hydroxynitrile Lyase from Sorghum bicolor in Complex with the Inhibitor Benzoic Acid: A Novel Cyanogenic Enzyme. *Biochemistry* **41**, 12043-12050 (2002).

38. M. Dadashipour *et al.*, S-selective hydroxynitrile lyase from a plant Baliospermum montanum: Molecular characterization of recombinant enzyme. *Journal of Biotechnology* **153**, 100-110 (2011).
39. S. Nakano, M. Dadashipour, Y. Asano, Structural and functional analysis of hydroxynitrile lyase from Baliospermum montanum with crystal structure, molecular dynamics and enzyme kinetics. *Biochimica et Biophysica Acta (BBA) - Proteins and Proteomics* **1844**, 2059-2067 (2014).
40. A. Nuylert, Y. Ishida, Y. Asano, Effect of Glycosylation on the Biocatalytic Properties of Hydroxynitrile Lyase from the Passion Fruit, Passiflora edulis: A Comparison of Natural and Recombinant Enzymes. *ChemBioChem* **18**, 257-265 (2017).
41. F. Motojima, A. Nuylert, Y. Asano, The crystal structure and catalytic mechanism of hydroxynitrile lyase from passion fruit, Passiflora edulis. *The FEBS Journal* **285**, 313-324 (2018).
42. Z. Zhai, A. Nuylert, K. Isobe, Y. Asano, Effects of codon optimization and glycosylation on the high-level production of hydroxynitrile lyase from Chamberlinius hualienensis in Pichia pastoris. *Journal of Industrial Microbiology and Biotechnology* **46**, 887-898 (2019).
43. F. Motojima *et al.*, R-hydroxynitrile lyase from the cyanogenic millipede, Chamberlinius hualienensis—A new entry to the carrier protein family Lipocalines. *The FEBS Journal* **288**, 1679-1695 (2021).
44. M. Dadashipour, Y. Ishida, K. Yamamoto, Y. Asano, Discovery and molecular and biocatalytic properties of hydroxynitrile lyase from an invasive millipede, <em>Chamberlinius hualienensis</em&gt. *Proceedings of the National Academy of Sciences* **112**, 10605 (2015).
45. A. Nuylert, M. Nakabayashi, T. Yamaguchi, Y. Asano, Discovery and Structural Analysis to Improve the Enantioselectivity of Hydroxynitrile Lyase from Parafontaria laminata Millipedes for (R)-2-Chloromandelonitrile Synthesis. *ACS Omega* **5**, 27896-27908 (2020).
46. R. Wiedner, M. Gruber-Khadjawi, H. Schwab, K. Steiner, Discovery of a novel (R)-selective bacterial hydroxynitrile lyase from Acidobacterium capsulatum. *Computational and Structural Biotechnology Journal* **10**, 58-62 (2014).
47. Z. Hussain *et al.*, Characterization of Two Bacterial Hydroxynitrile Lyases with High Similarity to Cupin Superfamily Proteins. *Applied and Environmental Microbiology* **78**, 2053-2055 (2012).
48. I. Hajnal *et al.*, Biochemical and structural characterization of a novel bacterial manganese-dependent hydroxynitrile lyase. *Febs j* **280**, 5815-5828 (2013).
49. E. Lanfranchi *et al.*, Enzyme discovery beyond homology: a unique hydroxynitrile lyase in the Bet v1 superfamily. *Scientific Reports* **7**, 46738 (2017).
50. L.-L. Xu, B. K. Singh, E. E. Conn, Purification and characterization of acetone cyanohydrin lyase from Linum usitatissimum. *Archives of Biochemistry and Biophysics* **263**, 256-263 (1988).
51. K. Trummler, H. Wajant, Molecular Cloning of Acetone Cyanohydrin Lyase from Flax (Linum usitatissimum): DEFINITION OF A NOVEL CLASS OF HYDROXYNITRILE LYASES *. *Journal of Biological Chemistry* **272**, 4770-4774 (1997).
52. K. Trummler *et al.*, Expression of the Zn2+-containing hydroxynitrile lyase from flax (Linum usitatissimum) in Pichia pastoris— utilization of the recombinant enzyme for enzymatic analysis and site-directed mutagenesis. *Plant Science* **139**, 19-27 (1998).
53. H. Breithaupt *et al.*, Cloning and expression of (R)-hydroxynitrile lyase from Linum usitatissimum (flax). *Journal of Molecular Catalysis B-enzymatic* **6**, 315-332 (1999).
54. C. Roberge, F. Fleitz, D. Pollard, P. Devine, Synthesis of optically active cyanohydrins from aromatic ketones: evidence of an increased substrate range and inverted stereoselectivity for the hydroxynitrile lyase from Linum usitatissimum. *Tetrahedron: Asymmetry* **18**, 208-214 (2007).
55. F. L. Cabirol *et al.*, Linum usitatissimum Hydroxynitrile Lyase Cross-Linked Enzyme Aggregates: A Recyclable Enantioselective Catalyst. *Advanced Synthesis & Catalysis* **350**, 2329-2338 (2008).

56. T. Touge *et al.*, Oxo-Tethered Ruthenium(II) Complex as a Bifunctional Catalyst for Asymmetric Transfer Hydrogenation and H2 Hydrogenation. *Journal of the American Chemical Society* **133**, 14960-14963 (2011).
57. A. Kišić, M. Stephan, B. Mohar, ansa-Ruthenium(II) Complexes of DPEN-SO2N(Me)(CH2)n(η6-aryl) Conjugate Ligands for Asymmetric Transfer Hydrogenation of Aryl Ketones. *Advanced Synthesis & Catalysis* **356**, 3193-3198 (2014).
58. M. Watanabe, K. Murata, T. Ikariya, Practical Synthesis of Optically Active Amino Alcohols via Asymmetric Transfer Hydrogenation of Functionalized Aromatic Ketones. *The Journal of Organic Chemistry* **67**, 1712-1715 (2002).
59. H. Vázquez-Villa, S. Reber, M. A. Ariger, E. M. Carreira, Iridium Diamine Catalyst for the Asymmetric Transfer Hydrogenation of Ketones. *Angewandte Chemie International Edition* **50**, 8979-8981 (2011).
60. C. Chen, L. Kong, T. Cheng, R. Jin, G. Liu, Facile construction of functionalized periodic mesoporous organosilica for Ir-catalyzed enantioselective reduction of α-cyanoacetophenones and α-nitroacetophenones. *Chemical Communications* **50**, 10891-10893 (2014).
61. O. Soltani, M. A. Ariger, H. Vázquez-Villa, E. M. Carreira, Transfer Hydrogenation in Water: Enantioselective, Catalytic Reduction of α-Cyano and α-Nitro Substituted Acetophenones. *Organic Letters* **12**, 2893-2895 (2010).
62. J.-E. Lee, J. Yun, Catalytic Asymmetric Boration of Acyclic α,β-Unsaturated Esters and Nitriles. *Angewandte Chemie International Edition* **47**, 145-147 (2008).
63. L. Zhu, T. Kitanosono, P. Xu, S. Kobayashi, A Cu(ii)-based strategy for catalytic enantioselective β-borylation of α,β-unsaturated acceptors. *Chemical Communications* **51**, 11685-11688 (2015).
64. S. Mun, J.-E. Lee, J. Yun, Copper-Catalyzed β-Boration of α,β-Unsaturated Carbonyl Compounds: Rate Acceleration by Alcohol Additives. *Organic Letters* **8**, 4887-4889 (2006).
65. Y. Suto, R. Tsuji, M. Kanai, M. Shibasaki, Cu(I)-Catalyzed Direct Enantioselective Cross Aldol-Type Reaction of Acetonitrile. *Organic Letters* **7**, 3757-3760 (2005).
66. Y. Suto, N. Kumagai, S. Matsunaga, M. Kanai, M. Shibasaki, Direct Catalytic Aldol-Type Reactions Using RCH2CN. *Organic Letters* **5**, 3147-3150 (2003).
67. J. Granander, J. Eriksson, G. Hilmersson, Highly enantioselective 1,2-additions of various organolithium reagents to aldehydes. *Tetrahedron: Asymmetry* **17**, 2021-2027 (2006).
68. K. Soai, Y. Hirose, S. Sakata, Highly enantioselective synthesis of β-hydroxy nitriles by the cyanomethylation of aldehydes using DPMPM as a chiral catalysts or ligand. *Tetrahedron: Asymmetry* **3**, 677-680 (1992).
69. O. Pàmies, J.-E. Bäckvall, Efficient Lipase-Catalyzed Kinetic Resolution and Dynamic Kinetic Resolution of β-Hydroxy Nitriles. A Route to Useful Precursors for γ-Amino Alcohols. *Advanced Synthesis & Catalysis* **343**, 726-731 (2001).
70. E. García-Urdiales, F. Rebolledo, V. Gotor, Study of the enantioselectivity of the CAL-B-catalysed transesterification of α-substituted α-propylmethanols and α-substituted benzyl alcohols. *Tetrahedron: Asymmetry* **12**, 3047-3052 (2001).
71. H. Ankati, D. Zhu, Y. Yang, E. R. Biehl, L. Hua, Asymmetric Synthesis of Both Antipodes of β-Hydroxy Nitriles and β-Hydroxy Carboxylic Acids via Enzymatic Reduction or Sequential Reduction/Hydrolysis. *The Journal of Organic Chemistry* **74**, 1658-1662 (2009).
72. M. L. Contente *et al.*, Preparation of enantiomerically enriched aromatic β-hydroxynitriles and halohydrins by ketone reduction with recombinant ketoreductase KRED1-Pglu. *Tetrahedron* **72**, 3974-3979 (2016).
73. D. Zhu *et al.*, Asymmetric Reduction of β-Ketonitriles with a Recombinant Carbonyl Reductase and Enzymatic Transformation to Optically Pure β-Hydroxy Carboxylic Acids. *Organic Letters* **9**, 2561-2563 (2007).

74. L.-J. Wang *et al.*, Highly efficient synthesis of chiral alcohols with a novel NADH-dependent reductase from Streptomyces coelicolor. *Bioresource Technology* **102**, 7023-7028 (2011).
75. C. Rodríguez *et al.*, Steric vs. electronic effects in the Lactobacillus brevis ADH-catalyzed bioreduction of ketones. *Organic & Biomolecular Chemistry* **12**, 673-681 (2014).
76. S. Kamila, D. Zhu, E. R. Biehl, L. Hua, Unexpected Stereorecognition in Nitrilase-Catalyzed Hydrolysis of β-Hydroxy Nitriles. *Organic Letters* **8**, 4429-4431 (2006).
77. C. Mukherjee, D. Zhu, E. R. Biehl, L. Hua, Exploring the Synthetic Applicability of a Cyanobacterium Nitrilase as Catalyst for Nitrile Hydrolysis. *European Journal of Organic Chemistry* **2006**, 5238-5242 (2006).
78. Y. Chen, F. Lie, Z. Li, Enantioselective Benzylic Hydroxylation with Pseudomonas monteilii TA-5: A Simple Method for the Syntheses of (R)-Benzylic Alcohols Containing Reactive Functional Groups. *Advanced Synthesis & Catalysis* **351**, 2107-2112 (2009).
79. S.-Y. Chen, C.-X. Yang, J.-P. Wu, G. Xu, L.-R. Yang, Multi-Enzymatic Biosynthesis of Chiral β-Hydroxy Nitriles through Co-Expression of Oxidoreductase and Halohydrin Dehalogenase. *Advanced Synthesis & Catalysis* **355**, 3179-3190 (2013).
80. T. G. G. Battye, L. Kontogiannis, O. Johnson, H. R. Powell, A. G. W. Leslie, iMOSFLM: a new graphical interface for diffraction-image processing with MOSFLM. *Acta Crystallographica Section D* **67**, 271-281 (2011).
81. P. Evans, Scaling and assessment of data quality. *Acta Crystallographica Section D* **62**, 72-82 (2006).
82. F. Long, A. A. Vagin, P. Young, G. N. Murshudov, BALBES: a molecular-replacement pipeline. *Acta Crystallographica Section D* **64**, 125-132 (2008).
83. P. Emsley, K. Cowtan, Coot: model-building tools for molecular graphics. *Acta Crystallographica Section D* **60**, 2126-2132 (2004).
84. G. N. Murshudov *et al.*, REFMAC5 for the refinement of macromolecular crystal structures. *Acta Crystallographica Section D* **67**, 355-367 (2011).
85. D. Liebschner *et al.*, Macromolecular structure determination using X-rays, neutrons and electrons: recent developments in Phenix. *Acta Crystallographica Section D* **75**, 861-877 (2019).
86. Schrodinger, LLC. (2015).
87. X. Robert, P. Gouet, Deciphering key features in protein structures with the new ENDscript server. *Nucleic Acids Research* **42**, W320-W324 (2014).
88. J. L. Lambert, J. Ramasamy, J. V. Paukstelis, Stable reagents for the colorimetric determination of cyanide by modified Koenig reactions. *Analytical Chemistry* **47**, 916-918 (1975).
89. C. Wiedemann, P. Bellstedt, M. Görlach, CAPITO—a web server-based analysis and plotting tool for circular dichroism data. *Bioinform.* **29**, 1750-1757 (2013).
90. P. T. Xie, T. D. Hurley, Methionine-141 directly influences the binding of 4-methylpyrazole in human σσ alcohol dehydrogenase. *Protein Science* **8**, 2639-2644 (1999).
91. F. Chen, P. Wang, Y. An, J. Huang, Y. Xu, Structural insight into the conformational change of alcohol dehydrogenase from Arabidopsis thaliana L. during coenzyme binding. *Biochimie* **108**, 33-39 (2015).
92. H. Eklund *et al.*, Structure of a triclinic ternary complex of horse liver alcohol dehydrogenase at 2.9 Å resolution. *Journal of Molecular Biology* **146**, 561-587 (1981).
93. P. C. Sanghani, H. Robinson, W. F. Bosron, T. D. Hurley, Human Glutathione-Dependent Formaldehyde Dehydrogenase. Structures of Apo, Binary, and Inhibitory Ternary Complexes. *Biochemistry* **41**, 10778-10786 (2002).
94. R. K. Wierenga, P. Terpstra, W. G. J. Hol, Prediction of the occurrence of the ADP-binding βαβ-fold in proteins, using an amino acid sequence fingerprint. *Journal of Molecular Biology* **187**, 101-107 (1986).
95. O. Rudyk, P. Eaton, Biochemical methods for monitoring protein thiol redox states in biological systems. *Redox Biology* **2**, 803-813 (2014).

96. B. Saville, A scheme for the colorimetric determination of microgram amounts of thiols. *Analyst* **83**, 670-672 (1958).
97. A. Yahashiri, J. K. Rubach, B. V. Plapp, Effects of Cavities at the Nicotinamide Binding Site of Liver Alcohol Dehydrogenase on Structure, Dynamics and Catalysis. *Biochemistry.* **53**, 881-894 (2014).
98. S. A. Benner, The stereoselectivity of alcohol dehydrogenases: A sterochemical imperative? *Experientia* **38**, 633-637 (1982).
99. A. Yahashiri, J. K. Rubach, B. V. Plapp, Effects of Cavities at the Nicotinamide Binding Site of Liver Alcohol Dehydrogenase on Structure, Dynamics and Catalysis. *Biochemistry* **53**, 881-894 (2014).
100. C. Wiedemann, P. Bellstedt, M. Görlach, CAPITO—a web server-based analysis and plotting tool for circular dichroism data. *Bioinformatics* **29**, 1750-1757 (2013).
101. I. M. Kolthoff, D. L. Leussing, T. S. Lee, Reaction of Ferrous and Ferric Iron with 1,10-Phenanthroline. III. The Ferrous Monophenanthroline Complex and the Colorimetric Determination of Phenanthroline. *Journal of the American Chemical Society* **72**, 2173-2177 (1950).
102. D. E. Drum, B. L. Vallee, Differential chemical reactivities of zinc in horsse liver alcohol dehydrogenase. *Biochemistry* **9**, 4078-4086 (1970).
103. A. Krężel, W. Maret, The biological inorganic chemistry of zinc ions. *Archives of Biochemistry and Biophysics* **611**, 3-19 (2016).
104. E. Magonet, P. Hayen, D. Delforge, E. Delaive, J. Remacle, Importance of the structural zinc atom for the stability of yeast alcohol dehydrogenase. *Biochemical Journal* **287**, 361-365 (1992).
105. B. V. Plapp *et al.*, Horse Liver Alcohol Dehydrogenase: Zinc Coordination and Catalysis. *Biochemistry* **56**, 3632-3646 (2017).
106. J. K. Rubach, B. V. Plapp, Mobility of Fluorobenzyl Alcohols Bound to Liver Alcohol Dehydrogenases as Determined by NMR and X-ray Crystallographic Studies. *Biochemistry* **41**, 15770-15779 (2002).
107. N. Tanaka, Y. Kusakabe, K. Ito, T. Yoshimoto, K. T. Nakamura, Crystal Structure of Formaldehyde Dehydrogenase from Pseudomonas putida: the Structural Origin of the Tightly Bound Cofactor in Nicotinoprotein Dehydrogenases. *Journal of Molecular Biology* **324**, 519-533 (2002).
108. M. E. Maguire, J. A. Cowan, Magnesium chemistry and biochemistry. *Biometals* **15**, 203-210 (2002).
109. J. Weston, in *PATAI'S Chemistry of Functional Groups*.
110. K. Gruber, C. Kratky, Biopolymers for biocatalysis: Structure and catalytic mechanism of hydroxynitrile lyases. *Journal of Polymer Science Part A: Polymer Chemistry* **42**, 479-486 (2004).
111. D. G. Isom, C. A. Castañeda, B. R. Cannon, B. García-Moreno E., Large shifts in pK_a values of lysine residues buried inside a protein. *Proceedings of the National Academy of Sciences* **108**, 5260-5265 (2011).
112. D. G. Isom, C. A. Castañeda, B. R. Cannon, P. D. Velu, B. García-Moreno E., Charges in the hydrophobic interior of proteins. *Proceedings of the National Academy of Sciences* **107**, 16096-16100 (2010).
113. T. Betke, P. Rommelmann, K. Oike, Y. Asano, H. Gröger, Cyanide-Free and Broadly Applicable Enantioselective Synthetic Platform for Chiral Nitriles through a Biocatalytic Approach. *Angewandte Chemie International Edition* **56**, 12361-12366 (2017).
114. T. Betke *et al.*, Biocatalytic Synthesis of Nitriles through Dehydration of Aldoximes: The Substrate Scope of Aldoxime Dehydratases. *ChemBioChem* **19**, 768-779 (2018).
115. C. Plass *et al.*, Approaching Bulk Chemical Nitriles from Alkenes: A Hydrogen Cyanide-Free Approach through a Combination of Hydroformylation and Biocatalysis. *ACS Catalysis* **9**, 5198-5203 (2019).
116. A. Hinzmann, S. Glinski, M. Worm, H. Gröger, Enzymatic Synthesis of Aliphatic Nitriles at a Substrate Loading of up to 1.4 kg/L: A Biocatalytic Record Achieved with a Heme Protein. *The Journal of Organic Chemistry* **84**, 4867-4872 (2019).

117. R. Metzner, S. Okazaki, Y. Asano, H. Gröger, Cyanide-free Enantioselective Synthesis of Nitriles: Synthetic Proof of a Biocatalytic Concept and Mechanistic Insights. *ChemCatChem* **6**, 3105-3109 (2014).
118. Y. Miao, R. Metzner, Y. Asano, Kemp Elimination Catalyzed by Naturally Occurring Aldoxime Dehydratases. *ChemBioChem* **18**, 451-454 (2017).
119. A. N. Alexandrova, D. Röthlisberger, D. Baker, W. L. Jorgensen, Catalytic Mechanism and Performance of Computationally Designed Enzymes for Kemp Elimination. *Journal of the American Chemical Society* **130**, 15907-15915 (2008).
120. M. L. Casey, D. S. Kemp, K. G. Paul, D. D. Cox, Physical organic chemistry of benzisoxazoles. I. Mechanism of the base-catalyzed decomposition of benzisoxazoles. *The Journal of Organic Chemistry* **38**, 2294-2301 (1973).
121. A. Li *et al.*, A redox-mediated Kemp eliminase. *Nature Communications* **8**, 14876 (2017).
122. Y. Asano, T. Yasuda, Y. Tani, H. Yamada, A New Enzymatic Method of Acrylamide Production. *Agricultural and Biological Chemistry* **46**, 1183-1189 (1982).
123. Y. Kato, R. Ooi, Y. Asano, Distribution of Aldoxime Dehydratase in Microorganisms. *Applied and Environmental Microbiology* **66**, 2290-2296 (2000).
124. K.-I. Oinuma *et al.*, Novel Aldoxime Dehydratase Involved in Carbon-Nitrogen Triple Bond Synthesis of Pseudomonas chlororaphis B23: SEQUENCING, GENE EXPRESSION, PURIFICATION, AND CHARACTERIZATION*. *Journal of Biological Chemistry* **278**, 29600-29608 (2003).
125. J. Nomura *et al.*, Crystal structure of aldoxime dehydratase and its catalytic mechanism involved in carbon-nitrogen triple-bond synthesis. *Proceedings of the National Academy of Sciences* **110**, 2810-2815 (2013).
126. Y. Kato, K. Nakamura, H. Sakiyama, S. G. Mayhew, Y. Asano, Novel heme-containing lyase, phenylacetaldoxime dehydratase from Bacillus sp. strain OxB-1: purification, characterization, and molecular cloning of the gene. *Biochemistry* **39**, 800-809 (2000).
127. Y. Kato, Y. Asano, High-level expression of a novel FMN-dependent heme-containing lyase, phenylacetaldoxime dehydratase of Bacillus sp. strain OxB-1, in heterologous hosts. *Protein Expression and Purification* **28**, 131-139 (2003).
128. Y. Asano, Y. Kato, Z-phenylacetaldoxime degradation by a novel aldoxime dehydratase from Bacillus sp. strain OxB-1. *FEMS Microbiology Letters* **158**, 185-190 (1998).
129. Y. Kato, S. Yoshida, S. X. Xie, Y. Asano, Aldoxime dehydratase co-existing with nitrile hydratase and amidase in the iron-type nitrile hydratase-producer Rhodococcus sp. N-771. *J Biosci Bioeng* **97**, 250-259 (2004).
130. H. Sawai *et al.*, X-ray Crystal Structure of Michaelis Complex of Aldoxime Dehydratase*♦. *Journal of Biological Chemistry* **284**, 32089-32096 (2009).
131. F. J. F. Castro *et al.*, The Addition of Diallylzinc to 5-Substituted 4,5-Dihydroisoxazoles. *Synlett* **6**, 798-800 (1999).
132. A. Pohjakallio, P. M. Pihko, U. M. Laitinen, Synthesis of 2-Isoxazolines: Enantioselective and Racemic Methods Based on Conjugate Additions of Oximes. *Chemistry – A European Journal* **16**, 11325-11339 (2010).
133. Y. Kato, K. Nakamura, H. Sakiyama, S. G. Mayhew, Y. Asano, Novel Heme-Containing Lyase, Phenylacetaldoxime Dehydratase from Bacillus sp. Strain OxB-1: Purification, Characterization, and Molecular Cloning of the Gene. *Biochemistry* **39**, 800-809 (2000).
134. R. Huisgen, M. Christl, 1,3-Dipolare Cycloadditionen, 72. Reaktionen der Knallsäure mit ungesättigten Verbindungen. *Chemische Berichte* **106**, 3291-3311 (1973).
135. A. Pohjakallio, P. M. Pihko, J. Liu, Base-Catalyzed Isomerization of 2-Isoxazolines Enables a Two-Step Enantioselective Synthesis of β-Hydroxynitriles from Enals. *The Journal of Organic Chemistry* **75**, 6712-6715 (2010).

136. A. Yashiro, Y. Nishida, K. Kobayashi, M. Ohno, β-Hydroxy Nitrile and β-Hydroxy Oxime Derivatives of [60]Fullerene by Nucleophilic Ring Cleavage of Fulleroisoxazoline and -Isoxazolidine in the Presence of Methanol. *Synlett* **2000**, 361-362 (2000).
137. M. H. Seo, Y. Y. Lee, Y. M. Goo, A New Method for the Preparation of β-Hydroxy Nitriles: Transformation of 3-Bromo-2-isoxazolines to β-Hydroxy Nitriles by Treatment of Alkanethiolates. *Synthetic Communications* **24**, 1433-1439 (1994).
138. R.-Z. Liao, W. Thiel, Why Is the Oxidation State of Iron Crucial for the Activity of Heme-Dependent Aldoxime Dehydratase? A QM/MM Study. *The Journal of Physical Chemistry B* **116**, 9396-9408 (2012).
139. E. Pinakoulaki *et al.*, Aldoxime Dehydratase: Probing the Heme Environment Involved in the Synthesis of the Carbon–Nitrogen Triple Bond. *The Journal of Physical Chemistry B* **115**, 13012-13018 (2011).
140. Y. Kato, S. Yoshida, S.-X. Xie, Y. Asano, Aldoxime dehydratase co-existing with nitrile hydratase and amidase in the iron-type nitrile hydratase-producer Rhodococcus sp. N-771. *Journal of Bioscience and Bioengineering* **97**, 250-259 (2004).
141. Y. Kato, R. Ooi, Y. Asano, Isolation and characterization of a bacterium possessing a novel aldoxime-dehydration activity and nitrile-degrading enzymes. *Archives of Microbiology* **170**, 85-90 (1998).
142. C. S. Chen, Y. Fujimoto, G. Girdaukas, C. J. Sih, Quantitative analyses of biochemical kinetic resolutions of enantiomers. *Journal of the American Chemical Society* **104**, 7294-7299 (1982).
143. T. R. Hoye, C. S. Jeffrey, F. Shao, Mosher ester analysis for the determination of absolute configuration of stereogenic (chiral) carbinol carbons. *Nature Protocols* **2**, 2451-2458 (2007).
144. Z. J. Wang *et al.*, Improved Cyclopropanation Activity of Histidine-Ligated Cytochrome P450 Enables the Enantioselective Formal Synthesis of Levomilnacipran. *Angewandte Chemie International Edition* **53**, 6810-6813 (2014).
145. T. K. Hyster, F. H. Arnold, P450BM3-Axial Mutations: A Gateway to Non-Natural Reactivity. *Israel Journal of Chemistry* **55**, 14-20 (2015).
146. Y. Yang *et al.*, Practical and Efficient Utilisation of (R)-3-chloro-1,2-Propanediol in Synthesis of L-Carnitine. *Journal of Chemical Research* **35**, 371-372 (2011).
147. N.-W. Wan, Z.-Q. Liu, F. Xue, Z.-Y. Shen, Y.-G. Zheng, A One-Step Biocatalytic Process for (S)-4-Chloro-3-hydroxybutyronitrile using Halohydrin Dehalogenase: A Chiral Building Block for Atorvastatin. *ChemCatChem* **7**, 2446-2450 (2015).
148. S. K. Ma *et al.*, A green-by-design biocatalytic process for atorvastatin intermediate. *Green Chemistry* **12**, 81-86 (2010).
149. M. Müller, Chemoenzymatic Synthesis of Building Blocks for Statin Side Chains. *Angewandte Chemie International Edition* **44**, 362-365 (2005).
150. C. C. J. Culvenor, W. Davies, F. G. Haley, 607. Reactions of ethylene oxides. Part V. The interaction of alkali cyanides with epichlorohydrin. *Journal of the Chemical Society (Resumed)*, 3123-3125 (1950).
151. N. Iranpoor, M. Shekarriz, Ring Opening of Epoxides with Sodium Cyanide Catalyzed with Ce(OTf)4. *Synthetic Communications* **29**, 2249-2254 (1999).
152. D. Mitchell, T. M. Koenig, ChemInform Abstract: Regiospecific Opening of 1,2-Epoxides with Acetone Cyanohydrin Under Mildly Basic Conditions. *ChemInform* **23**, (1992).
153. H.-X. Jin, X.-K. OuYang, Enzymatic approaches to the preparation of chiral epichlorohydrin. *RSC Advances* **5**, 92988-92994 (2015).
154. J. Wu *et al.*, Synthesis of chiral epichlorohydrin by chloroperoxidase-catalyzed epoxidation of 3-chloropropene in the presence of an ionic liquid as co-solvent. *Catalysis Communications* **11**, 727-731 (2010).
155. T. Nakamura, T. Nagasawa, F. Yu, I. Watanabe, H. Yamada, A new enzymatic synthesis of (R)-γ-chloro-β-hydroxybutyronitrile. *Tetrahedron* **50**, 11821-11826 (1994).

156. T. Nakamura, T. Nagasawa, Y. Fujio, I. Watanabe, H. Yamada, A new catalytic function of halohydrin hydrogen-halide-lyase, synthesis of β-hydroxynitriles from epoxides and cyanide. *Biochemical and Biophysical Research Communications* **180**, 124-130 (1991).
157. E. Lee, Enantioselective Hydrolysis of Epichlorohydrin in Organic Solvents Using Recombinant Epoxide Hydrolase. *Journal of Industrial and Engineering Chemistry* **13**, (2007).
158. H.-X. Jin, Z.-Q. Liu, Z.-C. Hu, Y.-G. Zheng, Biosynthesis of (R)-epichlorohydrin at high substrate concentration by kinetic resolution of racemic epichlorohydrin with a recombinant epoxide hydrolase. *Engineering in Life Sciences* **13**, 385-392 (2013).
159. J.-H. Woo *et al.*, Enantioselective hydrolysis of racemic epichlorohydrin using an epoxide hydrolase from Novosphingobium aromaticivorans. *Journal of Bioscience and Bioengineering* **110**, 295-297 (2010).
160. N. Kasai, T. Suzuki, Y. Furukawa, Optically active chlorohydrins as chiral C3 and C4 building units: Microbial resolution and synthetic applications. *Chirality* **10**, 682-692 (1998).
161. S. S. Mochalov, A. N. Fedotov, E. V. Trofimova, R. A. Gazzaeva, N. S. Zefirov, Isomerization of 3-unsubstituted 4,5-dihydroisoxazoles over alumina. A new synthesis of β-hydroxy nitriles. *Russian Journal of Organic Chemistry* **52**, 397-403 (2016).
162. A. N. Boa *et al.*, Cycloaddition of nitrile oxides to homochiral vinyl ethers. *Journal of the Chemical Society, Perkin Transactions 1*, 1277-1278 (1993).
163. A. Pohjakallio, P. M. Pihko, A Versatile Entry to 3-Unsubstituted 2-Isoxazolines. *Synlett* **2008**, 827-830 (2008).
164. A. Pohjakallio, P. M. Pihko, Enantioselective synthesis of 2-isoxazolines by a one-flask conjugate addition/oxime-transfer process. *Chemistry (Weinheim an der Bergstrasse, Germany)* **15**, 3960-3964 (2009).
165. D. Zheng, Y. Asano, Biocatalytic asymmetric ring-opening of dihydroisoxazoles: a cyanide-free route to complementary enantiomers of β-hydroxy nitriles from olefins. *Green Chemistry* **22**, 4930-4936 (2020).
166. K. Chen, Z. Wang, K. Ding, Y. Chen, Y. Asano, Recent progress on discovery and research of aldoxime dehydratases. *Green Synthesis and Catalysis* **2**, 179-186 (2021).
167. A. J. J. Straathof, J. A. Jongejan, The enantiomeric ratio: origin, determination and prediction. *Enzyme Microb. Technol.* **21**, 559-571 (1997).
168. A. J. J. Straathof, J. A. Jongejan, The enantiomeric ratio: origin, determination and prediction. *Enzyme and Microbial Technology* **21**, 559-571 (1997).
169. K. Kobayashi, S. Yoshioka, Y. Kato, Y. Asano, S. Aono, Regulation of Aldoxime Dehydratase Activity by Redox-dependent Change in the Coordination Structure of the Aldoxime-Heme Complex*. *Journal of Biological Chemistry* **280**, 5486-5490 (2005).

PUBLICATIONS

1. Biocatalytic asymmetric ring-opening of dihydroisoxazoles: a cyanide-free route to complementary enantiomers of β-hydroxy nitriles from olefins. *Green Chem,* 24th. June, 2020, Royal Society of Chemistry., **22**, 4930-4936 (2020).
2. A Cyanide-free Biocatalytic Process for Synthesis of Complementary Enantiomers of 4-Chloro-3-hydroxybutanenitrile From Allyl Chloride. *ChemCatChem,* 23rd, August, 2021, Wiley-VCH., **13,** 4237–4242 (2022).
3. Structural characterization of *Linum usitatissimum* hydroxynitrile lyase: a new cyanohydrin decomposition mechanism involving a cyano-zinc complex. Accepted by Journal of Biological chemistry at 19th, Jan, 2022. (DOI: https://doi.org/10.1016/j.jbc.2022.101650)

Appendices

Appendix I: NMR spectra for compounds **1a-1l** and **2a-2l**

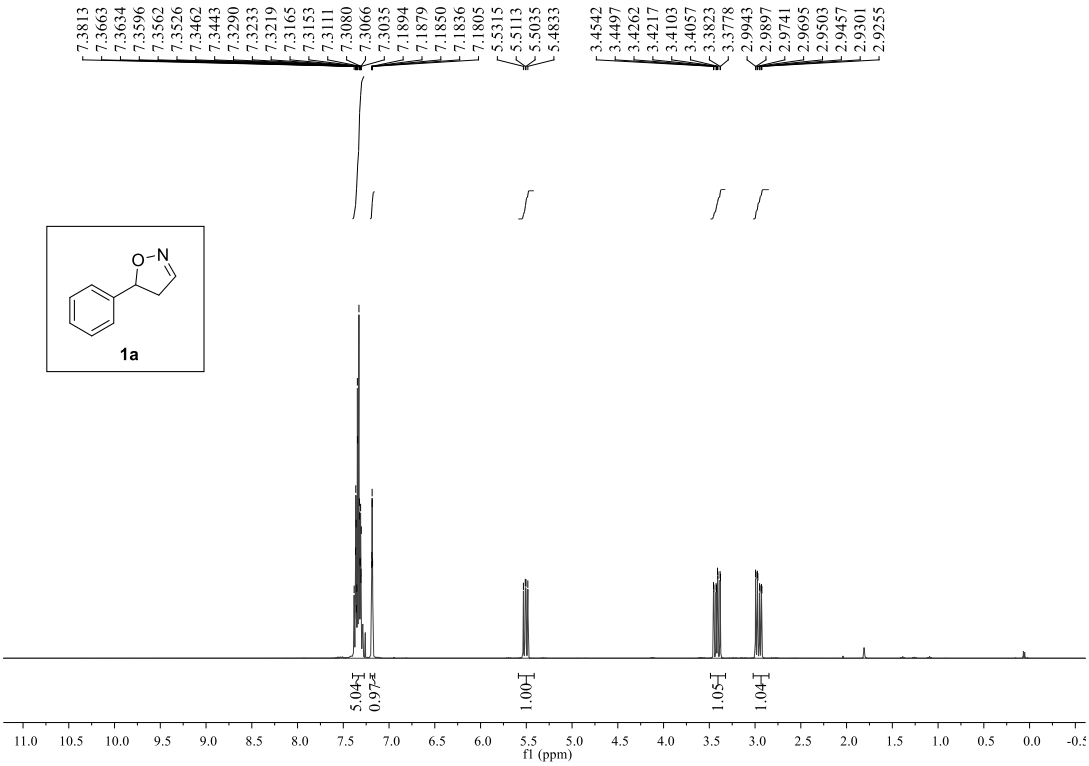

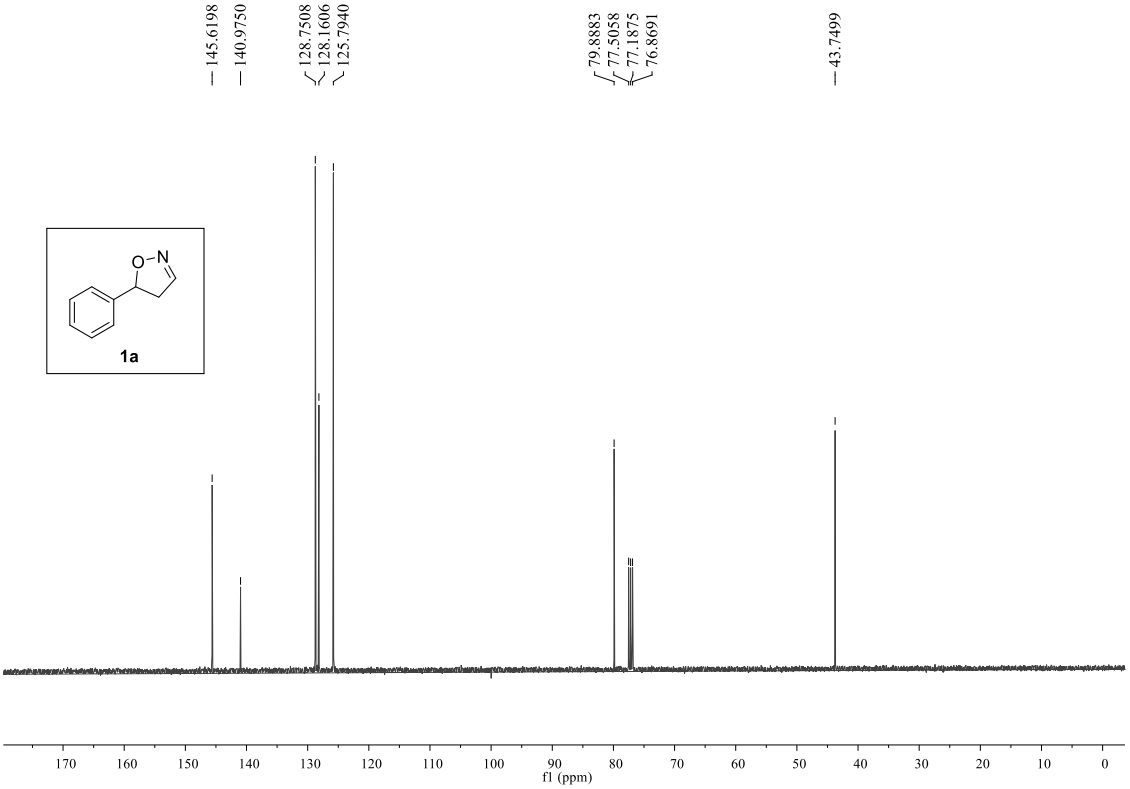

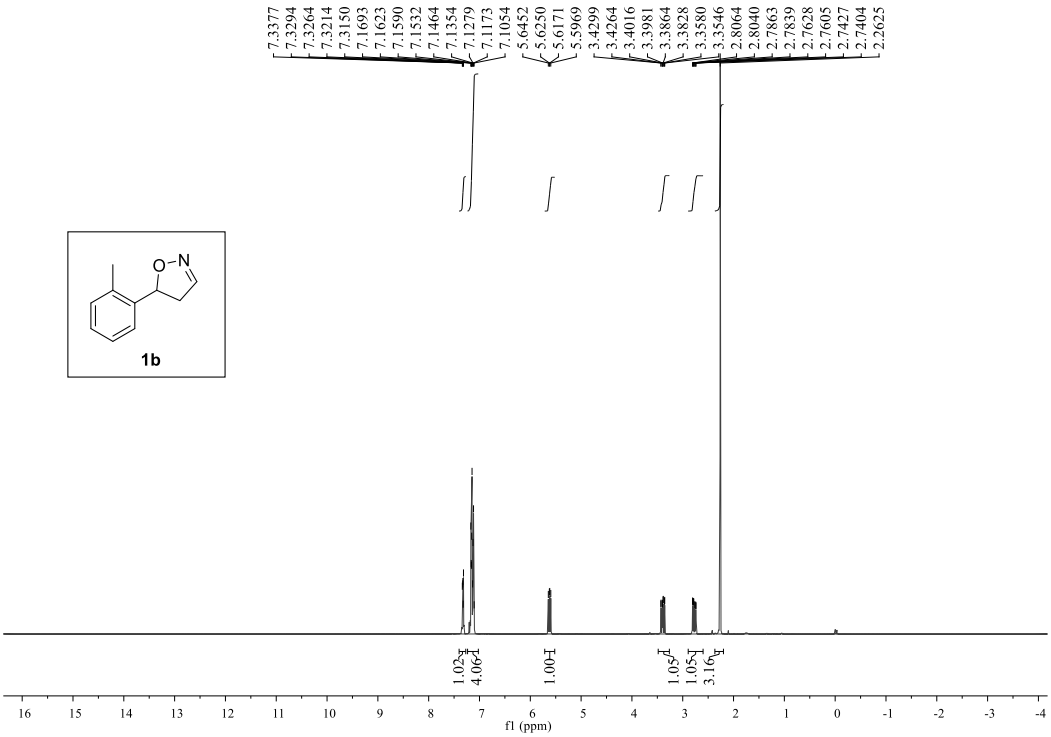
7.3377
7.3294
7.3264
7.3214
7.3150
7.1693
7.1623
7.1590
7.1532
7.1464
7.1354
7.1279
7.1173
7.1054
5.6452
5.6250
5.6171
5.5969
3.4299
3.4264
3.4016
3.3981
3.3864
3.3828
3.3580
3.3546
2.8064
2.8040
2.7863
2.7839
2.7628
2.7605
2.7427
2.7404
2.2625
1b
1.02
4.06
1.00
1.05
1.05
3.16
f1 (ppm)

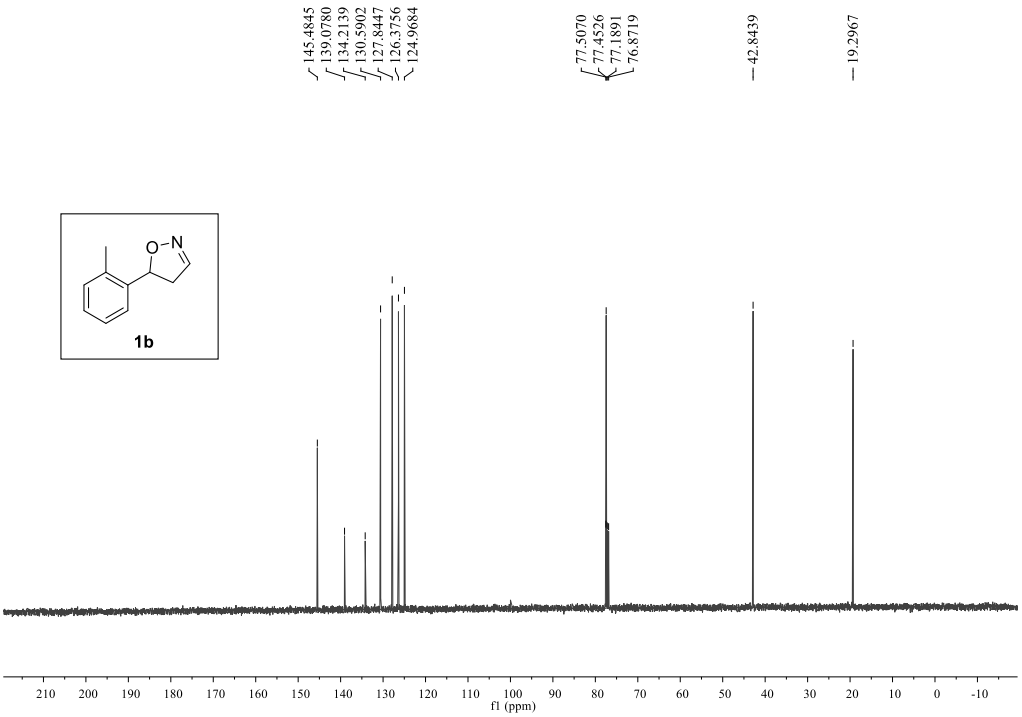
145.4845
139.0780
134.2139
130.5902
127.8447
126.3756
124.9684
77.5070
77.4526
77.1891
76.8719
42.8439
19.2967
1b
f1 (ppm)

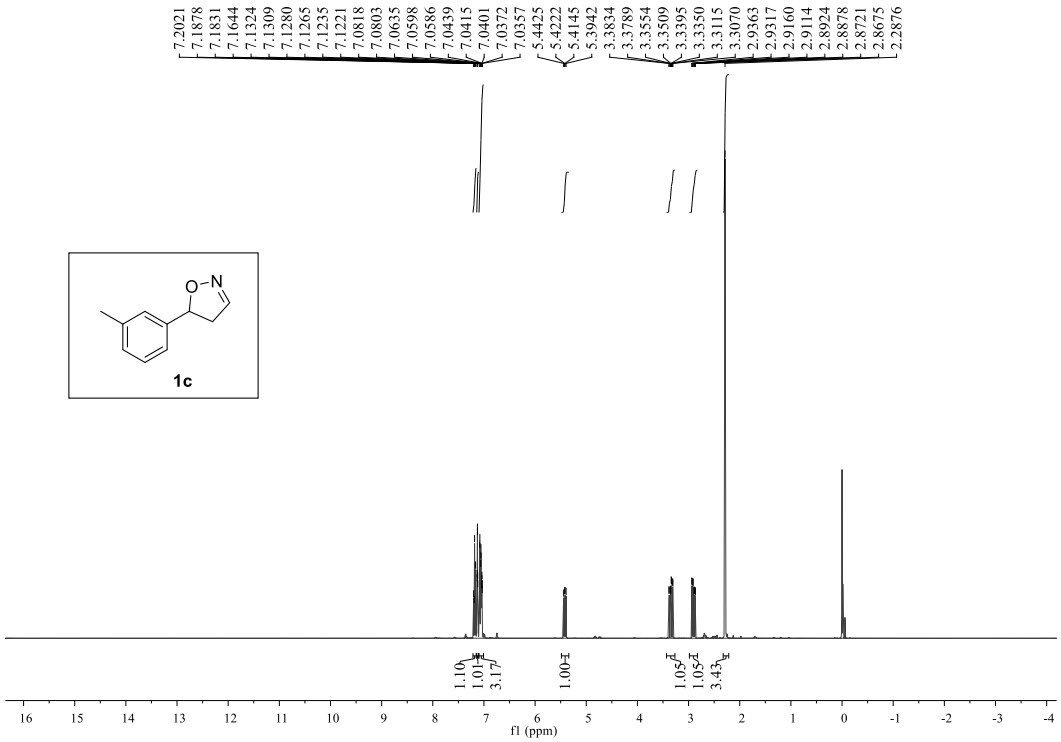
7.2021
7.1878
7.1831
7.1644
7.1324
7.1309
7.1280
7.1265
7.1235
7.1221
7.0818
7.0803
7.0635
7.0598
7.0586
7.0439
7.0415
7.0401
7.0372
7.0357
5.4425
5.4222
5.4145
5.3942
3.3834
3.3789
3.3554
3.3509
3.3395
3.3350
3.3115
3.3070
2.9363
2.9317
2.9160
2.9114
2.8924
2.8878
2.8721
2.8675
2.2876
1.10
1.01
3.17
1.00
1.05
1.05
3.43
O
N
1c
fl (ppm)

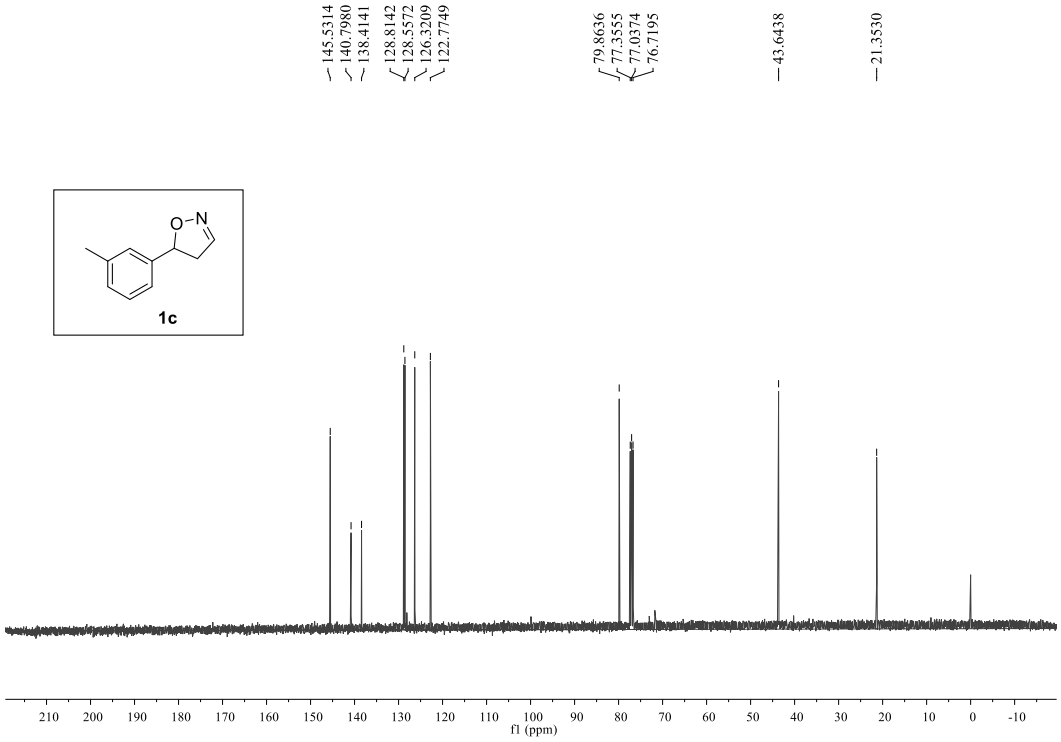
145.5314
140.7980
138.4141
128.8142
128.5572
126.3209
122.7749
79.8636
77.3555
77.0374
76.7195
43.6438
21.3530
O
N
1c
fl (ppm)

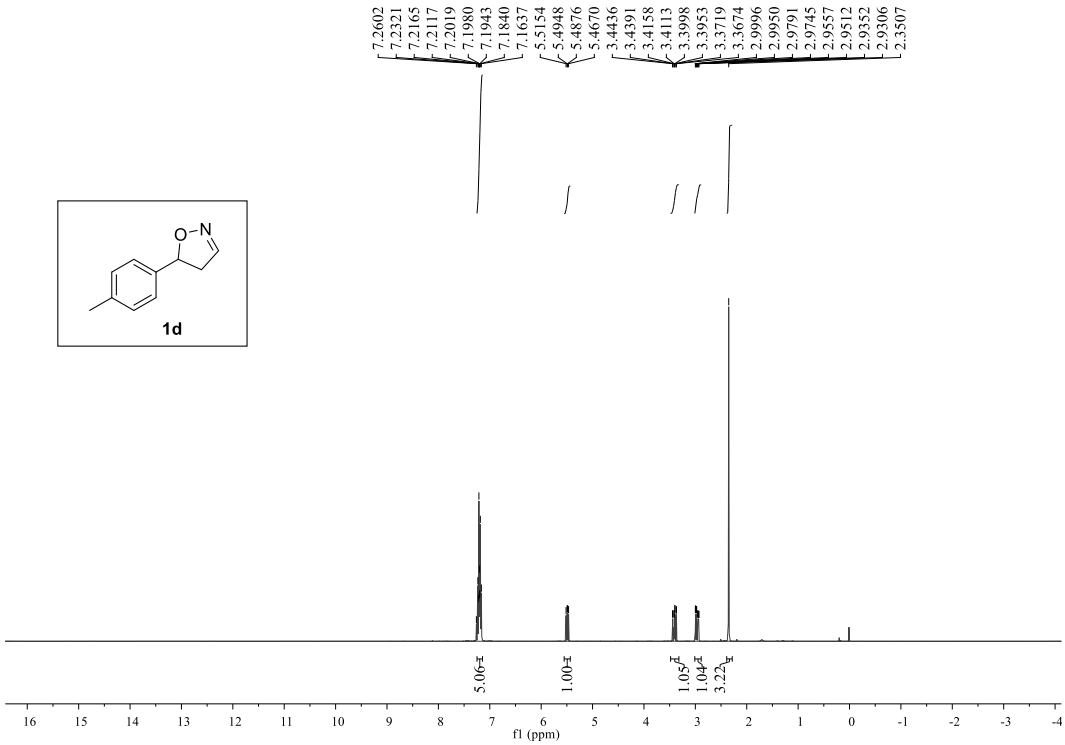
7.2602
7.2321
7.2165
7.2117
7.2019
7.1980
7.1943
7.1840
7.1637
5.5154
5.4948
5.4876
5.4670
3.4436
3.4391
3.4158
3.4113
3.3998
3.3953
3.3719
3.3674
2.9996
2.9950
2.9791
2.9745
2.9557
2.9512
2.9352
2.9306
2.3507
O
N
1d
5.06
1.00
1.05
1.04
3.22
16 15 14 13 12 11 10 9 8 7 6 5 4 3 2 1 0 -1 -2 -3 -4
f1 (ppm)

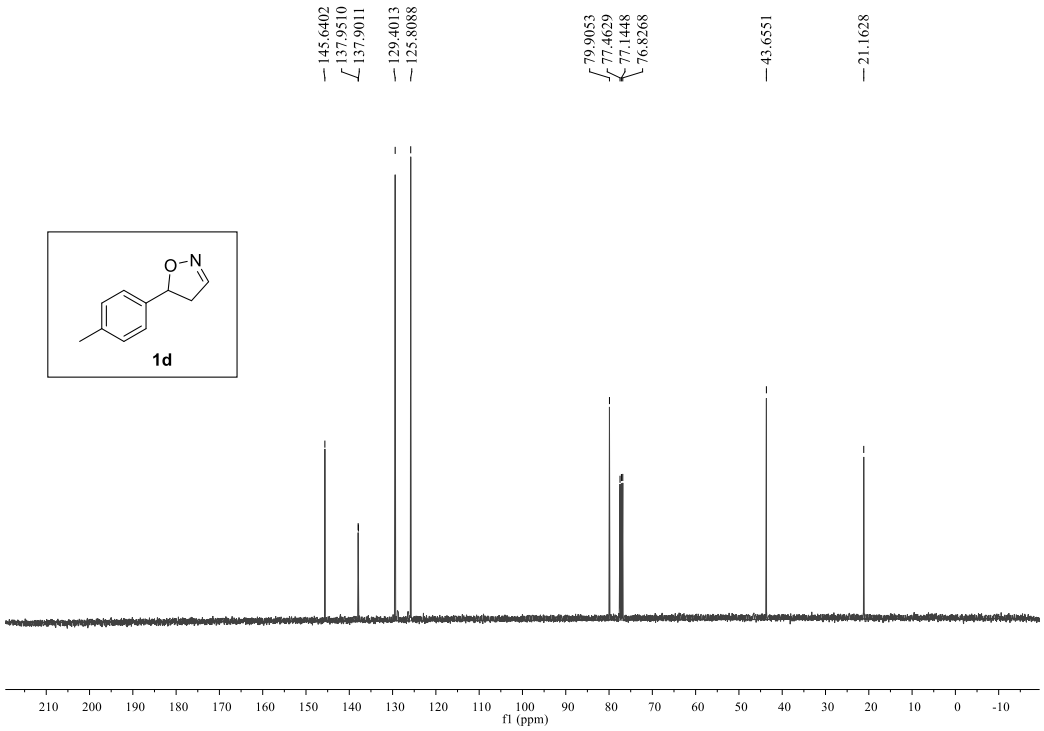
145.6402
137.9510
137.9011
129.4013
125.8088
79.9053
77.4629
77.1448
76.8268
43.6551
21.1628
O
N
1d
210 200 190 180 170 160 150 140 130 120 110 100 90 80 70 60 50 40 30 20 10 0 -10
f1 (ppm)

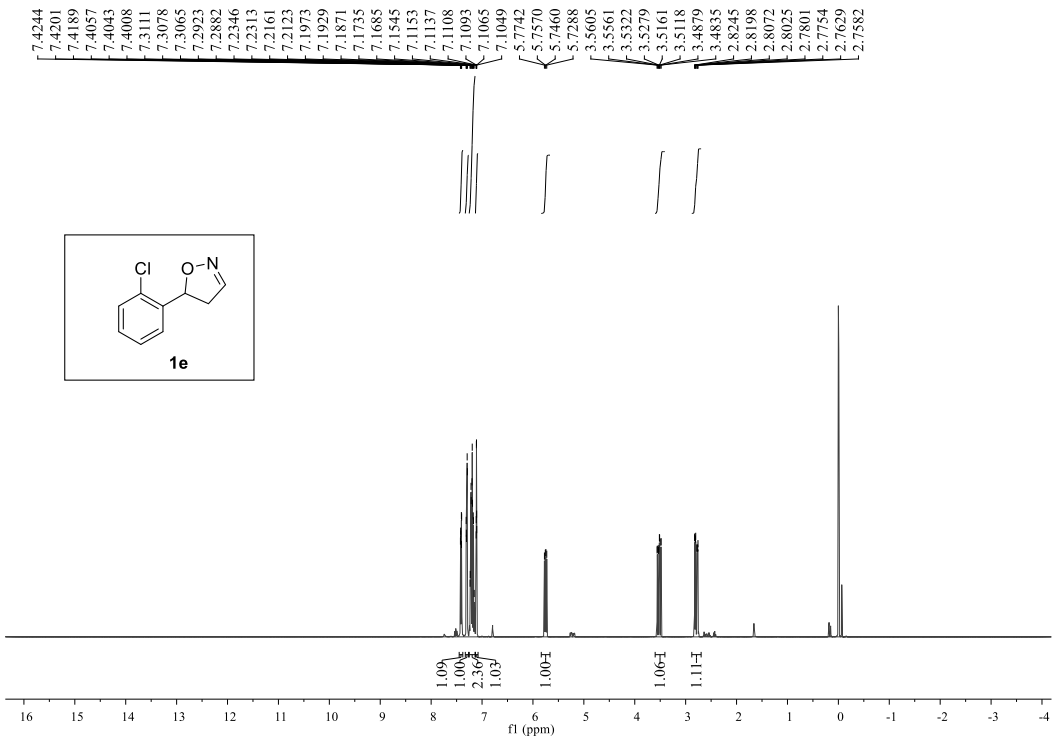
7.4244
7.4201
7.4189
7.4057
7.4043
7.4008
7.3111
7.3078
7.3065
7.2923
7.2882
7.2346
7.2313
7.2161
7.2123
7.1973
7.1929
7.1871
7.1735
7.1685
7.1545
7.1153
7.1137
7.1108
7.1093
7.1065
7.1049
5.7742
5.7570
5.7460
5.7288
3.5605
3.5561
3.5322
3.5279
3.5161
3.5118
3.4879
3.4835
2.8245
2.8198
2.8072
2.8025
2.7801
2.7754
2.7629
2.7582
Cl
O
N
1e
1.09
1.00
2.36
1.03
1.00
1.06
1.11
f1 (ppm)

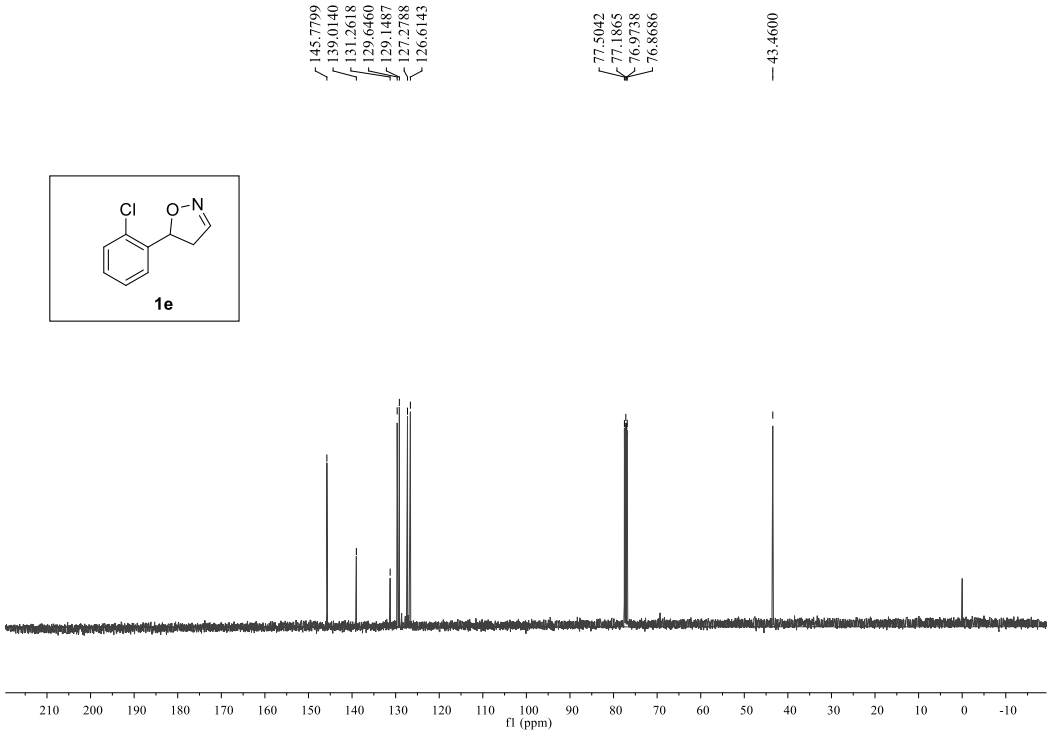
145.7799
139.0140
131.2618
129.6460
129.1487
127.2788
126.6143
77.5042
77.1865
76.9738
76.8686
43.4600
Cl
O
N
1e
f1 (ppm)

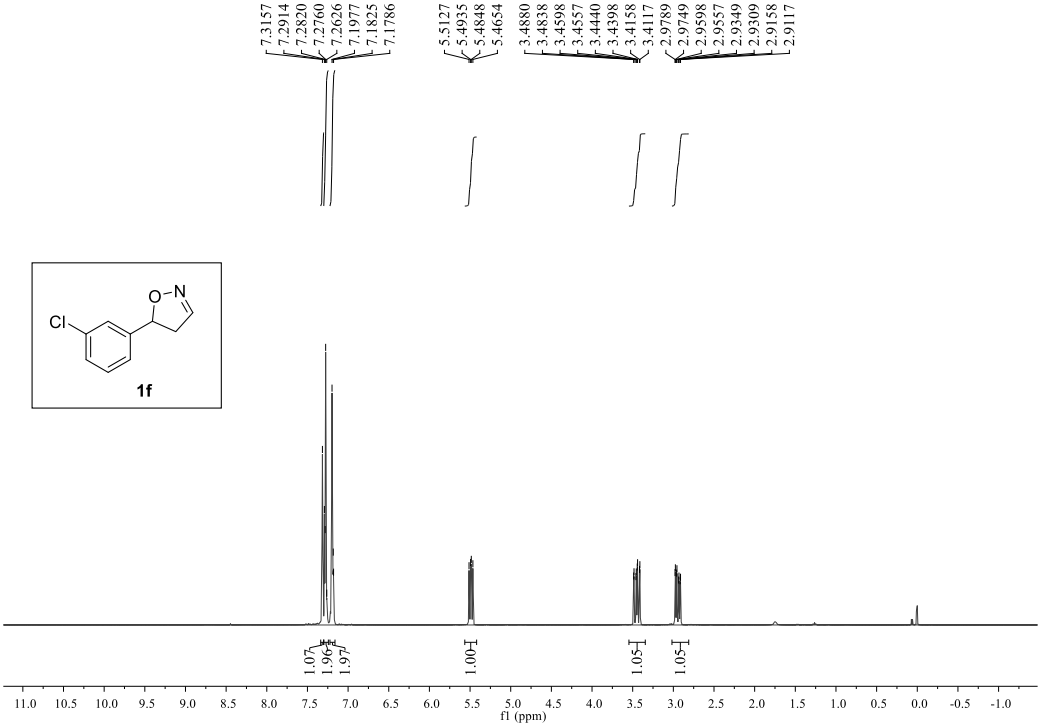
7.3157
7.2914
7.2820
7.2760
7.2626
7.1977
7.1825
7.1786
5.5127
5.4935
5.4848
5.4654
3.4880
3.4838
3.4598
3.4557
3.4440
3.4398
3.4158
3.4117
2.9789
2.9749
2.9598
2.9557
2.9349
2.9309
2.9158
2.9117
Cl
O
N
1f
1.07
1.96
1.97
1.00
1.05
1.05
11.0 10.5 10.0 9.5 9.0 8.5 8.0 7.5 7.0 6.5 6.0 5.5 5.0 4.5 4.0 3.5 3.0 2.5 2.0 1.5 1.0 0.5 0.0 -0.5 -1.0
f1 (ppm)

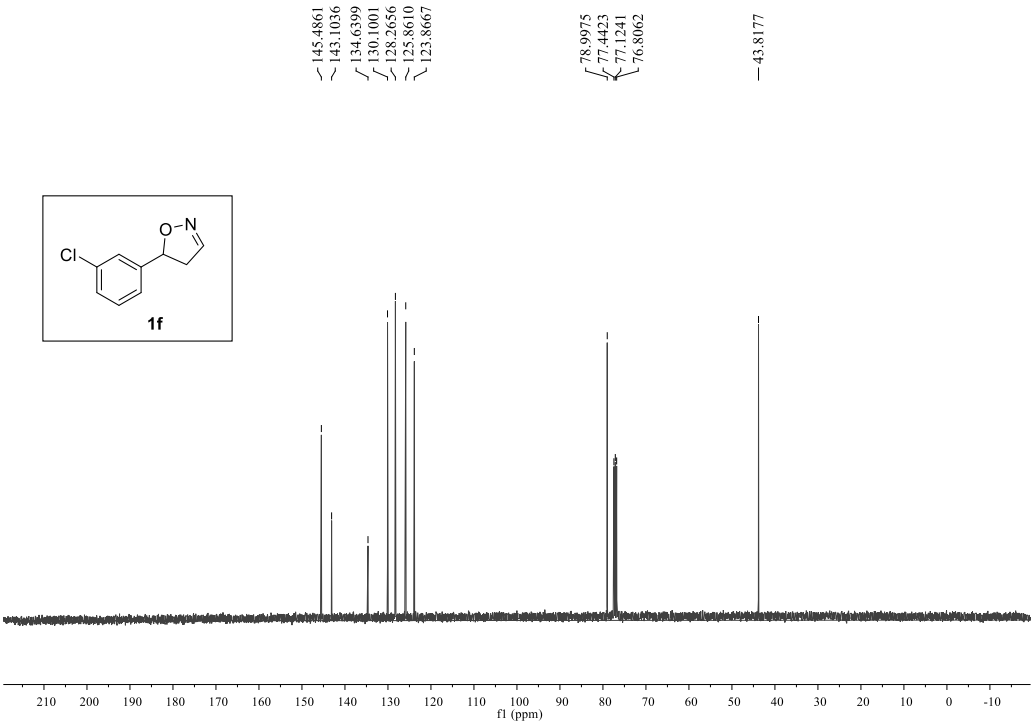
145.4861
143.1036
134.6399
130.1001
128.2656
125.8610
123.8667
78.9975
77.4423
77.1241
76.8062
43.8177
Cl
O
N
1f
210 200 190 180 170 160 150 140 130 120 110 100 90 80 70 60 50 40 30 20 10 0 -10
f1 (ppm)

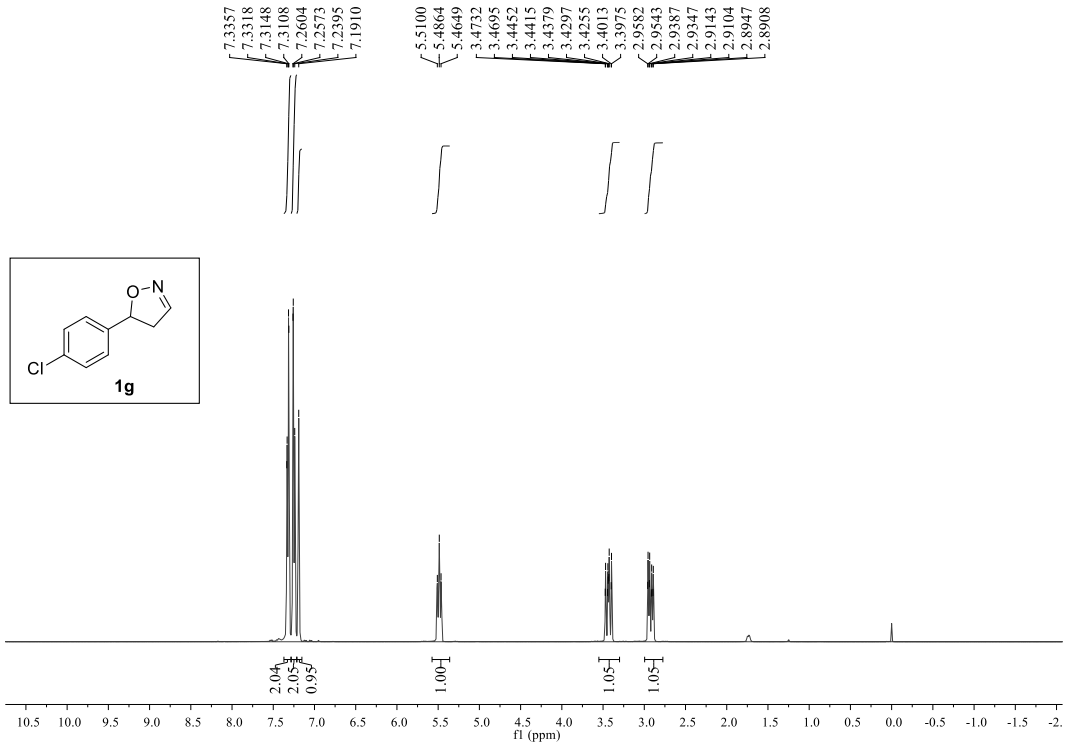
7.3357
7.3318
7.3148
7.3108
7.2604
7.2573
7.2395
7.1910
5.5100
5.4864
5.4649
3.4732
3.4695
3.4452
3.4415
3.4379
3.4297
3.4255
3.4013
3.3975
2.9582
2.9543
2.9387
2.9347
2.9143
2.9104
2.8947
2.8908
O
N
Cl
1g
2.04
2.05
0.95
1.00
1.05
1.05
f1 (ppm)

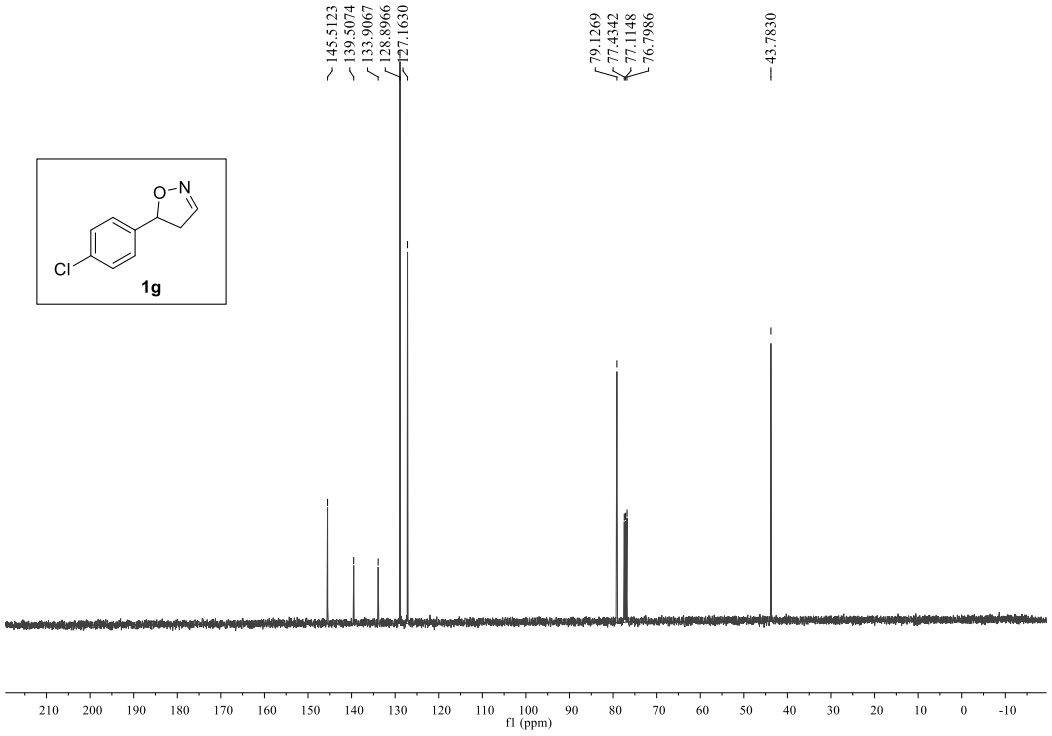
145.5123
139.5074
133.9067
128.8966
127.1630
79.1269
77.4342
77.1148
76.7986
43.7830
O
N
Cl
1g
f1 (ppm)

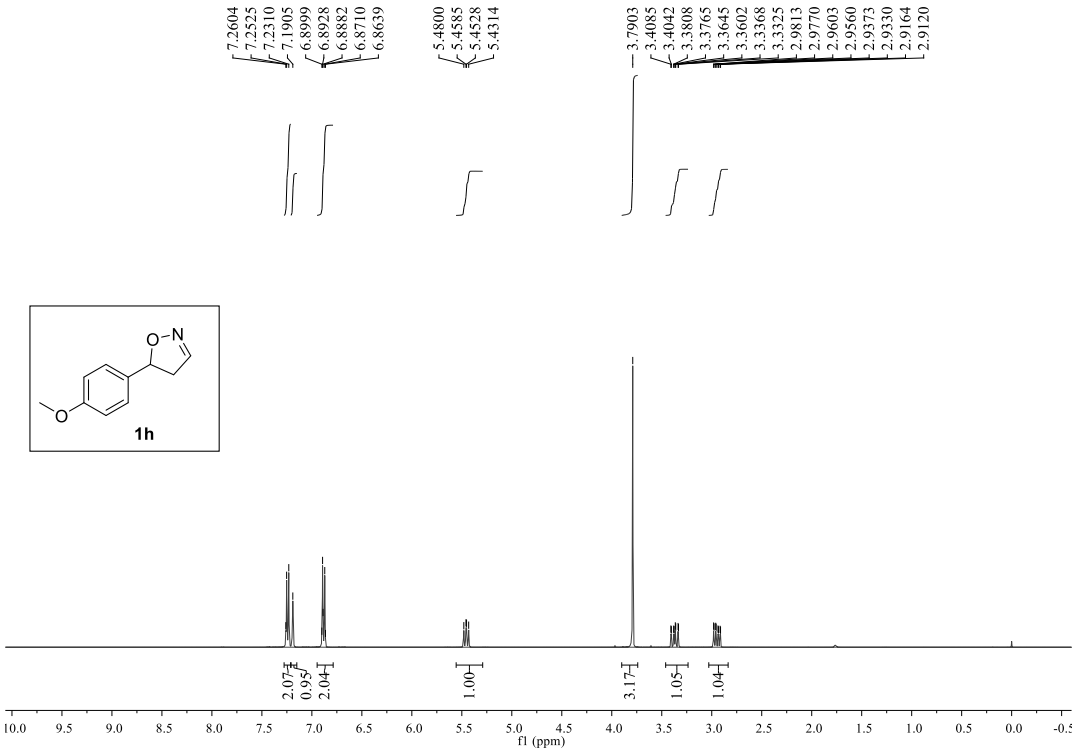
7.2604
7.2525
7.2310
7.1905
6.8999
6.8928
6.8882
6.8710
6.8639
5.4800
5.4585
5.4528
5.4314
3.7903
3.4085
3.4042
3.3808
3.3765
3.3645
3.3602
3.3368
3.3325
2.9813
2.9770
2.9603
2.9560
2.9373
2.9330
2.9164
2.9120
1h
2.07
0.95
2.04
1.00
3.17
1.05
1.04
f1 (ppm)

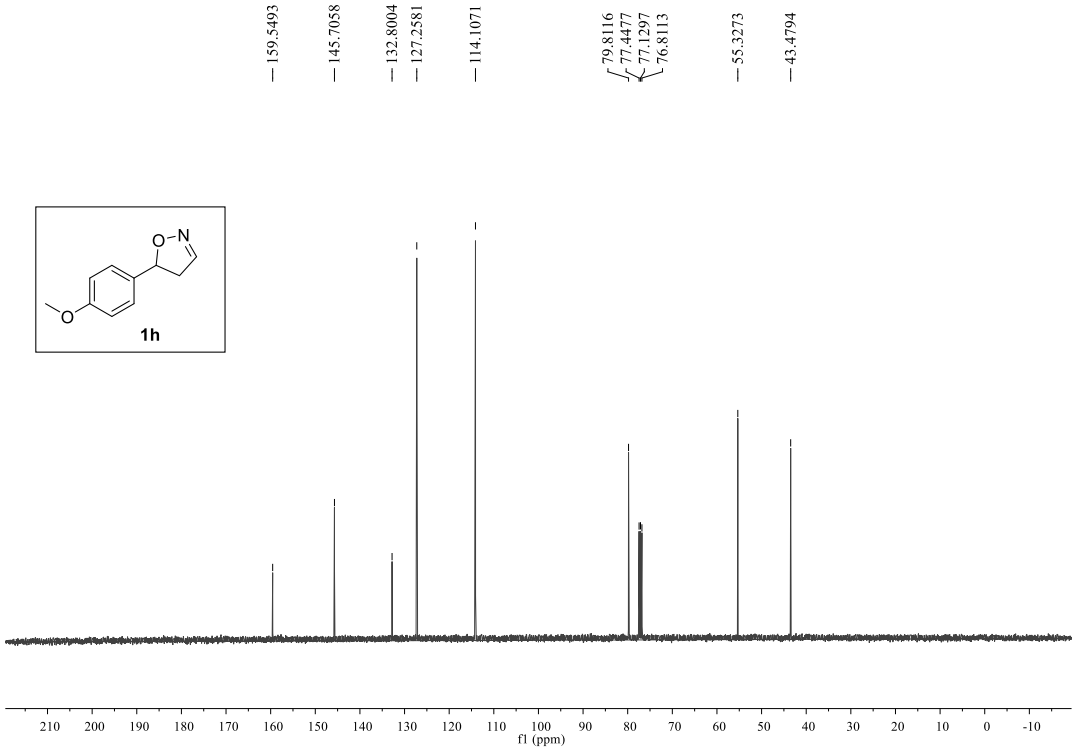
159.5493
145.7058
132.8004
127.2581
114.1071
79.8116
77.4477
77.1297
76.8113
55.3273
43.4794
1h
f1 (ppm)

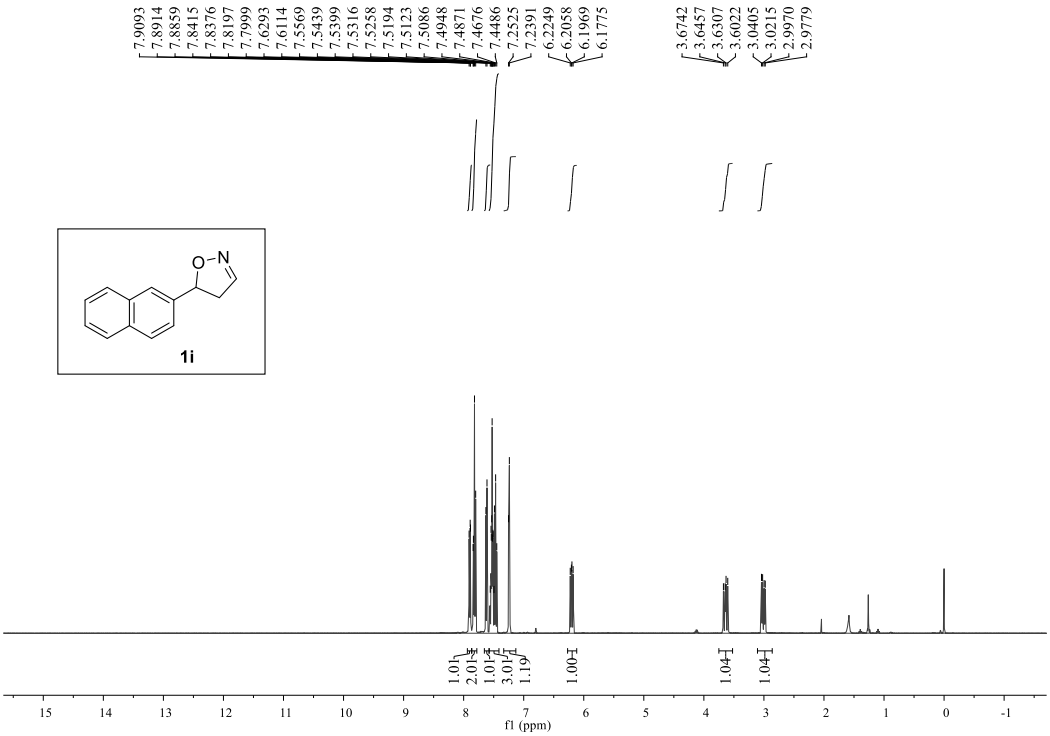
7.9093
7.8914
7.8859
7.8415
7.8376
7.8197
7.7999
7.6293
7.6114
7.5569
7.5439
7.5399
7.5316
7.5258
7.5194
7.5123
7.5086
7.4948
7.4871
7.4676
7.4486
7.2525
7.2391
6.2249
6.2058
6.1969
6.1775
3.6742
3.6457
3.6307
3.6022
3.0405
3.0215
2.9970
2.9779
O
N
1i
1.01
2.01
1.01
3.01
1.19
1.00
1.04
1.04
15 14 13 12 11 10 9 8 7 6 5 4 3 2 1 0 -1
f1 (ppm)

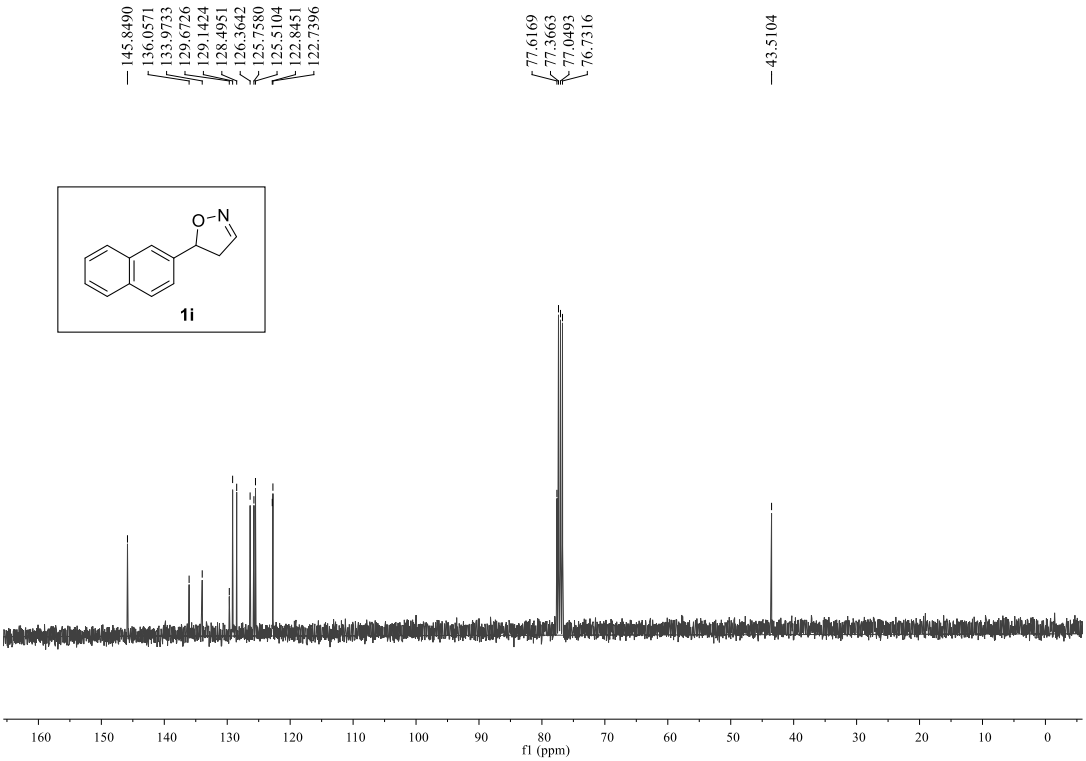
145.8490
136.0571
133.9733
129.6726
129.1424
128.4951
126.3642
125.7580
125.5104
122.8451
122.7396
77.6169
77.3663
77.0493
76.7316
43.5104
O
N
1i
160 150 140 130 120 110 100 90 80 70 60 50 40 30 20 10 0
f1 (ppm)

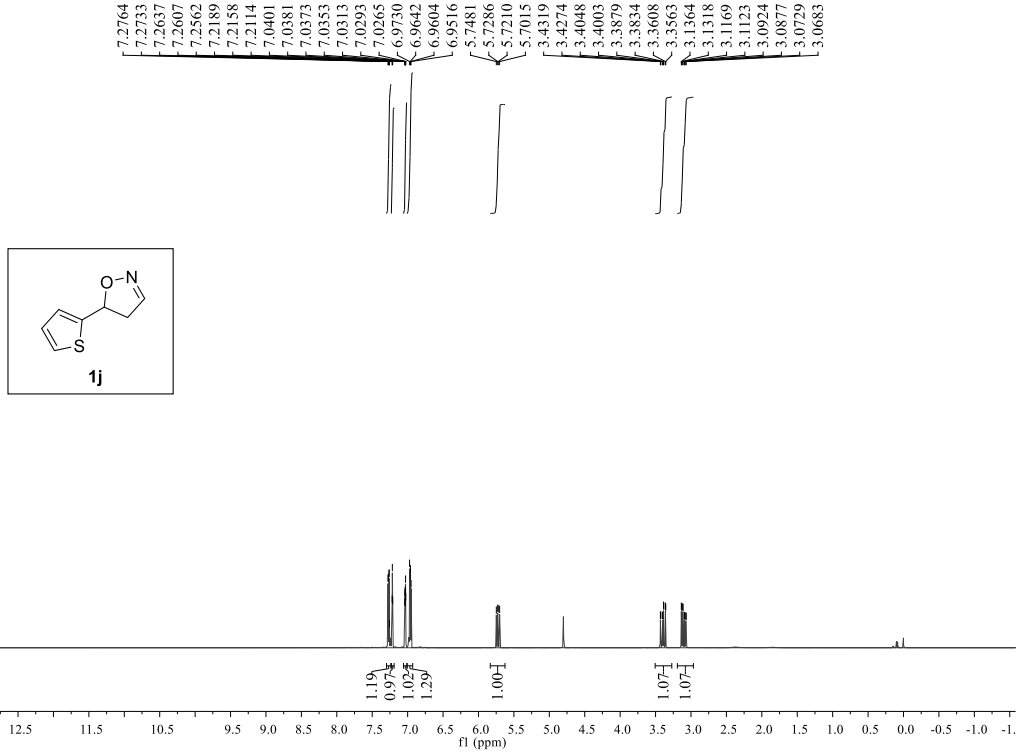
7.2764
7.2733
7.2637
7.2607
7.2562
7.2189
7.2158
7.2114
7.0401
7.0381
7.0373
7.0353
7.0313
7.0293
7.0265
6.9730
6.9642
6.9604
6.9516
5.7481
5.7286
5.7210
5.7015
3.4319
3.4274
3.4048
3.4003
3.3879
3.3834
3.3608
3.3563
3.1364
3.1318
3.1169
3.1123
3.0924
3.0877
3.0729
3.0683
1j
1.19
0.97
1.02
1.29
1.00
1.07
1.07
f1 (ppm)

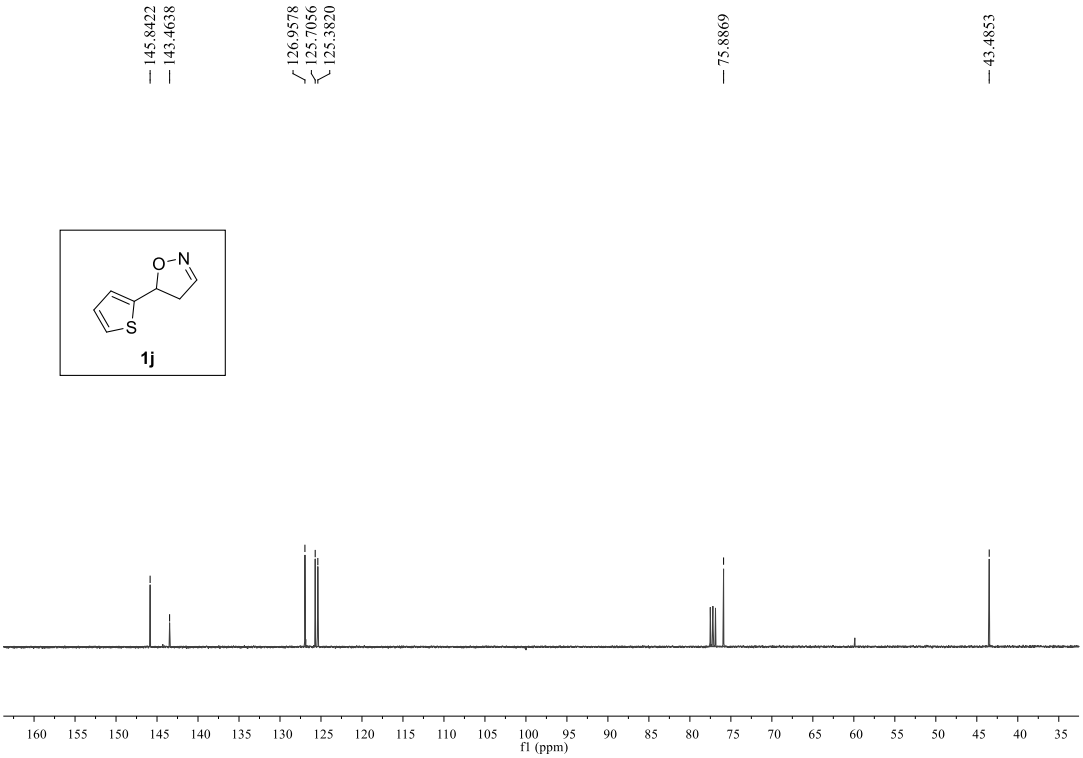
145.8422
143.4638
126.9578
125.7056
125.3820
75.8869
43.4853
1j
f1 (ppm)

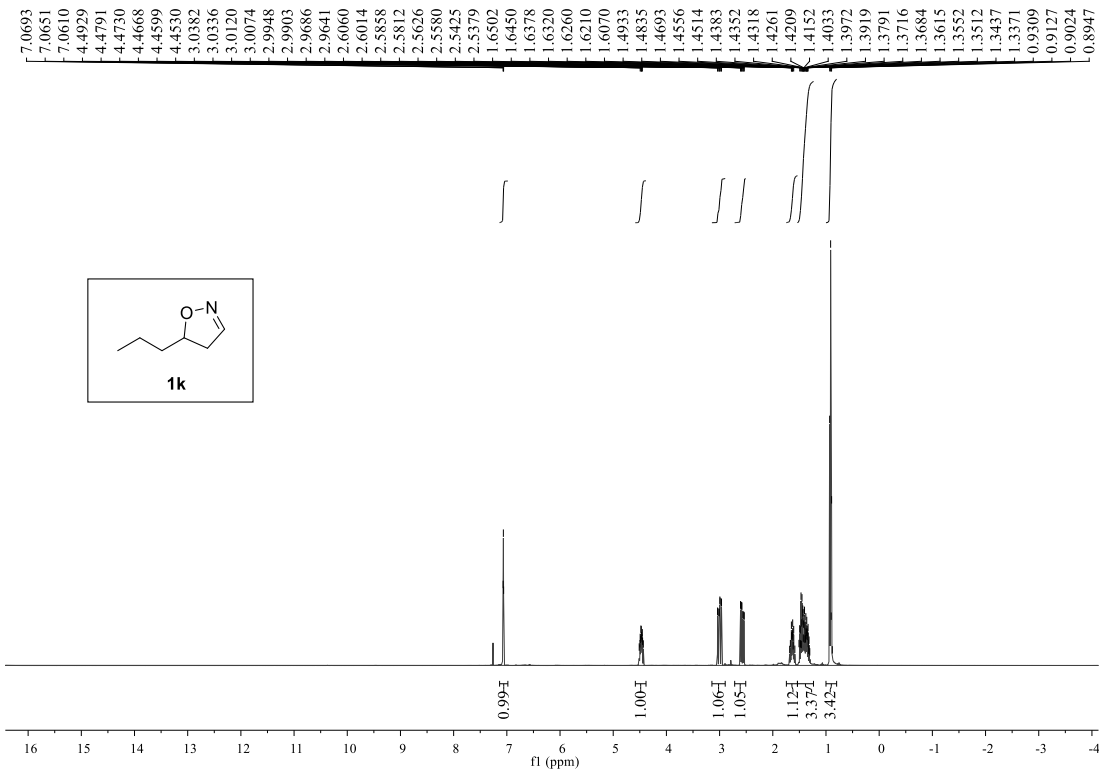
7.0693
7.0651
7.0610
4.4929
4.4791
4.4730
4.4668
4.4599
4.4530
3.0382
3.0336
3.0120
3.0074
2.9948
2.9903
2.9686
2.9641
2.6060
2.6014
2.5858
2.5812
2.5626
2.5580
2.5425
2.5379
1.6502
1.6450
1.6378
1.6320
1.6260
1.6210
1.6070
1.4933
1.4835
1.4693
1.4556
1.4514
1.4383
1.4352
1.4318
1.4261
1.4209
1.4152
1.4033
1.3972
1.3919
1.3791
1.3716
1.3684
1.3615
1.3552
1.3512
1.3437
1.3371
0.9309
0.9127
0.9024
0.8947
O
N
1k
0.99
1.00
1.06
1.05
1.12
3.37
3.42
f1 (ppm)

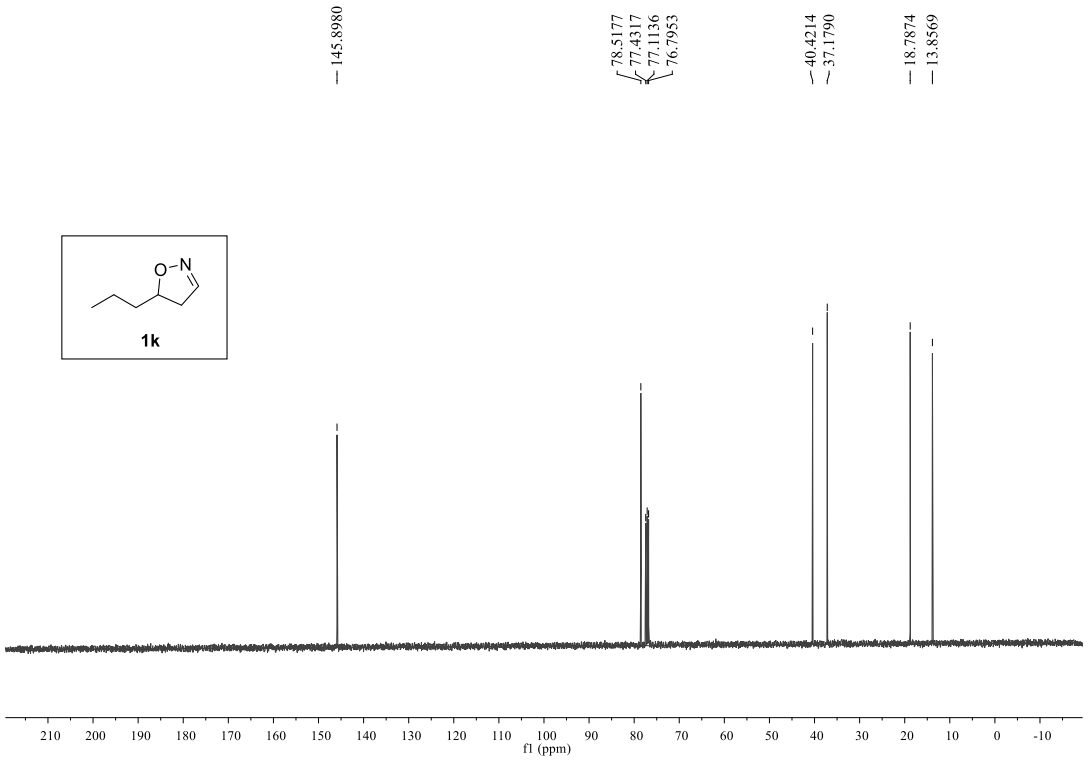
145.8980
78.5177
77.4317
77.1136
76.7953
40.4214
37.1790
18.7874
13.8569
O
N
1k
f1 (ppm)

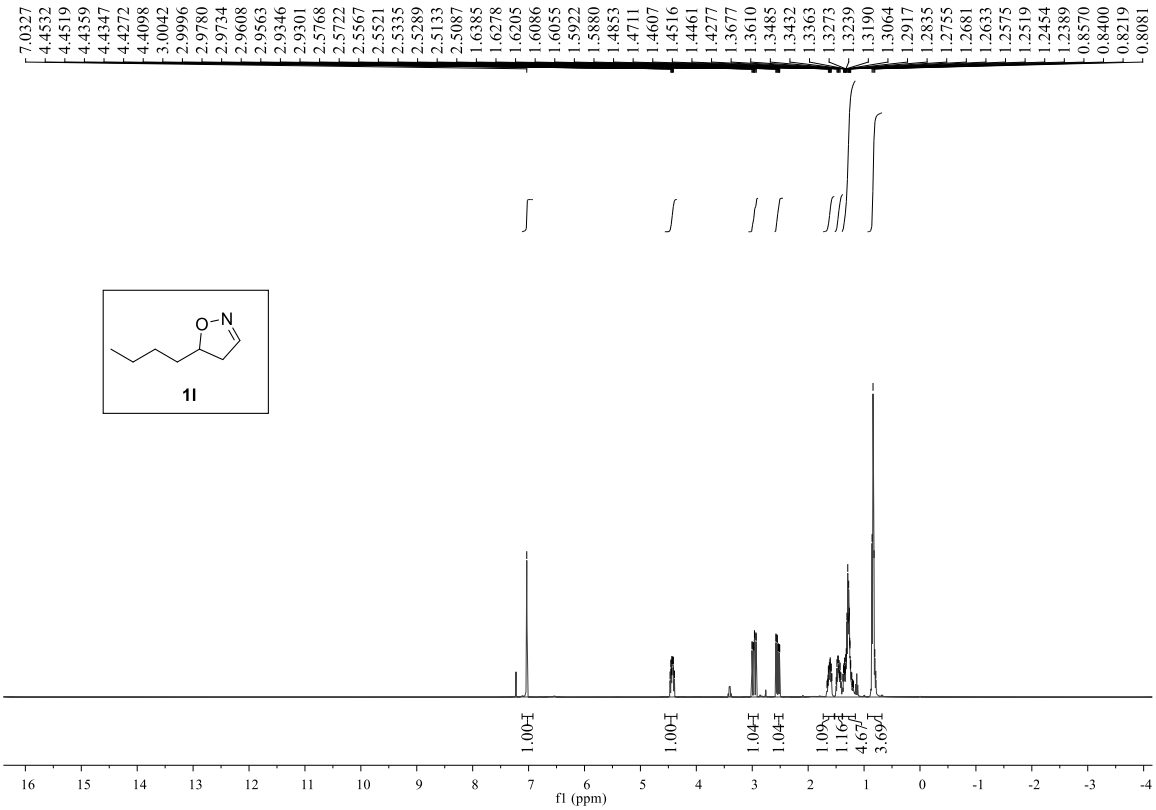
7.0327
4.4532
4.4519
4.4359
4.4347
4.4272
4.4098
3.0042
2.9996
2.9780
2.9734
2.9608
2.9563
2.9346
2.9301
2.5768
2.5722
2.5567
2.5521
2.5335
2.5289
2.5133
2.5087
1.6385
1.6278
1.6205
1.6086
1.6055
1.5922
1.5880
1.4853
1.4711
1.4607
1.4516
1.4461
1.4277
1.3677
1.3610
1.3485
1.3432
1.3363
1.3273
1.3239
1.3190
1.3064
1.2917
1.2835
1.2755
1.2681
1.2633
1.2575
1.2519
1.2454
1.2389
0.8570
0.8400
0.8219
0.8081
O
N
1l
1.00
1.00
1.04
1.04
1.09
1.16
4.67
3.69
16 15 14 13 12 11 10 9 8 7 6 5 4 3 2 1 0 -1 -2 -3 -4
f1 (ppm)

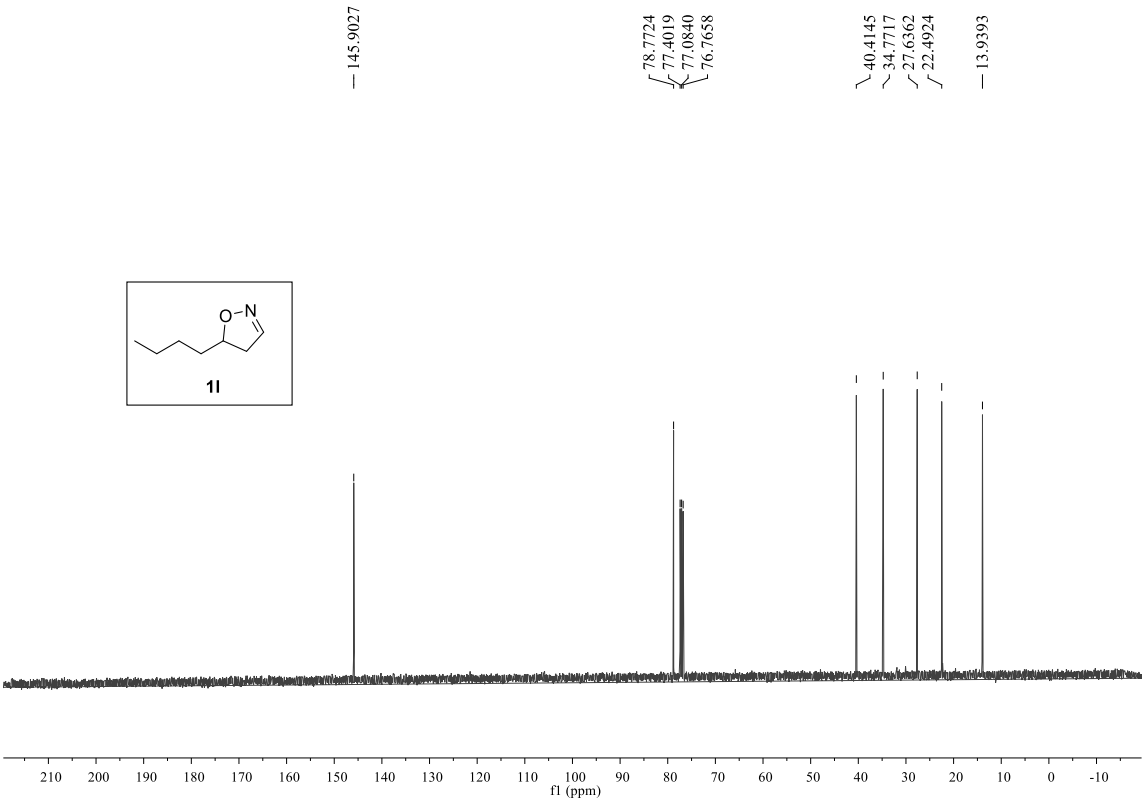
145.9027
78.7724
77.4019
77.0840
76.7658
40.4145
34.7717
27.6362
22.4924
13.9393
O
N
1l
210 200 190 180 170 160 150 140 130 120 110 100 90 80 70 60 50 40 30 20 10 0 -10
f1 (ppm)

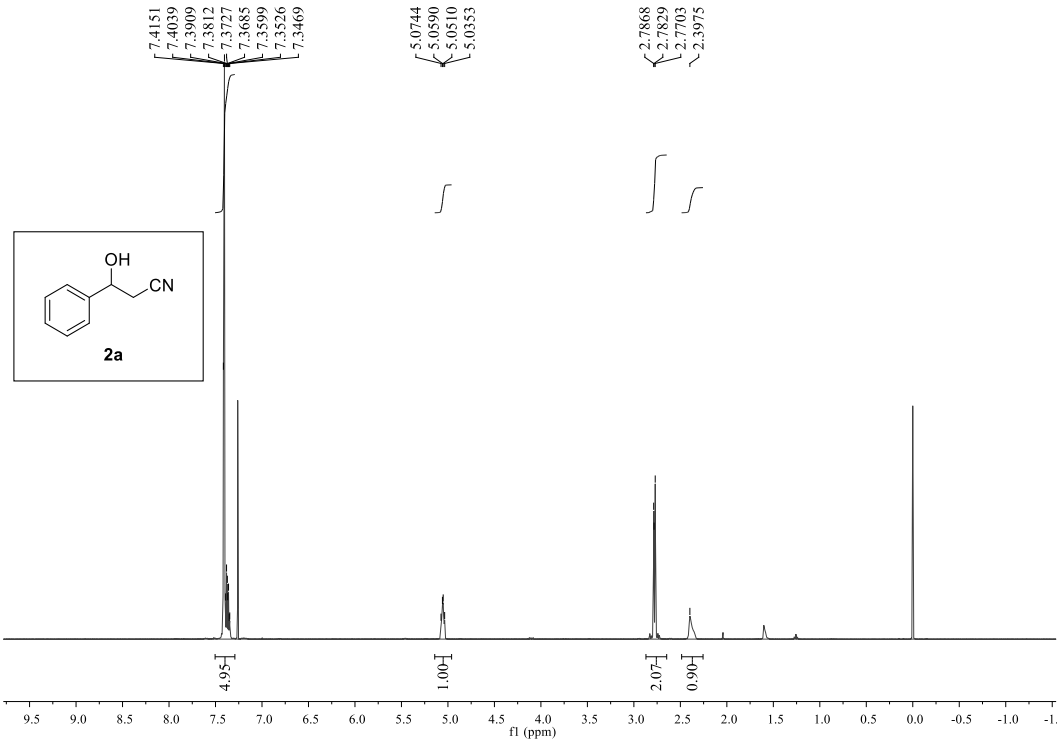
7.4151
7.4039
7.3909
7.3812
7.3727
7.3685
7.3599
7.3526
7.3469
5.0744
5.0590
5.0510
5.0353
2.7868
2.7829
2.7703
2.3975
OH
CN
2a
4.95
1.00
2.07
0.90
f1 (ppm)

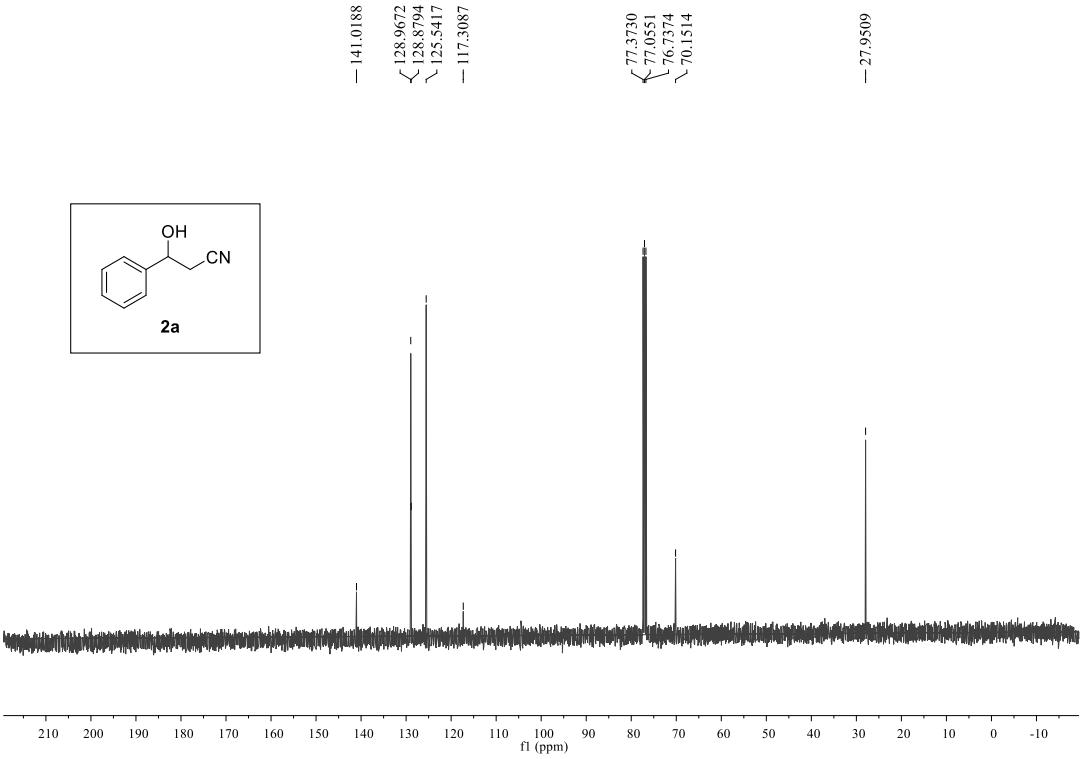
141.0188
128.9672
128.8794
125.5417
117.3087
77.3730
77.0551
76.7374
70.1514
27.9509
OH
CN
2a
f1 (ppm)

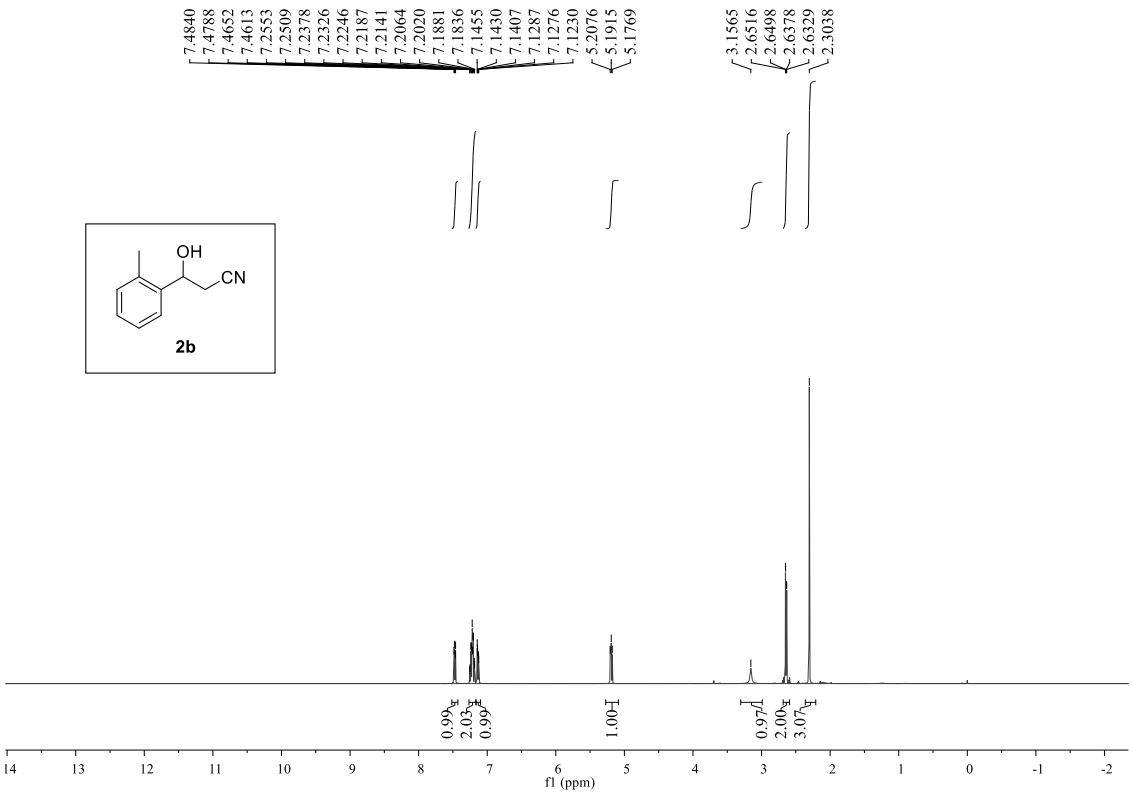
7.4840
7.4788
7.4652
7.4613
7.2553
7.2509
7.2378
7.2326
7.2246
7.2187
7.2141
7.2064
7.2020
7.1881
7.1836
7.1455
7.1430
7.1407
7.1287
7.1276
7.1230
5.2076
5.1915
5.1769
3.1565
2.6516
2.6498
2.6378
2.6329
2.3038
OH
CN
2b
0.99
2.03
0.99
1.00
0.97
2.00
3.07
f1 (ppm)

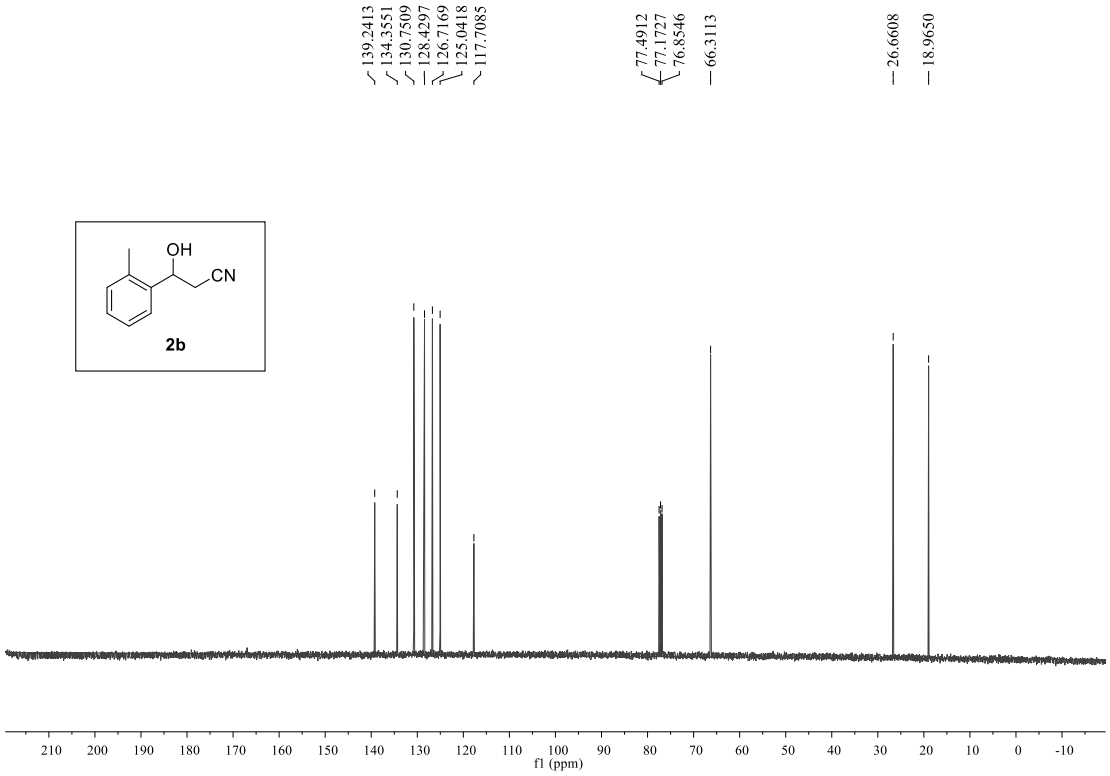
139.2413
134.3551
130.7509
128.4297
126.7169
125.0418
117.7085
77.4912
77.1727
76.8546
66.3113
26.6608
18.9650
OH
CN
2b
f1 (ppm)

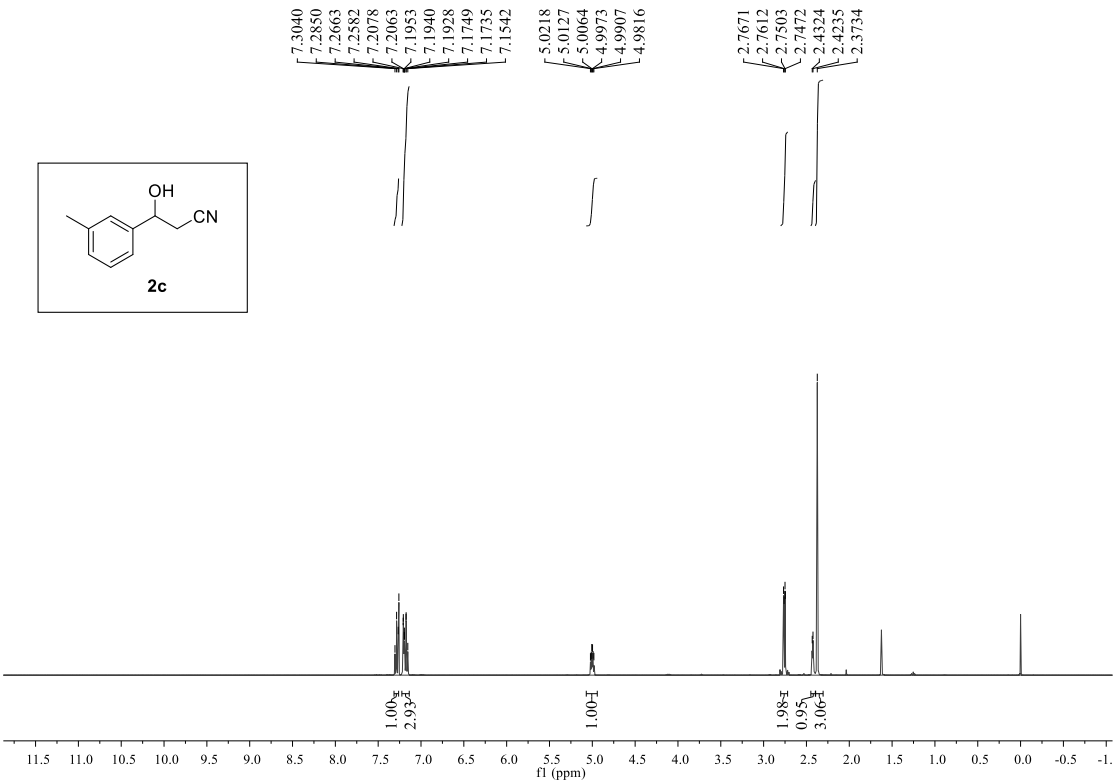
7.3040
7.2850
7.2663
7.2582
7.2078
7.2063
7.1953
7.1940
7.1928
7.1749
7.1735
7.1542
5.0218
5.0127
5.0064
4.9973
4.9907
4.9816
2.7671
2.7612
2.7503
2.7472
2.4324
2.4235
2.3734
OH
CN
2c
1.00
2.93
1.00
1.98
0.95
3.06
f1 (ppm)

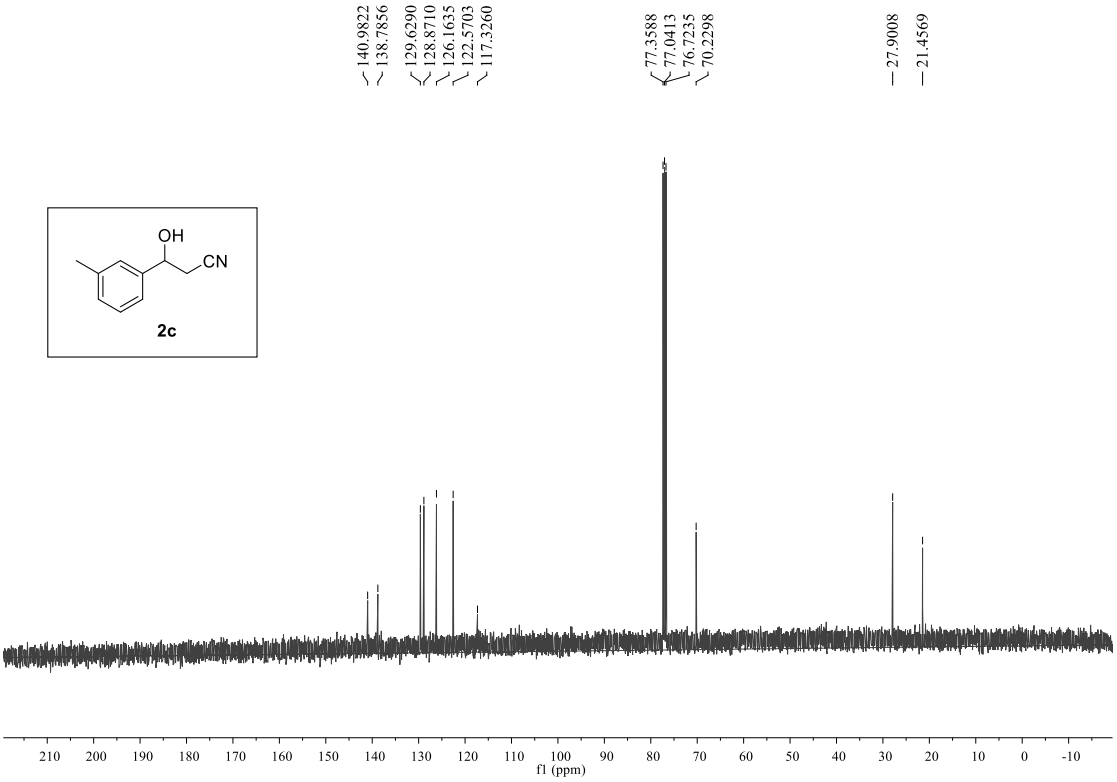
140.9822
138.7856
129.6290
128.8710
126.1635
122.5703
117.3260
77.3588
77.0413
76.7235
70.2298
27.9008
21.4569
OH
CN
2c
f1 (ppm)

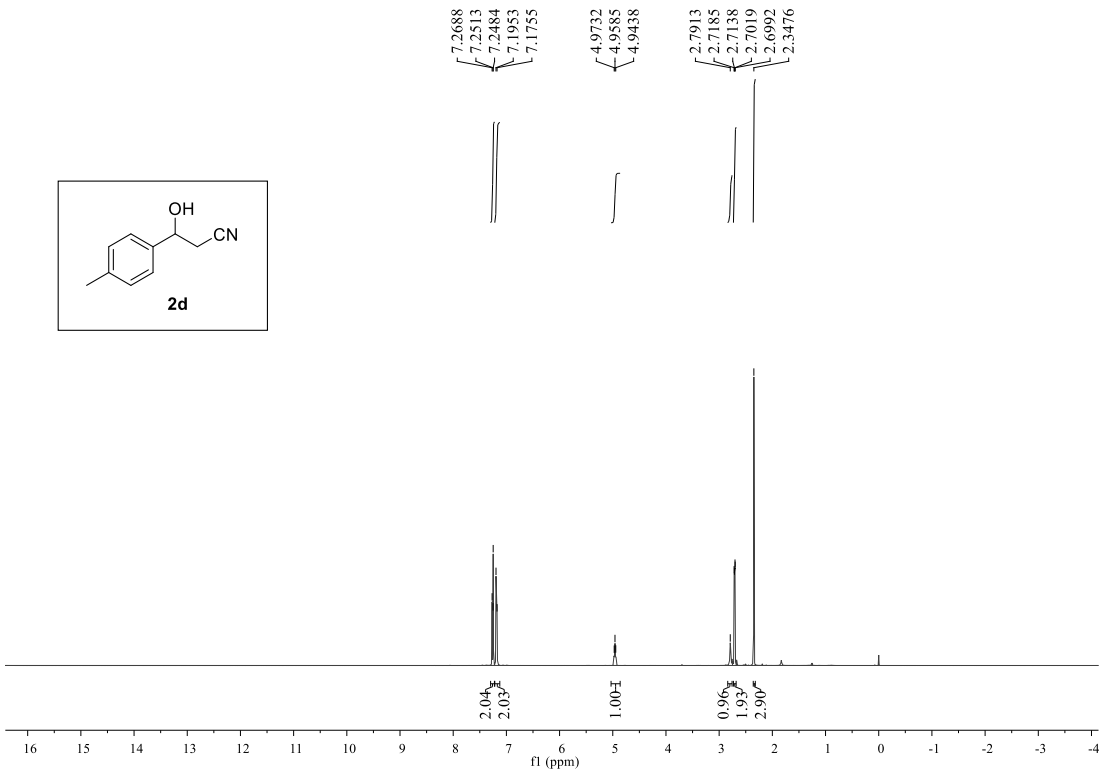
7.2688
7.2513
7.2484
7.1953
7.1755
4.9732
4.9585
4.9438
2.7913
2.7185
2.7138
2.7019
2.6992
2.3476
OH
CN
2d
2.04
2.03
1.00
0.96
1.93
2.90
f1 (ppm)

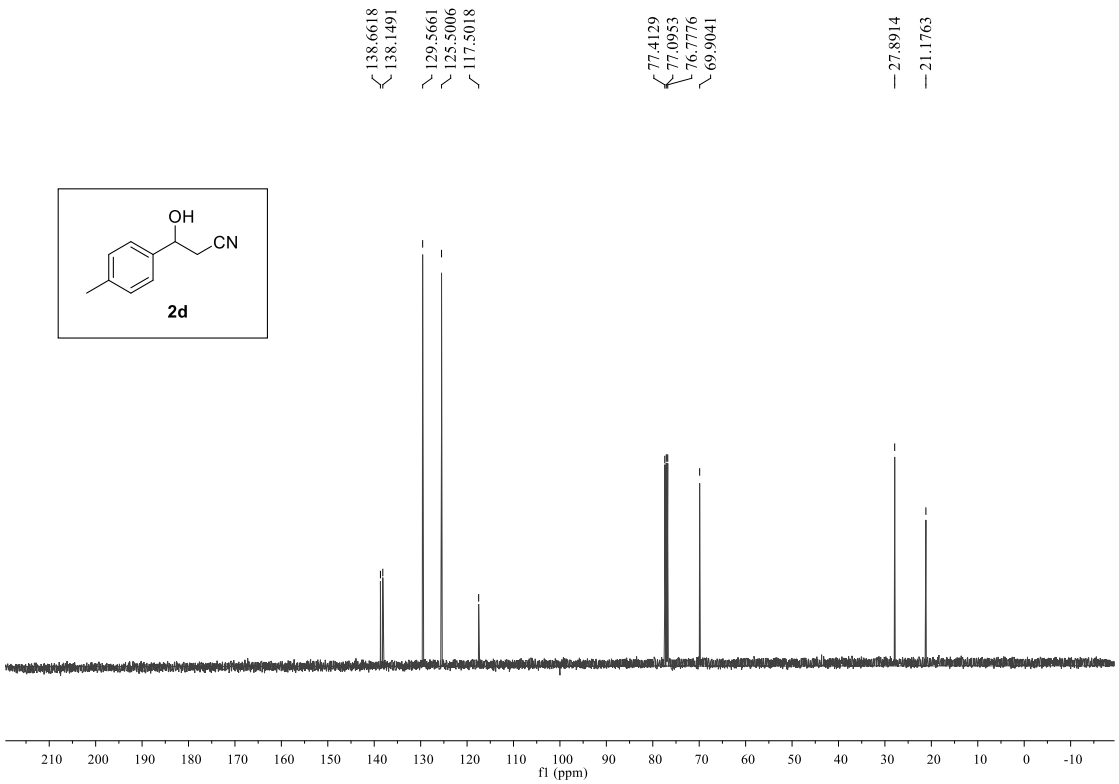
138.6618
138.1491
129.5661
125.5006
117.5018
77.4129
77.0953
76.7776
69.9041
27.8914
21.1763
OH
CN
2d
f1 (ppm)

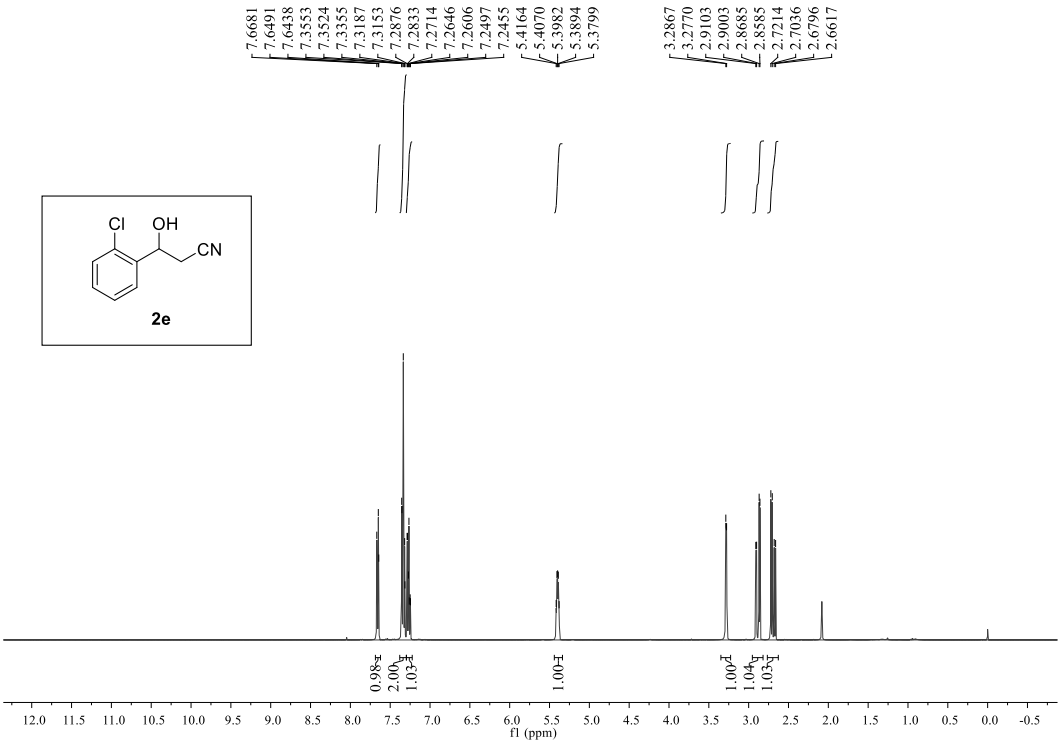
7.6681
7.6491
7.6438
7.3553
7.3524
7.3355
7.3187
7.3153
7.2876
7.2833
7.2714
7.2646
7.2606
7.2497
7.2455
5.4164
5.4070
5.3982
5.3894
5.3799
3.2867
3.2770
2.9103
2.9003
2.8685
2.8585
2.7214
2.7036
2.6796
2.6617
Cl
OH
CN
2e
0.98
2.00
1.03
1.00
1.00
1.04
1.03
f1 (ppm)

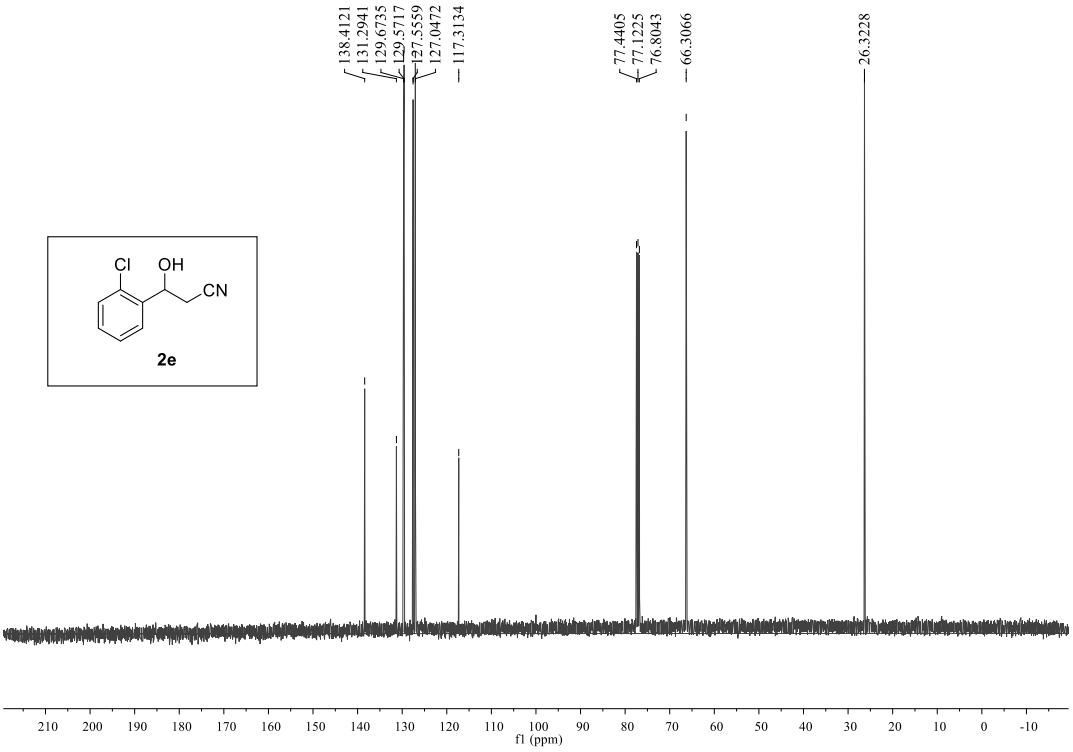
138.4121
131.2941
129.6735
129.5717
127.5559
127.0472
117.3134
77.4405
77.1225
76.8043
66.3066
26.3228
Cl
OH
CN
2e
f1 (ppm)

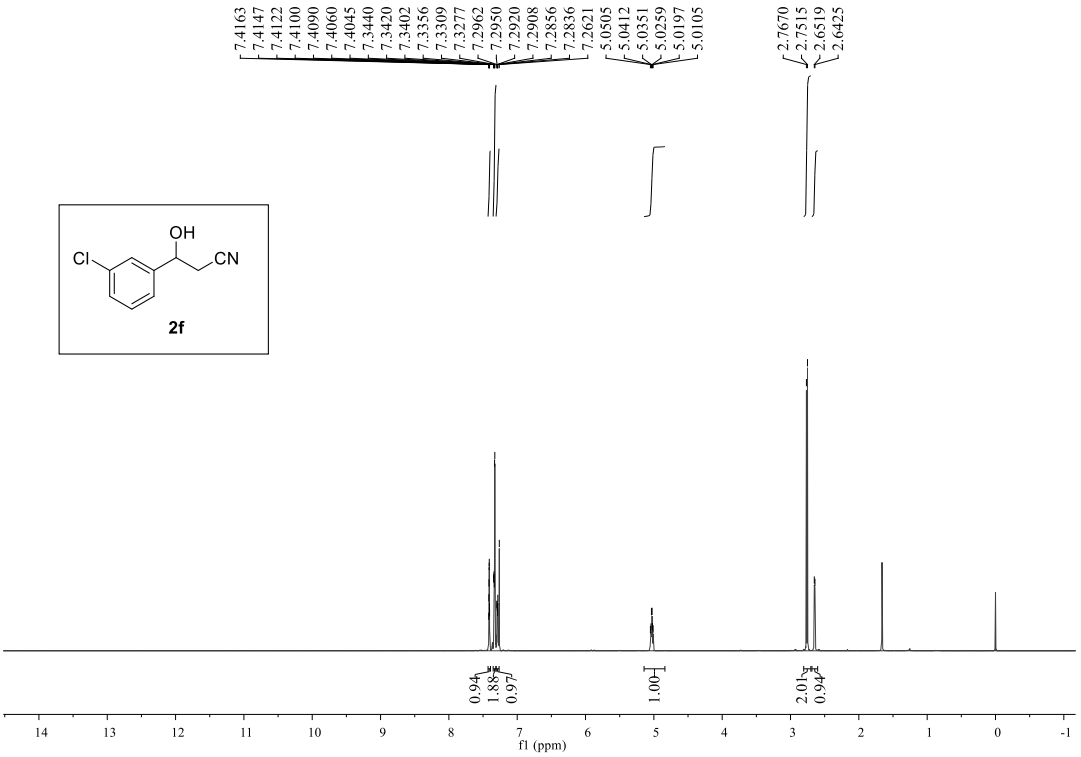
7.4163
7.4147
7.4122
7.4100
7.4090
7.4060
7.4045
7.3440
7.3420
7.3402
7.3356
7.3309
7.3277
7.2962
7.2950
7.2920
7.2908
7.2856
7.2836
7.2621
5.0505
5.0412
5.0351
5.0259
5.0197
5.0105
2.7670
2.7515
2.6519
2.6425
OH
Cl
CN
2f
0.94
1.88
0.97
1.00
2.01
0.94
f1 (ppm)

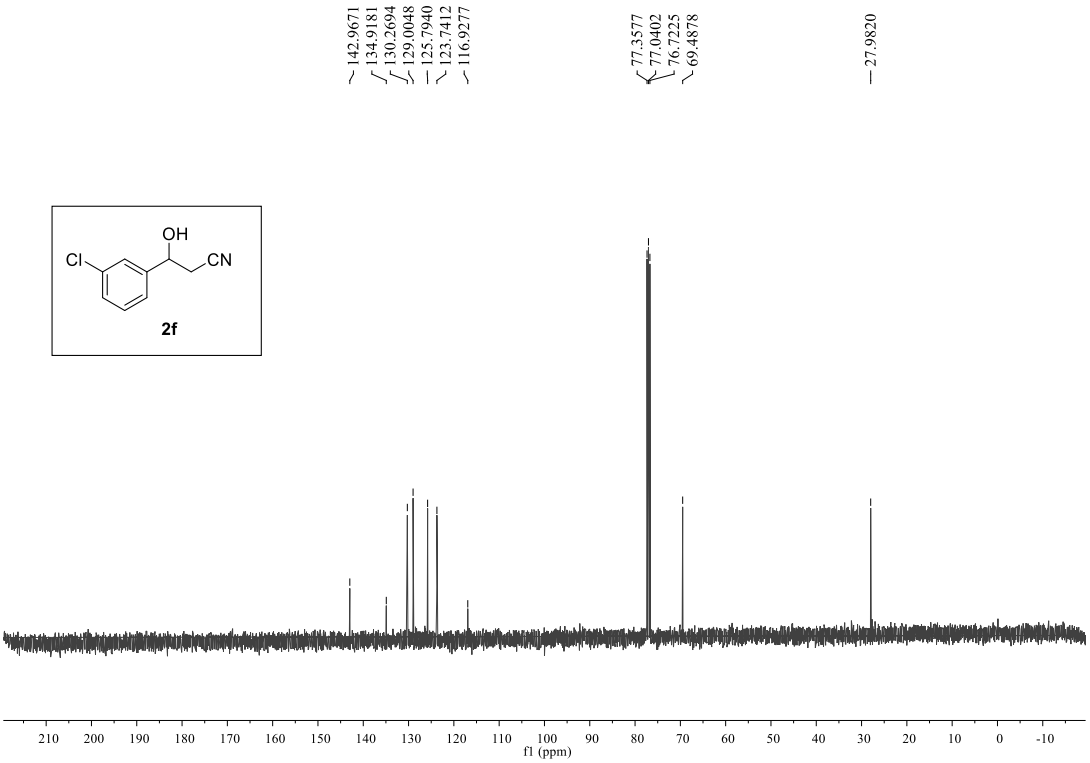
142.9671
134.9181
130.2694
129.0048
125.7940
123.7412
116.9277
77.3577
77.0402
76.7225
69.4878
27.9820
OH
Cl
CN
2f
f1 (ppm)

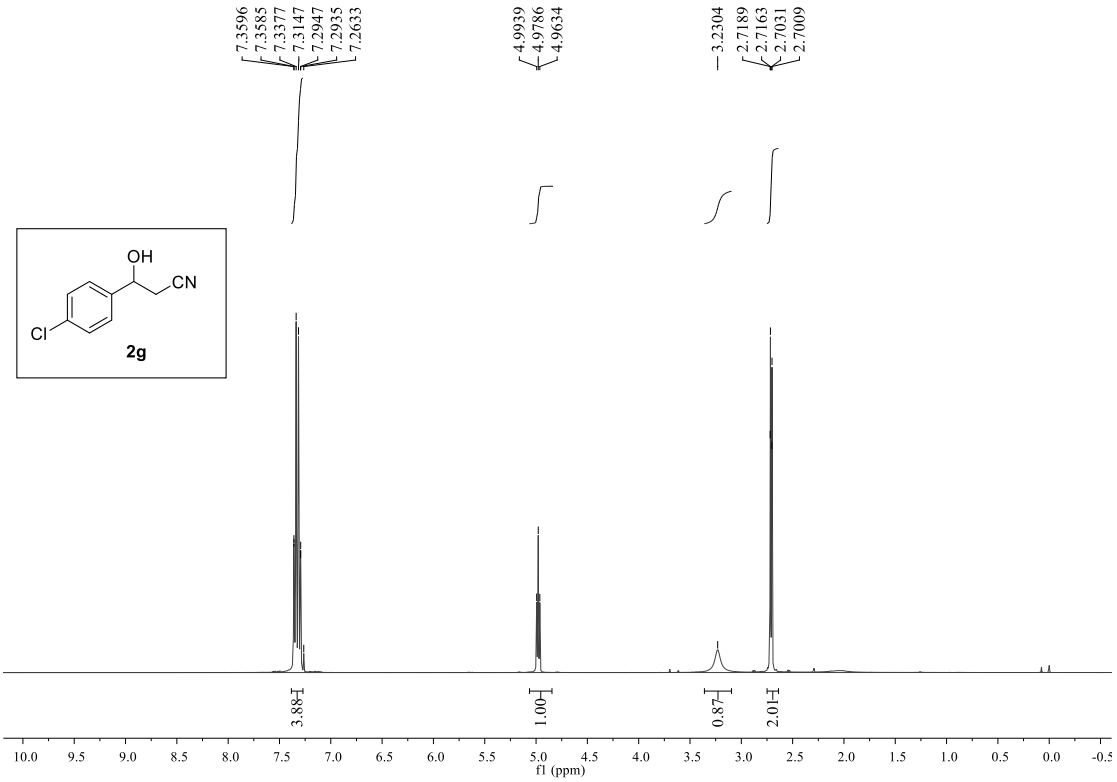
7.3596
7.3585
7.3377
7.3147
7.2947
7.2935
7.2633
4.9939
4.9786
4.9634
3.2304
2.7189
2.7163
2.7031
2.7009
OH
CN
Cl
2g
3.88
1.00
0.87
2.01
f1 (ppm)

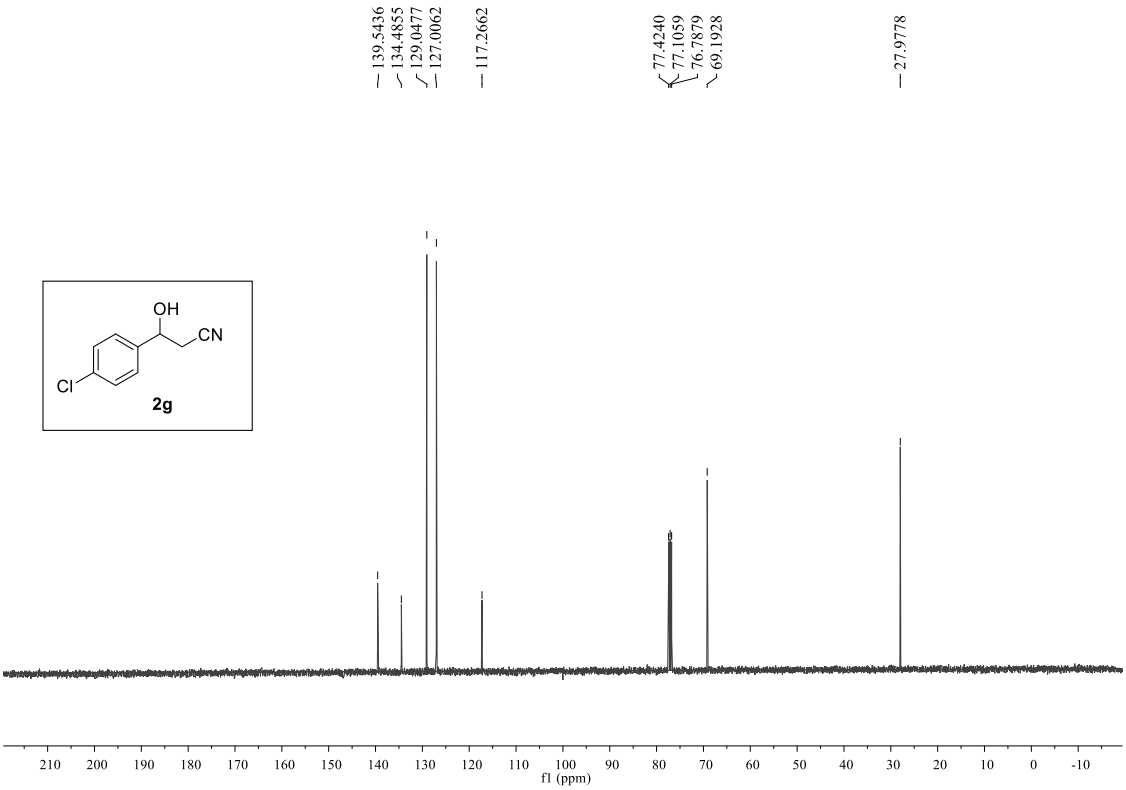
139.5436
134.4855
129.0477
127.0062
117.2662
77.4240
77.1059
76.7879
69.1928
27.9778
OH
CN
Cl
2g
f1 (ppm)

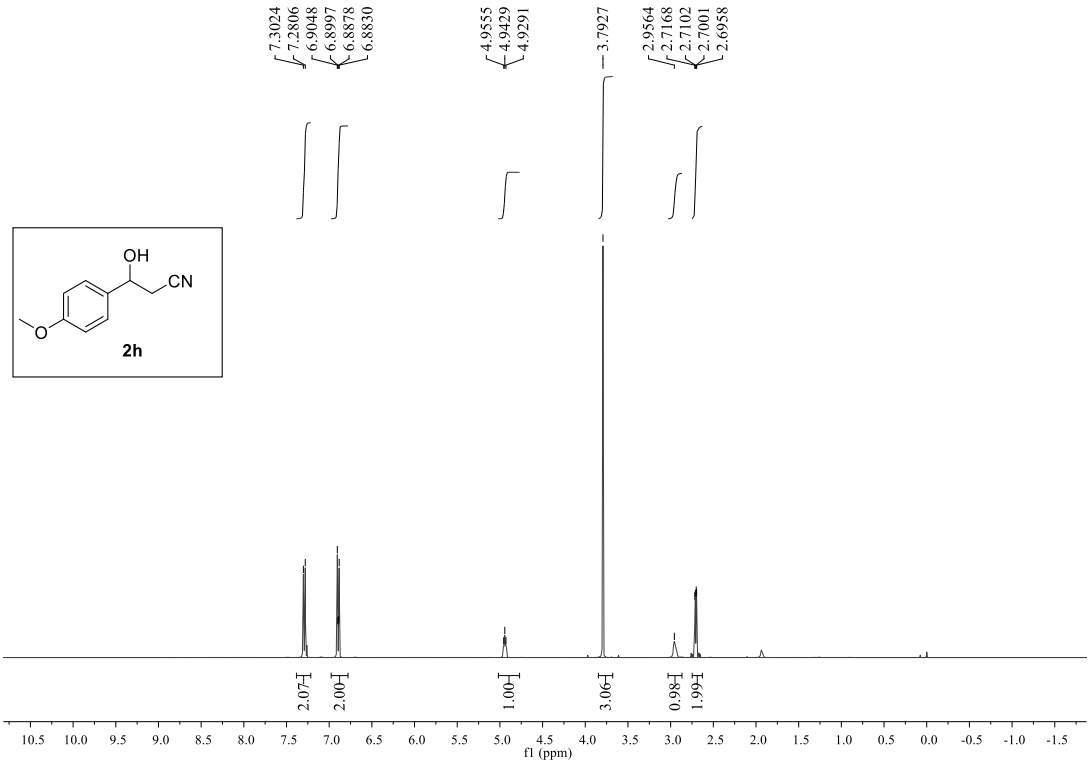
7.3024
7.2806
6.9048
6.8997
6.8878
6.8830
4.9555
4.9429
4.9291
3.7927
2.9564
2.7168
2.7102
2.7001
2.6958
OH
CN
O
2h
2.07
2.00
1.00
3.06
0.98
1.99
f1 (ppm)

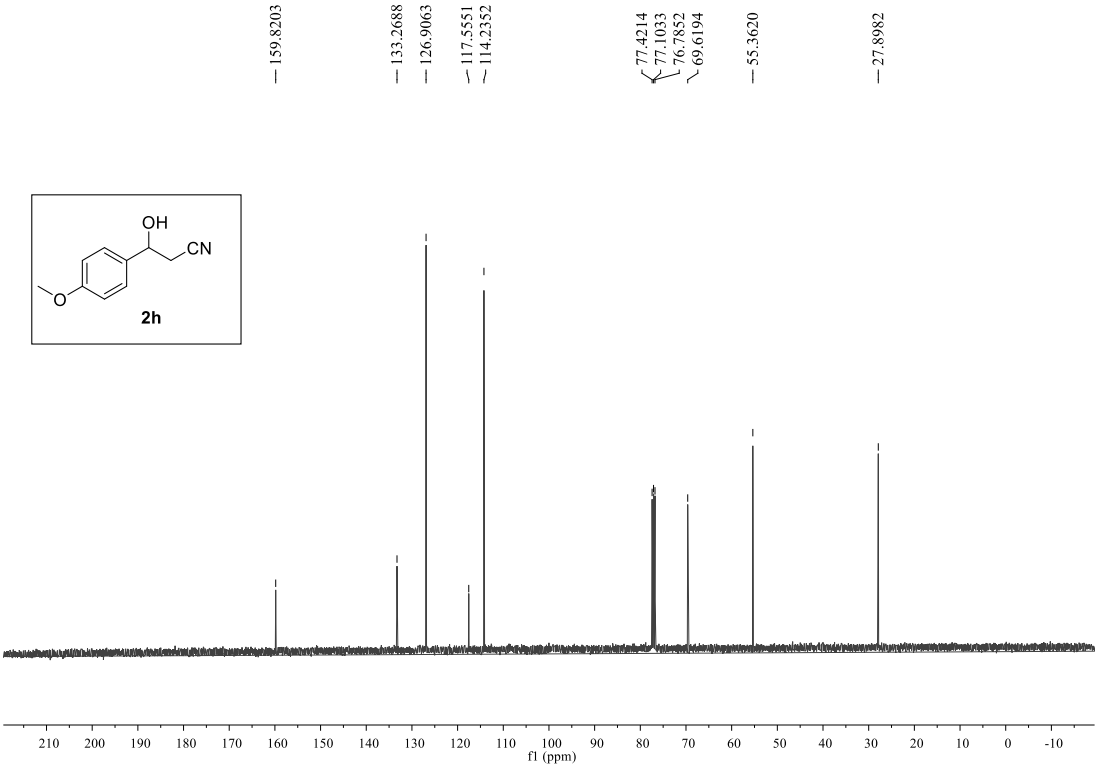
159.8203
133.2688
126.9063
117.5551
114.2352
77.4214
77.1033
76.7852
69.6194
55.3620
27.8982
OH
CN
O
2h
f1 (ppm)

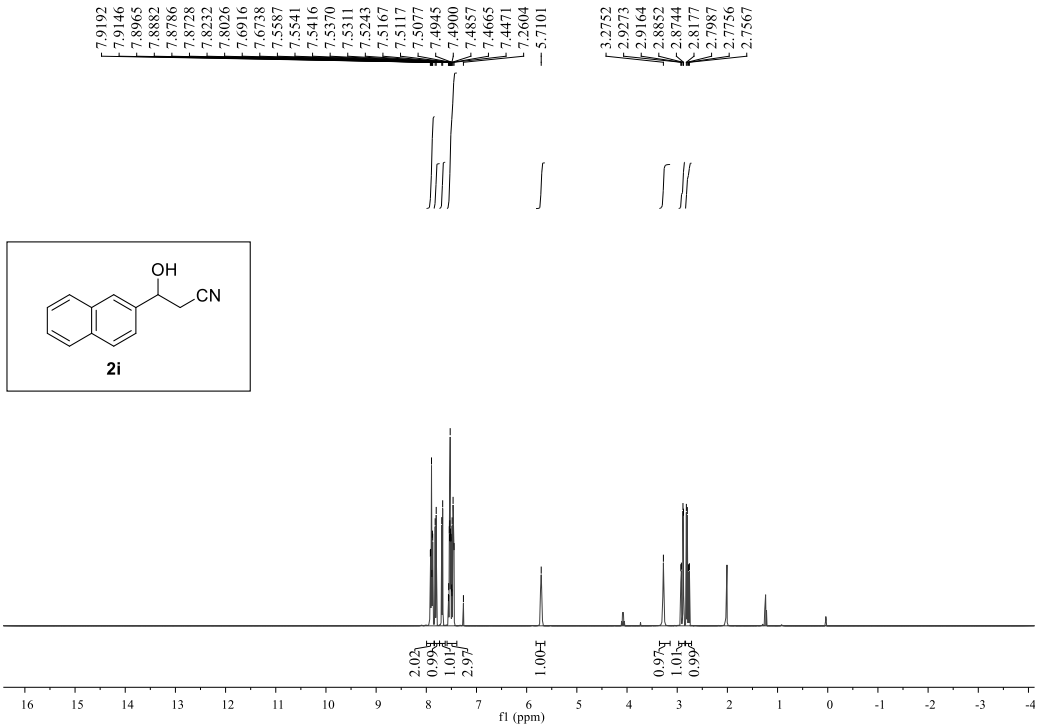
7.9192
7.9146
7.8965
7.8882
7.8786
7.8728
7.8232
7.8026
7.6916
7.6738
7.5587
7.5541
7.5416
7.5370
7.5311
7.5243
7.5167
7.5117
7.5077
7.4945
7.4900
7.4857
7.4665
7.4471
7.2604
5.7101
3.2752
2.9273
2.9164
2.8852
2.8744
2.8177
2.7987
2.7756
2.7567
OH
CN
2i
2.02
0.99
1.01
2.97
1.00
0.97
1.01
0.99
f1 (ppm)

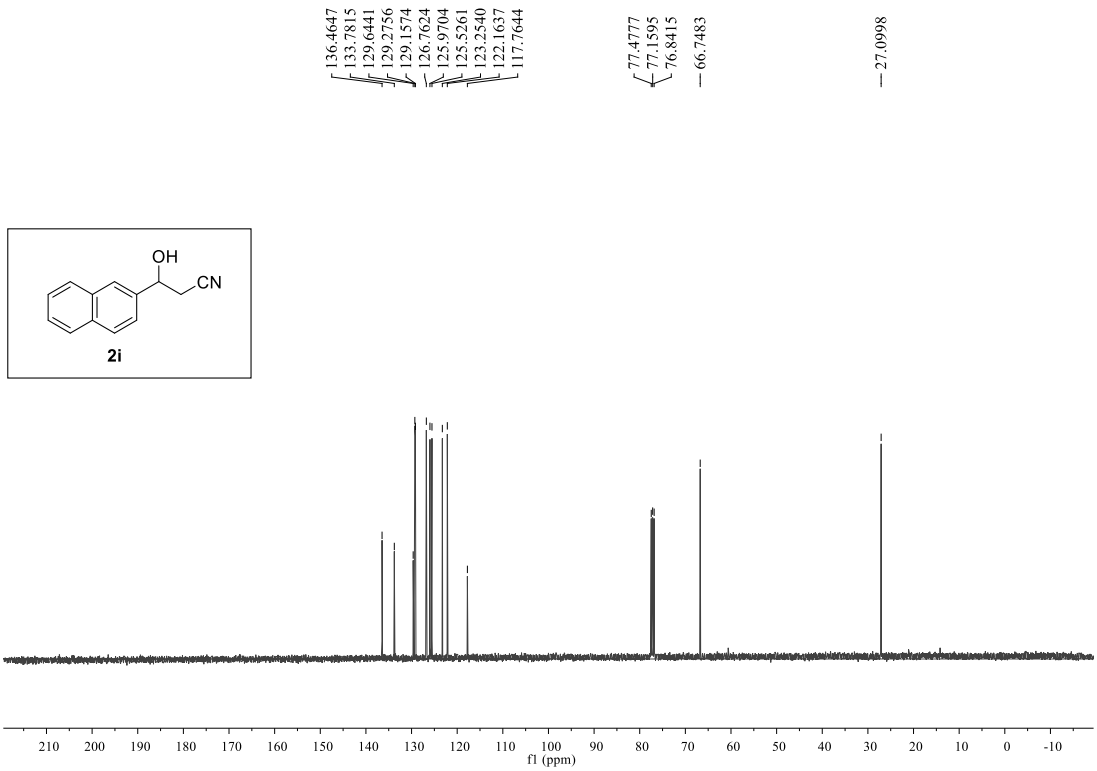
136.4647
133.7815
129.6441
129.2756
129.1574
126.7624
125.9704
125.5261
123.2540
122.1637
117.7644
77.4777
77.1595
76.8415
66.7483
27.0998
OH
CN
2i
f1 (ppm)

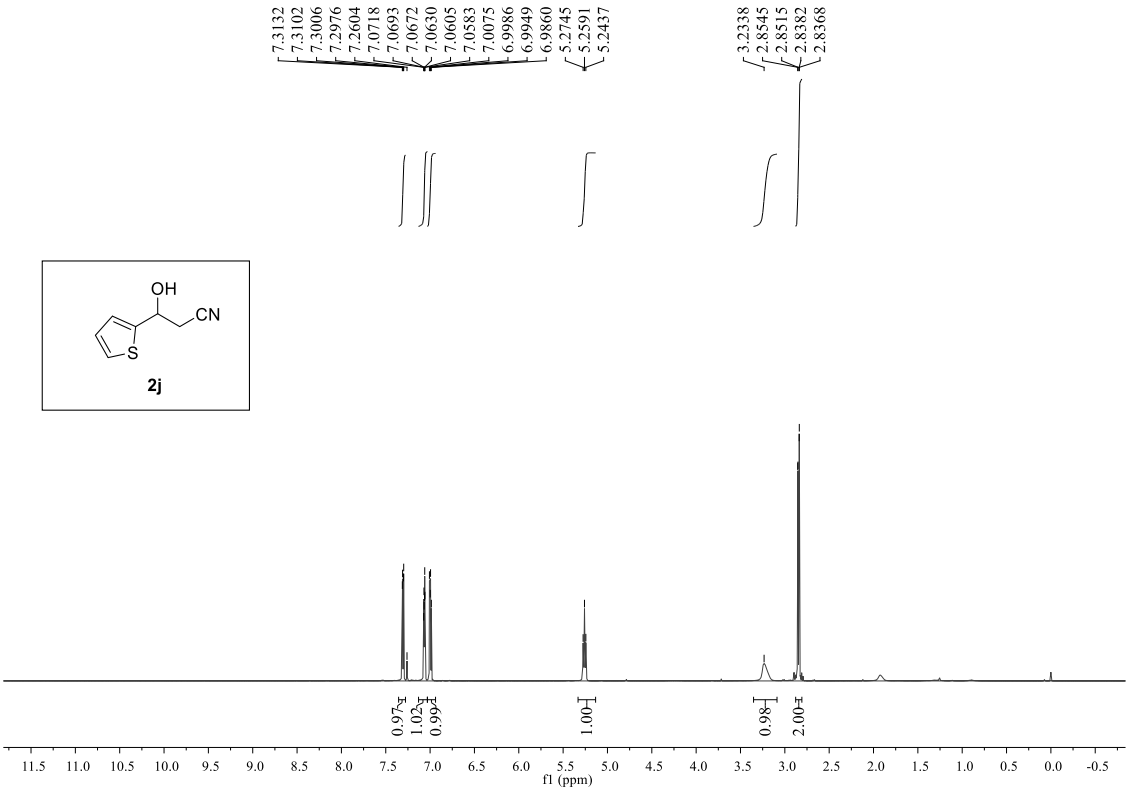
7.3132
7.3102
7.3006
7.2976
7.2604
7.0718
7.0693
7.0672
7.0630
7.0605
7.0583
7.0075
6.9986
6.9949
6.9860
5.2745
5.2591
5.2437
3.2338
2.8545
2.8515
2.8382
2.8368
OH
CN
S
2j
0.97
1.02
0.99
1.00
0.98
2.00
11.5 11.0 10.5 10.0 9.5 9.0 8.5 8.0 7.5 7.0 6.5 6.0 5.5 5.0 4.5 4.0 3.5 3.0 2.5 2.0 1.5 1.0 0.5 0.0 -0.5
f1 (ppm)

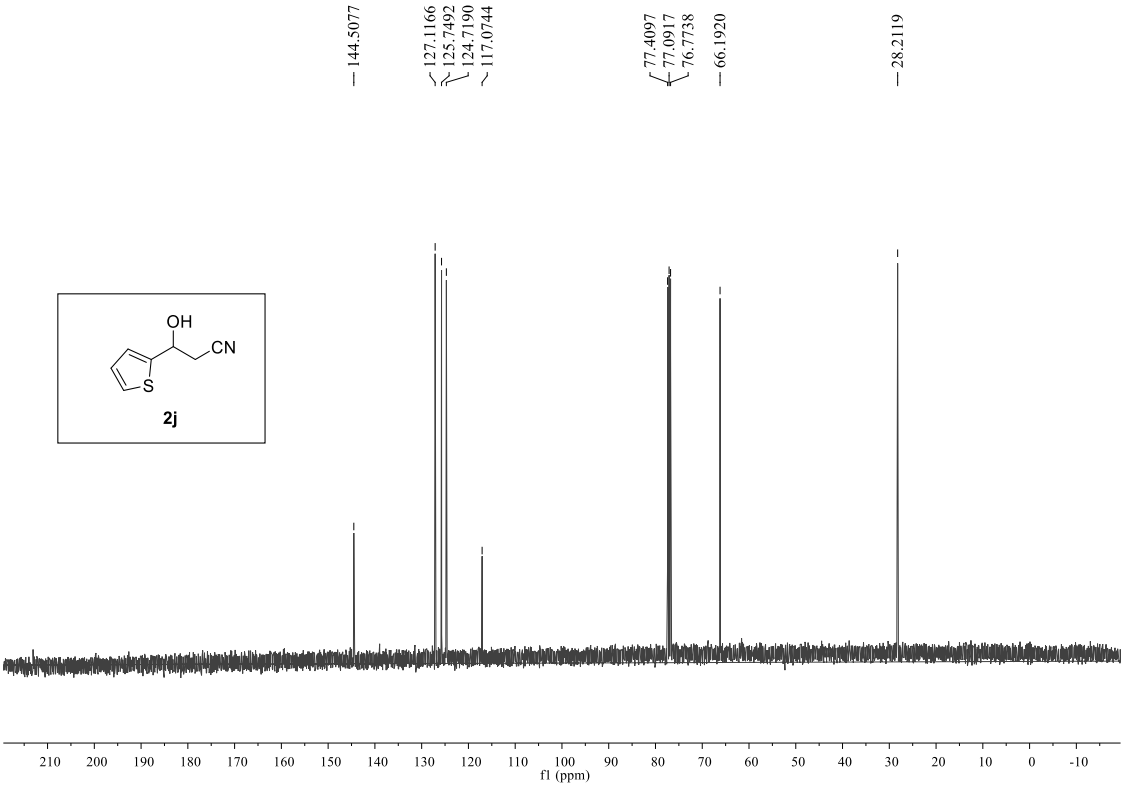
144.5077
127.1166
125.7492
124.7190
117.0744
77.4097
77.0917
76.7738
66.1920
28.2119
OH
CN
S
2j
210 200 190 180 170 160 150 140 130 120 110 100 90 80 70 60 50 40 30 20 10 0 -10
f1 (ppm)

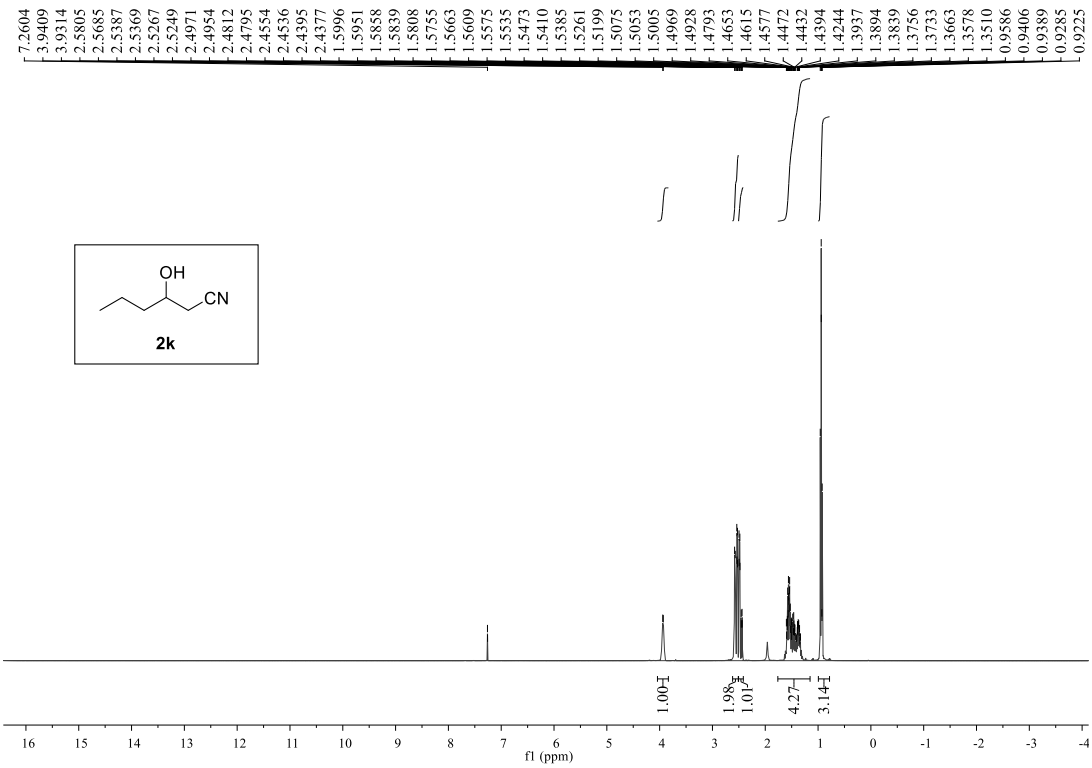
7.2604
3.9409
3.9314
2.5805
2.5685
2.5387
2.5369
2.5267
2.5249
2.4971
2.4954
2.4812
2.4795
2.4554
2.4536
2.4395
2.4377
1.5996
1.5951
1.5858
1.5839
1.5808
1.5755
1.5663
1.5609
1.5575
1.5535
1.5473
1.5410
1.5385
1.5261
1.5199
1.5075
1.5053
1.5005
1.4969
1.4928
1.4793
1.4653
1.4615
1.4577
1.4472
1.4432
1.4394
1.4244
1.3937
1.3894
1.3839
1.3756
1.3733
1.3663
1.3578
1.3510
0.9586
0.9406
0.9389
0.9285
0.9225
OH
CN
2k
1.00
1.98
1.01
4.27
3.14
f1 (ppm)

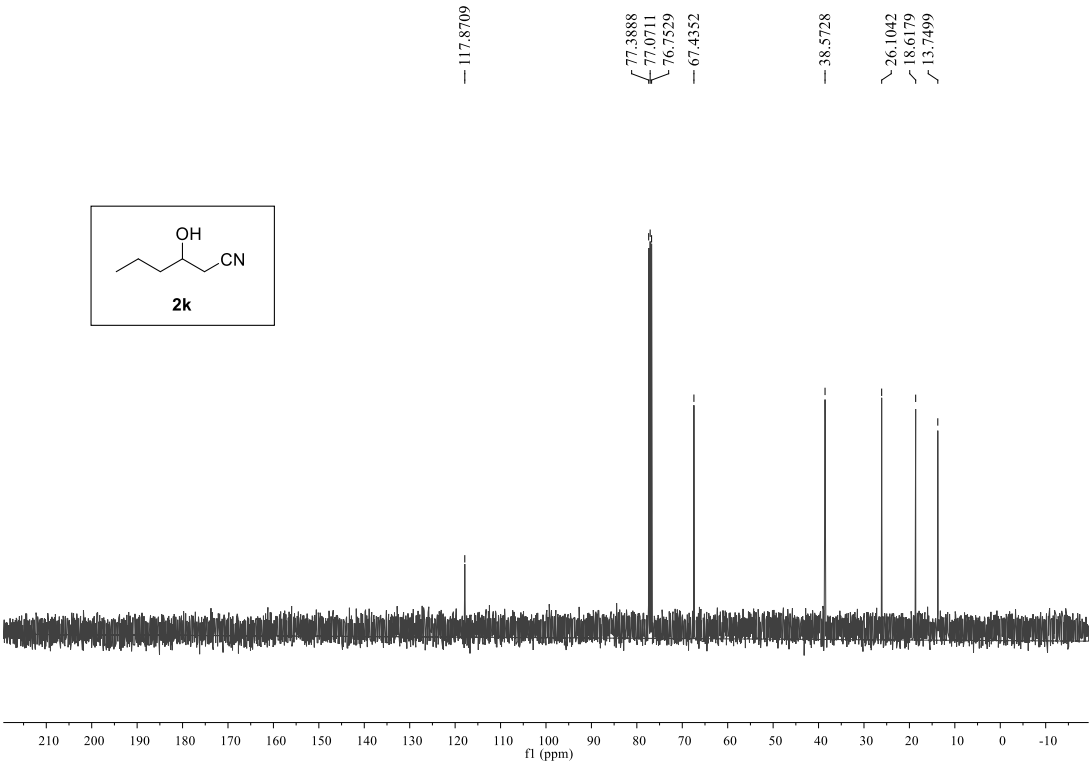
117.8709
77.3888
77.0711
76.7529
67.4352
38.5728
26.1042
18.6179
13.7499
OH
CN
2k
f1 (ppm)

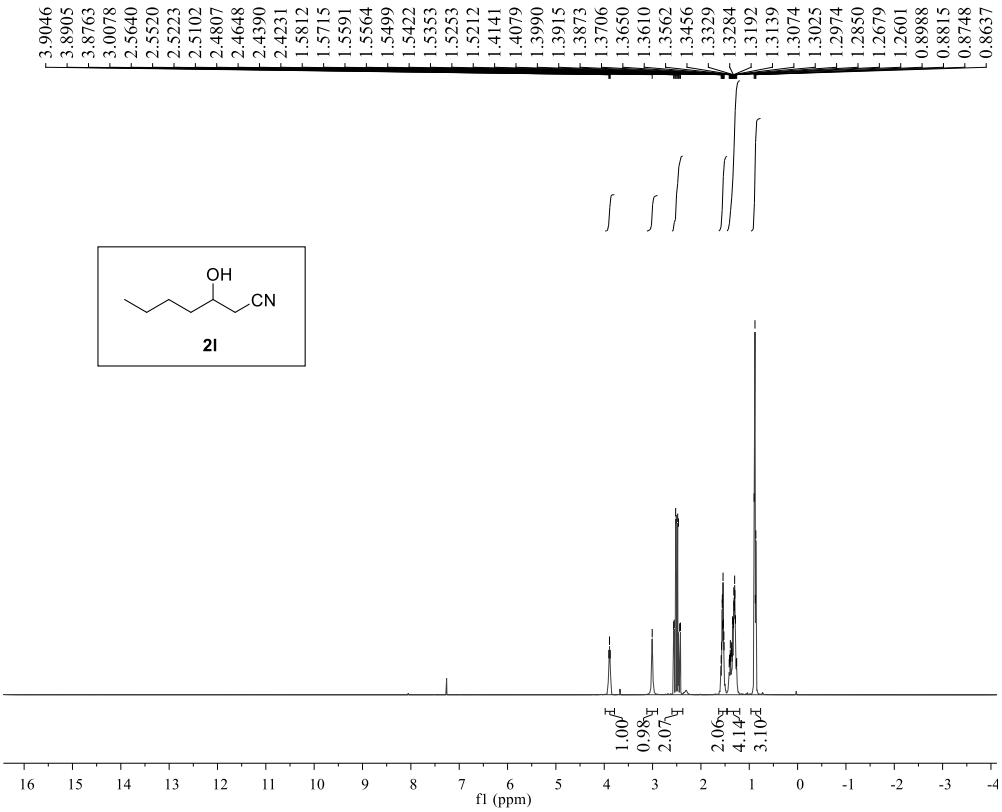
3.9046
3.8905
3.8763
3.0078
2.5640
2.5520
2.5223
2.5102
2.4807
2.4648
2.4390
2.4231
1.5812
1.5715
1.5591
1.5564
1.5499
1.5422
1.5353
1.5253
1.5212
1.4141
1.4079
1.3990
1.3915
1.3873
1.3706
1.3650
1.3610
1.3562
1.3456
1.3329
1.3284
1.3192
1.3139
1.3074
1.3025
1.2974
1.2850
1.2679
1.2601
0.8988
0.8815
0.8748
0.8637
OH
CN
2l
1.00
0.98
2.07
2.06
4.14
3.10
16 15 14 13 12 11 10 9 8 7 6 5 4 3 2 1 0 -1 -2 -3 -4
f1 (ppm)

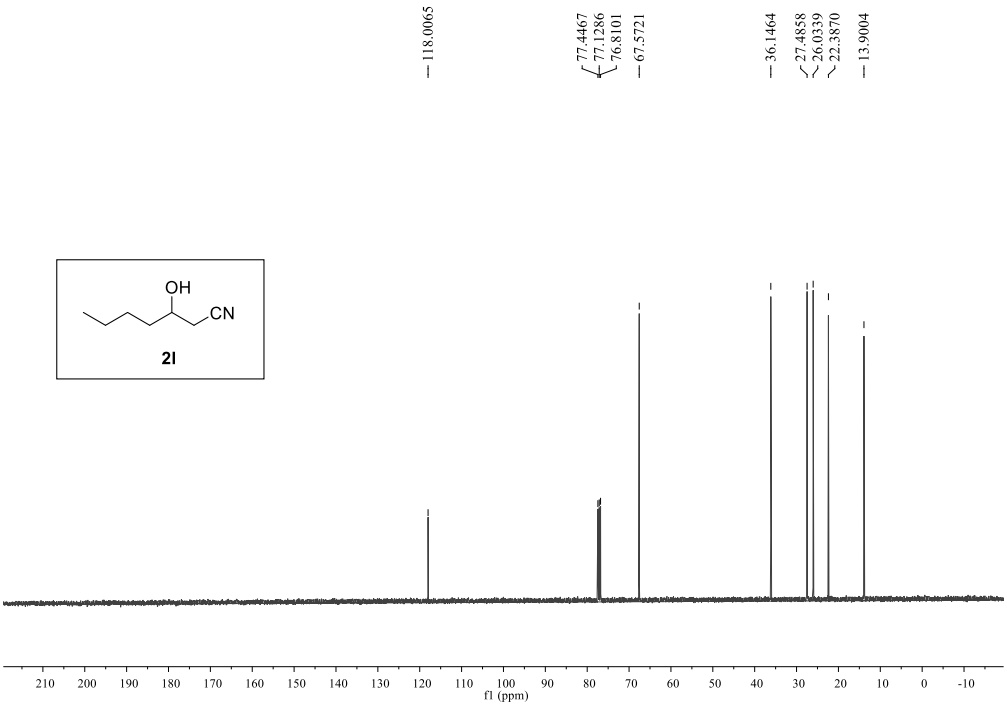
118.0065
77.4467
77.1286
76.8101
67.5721
36.1464
27.4858
26.0339
22.3870
13.9004
OH
CN
2l
210 200 190 180 170 160 150 140 130 120 110 100 90 80 70 60 50 40 30 20 10 0 -10
f1 (ppm)

Appendix II: Absolute configuration measurement of compounds of **2e, 2g, 2k, 2l** using mosher ester method.

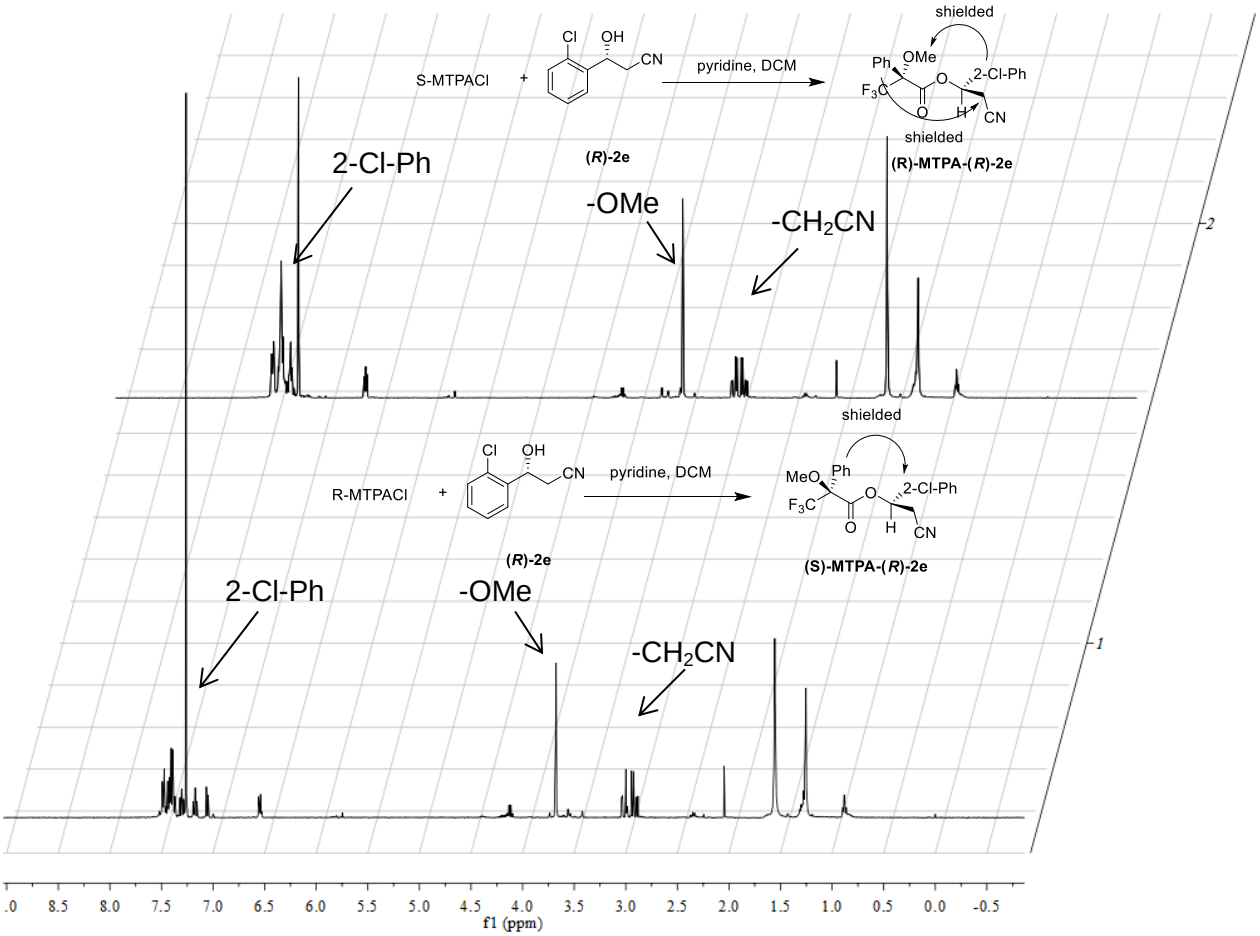

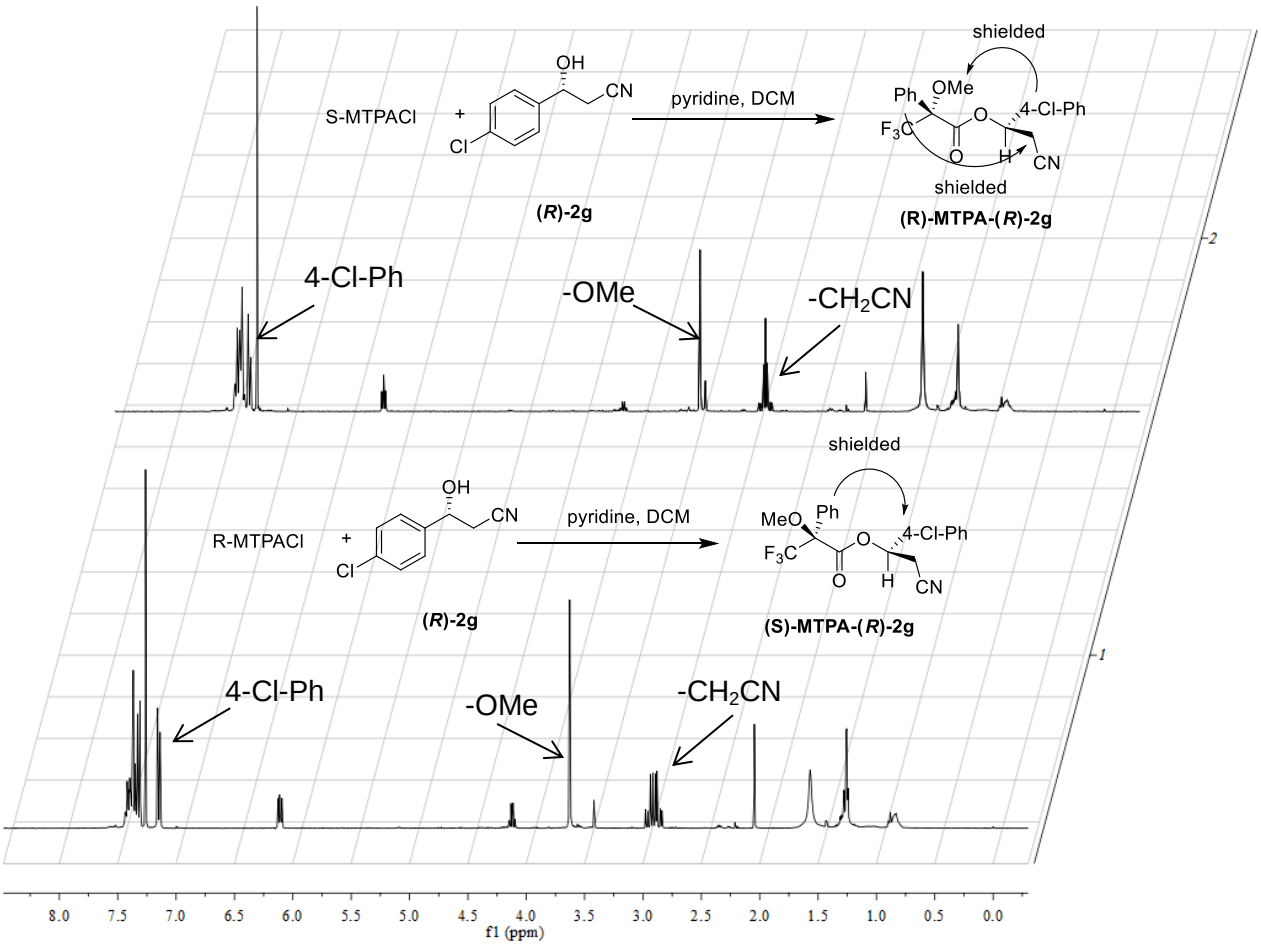
S-MTPACl
OH
CN
Cl
pyridine, DCM
shielded
Ph
OMe
4-Cl-Ph
F3C
O
H
CN
shielded
(R)-2g
(R)-MTPA-(R)-2g
4-Cl-Ph
-OMe
-CH2CN
R-MTPACl
OH
CN
Cl
pyridine, DCM
shielded
MeO
Ph
4-Cl-Ph
F3C
O
H
CN
(R)-2g
(S)-MTPA-(R)-2g
4-Cl-Ph
-OMe
-CH2CN
8.0 7.5 7.0 6.5 6.0 5.5 5.0 4.5 4.0 3.5 3.0 2.5 2.0 1.5 1.0 0.5 0.0
f1 (ppm)

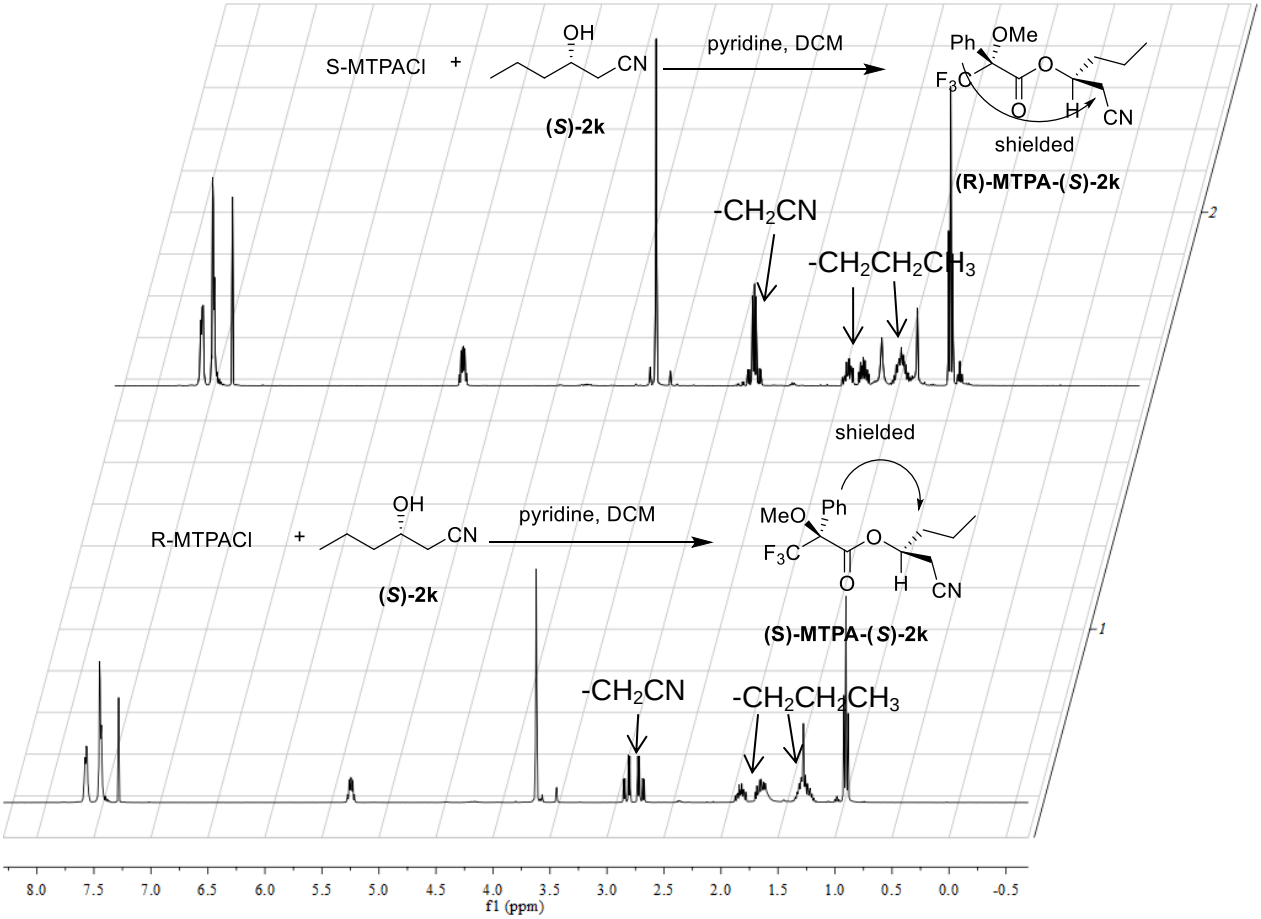
S-MTPACl
OH
CN
(S)-2k
pyridine, DCM
Ph
OMe
F3C
O
H
CN
shielded
(R)-MTPA-(S)-2k
-CH2CN
-CH2CH2CH3
shielded
R-MTPACl
OH
CN
(S)-2k
pyridine, DCM
MeO
Ph
F3C
O
H
CN
(S)-MTPA-(S)-2k
-CH2CN
-CH2CH2CH3
8.0 7.5 7.0 6.5 6.0 5.5 5.0 4.5 4.0 3.5 3.0 2.5 2.0 1.5 1.0 0.5 0.0 -0.5
f1 (ppm)

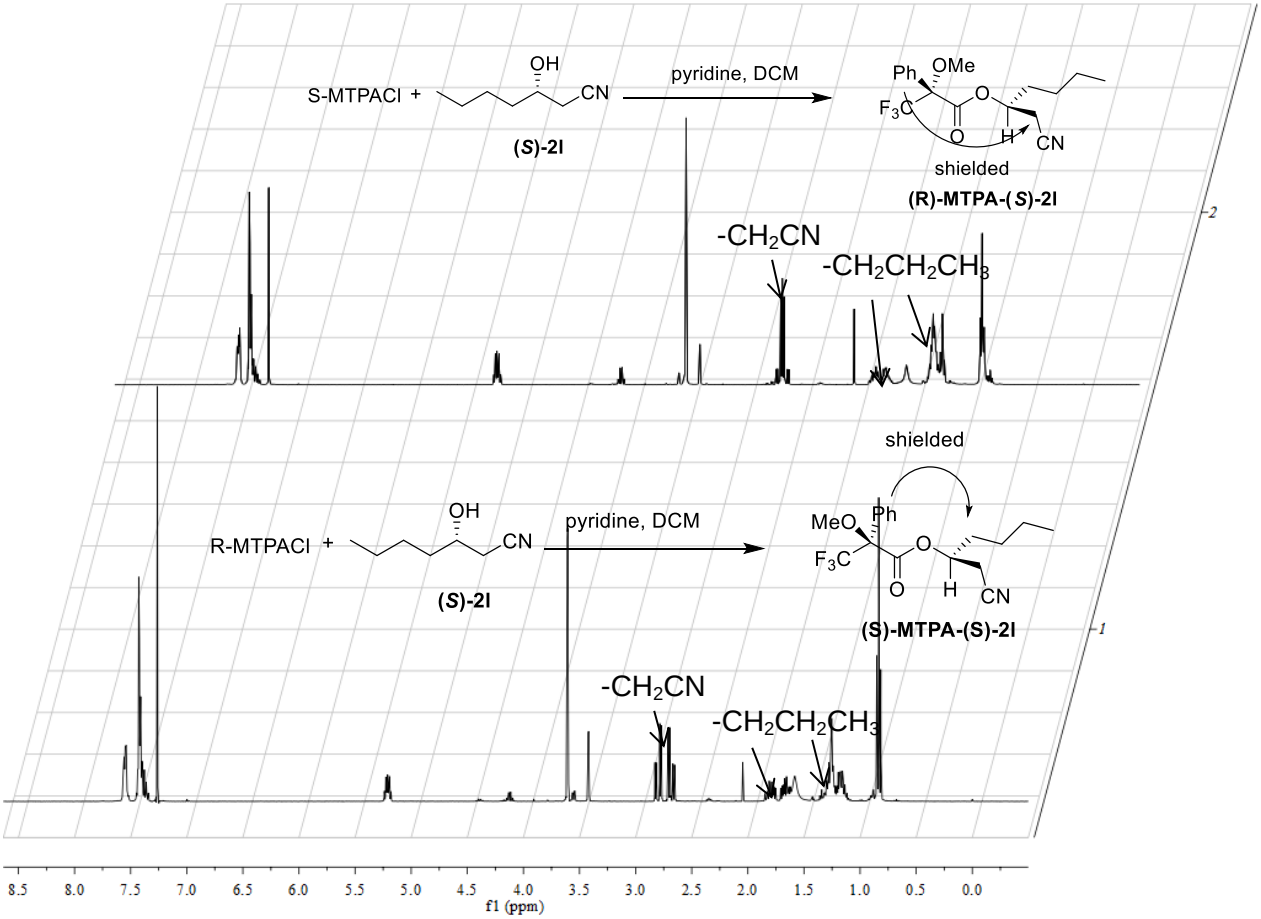
S-MTPACl +
OH
CN
(S)-2l
pyridine, DCM
Ph
OMe
F3C
O
O
H
CN
shielded
(R)-MTPA-(S)-2l
-CH2CN
-CH2CH2CH3
shielded
R-MTPACl +
OH
CN
(S)-2l
pyridine, DCM
MeO
Ph
F3C
O
O
H
CN
(S)-MTPA-(S)-2l
-CH2CN
-CH2CH2CH3
8.5 8.0 7.5 7.0 6.5 6.0 5.5 5.0 4.5 4.0 3.5 3.0 2.5 2.0 1.5 1.0 0.5 0.0
f1 (ppm)

Appendix III. The NMR spectra of 5-(chloromethyl)-4, 5-dihydroisoxazole and 4-chloro-3-hydroxybutanenitrile

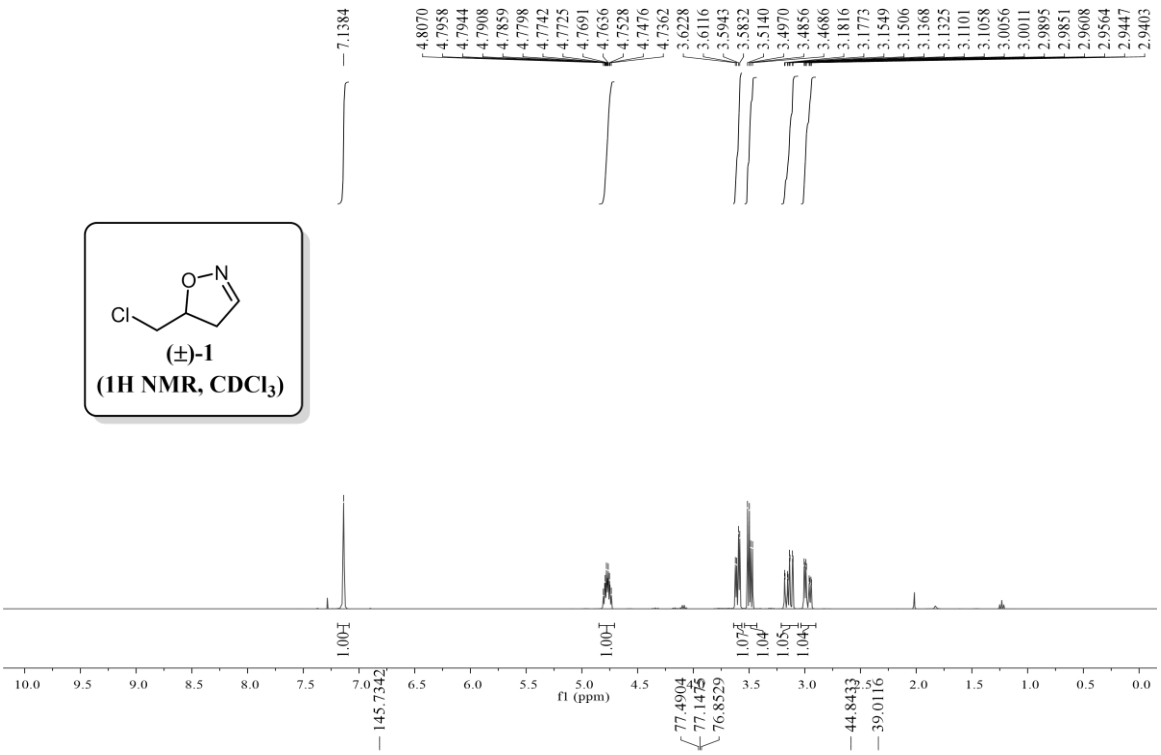

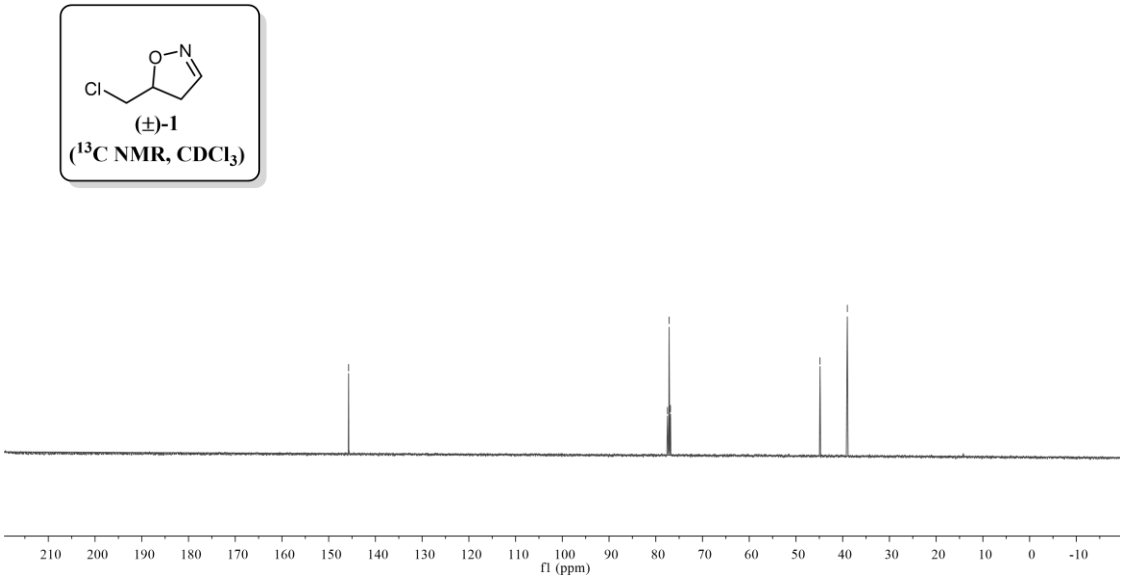

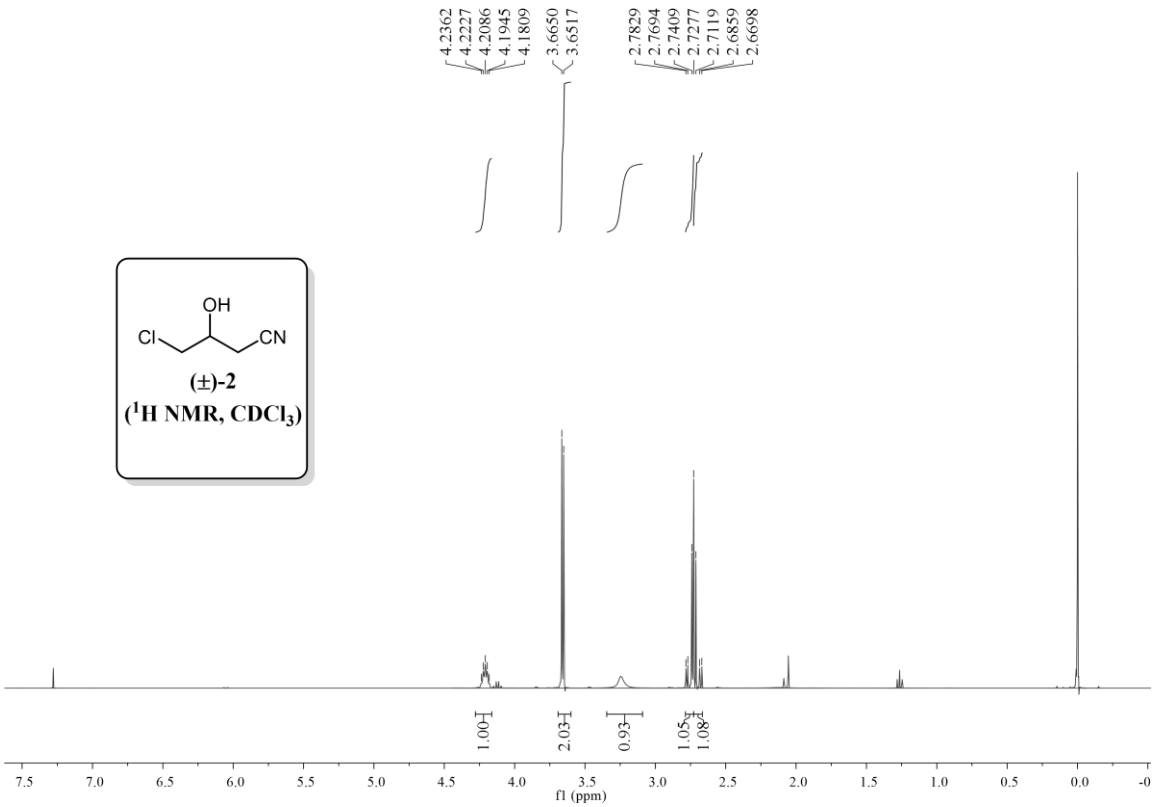
4.2362
4.2227
4.2086
4.1945
4.1809
3.6650
3.6517
2.7829
2.7694
2.7409
2.7277
2.7119
2.6859
2.6698
OH
Cl
CN
(±)-2
(1H NMR, CDCl3)
1.00
2.03
0.93
1.05
1.08
7.5 7.0 6.5 6.0 5.5 5.0 4.5 4.0 3.5 3.0 2.5 2.0 1.5 1.0 0.5 0.0 -0
f1 (ppm)

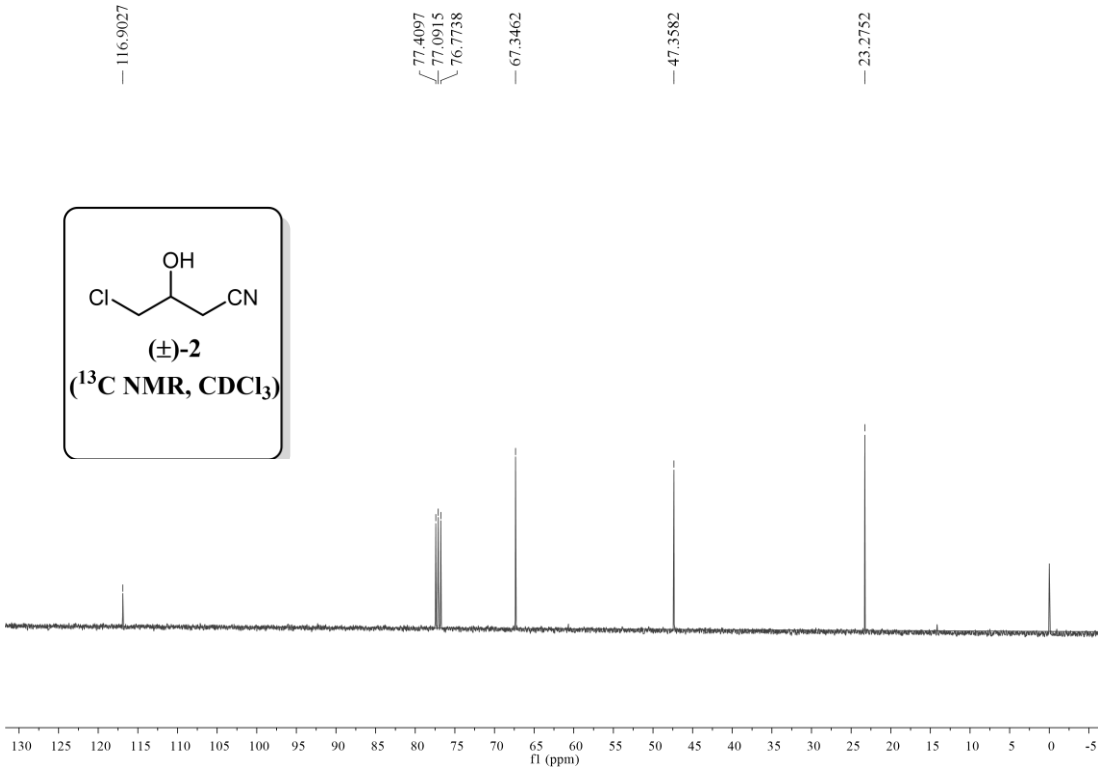
116.9027
77.4097
77.0915
76.7738
67.3462
47.3582
23.2752
OH
Cl
CN
(±)-2
(13C NMR, CDCl3)
130 125 120 115 110 105 100 95 90 85 80 75 70 65 60 55 50 45 40 35 30 25 20 15 10 5 0 -5
f1 (ppm)

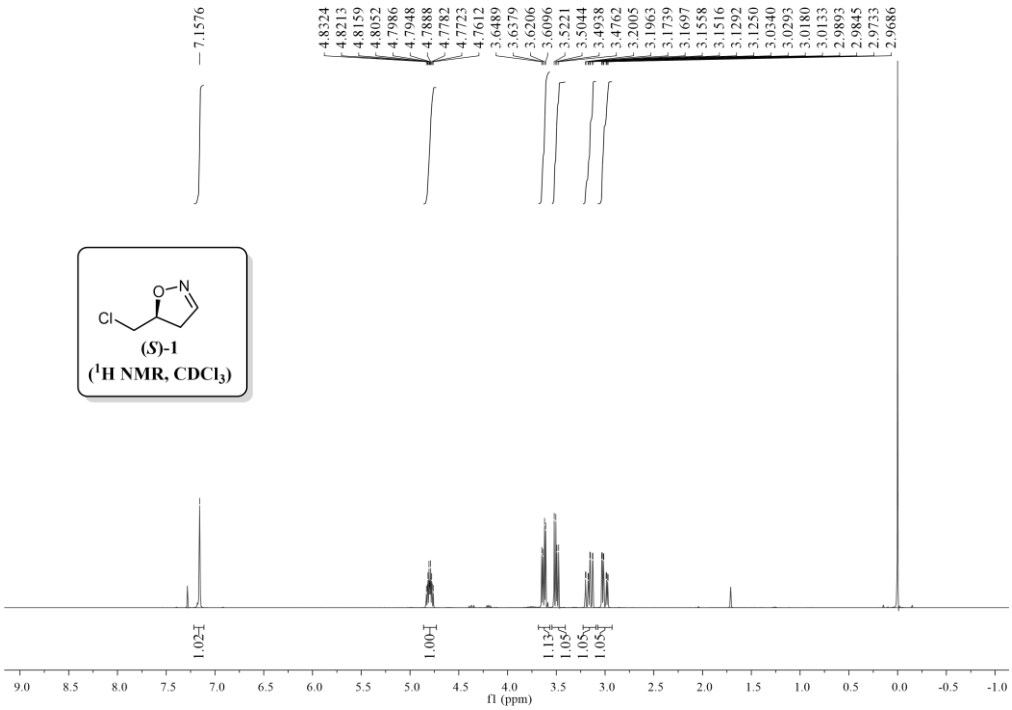

(*S*)-1
(^{1}H NMR, $CDCl_3$)

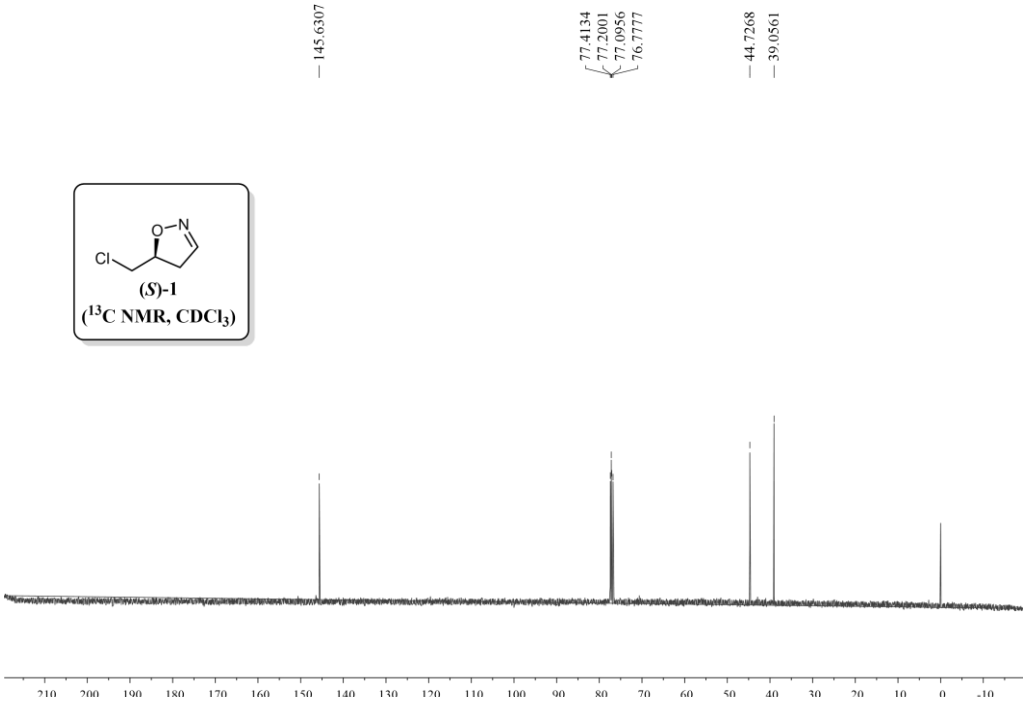

(*S*)-1
(^{13}C NMR, $CDCl_3$)

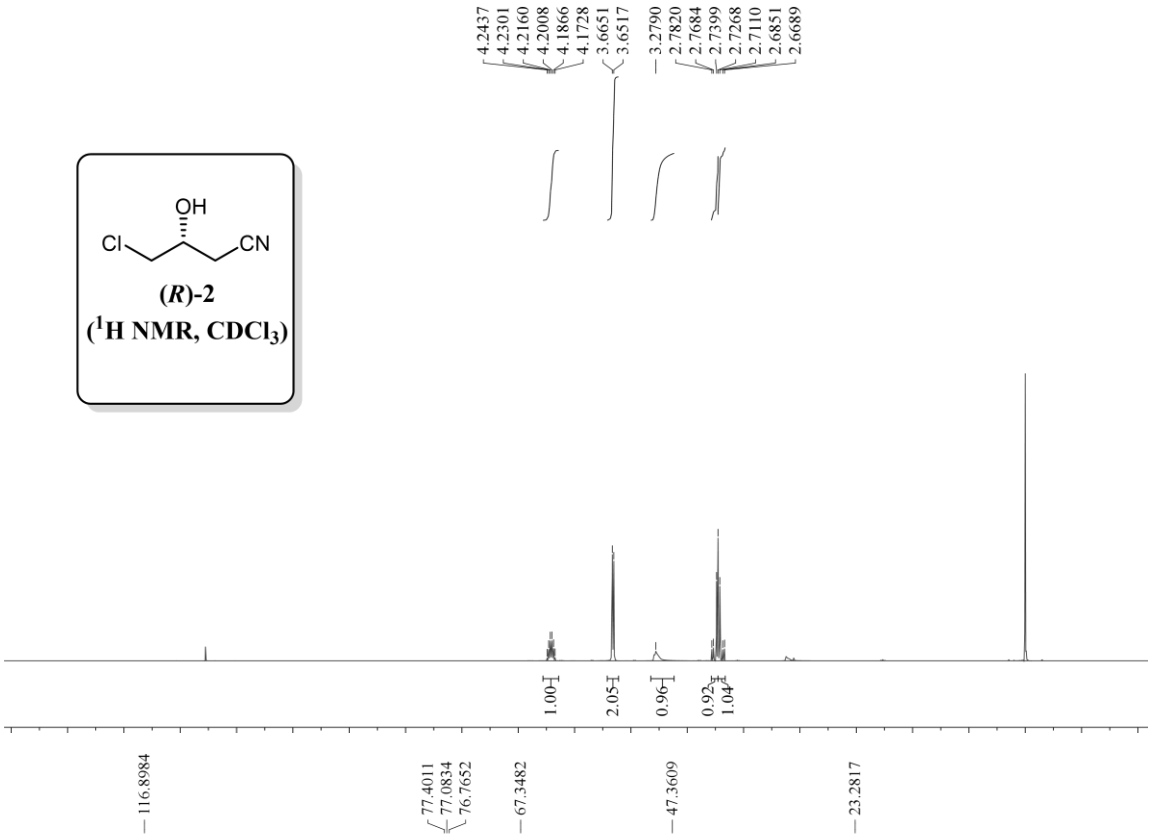
OH
Cl
CN
(R)-2
(1H NMR, CDCl3)
4.2437
4.2301
4.2160
4.2008
4.1866
4.1728
3.6651
3.6517
3.2790
2.7820
2.7684
2.7399
2.7268
2.7110
2.6851
2.6689
1.00
2.05
0.96
0.92
1.04
116.8984
77.4011
77.0834
76.7652
67.3482
47.3609
23.2817

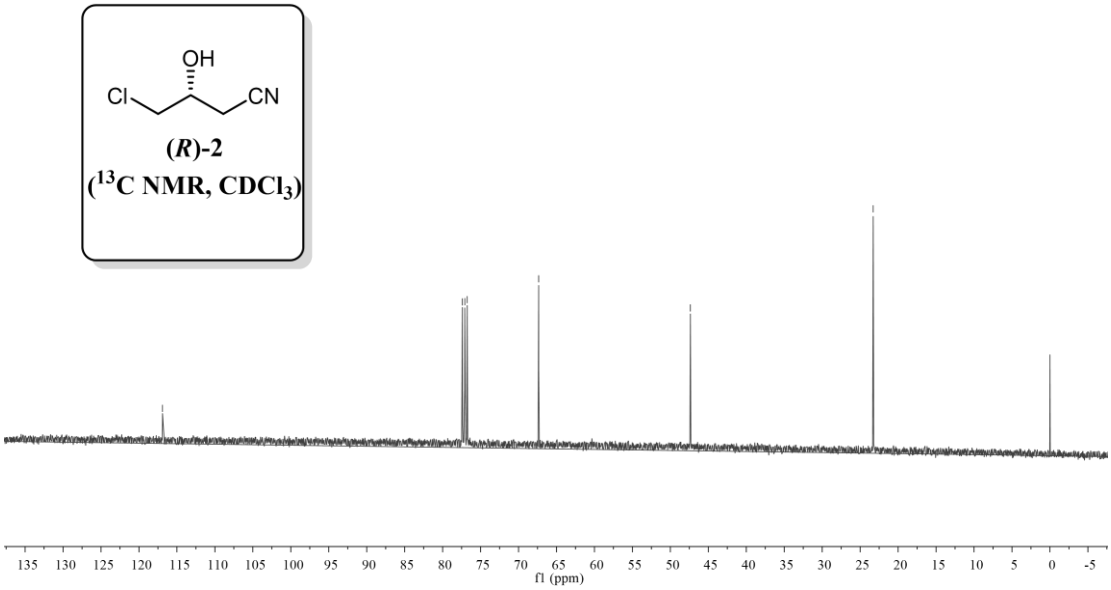
OH
Cl
CN
(R)-2
(13C NMR, CDCl3)
135 130 125 120 115 110 105 100 95 90 85 80 75 70 65 60 55 50 45 40 35 30 25 20 15 10 5 0 -5
f1 (ppm)

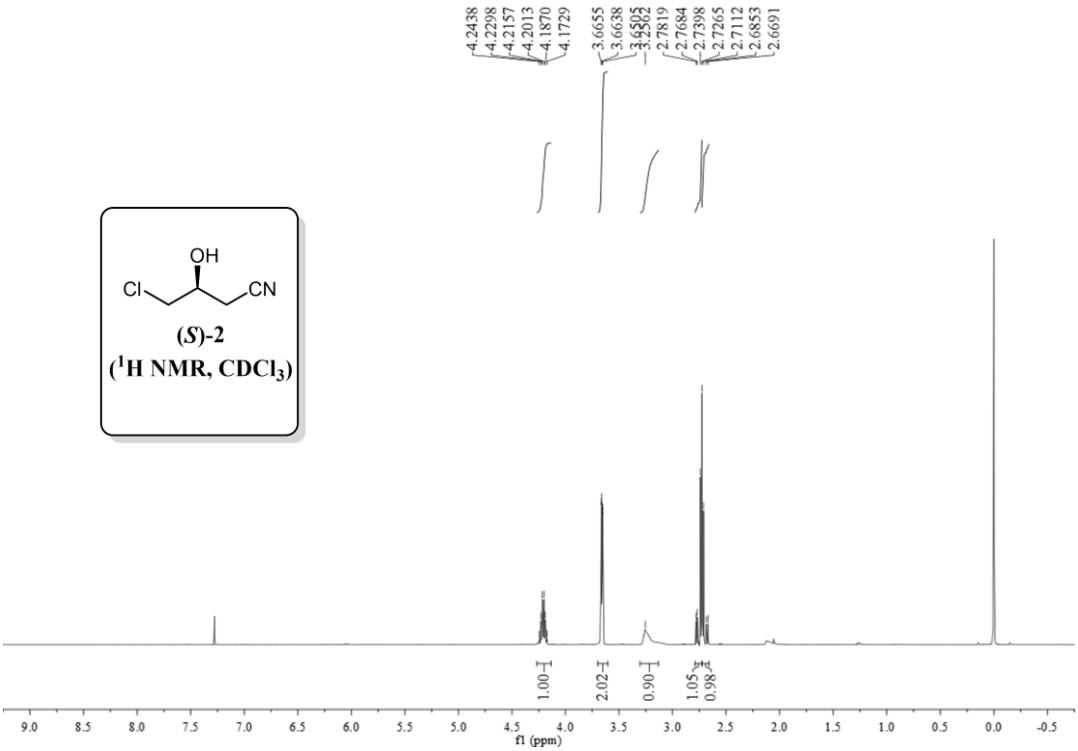
4.2438
4.2298
4.2157
4.2013
4.1870
4.1729
3.6655
3.6638
3.6505
3.2562
2.7819
2.7684
2.7398
2.7265
2.7112
2.6853
2.6691
OH
Cl
CN
(S)-2
(1H NMR, CDCl3)
1.00
2.02
0.90
1.05
0.98
f1 (ppm)

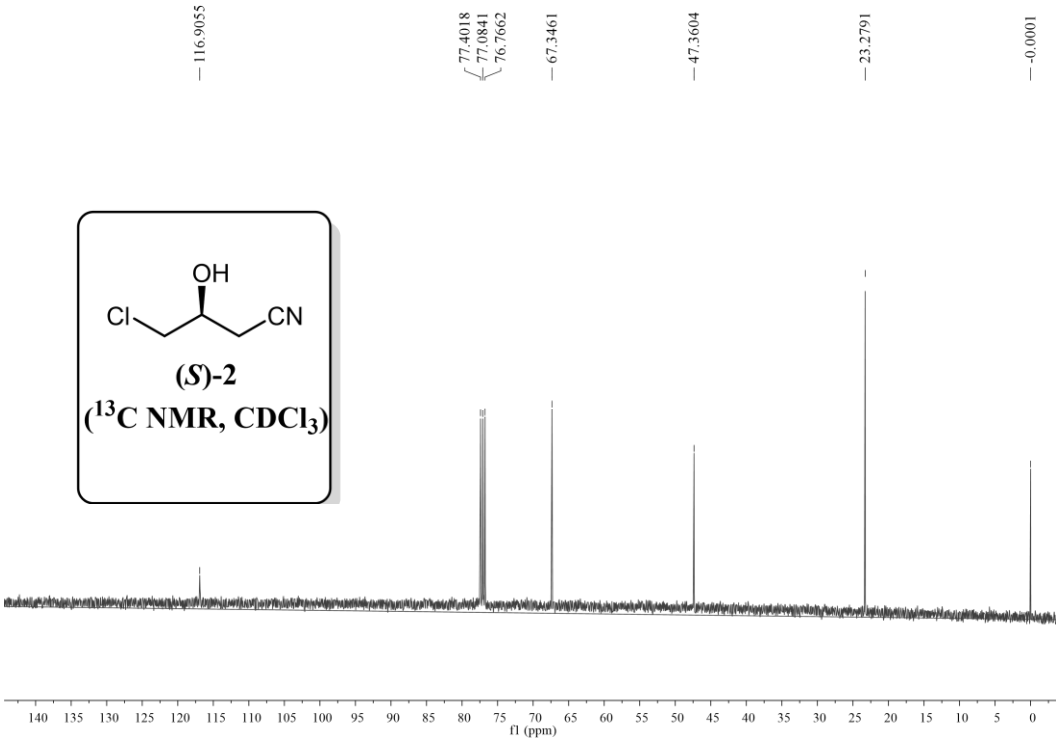
116.9055
77.4018
77.0841
76.7662
67.3461
47.3604
23.2791
-0.0001
OH
Cl
CN
(S)-2
(13C NMR, CDCl3)
f1 (ppm)

Appendix IV: GC analysis result for large scale reactions.

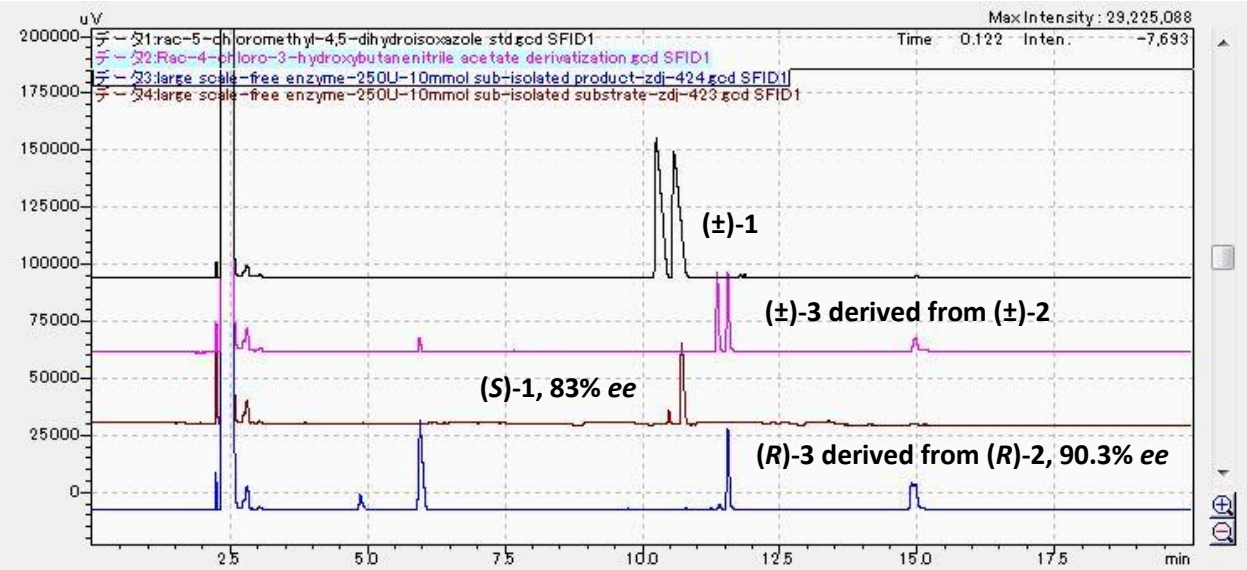

AppendixIV-1: The GC analysis result of the isolated products in gram-scale reaction (10 min) using OxdA-L318I enzyme as catalyst **(Table 8, entry 1)**

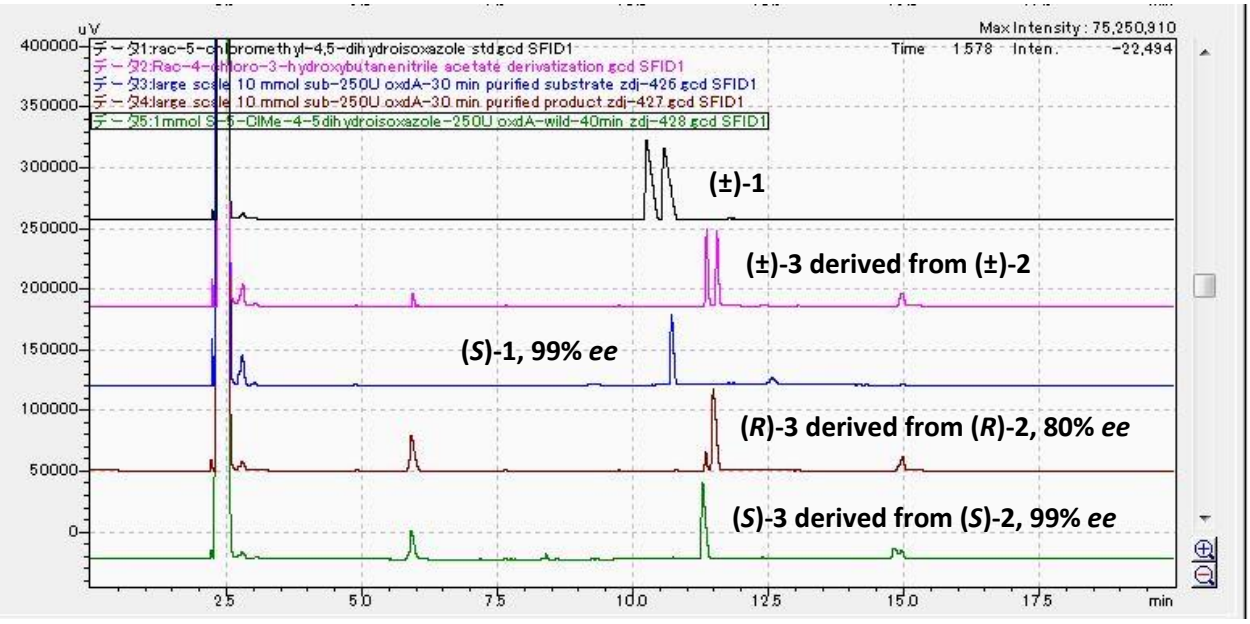

AppendixIV-2: The GC analysis result of the isolated products in gram-scale reaction (30 min) using OxdA-L318I enzyme as catalyst (**Table 8, entry 2**) and the enzymatic reaction to convert **(*S*)-1** to **(*S*)-2**.

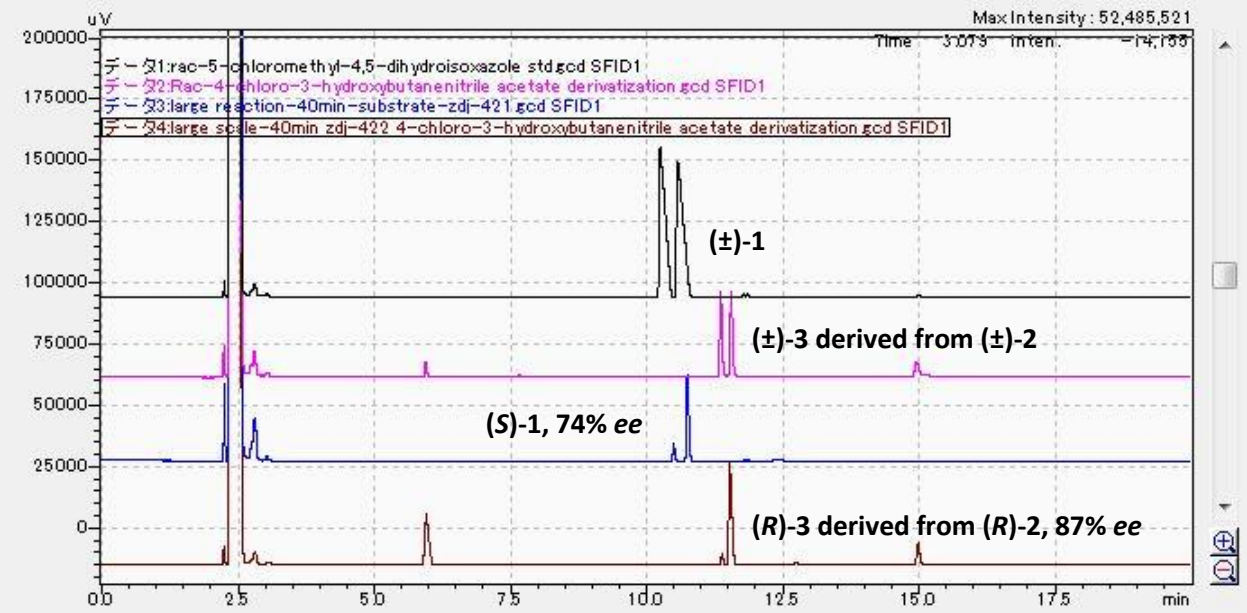

AppendixIV-3: The GC analysis result of the isolated products in gram-scale reaction (40 min) using OxdA-L318I whole cell as catalyst **(Table 8, entry 3)**

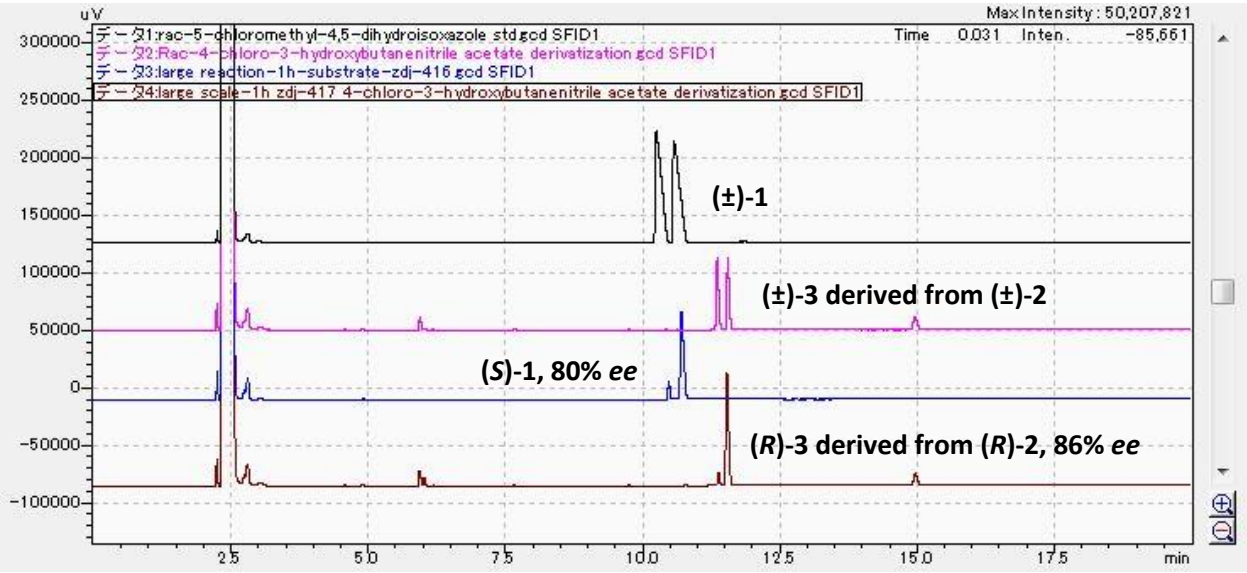

AppendixIV-4: The GC analysis result of the isolated products in gram-scale reaction (60 min) using OxdA-L318I whole cell as catalyst **(Table 8, entry 4)**

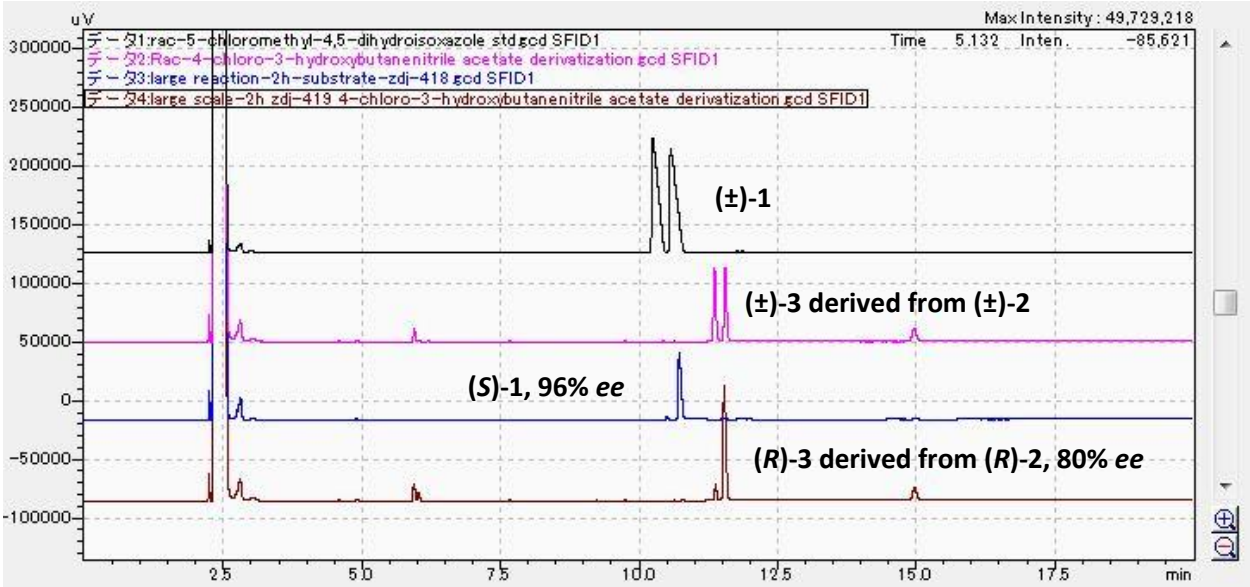

AppendixIV-5: The GC analysis result of the isolated products in gram-scale reaction (120 min) using OxdA-L318I whole cell as catalyst **(Table 8, entry 5)**

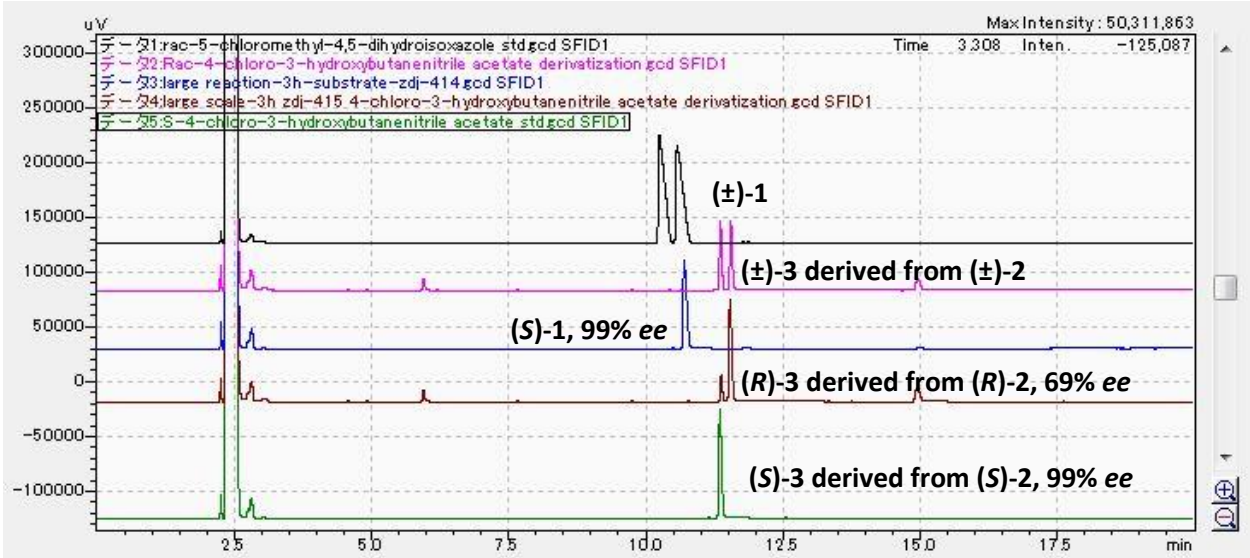

AppendixIV-6: The GC analysis result of the isolated products in gram-scale reaction (180 min) using OxdA-L318I whole cell as catalyst **(Table 8, entry 6)** and the chemical reaction to convert **(*S*)-1** to **(*S*)-2**.